1991

Petrogenesis Of The Prairie Creek, Arkansas, Diamondiferous Olivine Lamproite

Edward C. Walker

PETROGENESIS OF THE PRAIRIE CREEK, ARKANSAS, DIAMONDIFEROUS OLIVINE LAMPROITE

by

Edward C. Walker

Department of Geology

Submitted in partial fulfilment
of the requirements for the degree of
Doctor of Philosophy

Faculty of Graduate Studies
The University of Western Ontario
London, Ontario
August 1991

ISBN 0-315-66296-4

ABSTRACT

The Prairie Creek, Arkansas olivine lamproite intrusion consists of three facies of rock: tuff, breccia and hypabyssal facies of rock; and two suites of cognate xenoliths. Suprasolidus experiments on the hypabyssal rock were undertaken between 10 and 40 kilobars, and 1000 and 1400 °C, with three different volatile conditions. A petrogenetic model for the intrusion is proposed based on the integration of phase relations and mineral chemistry.

Clinopyroxene, phlogopite, spinel and titan potassic richterite mineral analyses from the intrusion independently define a single continuous compositional trend. Comparison of the mineral analyses from the intrusion to those from the experiments suggests that the composition of phlogopite and clinopyroxene may be controlled by pressure, and spinel by temperature. In addition, the paragenetic sequence defined by the tuff and breccia facies of rock is similar to that observed in the experiments on the hypabyssal rock, with H_2O and F as additional components.

The data indicate that the crystallization of an olivine lamproite magma, ascending from below the diamond-graphite transition to the surface in a buoyancy-driven magma fracture, can model the petrogenesis of the intrusion. Increased abundance of water, and possibly fluorine, at the top of the magma fracture resulted in the crystallization of olivine followed by phenocrystic phlogopite at depths greater than 30 kilometers. This magma erupted explosively at the surface, and formed the tuff and breccia facies of rock. Below the volatile enriched portion of the magma column, olivine, spinel, perovskite,

apatite and clinopyroxene crystallized before poikilitic phlogopite. The poikilitic phlogopite is compositionally different than the phenocrystic phlogopite, and crystallized at depths less than 30 kilometers. The magma in which the poikilitic phlogopite crystallized ascended more slowly, intruded the tuff and breccia facies, and is represented by the hypabyssal facies of rock.

As the hypabyssal facies ascended through the conduit produced by the eruption of the tuff and breccia magma, remnant magma within the conduit was incorporated as cognate xenoliths into the ascending hypabyssal facies at successively lower pressures. These cognate xenoliths host a similar paragenetic sequence and mineral chemistry, with respect to clinopyroxene, phlogopite and amphibole, to that observed in the tuff, breccia and hypabyssal facies of rock.

The paragenetic sequence and mineral compositions of the Prairie Creek intrusion are similar to those in the Kapamba and Western Australia olivine lamproites, described by other authors. Such a correlation is considered to suggest that crystallization within a buoyancy driven magma fracture may be an important petrogenetic process for the genesis of olivine lamproite magmas.

ACKNOWLEDGEMENTS

I wish to express my gratitude and thanks to the people who have assisted me during the many phases of my thesis.

I would like to acknowledge and thank Dr. Alan D. Edgar for the opportunity to undertake this project, his funding, assistance and critical review.

Special acknowledgement is due to Robert Barnett, Dr. Norm Duke, Dr. Yves Thibault, and Andrew McNeil who supported and inspired me with inciteful discussions, and encouragement.

Appreciation and thanks go to Robert Barnett, Ron Shirran, John Forth and Charles Wu for their technical assistance, and David Kingston who assisted both technically and editorially.

I owe a large debt of gratitude to Barbara Holman, who read the entire manuscript and helped bring clarity to my thoughts. And to Dr. Richard Sutcliffe who provided critical review, enthusiasm, support, and much needed encouragement during the final stages of preparation.

It is with fondness that I remember my father, Jerry Walker. It was through him that I learned to be inquisitive, perseverant, and to never accept obstructions or limitations. These have been the attributes that have brought me to this point, and will serve me both with frustration and elation in the future.

I wish also to thank my mother, Linda Walker, as well as, Patrica and David Holman, who continually supported me, and helped me throughout the years.

Lastly, but by no means least, to my wife, Cheri, I extend my love and appreciation. Without her support, patience, assistance, and encouragement, none of this would have been possible.

TABLE OF CONTENTS

LIST OF PHOTOGRAPHIC PLATES

LIST OF TABLES

LIST OF FIGURES

LIST OF APPENDICES

CHAPTER 1

INTRODUCTION

1.1 Lamproite

Lamproites are low CaO, Al_2O_3, and Na_2O, and high K_2O/Al_2O_3 and Mg/(Mg+Fe) (Mg number) ultrapotassic rocks which commonly occur as diatremes, sills, and dykes (Foley et al. 1987; Bergman 1987; Mitchell and Bergman 1991). The diagnostic minerals of lamproites are: titanium-fluorine-rich phlogopite; titanium-rich, aluminum-chromium-poor diopside; titanium-rich, aluminum-poor potassium richterite[1]; priderite[2]; and wadeite[3] (Barton 1979; Jaques et al. 1984a; 1984b; Scott-Smith and Skinner 1984b; Mitchell 1985; Bergman 1987). The lamproites with greater than 10 percent modal abundance of olivine, higher Mg number, Ni, and Cr values, and lower SiO_2, K_2O, and TiO_2 values are called olivine lamproites (Scott-Smith and Skinner 1984a; Jaques et al. 1984a). Olivine lamproites have been documented to occur in Argyle and West Kimberley, Western Australia (Jaques et al. 1984; Atkinson et al. 1984); Prairie Creek, Arkansas, United States (Scott-Smith and Skinner 1984a); Woodson County, Kansas, United States (Cullers et al. 1985) and Kapamba, Zambia, Africa (Skinner et al. 1989). Each of these olivine lamproite occurrences, with the exception of Woodson County, has associated diamonds.

The recognition in the early 1980's of olivine lamproite as an important source for diamonds prompted an interest in the petrogenesis of the lamproites.

1 Potassium richterite $(K,Na,Ca)_3(Mg,Fe)_5Si_8O_{22}(OH)_2$
2 Priderite $(K,Ba)(Ti,Fe)_8O_{16}$
3 Wadeite $K_4Zr_2Si_6O_{18}$

Petrogenetic studies (Jaques et al. 1984a, 1986, 1989a, 1989b; Scott-Smith and Skinner 1984a; Atkinson et al. 1984; Scott-Smith et al. 1989), including high-pressure, high-temperature suprasolidus experiments on a synthetic Western Australian olivine lamproite composition (Foley 1989), have suggested that olivine lamproites may represent the partial melt composition of a mica-harzburgite at pressures between 45 and 55 kilobars (kb). The partial melting has been considered to occur in reduced oxygen fugacity conditions where H_2O, CH_4, and F are the dominant volatile species. Petrogenetic studies have also suggested that olivine lamproites are differentiated magma compositions, and that they may be derived from complex high-pressure and high-temperature differentiation of a more siliceous and Fe-rich phlogopite lamproite parental magma (Mitchell 1985; Mitchell and Bergman 1991).

1.2 Previous Work on the Prairie Creek Olivine Lamproite.

The Prairie Creek olivine lamproite is located within the Crater of Diamonds State Park, approximately 4 km south, south-east of Murfreesboro, Arkansas (Figure 1). In 1842, W. B. Powell reported the occurrence of an ultramafic rock which is now identified to be the Prairie Creek olivine lamproite intrusion (cited by Miser and Ross 1923). Diamonds were mined from the intrusion between 1911 and 1921 (Miser and Ross 1923). In 1922, the State of Arkansas designated the area as a State Park, thus restricting mining activity. As a result, the diamond potential of Prairie Creek has not been fully evaluated.

A total of five separate lamproite intrusions have been outlined in the Murfreesboro area (Figure 2). The Prairie Creek intrusion, which is the focus of the current study, and the Twin Knobs #1 intrusion, were classified as olivine

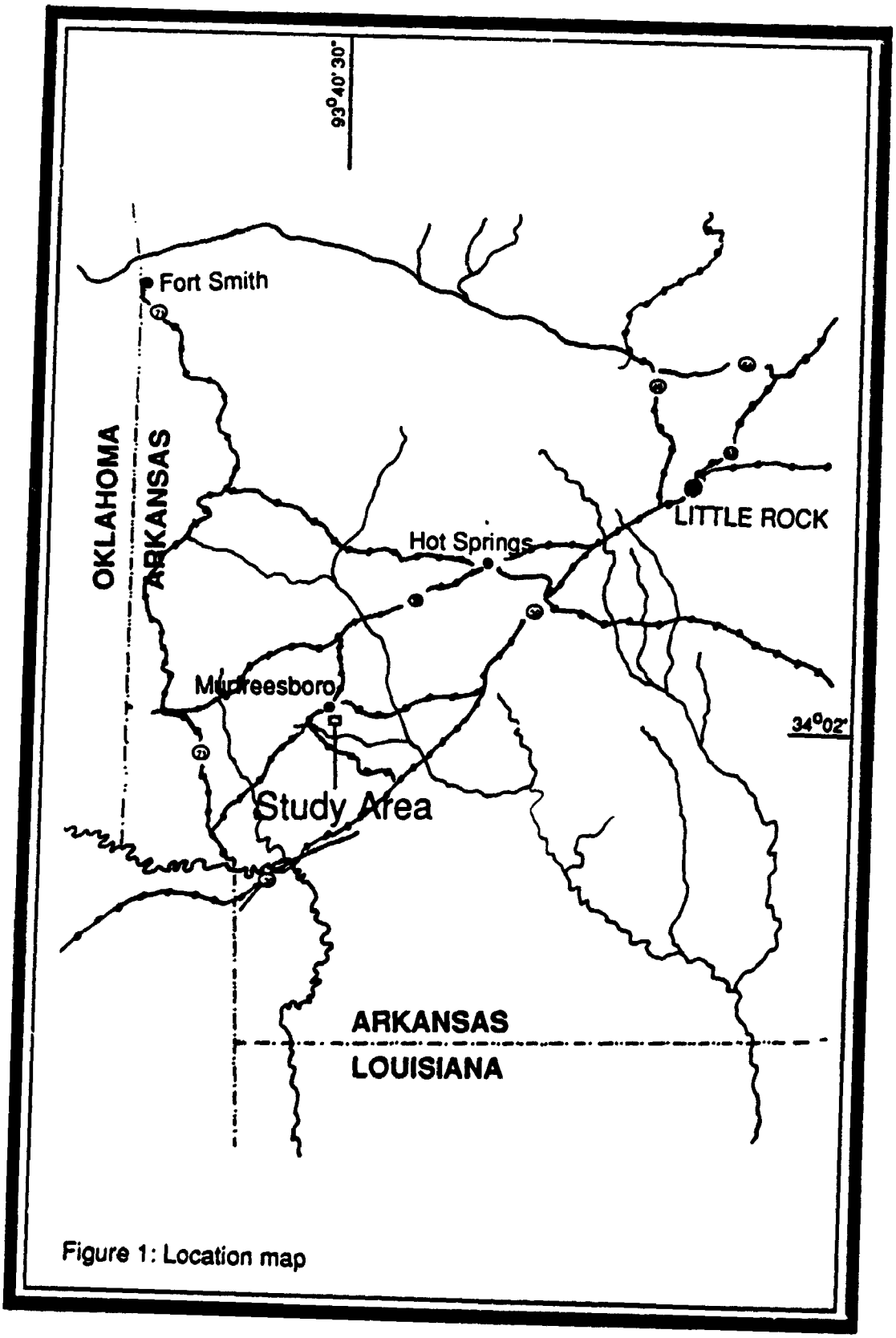

Figure 1: Location map

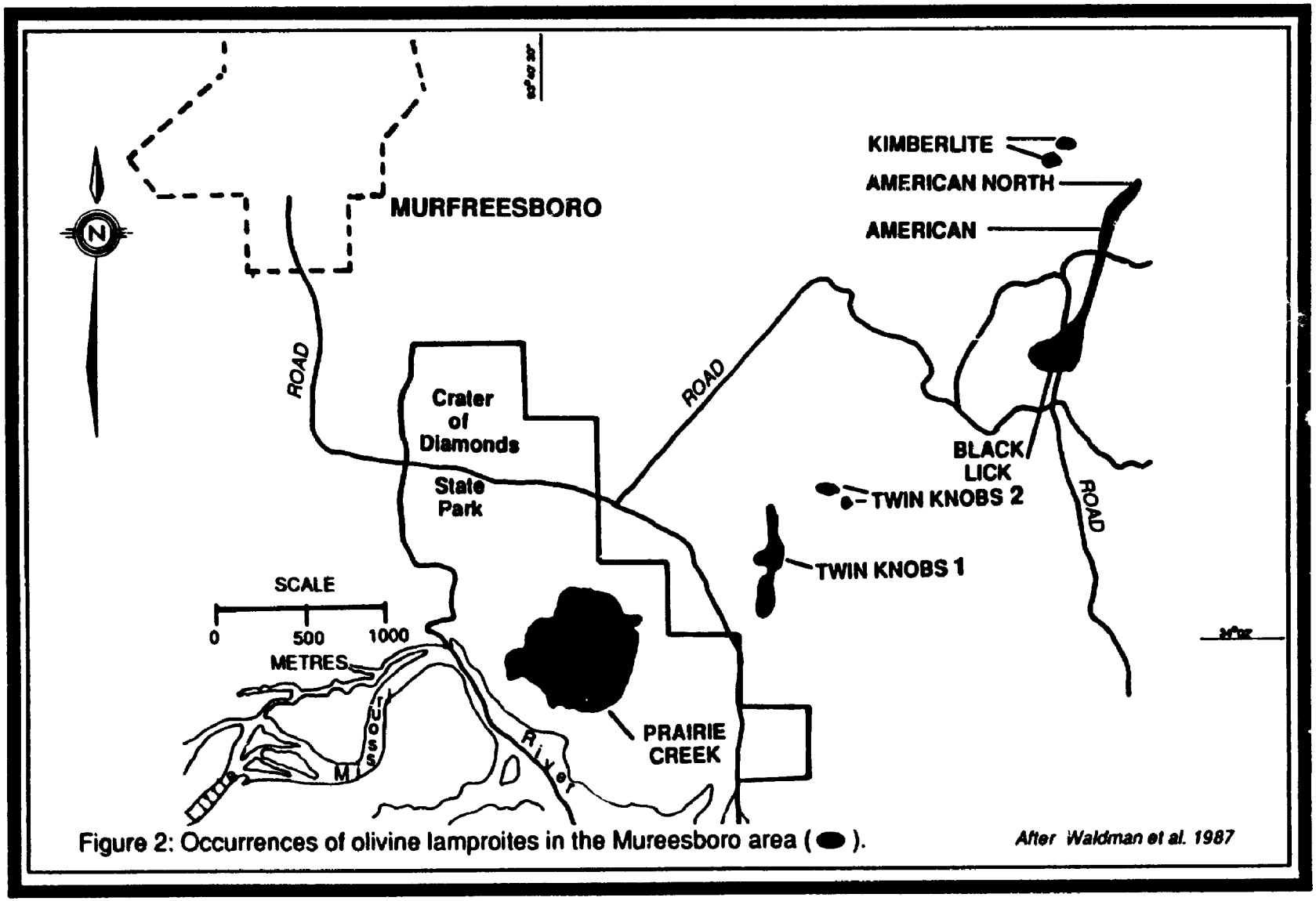

Figure 2: Occurrences of olivine lamproites in the Mureesboro area (●).

After Waldman et al. 1987

lamproites (Scott-Smith and Skinner 1984a; Waldman et al. 1987). The remaining three intrusions - the Kimberlite, the American/Black Lick, and the Twin Knobs #2 intrusions - have been described as having olivine lamproite affinities (Scott-Smith and Skinner 1984c; Waldman et al. 1987). Diamonds are hosted in every lamproite intrusion in the Murfreesboro area, except the Twin Knobs # 2 (Miser and Ross 1923; Waldman et al. 1987).

Branner and Brackett (1889) were the first to identify the Prairie Creek intrusion. Detailed petrographic studies were subsequently made by Miser and Ross (1923), and Scott-Smith and Skinner (1984a). These two studies outlined three rock facies within the Prairie Creek intrusion: tuff, breccia, and hypabyssal (HYP) facies. Petrographic and geochemical studies by Gogineni et al. in 1978, classified the Prairie Creek intrusion as a micaceous kimberlite. Scott-Smith and Skinner (1984a) reclassified the intrusion as an olivine lamproite, and suggested that the Prairie Creek olivine lamproite could be a transitional composition between the kimberlite and lamproite groups of rocks. Other works include: petrographic and geochemical studies by Steele and Wagner (1979); geophysical and isotopic work by Bolivar and Brookins (1979); petrographic descriptions of lamproitic cognate xenoliths within the HYP facies by Mitchell and Lewis (1983); and descriptive observations of cavities within the diamonds that occur in the breccia by Giardini and Melton (1975).

1.3 Purpose and Scope

The main objectives of the present study are:

1/ to determine the suprasolidus mineral phase relations and the possible source rock of the Prairie Creek HYP olivine lamproite using a piston cylinder apparatus at pressures between 10 and 40 kb and temperatures between 1000°C and 1500°C;

2/ to develop an integrated petrogenetic model which explains: a) the mineral phase relations and mineral chemistry of the the tuff, breccia and HYP facies of the Prairie Creek olivine lamproite; b) the mineral chemistry and phase relations of the cognate xenoliths; and c) the high-pressure and high-temperature suprasolidus experiments of the HYP facies;

3/ to evaluate the role of water and fluorine during the genesis of the Prairie Creek olivine lamproite from strictly an orthomagmatic point view;

4/ to compare and contrast the Prairie Creek olivine lamproite mineral phase relations and chemistry to the Zambia (Skinner et al. 1989) and Western Australian olivine lamproite and phlogopite lamproite petrogenetic model (Jaques et al. 1984a, 1986, 1989; Foley 1989; Mitchell and Bergman 1991).

CHAPTER 2

GEOLOGY, STRUCTURE, AND PETROGRAPHY

2.1 Geology and Structure

The Prairie Creek olivine lamproite intrusion is one of five lamproite intrusions located within the American Gulf Coastal Plain, south of the Ouachita fold belt. (Steele and Wagner 1979). The Ouachita fold belt consists of Late Pennsylvanian to Permian platform sediments which have been intensely folded and thrusted during the Ouachita orogeny. The southern margin of the Ouachita fold belt is unconformably overlain by the Gulf Coastal Plain (Nelson et al. 1982), which is comprised of gently south-dipping, Carboniferous and Cretaceous shales, and sandstones (Miser and Ross 1923).

The five lamproite intrusions in the Murfreesboro, Arkansas area (Figure 2), have erupted through, and been emplaced within, the Gulf Coastal Plain sediments. The intrusions are distributed along a north to north-easterly oriented trend. This trend parallels the Mississippi embayment rift system (Waldman et al. 1987), which has been active since the early Paleozoic. Extensional events along the rift system have occurred during the Cambrian, Carboniferous and late Mesozoic (Kane et al. 1981). The location of the lamproite intrusions has also been statistically correlated with a 90% confidence to hot spot activity by reconstructing post-Triassic plate motion of the North American continental plate (Crough et al. 1980). The age of the Prairie Creek tuff has been determined by K-Ar dating, using phlogopite separates, as 106 ± 3 million years (Gogineni et al. 1978).

The Prairie Creek intrusion is a diatreme facies lamproite, with a cylindrical surface expression (Figure 3) and a typical lamproite "champagne glass-like" cross section (Figure 4, after Bolivar and Steele 1979; Bergman 1987). The surface occurrence of the tuff, breccia and HYP facies are illustrated in Figure 3 (from Miser and Ross 1923).

2.2 Petrography of the Prairie Creek Intrusion

The petrography of the tuff, breccia and HYP facies of the Prairie Creek intrusion is based primarily on the descriptions by Miser and Ross (1923), and Scott-Smith and Skinner (1984a). These descriptions are augmented in the present work by the descriptive analysis of hand specimens and thin sections of 75 samples selected from the three facies of the Prairie Creek intrusion. The samples were collected by Makoto Arima and Reidar Trønnes in 1984.

2.2.1 Tuff facies

The tuff is the most altered and has the most varied texture of the three facies of rock. It is distinguished from the other facies by its blue-gray color, the presence of secondary chlorite, and abundance of quartz derived from the surrounding host sandstones. In addition to the chlorite and quartz, the tuff contains completely serpentinized inclusion-free olivine, variable amounts of small lath-like phlogopite phenocrysts (Plate 1), rounded apatite-filled vesicles and numerous shale and sandstone xenoliths. The serpentinized olivine occurs as either large anhedral or small euhedral grains. The phlogopite phenocrysts contain a distinct inclusion-free mantling of slightly darker red-

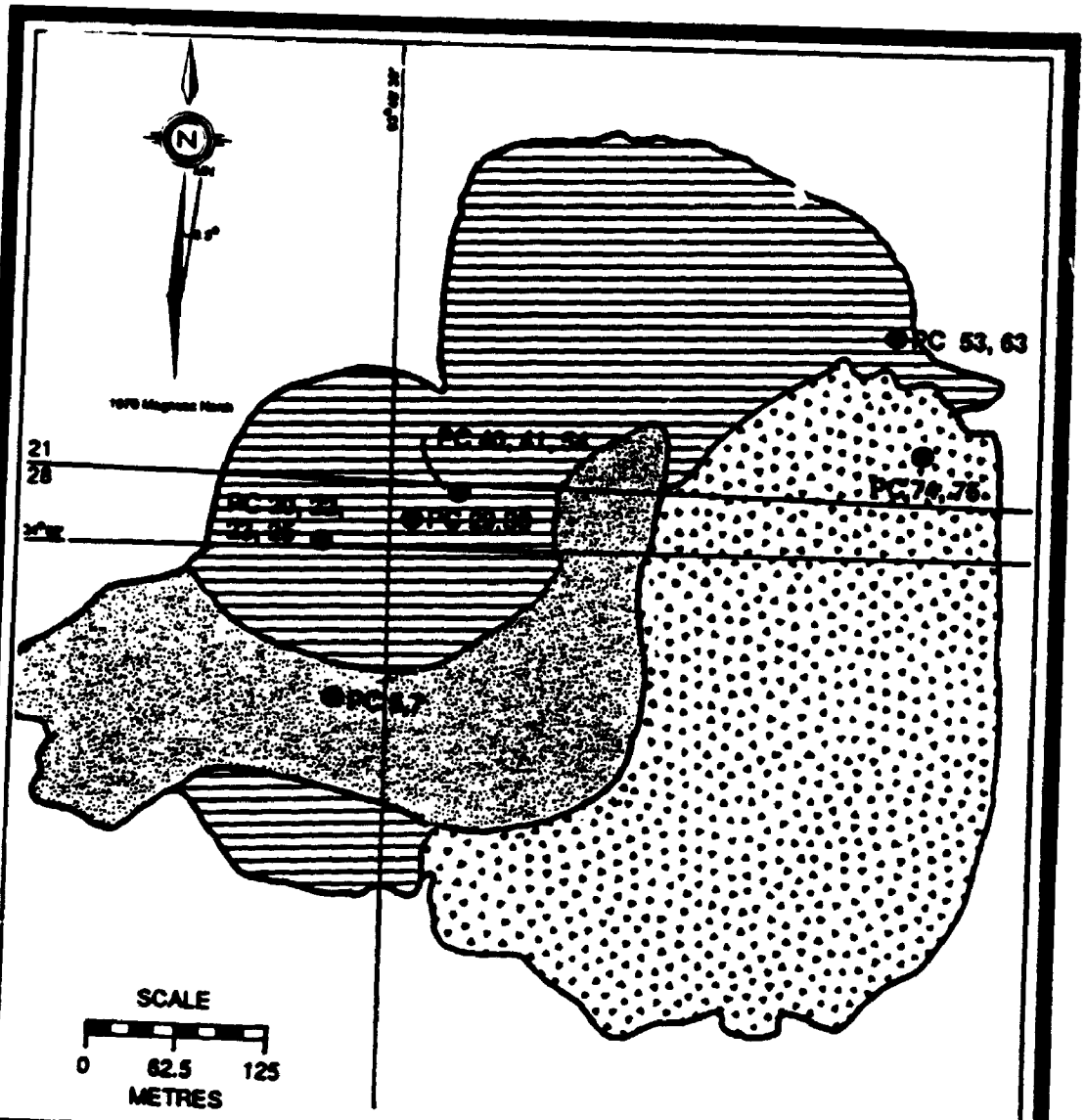

After Miser and Ross 1923

KEY

PRAIRIE CREEK INTRUSION

hypabyssal facies

tuff facies

breccia facies

sample location

Figure 3: Geology and sample location of the Praire Creek Intrusion

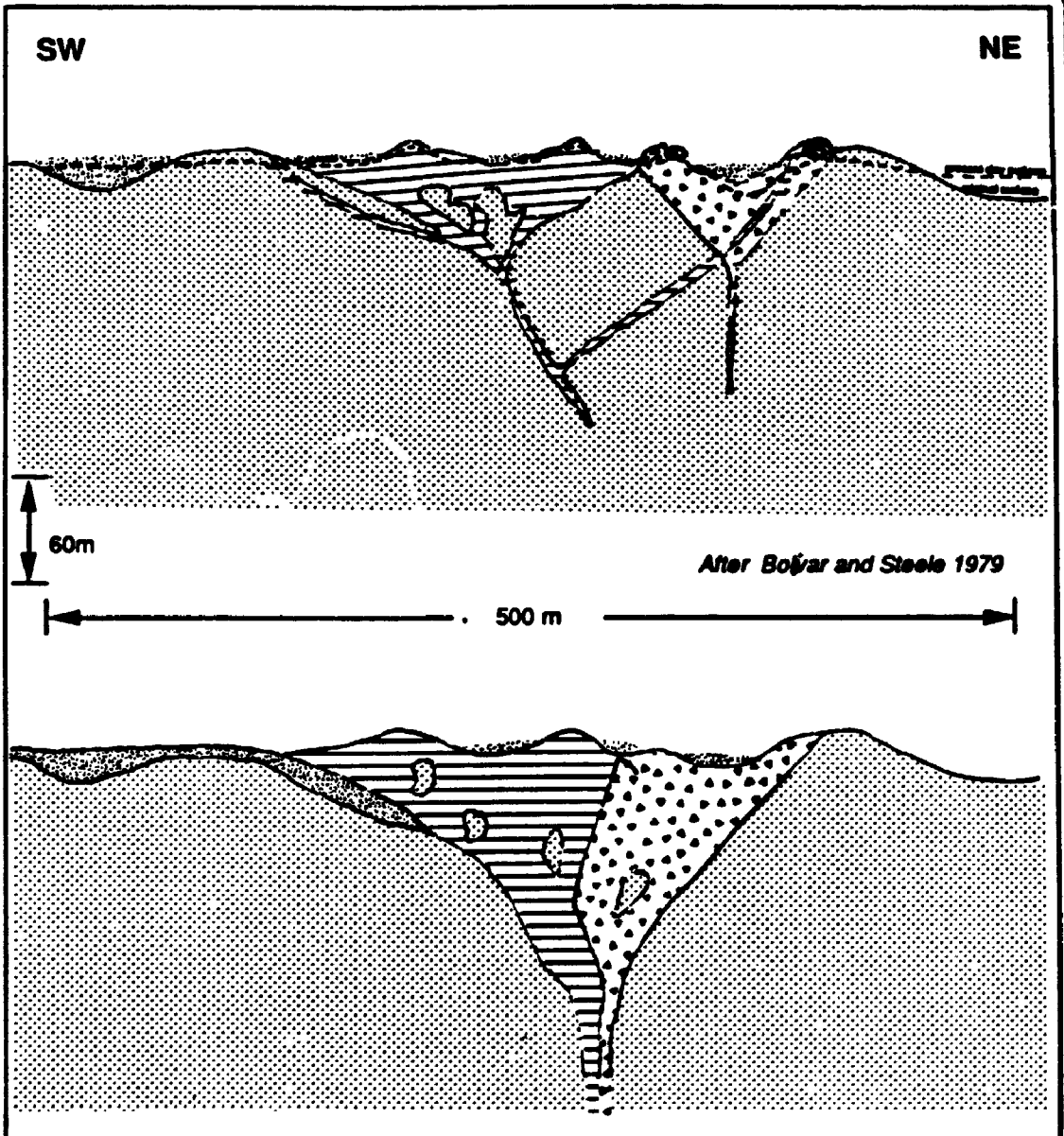

Figure 4: Hypothetical cross section of the Praire Creek Intrusion

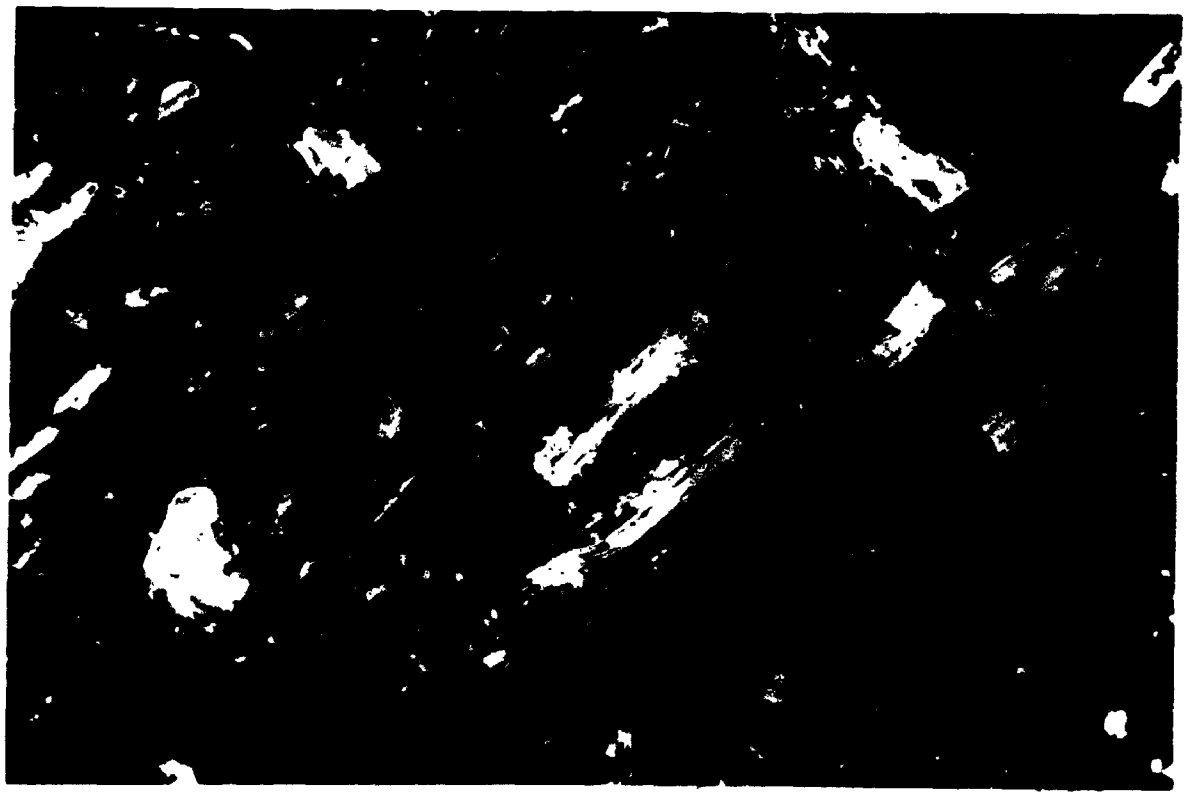

Plate 1: Photomicrograph of the phlogopite-rich tuff facies. Inclusion-free phenocrystic phlogopite and a groundmass of serpentine, illite and chalcedony. Field of view is 4 mm; cross-polarized light.

brown, pleochroic phlogopite, and are occasionally broken along the cleavage planes. The olivine and phlogopite phenocrysts have an antipathetic relationship. As a result, the tuff is categorized into phlogopite-rich, olivine-poor; and phlogopite-poor, olivine-rich sub-groups. In their study, Scott-Smith and Skinner (1984a) observed the phlogopite-rich olivine-poor sub-group to be the most abundant of the two categories.

2.2.2 Breccia facies

In hand specimen the breccia is brown to buff in color and variable in texture. It is sub-divided into two groups: a clast-supported lapilli; and a matrix-supported lapilli (Scott-Smith and Skinner 1984a). The matrix-supported lapilli consist of fragmented components of the breccia lapilli and quartz. This matrix is very similar to the tuff facies, except for the absence of chlorite, and the abundance of phlogopite and quartz. The breccia is dominated by serpentinized inclusion-free olivine, rare lath-like phlogopite phenocrysts, and numerous vesicles, in what appears to be serpentinized glass (Plate 2). The serpentinized olivine occurs as either large anhedral or small euhedral grains. The large anhedral grains have a serrate boundary. An interesting characteristic of the breccia is the rare occurrence of lapilli that are entirely made up of small lath-like phlogopite and devitrified glass (Plate 3). Although it was not observed in this study, Scott-Smith and Skinner (1984a) reported the rare occurrence of serpentinized olivine inclusions in these lapilli. Xenoliths of shale and sandstone are also present within the breccia facies.

Plate 2: Photomicrograph of the breccia facies of rock. The photograph consists mostly of serpentinized large anhedral and small euhedral olivine hosted in a fine grained groundmass. A single lath of phenocrystic phlogopite is located at the center of the photo. Field of view is 4 mm; cross-polarized light.

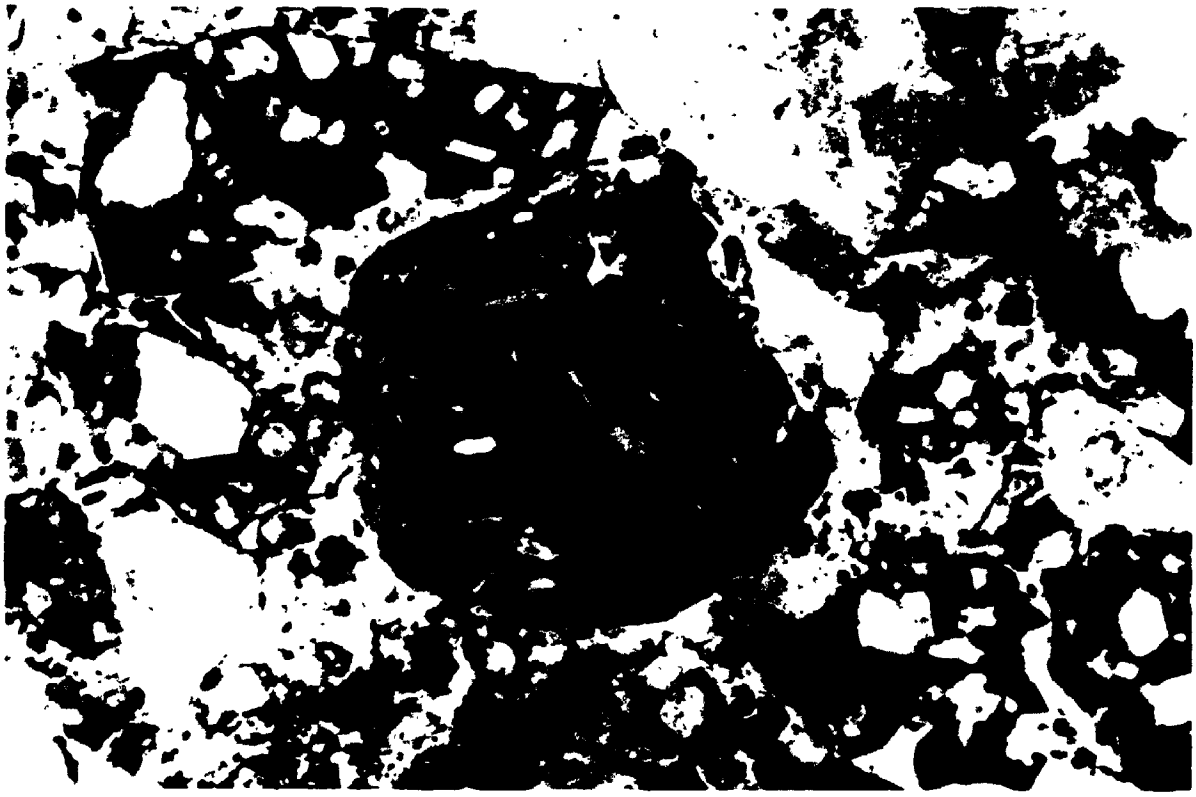

Plate 3: Photomicrograph of rare phlogopite + glass lapilli hosted within the breccia facies of rock. Field of view is 4 mm; plain light.

2.2.3 Hypabyssal (HYP) facies

The HYP facies of the Prairie Creek intrusion is a massive, black, porphyritic facies that is much less altered and contains fewer shale and sandstone xenoliths than the pyroclastic facies. The HYP facies, like the tuff and breccia, is characterized by two sizes of inclusion-free olivine. The large olivine crystals, which make up to 22 modal % of this rock, are subhedral to anhedral, and greater than 1 mm in size. They have serrate outlines (Plate 4), and occasionally exhibit undulose extinction. The smaller olivine crystals (Plate 5) make up 17 modal % of the rock, are euhedral, less than 1 mm in size, and do not have serrate outlines. All the olivine crystals are serpentinized around the edges, and some of the smaller grains are completely serpentinized.

Although there is no clinopyroxene in the tuff and breccia, it is present in amounts of up to 21 modal % in the HYP facies. It occurs as euhedral microphenocrysts, and occurs in the same proportion both in the devitrified glass and in the poikilitic phlogopite. Some clinopyroxene prisms are randomly oriented, and others are preferentially oriented in a flow-like arrangement around the large and small olivine crystals. Both orientations are displayed in the devitrified glass and in the poikilitic phlogopite (Plate 6).

The phlogopite in the HYP facies has textural differences to the phlogopite in the tuff and breccia. In the HYP facies, the phlogopite occurs as unzoned, rounded, anhedral, poikilitic masses. These masses are often found at the margins of the large olivine crystals, preserving a pristine serrate olivine grain boundary (Plate 4). The poikilitic phlogopites contain olivine,

Plate 4: Poikilitic phlogopite in contact with a large anhedral olivine grain (LAO) with a serrate grain boundary. Field of view is 16 mm; cross-polarized light.

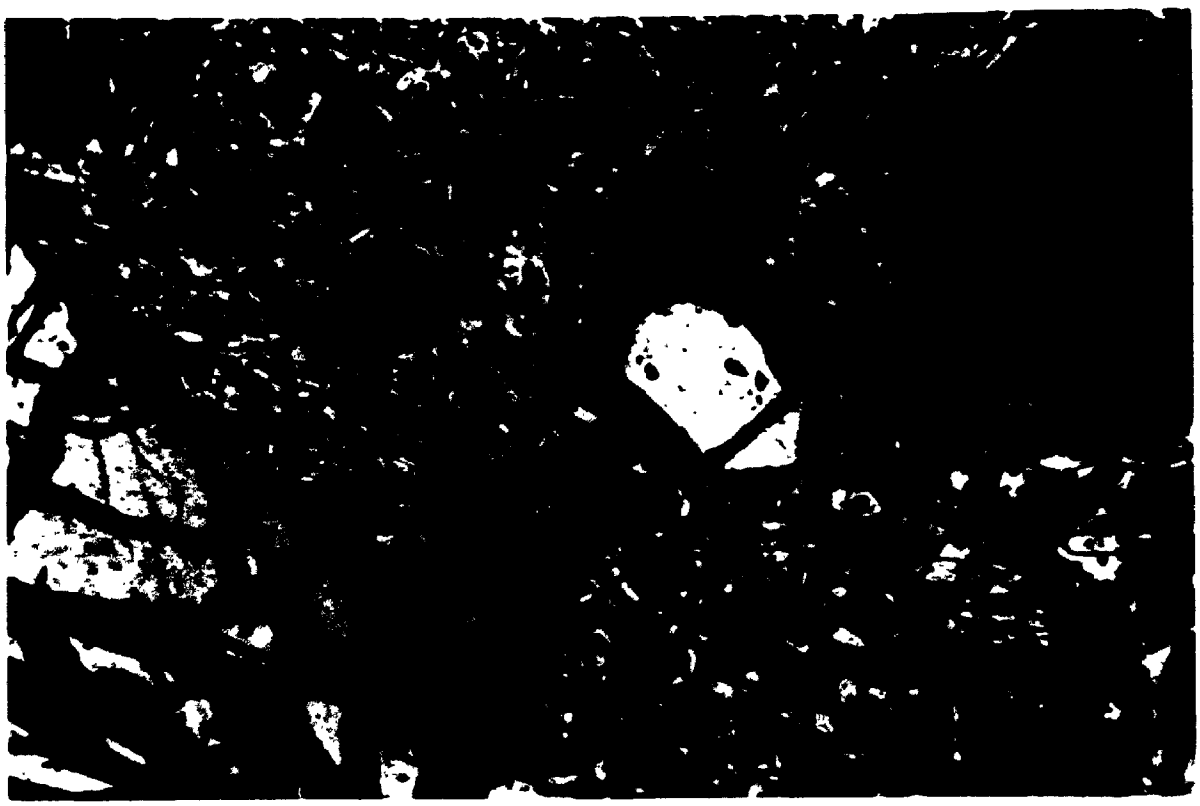

Plate 5: Photomicrograph of a small euhedral olivine phenocryst (SEO) an inclusion within the poikilitic phlogopite of the hypabyssal facies. Field of view is 4 mm; cross-polarized light.

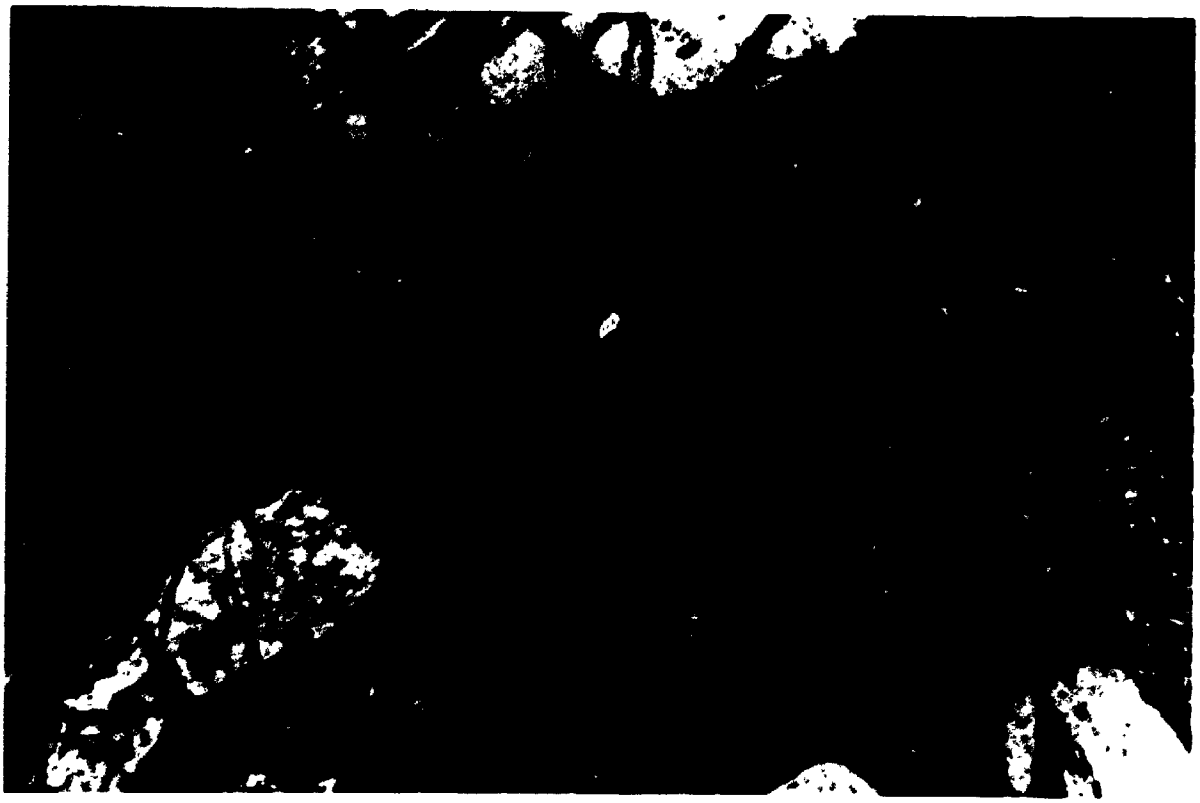

Plate 6: Photomicrograph of aligned clinopyroxene around small and large olivine grains in poikilitic phlogopite of the hypabyssal facies. Field of view is 4 mm; cross-polarized light.

clinopyroxene, perovskite, chrome spinel, and apatite as inclusions. Also occurring in the phlogopite are rounded to oblong-shaped inclusions, which may represent either magma or gas bubbles that were trapped during the time of phlogopite crystallization, and subsequently replaced by secondary minerals.

The remaining minerals in the HYP facies are: Ti-K richterite; perovskite; spinel; apatite; wadeite; priderite; an unidentified inclusion in clinopyroxene; and devitrified glass. Their petrographic characteristics are more straightforward, and are outlined in Table 1.

2.3 Petrography of the Prairie Creek Xenoliths

The HYP facies of the Prairie Creek intrusion hosts a limited number of "diopside-richterite" (Mitchell and Lewis 1983; Mitchell and Bergman 1991) "phlogopite-bearing", dunite and wehrlite xenoliths. Based on mineral chemistry (Chapter 5), both the diopside-richterite and phlogopite-bearing types are considered to be cognate xenoliths, and the dunite and wehrlite xenoliths are not considered to be cognate. They range in size from 2 mm to 2 cm, and have varying mineralogies.

2.3.1 Diopside-Richterite Cognate Xenoliths (DRX)

Of the 14 cognate xenoliths studied from the HYP facies, 11 are diopside-richterite cognate xenoliths (DRX). They were first described by Mitchell and Lewis in 1983. The present study reveals that although all 11 share similar characteristics to those described by Mitchell and Lewis (1983), they are

Table 1: Summary of the petrography of the minerals present in the Prairie Creek hypabyssal facies.

Mineral	Habit	Modal%	Size	Associations and Occurrences
Olivine serrate	anhedral to euhedral	39	50μm to 4mm	Occurs as large anhedral grains with a serrate boundary and small euhedral grains without a boundary. Anhedral grains are much larger than the euhedral grains.
Clinopyroxene inclusions of	euhedral	21	15μm	Discrete euhedral laths. Sometimes aligned parallel to olivine grain boundaries. Hosts perovskite, spinel and apatite.
Phlogopite apatite	anhedral	2	<4mm	Irregular poikilitic masses with inclusions of olivine, clinopyroxene, perovskite, spinel and
Ti-K Richterite	anhedral to subhedral	<1	<50μm	Euhedral minute grains or sub-poikilitic masses along poikilitic phlogopite grain boundaries. Clinopyroxene and perovskite occur as inclusions in the sub-poikilitic grains.
Perovskite	subhedral to euhedral	6	5 to 10μm	Discrete grains distributed randomly throughout the devitrified glass and within the poikilitic phlogopite.
Spinel poikilitic	subhedral to euhedral	3	5 to15μm	Discrete grains distributed randomly throughout the devitrified glass, and as inclusions in phlogopite, clinopyroxene, and wadeite. Has a narrow <10μm mantling.
Apatite along the	anhedral	<0.5	<10μm	Occurs within devitrified glass or as inclusions in clinopyroxene and wadeite. Also present cleavage planes of phlogopite.
Wadeite	anhedral	<0.5	150μm	Poikilitic with high birefringence. Has inclusions of chrome spinel, perovskite, and apatite.
Priderite	subhedral	<0.5	<75μm	Occurs as columnar, reddish-brown mineral aggregates.
Inclusion in properties. Clinopyroxene	anhedral	<0.5	<5μm	Rounded to angular inclusions within clinopyroxene. Unable to determine any optical
Devitrified glass Glass	anhedral	27	<2μm	Completely devitrified glass, representing a combination of serpentine and illite. Amount of easily recognized under plain light.

usefully subdivided into three different types, differentiated on the basis of the xenolith shape and mineralogy (discussed in this section) and mineral chemistry (discussed in Chapter 5).

The cognate xenolith type Mitchell and Lewis (1983) described is referred to in the present study as "round" DRX. The two additional types will be referred to as "columnar" and "lenticular". The round and columnar DRX consist of 15 to 35 μm subhedral Ti-K richterite, diopside and priderite grains. The diopside and Ti-K richterite crystals found within the xenoliths are larger than those found in the surrounding corona and the host HYP facies, and they appear to have grown inward from the margin of the xenolith (Plate 7). The lenticular DRX are distinguished from the round and columnar DRX not only by their shape, but also by the presence of phlogopite and a shcherbakovite-like mineral, and an absence of Ti-K richterite. One of the round DRX observed differs from the others by having abundant pyrite.

The DRX typically contain approximately 20 modal % combined diopside, Ti-K richterite and priderite. The remaining 80 % consists of two types of secondary alteration. The first type, which represents approximately 40 % of the alteration, is associated with the pseudomorphing of Ti-K richterite. The second type, which represents up to 60 % of the alteration, does not appear to be a pseudomorph of a primary mineral.

Each of the DRX are surrounded by a corona consisting of three rims (Plate 8). The innermost rim, which encompasses the xenolith, is one mm wide, composed of diopside, and will be referred to throughout the study as corona rim 1 (CR1). The intermediate rim is one to two mm wide, composed of

Plate 7: Photomicrograph of five diopside minerals within the diopside-richterite cognate xenolith. These minerals are aligned perpendicular to the contact of the cognate xenolith with the corona rim 1. The cognate xenolith is located at the top of the photo. Field of view is 4 mm; cross-polarized light.

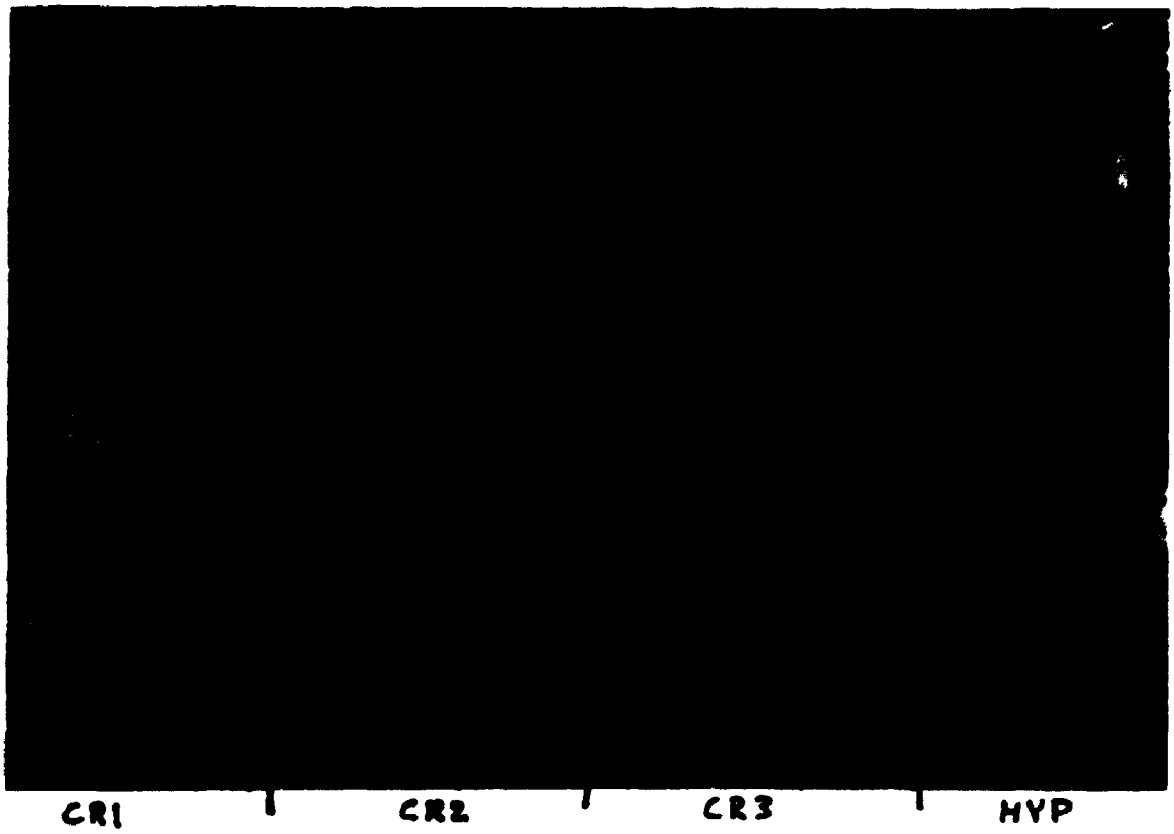

Plate 8: Photomicrograph of the corona around the diopside-richterite cognate xenoliths. The cognate xenolith occurs on the left side of the photo, corona rim 1, 2, and 3, from left to right are in the middle, and HYP facies occurs on the far right side. Field of view is 4 mm; cross-polarized light.

diopside, phlogopite, and Ti-K richterite, and will be referred to as corona rim 2 (CR2). The outermost rim is up to four mm wide, composed of typical Prairie Creek olivine lamproite HYP facies which lacks perovskite, and will be referred to as corona rim 3 (CR3). There is a sharp contact between the DRX and CR1, and a gradational contact between CR2 and CR3, and between CR3 and the host HYP facies. The clinopyroxene in each of the three coronas, host minute inclusions identical to the inclusions found in the microphenocryst clinopyroxene from the HYP facies.

2.3.2 Phlogopite-bearing Cognate Xenoliths (PBX)

Three of the fourteen cognate xenoliths studied from the Prairie Creek olivine lamproite HYP facies are phlogopite-bearing cognate xenoliths (PBX). They are distinguished from the DRX by their abundance of phlogopite, and their absence of Ti-K richterite, priderite, and a clinopyroxene - dominated corona. They also have a greater variability in texture and secondary alteration.

The PBX typically consist of subhedral poikilitic phlogopite plates which make up 15 to 75 percent of the xenolith. The phlogopite plates are dominated by inclusions and are often broken along their cleavage planes (Plate 9). The inclusions vary in type and abundance. The inclusions are: a trapped liquid or gas vesicles similar to the inclusions in the poikilitic phlogopite from the HYP facies; and inclusions similar to the unidentified inclusions in the clinopyroxene from the HYP facies. The groundmass within the xenolith is completely altered; in some areas of the xenolith, it appears to be pseudomorphing a primary phase.

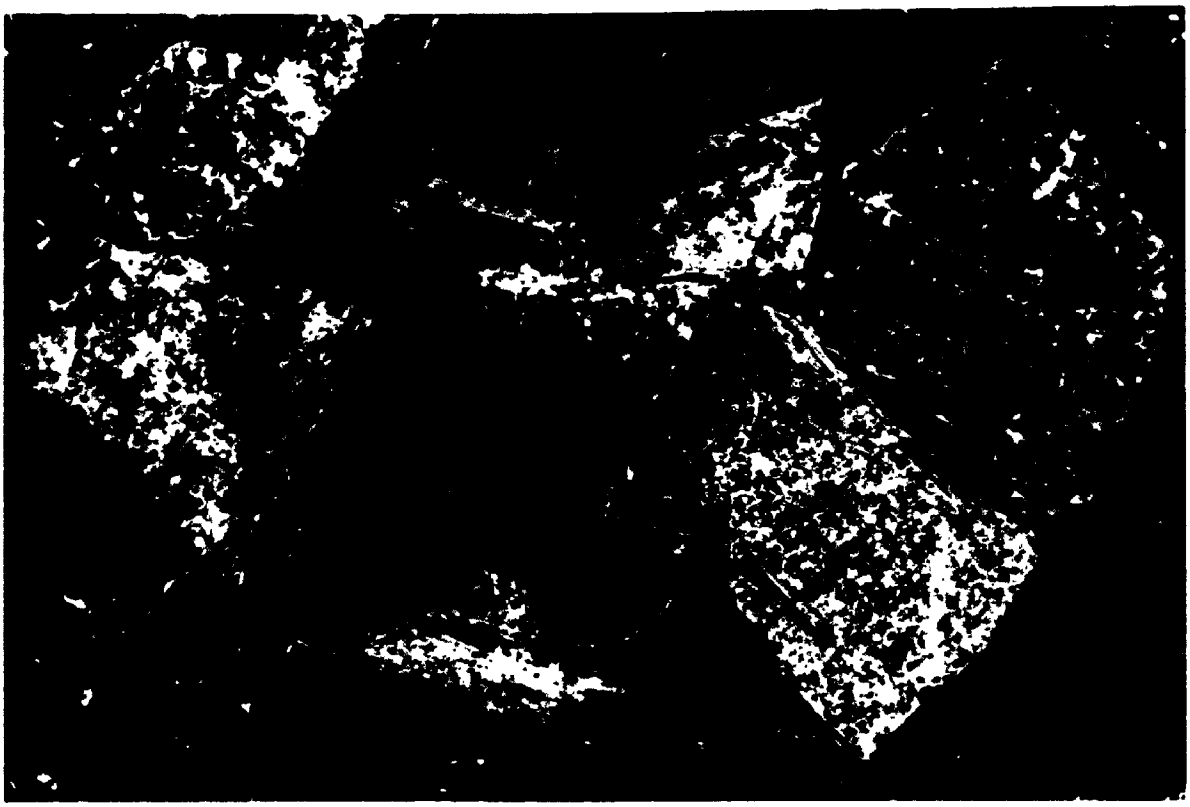

Plate 9: Photomicrograph of a phlogopite-bearing cognate xenolith. The inclusions in the phlogopite may be trapped devitrified glass. Between the phlogopite grains are secondary minerals which consist mainly of serpentine and illite. Field of view is 4 mm; cross-polarized light.

The contact of the PBX with the host HYP facies is characterized by a 10 µm wide complex zone consisting of poikilitic phlogopite, perovskite, spinel, and minor clinopyroxene, associated with what appears to be either devitrified glass or gas vesicles filled with secondary minerals. The composition of the secondary minerals and their physical characteristics are analogous to the altered glass trapped within both the phlogopite in the xenolith and the poikilitic phlogopite in the HYP facies. Microphenocrysts of clinopyroxene within the HYP facies are often aligned parallel to the contact with the phlogopite-bearing cognate xenolith.

2.3.3 Other Xenoliths

Dunite and wehrlite xenoliths less than 5 mm in diameter occur within the HYP facies. The dunite is made up of irregular shaped, rounded olivine aggregates, which are serpentinized around the grain boundaries. The wehrlite xenoliths consist mainly of olivine, and round to oblong clinopyroxene. The outer margins of the olivine crystals in the wehrlite xenoliths are also serpentinized.

2.4 Paragenetic Sequence

The five different rock types of the Prairie Creek intrusion can be divided into two different paragenetic sequences. Tuff and breccia facies of rock and PBX, are characterized by the occurrence of phlogopite phenocrysts crystallizing before or without clinopyroxene, whereas, the HYP facies of rock and the DRX, phlogopite occurs as poikilitic grains crystallizing after clinopyroxene. In the case of the HYP rock, the paragenetic sequence of LAO crystallization, development of a serrate boundary around the LAO, and the

crystallization of the SEO, is identical to that in the tuff and breccia facies of rock. The primary difference between the three facies of rock, is the crystallization of spinel, perovskite, apatite and clinopyroxene before phlogopite in the hypabyssal rock.

CHAPTER 3

EXPERIMENTAL AND ANALYTICAL METHODS

3.1 Starting Material

Previous work on lamproites has suggested that the change from high Mg number (approximately 85) and low SiO_2 (approximately 40 wt. %) to low Mg number (approximately 70) and high SiO_2 (approximately 50 wt. %) within the lamproite group of rocks is a result of the derivation of primitive lamproitic magmas from the partial melting of a mica-harzburgite at successively lower pressures (Jaques et al. 1984a; Foley 1989). Based on this model, the high Mg number and low SiO_2 of olivine lamproites is indicative of a primitive lamproite magma derived from the highest pressure of partial melting of a mica harzburgite. As a result, the Prairie Creek olivine lamproite was investigated to determine its suitability for suprasolidus experiments.

Petrographic analysis of the three facies of the Prairie Creek intrusion, demonstrated that the HYP facies was the least contaminated by xenolithic material. Four of the most pristine rock samples were chosen for whole rock analyses (Table 2) in order to try and select a representative HYP facies composition. The absence of a significant chemical variation between the four samples was considered to indicate that each was equally representative of the HYP magma. Of the four samples, PC-30 was selected as the composition for suprasolidus experiments due to its limited amount of olivine serpentinization relative to the other three samples.

Table 2. Chemical composition of the Prairie Creek olivine lamproite, and olivine lamproites from Ellendale, and Argyle, Western Australia.

	PC-30	PC-29	PC-41	PC-45	El	Ak
SiO_2	39.50	39.10	39.20	39.40	41.50	40.98
TiO_2	2.40	2.35	2.34	2.35	2.68	2.65
Al_2O_3	3.67	3.69	3.60	3.63	3.54	4.38
Cr_2O_3	0.23	0.22	0.23	0.23	0.18	0.17
Fe_2O_3	4.16	8.27*	8.35*	8.43*	4.57	3.40
FeO	4.13	nd	nd	nd	3.90	4.27
MnO	0.14	0.14	0.13	0.13	0.13	0.10
MgO	27.70	26.70	27.40	27.70	26.90	22.93
CaO	4.74	4.64	4.63	4.67	4.38	5.71
K_2O	2.91	3.65	3.43	3.43	4.10	4.26
Na_2O	0.34	0.36	0.41	0.37	0.36	0.09
BaO	0.29	0.37	0.29	0.29	1.10	0.09
NiO	0.18	0.17	0.18	0.18	0.18	0.13
P_2O_5	0.34	0.47	0.44	0.45	0.62	0.88
H_2O^+	6.40	nd	nd	nd	4.13	5.69
H_2O^-	2.09	nd	nd	nd	1.60	0.86
CO_2	0.26	nd	nd	nd	0.19	2.40
F^-	0.17	0.18	0.18	0.18	0.20	0.35
Cl^-	0.01	0.02	0.03	0.03	0.50	nd
LOI	-	8.88	8.49	8.17	-	-
Total	99.66	99.21	99.33	99.64	100.76	99.34
Trace Elements ppm						
Rb	190	200	190	180	386	317
Sr	1150	1190	1150	1130	959	930
Y	20	20	20	10	16	16
Zr	630	650	620	660	564	575
Nb	90	90	90	100	118	182
Mg num.	86.7	86.5	86.7	86.7	85.7	84.8
K_2O"/Na_2O"	8.6	10.1	8.4	9.3	11.4	47.3
K_2O"/Al_2O_3"	0.8	1.0	1.0	1.0	1.2	1.0

PC-30, PC-29, PC-41 and PC-45 analyses of Prairie Creek from present study. * = Total Fe as Fe_2O_3. El = Ellendale, Western Australia olivine lamproite (Jaques et al. 1984a). Ak = Argyle, Western Australia olivine lamproite (Jaques et al. 1989a). nd = not determined. LOI = loss on ignition. Mg num. = Mg / ($Mg+Fe_{total}$) *100. " = weight percent.

The high Mg number, NiO and Cr_2O_3, and low SiO_2, of the HYP facies are consistent with mantle derivation. The Prairie Creek HYP facies is also similar to olivine lamproite compositions elsewhere in the world (Table 2). Owing to the absence of petrographic and mineral chemical data indicative of a differentiation, such as zoned or compositionally different olivine compositions, sample PC-30 was considered to be a primitive olivine lamproite composition. As a result, the HYP facies was considered representative of a olivine lamproite composition, and a greater than 200 mesh powder of sample PC-30 was prepared for suprasolidus experiments according to the procedure outlined in Appendix 1.

3.2 Experimental Procedure

3.2.1 Preparation Of Sample Charges

Approximately seven milligrams of the prepared sample of PC-30 was encapsulated; in $Ag_{50}Pd_{50}$ for experiments which were to be run at temperatures less than 1225°C, and in Fe soaked Pt capsules for experiments which were to be run at temperatures greater than 1225°C. Capsules were made from seven millimeter long tubes, with a one millimeter inside diameter. Before putting the sample in the capsule, one end was crimped and welded. After filling the capsule with approximately seven milligrams of PC-30, the open end was also crimped and welded. The completely sealed capsule was then formed to fit the appropriate specifications of the charge assembly for the piston cylinder apparatus. A detailed outline of the charge preparation and sample recovery is outlined in Appendix 2.

3.2.2 Apparatus and Experimental Technique

The capsules were placed in a 1.27 cm diameter piston cylinder apparatus (modified from Boyd and England 1960), with a talc-Pyrex glass single capsule assemblage. The pressure transmitting media in each of the experiments were talc and Pyrex glass. No correction was made for the loss of pressure due to friction. All experiments were completed using the "piston out" technique (Richardson et al. 1968). The pressure was calibrated using the kyanite-sillimanite transition at 22 kb and 1200°C (Richardson et al. 1968) and the albite = jadeite + quartz transition at 16.3 kb and 600°C (Johannes et al. 1971) to within an accuracy of ±0.5 kb. Temperature was maintained within ±5°C using a $Pt\text{-}Pt_{90}\ Rh_{10}$ thermocouple. No pressure correction was applied to the emf of the thermocouple. Each experiment ended with an isobaric quench to below 700°C within five seconds, and to room temperature in twenty seconds.

The oxygen fugacity of the capsule was not buffered. Based on the buffering capacity of the graphite furnace in the piston cylinder furnace assemblage, Brey and Green (1975) estimated the oxygen fugacity to be between Ni-NiO and Quartz-Fayalite-Magnetite. The estimated oxygen fugacity of the present study and its effects on the genesis of the Prairie Creek olivine lamproite are discussed in Chapter 6.

3.2.3 Loss of iron to the capsules

A common problem when using Pt as the capsule material is the loss of iron from the sample to the capsule during the experiment. The loss of Fe was reduced by using $Ag_{50}Pd_{50}$ capsules, short experimental run times (as low as 5 minutes), and by using Fe soaked Pt capsules. The method for soaking Pt in Fe was modified from Ford's (1978) procedure, and is outlined in Appendix 3. Although these precautions were undertaken, the loss of Fe to the Fe soaked Pt capsule was still evident. This is best illustrated in the "no added volatile" system at 10 kb where the Mg number of olivine increases by 1.7 when $Ag_{50}Pd_{50}$ is replaced by Fe soaked Pt capsules above 1225°C (Chapter 4). The specific effects caused by the loss of Fe to Pt, and by a lesser degree to the $Ag_{50}Pd_{50}$ capsules (Stern and Wyllie 1975; Ford 1978), were not determined. However, it can be assumed that the loss of Fe^{2+} to the capsule would decrease the Fe in the sample, increase the Mg number of the minerals and the liquid, cause a shift in the phase boundaries to higher temperatures (but not the relative stability of the minerals (Barton and Hamilton 1982)), and make the attainment of equilibrium difficult.

3.2.4 Addition of Volatiles

During the explosive emplacement of the Prairie Creek olivine lamproite, H_2O, CO_2 F and Cl may have degassed from the Prairie Creek HYP magma. The importance of the volatiles H_2O and F, during the partial melting of the lamproite source rock, and during the crystallization of the lamproite magma, has been demonstrated by Jaques et al. 1984a, Foley et al. 1986, and Foley 1989. In order to replace the loss of important volatiles, experiments were undertaken with the addition H_2O and F to sample PC-30.

In this study, three experimental systems with different volatile conditions were investigated. The first was the "no added volatile" system, which represented the volatiles in sample PC-30; 6.4 wt. % H_2O, 0.17 wt. % F, and 0.26 wt. % CO_2 (Table 2). The other two systems were based on the addition of H_2O ("water added"), and the addition of F ("fluorine added"). The amount of H_2O and F added to the experimental systems should ideally be equal to the amount lost during eruption, however, this amount can not be quantified. As a result, the addition of H_2O was based on an assumption that approximately half of the H_2O currently in PC-30 was lost during eruption. The addition of F was based on the F values of other olivine lamproites from Western Australia (Jaques et al. 1984), which are much higher than the F values in the Prairie Creek intrusion. As a result, H_2O was increased to 15 wt. % by the addition of 8.6 wt. % deionized water, and F was increased to 0.5 wt. % by the addition of a greater than 200 mesh 98 % pure lithium fluoride.

Retention of the volatiles within the experimental charge was tested after the completion of each run. The capsule was weighted then pierced with a sharpened rod. The pierced capsule was then dried at 110°C for 60 minutes and reweighed. If a weight loss was observed, the volatiles in the sample charge would be considered to have been retained during the experiment. If there was no weight loss, it was assumed that the capsule was not sealed and volatiles had escaped during the experiment. Unsuccessfully sealed charges were discarded.

During the experimental run, lithium fluoride in the "fluorine added" system is assumed to have broken down to Li and F. Lithium fluoride decomposes at 845°C, and the lowest temperature studied in the "fluorine added" system was 1000°C. The change in the temperature of the phase boundaries by up to a 100°C, and the higher F atoms per formula unit in phlogopites, with respect to the "no added volatile" experiments (Chapter 4 and 5), is considered to substantiate the breakdown of lithium fluoride and the increase of F during the "fluorine added" experimental procedure. The depolymerizing effect of Li on the silicate melt is considered negligible due to the high percentage of F in the lithium fluoride compound (73.2 wt. %), and the low weight percentage of lithium fluoride added to the sample charge.

Each of the experimental runs from the three experimental systems is considered to have been in vapor absent conditions, due to the absence of gas bubbles in the experimental run products.

3.3 Techniques for Identification of Experimental Run Products

The identification of run products were based on two procedures: 1/ optical observation in immersion oils; and 2/ electron microprobe analyses.

Optical identification with immersion oils enabled the determination of the minerals, and their habit and texture. This method provided only qualitative results for the identification of mineral phases.

The electron microprobe was used to quantitatively analyses of the minerals present in the experimental run products. In order to prepare the samples for mineral analysis, the run products were embedded in epoxy on a glass thin section, then polished and carbon coated. The majority of the electron microprobe analyses were obtained from the JEOL 8600 electron microprobe with four wavelength spectrometers, back scatter electron detector and a Tracor Northern 5500 automation and energy dispersive system. Electron microprobe analyses were also obtained from a Materials Analysis Company (MAC) model 400 electron microprobe with three spectrometers, and a KRISEL CONTROL automation system. No significant differences in the mineral analyses were observed between the two electron microprobes. The operating conditions, standards, reproducibility, and accuracy of both microprobes are given in Appendix 4.

3.4 Distinction Between Primary and Quench Minerals

When suprasolidus experiments are rapidly cooled to room temperature at the completion of an experiment, minerals commonly crystallize from the liquid. These minerals are referred to as quench minerals, and they must be distinguished from the primary minerals which crystallized at the pressure and temperature conditions selected for the experiment. The criteria used to distinguish primary minerals from quench minerals are only guidelines, and are specific to the present study. They were established by careful interpretation of the mineral chemistry and crystal morphology from each of the experimental run products. A minimum of three chemically similar analyses from different mineral grains, were obtained before the mineral was confirmed to be a primary mineral. Examples of quench and primary mineral analyses are give in Table 3. The criteria used for each mineral are discussed below.

The minerals in all three experimental run products are fine grained, not greater than 30 μm, and typically less than 10 μm. The minerals identified to have crystallized are: olivine, clinopyroxene, phlogopite, spinel, perovskite, apatite, armalcolite and a sanidine-like mineral. The olivine, clinopyroxene, phlogopite and spinel have both primary and quench versions. Perovskite, apatite and armalcolite are present only as primary minerals, and the sanidine-like mineral is present only as a quench mineral.

Quench olivine grains are identified by their acicular, feather-shape, or branch-like morphology. The TiO_2 content of the quench olivine grains was greater than 0.5 weight percent (wt. %), and displayed a low Mg number relative to the primary olivine. In contrast, the primary olivines are euhedral to subhedral, equant in form, have less than 0.5 wt. % TiO_2, and a Mg number not higher than 96.5 near the liquidus phase boundary or lower than 89.0 furthest from the liquidus phase boundary.

Quench clinopyroxene occurs as acicular crystals or as masses interstitial to the olivine grains, with Al_2O_3 and TiO_2 values each greater than three wt. %. Primary clinopyroxene has a euhedral, lath-shaped morphology, TiO_2, and Al_2O_3 each less than three wt. %, and a Mg number value not greater than three less than the accompanying primary olivine (Table 3).

The distinction between quench and primary phlogopite crystals was the most difficult to discern, as relatively high Al_2O_3 and TiO_2 wt. % values are present in the primary minerals, and the morphologies of the primary phases are varied. It was common for quench phlogopite to occur as long fibrous

grains with variable compositions, and for the stoichiometric structural formula to indicate a large deficiency in the octahedral and tetrahedral sites. Primary phlogopite grains have less than five wt.. % TiO_2, a stoichiometric structural formula, and a Mg number difference of not more than six when compared to the accompanying primary olivine and clinopyroxene

Table 3: Comparison of olivine, clinopyroxene and phlogopite quench and primary electron microprobe analyses.

	Olivine		Clinopyroxene		Phlogopite	
	Quench	Primary	Quench	Primary	Quench	Primary
Sample	PCW 6	PCW 6	EPC 25	EPC 25	EPC 45	EPC 45
SiO_2	42.01	41.05	43.33	51.84	43.05	41.97
TiO_2	1.91	0.02	6.22	1.51	2.11	1.42
Al_2O_3	0.00	0.00	4.95	0.44	8.77	11.71
Cr_2O_3	0.02	0.00	0.50	0.37	0.29	0.15
MnO	0.19	0.13	0.46	0.12	0.11	0.00
FeO	9.40	8.54	11.33	2.76	8.53	5.66
MgO	45.79	49.82	8.53	17.05	21.89	23.98
CaO	0.06	0.05	23.5	25.31	0.03	0.03
BaO	nd	nd	nd	nd	0.00	0.34
K_2O	0.02	0.02	0.18	0.01	9.22	9.1
Na_2O	0.03	0.00	0.50	0.41	0.01	0.04
NiO	0.00	0.4	nd	nd	nd	nd
F	nd	nd	nd	nd	0	0.11
Total	99.43	100.03	99.5	99.82	94.01	94.51
Mg number	89.7	91.2	57.3	91.7	82.1	88.3

nd = not determined

Quench spinel crystals are typically less than two µm in size, have a pyramidal morphology and are often directly associated with the outer grain boundaries of quench and primary olivines grains. Primary spinels are greater than two µm, have a euhedral cubic crystal form, and a stoichiometric structural formula.

The minerals perovskite, apatite, and armalcolite are considered primary based on their subhedral to euhedral crystal morphology, and stoichiometric structural formula.

A quench sanidine-like mineral was present in several low temperature 10 kb experiments, occurring above and below the stability of phlogopite, and closely associated with the incoming of clinopyroxene. When present, the sanidine-like minerals occur along the olivine grain boundaries. It was considered to be a quench mineral phase due to its anhedral morphology, and its Si deficiency, and Al excess in the structural formula.

3.5 Estimation of Equilibrium and Reproducibility

Equilibrium was established in the "no added volatile" system across the liquidus phase boundary at 20 and 30 kb. It was tested by completing reversal and heating isobaric experiments across the liquidus phase boundary. Heating experiments were accomplished by running an experiment at conditions identical to a previously completed experiment located near, but below, the liquidus phase boundary. When the duration of the heating experiment equaled that of the original experiment at those conditions, instead of quenching the experiment to room temperature, the temperature was increased to a previously completed experiment on the high temperature side of the liquidus phase boundary. The experiment was again held at these conditions for a time identical to the previously completed experiment, before it was finally quenched to room temperature. Reversal experiments were completed with an opposite procedure as the heating experiment: reversal experiments began on

the high temperature side of the liquidus phase boundary. Two isobaric heating-reversal experiments were completed in the present study, one at 20 kb, and the other at 30 kb. Both reversal experiments reproduced the assemblage olivine + liquid on the low temperature side of the phase boundary, and the heating experiments reproduced the assemblage of liquid on the high temperature side of the phase boundary. As a result, the liquidus phase boundary in the "no added volatile" system was considered to be in equilibrium

In order to determine the reproducibility of the experiments, four experimental conditions were duplicated, three in the "no water added" system, and one in the "water added" system. The replication of the experiments were accurate within the precision of the apparatus and experimental technique.

CHAPTER 4

EXPERIMENTAL RESULTS

4.1 "No Added Volatile" System

The results of the "no added volatile" system are listed in Table 4, and plotted in Figure 5. The liquidus occurs at 1470°C at 40 kb, and 1440°C at 10 kb. Olivine is the only liquidus phase present in the "no added volatile" experiments, and occurs as a mineral phase in all experiments below the liquidus. As temperature decreases from the liquidus, between 10 and 20 kb, spinel is the next phase to crystallize with olivine. Above approximately 25 ± 5 kb, the "spinel in" phase boundary no longer represents the second phase to crystallize. At these pressures, as temperature decreases, clinopyroxene and phlogopite are stable after the incoming of olivine. The change in spinel stability corresponds to a change in chemical composition from chromite to ulvospinel-magnetite as a function of temperature, and to some extent pressure. The variation in spinel chemical composition is discussed further in Chapter 5.4.

At approximately 25 ± 5 kb, a reaction point involving olivine, clinopyroxene, phlogopite and liquid is apparently present. The reaction line extending to higher pressures from the reaction point at 25 kb is the first mineral phase boundary below the liquidus as temperature decreases. It will be shown in the "water added" and "fluorine added" systems that the clinopyroxene and phlogopite phase boundaries are sensitive to the type and amount of volatiles in the system. Rather than being a reaction relationship, it is also possible that

Table 4: Results from the "no added volatile" experimental system.

Charge #	Cap	Pres	Temp	Time	Mineralogy
EPC 2	Pt_{Fe}	20	1350	10	$ol_{95.5}$
EPC 3	Pt_{Fe}	30	1450	10	$ol_{94.7}$
EPC 4	Pt_{Fe}	30	1400	10	$ol_{94.3}$
EPC 6	Pt_{Fe}	10	1450	10	quench liquid
EPC 7	Pt_{Fe}	30	1250	30	$ol_{92.5}$, $cpx_{91.8}$, $ph_{89.5}$
EPC 8	Pt_{Fe}	10	1250	30	$ol_{93.5}$
EPC 10	$Ag_{50}Pd_{50}$	20	1200	45	$ol_{92.5}$, sp_{chr}
EPC 11	Pt_{Fe}	20	1280	30	$ol_{94.1}$
EPC 16	Pt_{Fe}	10	1300	20	$ol_{95.2}$
EPC 19	Pt_{Fe}	30	1310	20	$ol_{93.7}$
EPC 22	Pt_{Fe}	10	1380	10	$ol_{96.0}$
EPC 25	$Ag_{50}Pd_{50}$	10	1120	240	$ol_{92.2}$, $cpx_{92.2}$ sp_{trans}
EPC 28	Pt_{Fe}	30	1350	10	ol
EPC 31	Pt_{Fe}	30	1500	5	quench liquid
EPC 33	Pt_{Fe}	20	1315	5	$ol_{94.6}$
EPC 34	$Ag_{50}Pd_{50}$	10	1200	30	$ol_{92.5}$
EPC 37	$Ag_{50}Pd_{50}$	20	1240	30	$ol_{93.7}$
EPC 41	$Ag_{50}Pd_{50}$	40	1460	10	$ol_{95.2}$
EPC 42	$Ag_{50}Pd_{50}$	35	1380	15	$ol_{95.0}$
EPC 43	$Ag_{50}Pd_{50}$	20	1050	240	$ol_{91.7}$, $cpx_{90.9}$, $ph_{88.3}$, $sp_{ulvo-mag}$
EPC 45	$Ag_{50}Pd_{50}$	30	1150	180	$ol_{92.5}$, $cpx_{91.7}$, $ph_{89.1}$, $sp_{ulvo-mag}$
EPC 47	Pt_{Fe}	20	1450	5	quench liquid
EPC 50	$Ag_{50}Pd_{50}$	15	1050	360	$ol_{92.1}$, $cpx_{91.5}$, sp_{mag}
EPC 51	$Ag_{50}Pd_{50}$	10	1000	420	$ol_{91.5}$, $cpx_{89.5}$, sp_{mag}, pv
EPC 52	$Ag_{50}Pd_{50}$	10	1070	360	$ol_{91.5}$, $cpx_{90.3}$, sp_{trans}
EPC 54	Pt_{Fe}	20	1400	5	$ol_{96.5}$
EPC 55	Pt_{Fe}	40	1300	20	$ol_{93.1}$
EPC 56	Pt_{Fe}	40	1380	10	$ol_{94.7}$
EPC 59	$Ag_{50}Pd_{50}$	20	1120	180	$ol_{92.4}$, $cpx_{91.7}$, sp_{trans}
EPC 60	$Ag_{50}Pd_{50}$	35	1200	180	$ol_{94.3}$, $cpx_{91.5}$, $ph_{89.8}$, $sp_{ulvo-mag}$

ol = olivine; cpx = clinopyroxene; ph = phlogopite; sp = spinel; chr = chromite; mag = magnetite; ulvo-mag = ulvospinel-magnetite; trans = transitional; pv = perovskite; ap = apatite; arm = armalcolite; Cap = capsule; Pres = pressure in kilobars; Temp = temperature in degrees Celsius; Time = minutes; Number after mineral symbol is the average Mg number for that mineral.

FIGURE 5: Pressure-temperature diagram for phase relations in the Prairie Creek olivine lamproite, sample PC-30, under "no added volatile" conditions. Solid lines represent experimentally determined boundary curves; dashed lines inferred boundary curves. Horizontal lines with arrows adjoining experimental points indicate reversals runs.

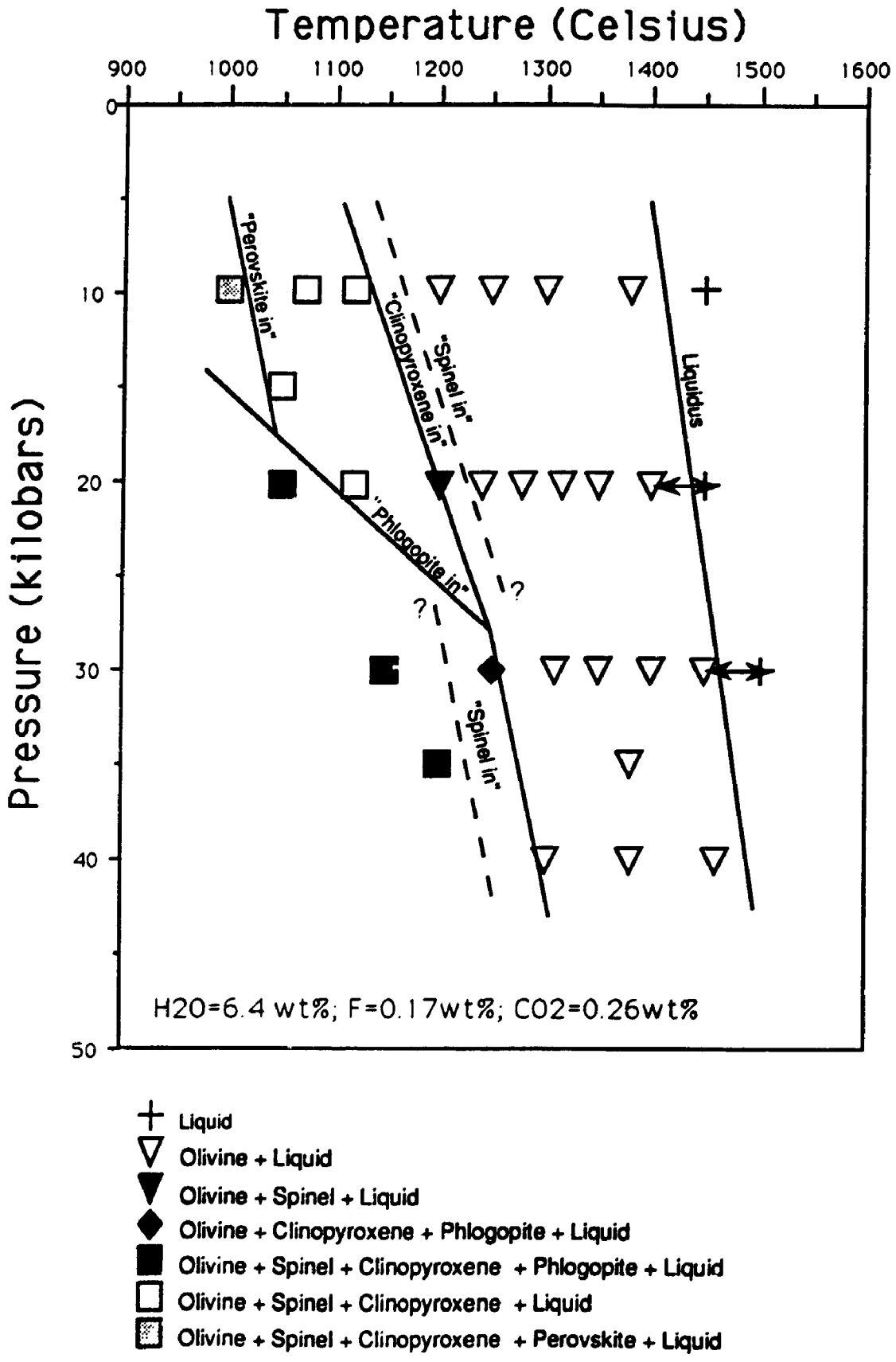
Temperature (Celsius)
900
1000
1100
1200
1300
1400
1500
1600
Pressure (kilobars)
0
10
20
30
40
50
"Perovskite in"
"Clinopyroxene in"
"Spinel in"
Liquidus
"Phlogopite in"
"Spinel in"
?
?
H20=6.4 wt%; F=0.17wt%; C02=0.26wt%
Liquid
Olivine + Liquid
Olivine + Spinel + Liquid
Olivine + Clinopyroxene + Phlogopite + Liquid
Olivine + Spinel + Clinopyroxene + Phlogopite + Liquid
Olivine + Spinel + Clinopyroxene + Liquid
Olivine + Spinel + Clinopyroxene + Perovskite + Liquid

the clinopyroxene and phlogopite phase boundaries in the "no added volatile" system are indistinguishable within the precision and accuracy of the experimental technique.

When the mineral phase boundaries are extrapolated to higher pressures (up to 50 kb), there is no evidence of a multiple saturation point on the liquidus. A multiple saturation point may represent the pressure, temperature and mineralogy of the source region from which the Prairie Creek olivine lamproite magma was extracted.

Below approximately 25 kb, the "phlogopite in" phase boundary diverges from the "clinopyroxene in" phase boundary at a lower slope (Figure 5). Phlogopite is not a stable phase at or below 15 kb within the temperature and pressure conditions studied. The low-temperature mineral phase assemblages observed below 15 kb are: olivine + clinopyroxene + spinel + liquid occurring at 1070°C; and olivine + clinopyroxene + spinel + perovskite + liquid at 1000°C.

4.2 "Water Added" System

The results of the experiments performed on the "water added" system are listed in Table 5 and plotted in Figure 6. The liquidus occurs at 1340°C at 30 kb and 1320°C at 10 kb. Olivine is the only liquidus mineral phase in the experimental runs, and is present in all sub-liquidus experiments. Below 15 kb, within 100°C of the liquidus, spinel is the first phase to crystallize with olivine, then phlogopite, followed by clinopyroxene. Above 15 ± 5 kb, the "spinel in" phase boundary appears to shift to a lower temperature. As a result, above 15 kb, phlogopite is the first phase to crystallize with olivine, then clinopyroxene

Table 5: Results from the "water added" experimental system.

Charge #	Cap	Pres	Temp	Time	Mineralogy
PCW 5	$Ag_{50}Pd_{50}$	20	1200	180	$ol_{94.5}$
PCW 6	$Ag_{50}Pd_{50}$	10	1100	360	$ol_{91.8}$, sp_{trans}, arm
PCW 13	Pt_{Fe}	20	1280	30	$ol_{95.8}$
PCW 14	Pt_{Fe}	10	1300	30	$ol_{93.9}$
PCW 16	Pt_{Fe}	30	1350	15	quench liquid
PCW 18	Pt_{Fe}	20	1390	15	quench liquid
PCW 21	Pt_{Fe}	20	1250	30	ol
PCW 22	Pt_{Fe}	30	1250	20	ol
PCW 23	Pt_{Fe}	30	1300	15	$ol_{95.5}$
PCW 25	Pt_{Fe}	10	1200	90	$ol_{93.0}$, sp_{chr}
PCW 26	$Ag_{50}Pd_{50}$	30	1150	270	$ol_{91.9}$, $cpx_{91.0}$, $ph_{89.6}$
PCW 28	$Ag_{50}Pd_{50}$	10	1150	270	$ol_{91.6}$, sp_{trans}
PCW 31	$Ag_{50}Pd_{50}$	10	1000	60	$ol_{91.8}$, $cpx_{90.6}$, $ph_{83.7}$, sp_{mag}, pv, ap
PCW 32	$Ag_{50}Pd_{50}$	20	1020	360	$ol_{92.8}$, $cpx_{91.1}$, $ph_{88.8}$, $sp_{ulvo\text{-}mag}$
PCW 33	$Ag_{50}Pd_{50}$	20	1130	240	$ol_{93.8}$, $ph_{90.0}$
PCW 35	$Ag_{50}Pd_{50}$	30	1050	240	$ol_{92.6}$, $cpx_{91.1}$, $ph_{89.4}$, sp_{mag}
PCW 41	$Ag_{50}Pd_{50}$	30	1200	210	$ol_{94.4}$

ol = olivine; cpx = clinopyroxene; ph = phlogopite; sp = spinel; chr = chromite; mag = magnetite; ulvo-mag = ulvospinel-magnetite; trans = transitional; pv = perovskite; ap = apatite; arm = armalcolite; Cap = capsule; Pres = pressure in kilobars; Temp = temperature in degrees Celsius; Time = minutes; Number after mineral symbol is the average Mg number for that mineral.

FIGURE 6: Pressure-temperature diagram for phase relations in the Prairie Creek olivine lamproite, sample PC-30, under "water added" conditions. Solid lines represent experimentally determined boundary curves; dashed lines inferred boundary curves.

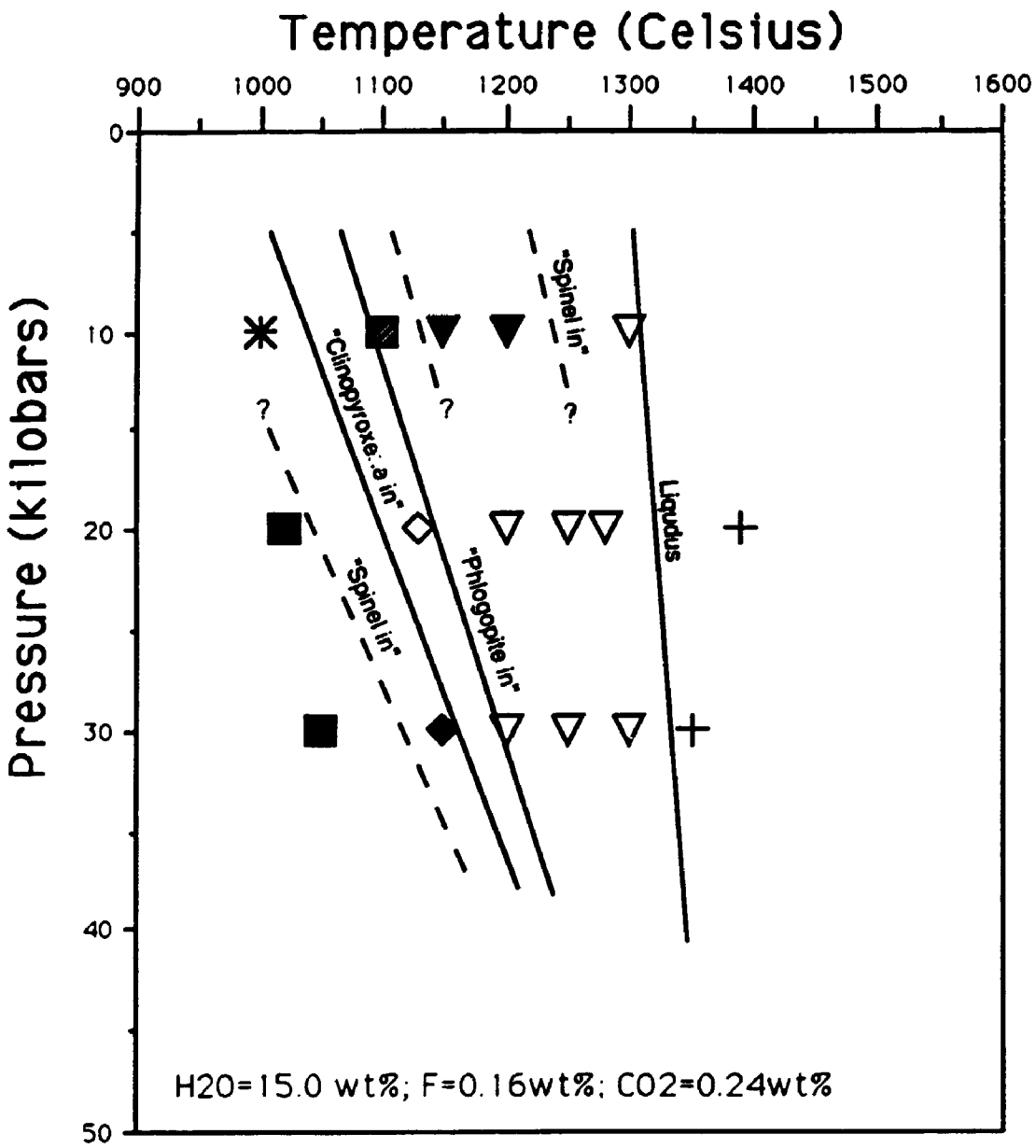

Liquid
Olivine + Liquid
Olivine + Spinel + Liquid
Olivine + Clinopyroxene + Phlogopite + Liquid
Olivine + Phlogopite + Liquid
Olivine + Spinel + Clinopyroxene + Phlogopite + Liquid
Olivine + Spinell + Armalcolite+ Liquid
Olivine + Spinel + Clinopyroxene + Phlogopite + Perovskite + Apatite + Liquid

followed by spinel. The low-temperature and low-pressure stable phase assemblages in the "water added" system are olivine + clinopyroxene + phlogopite + spinel, with armalcolite present at 1100°C and 10 kb, and perovskite and apatite present at 1000°C and 10 kb.

The most significant difference between the"water added" and "no added volatile" (Figure 5) systems is the change in the "phlogopite in" phase boundary. In the "water added" system, the line has an increased slope, occurs at a point 50°C higher at 20 kb, is present at 10 kb, and occurs up to 60°C higher than the "clinopyroxene in" phase boundary between 10 - 30 kb in the "no added volatile" system. The stability of phlogopite before clinopyroxene in the "water added" system is also a function of the "clinopyroxene in" phase boundary, occurring more than 100°C lower at 10 and 20 kb than in the "no added volatile" system. The liquidus phase boundary also occurs at a temperature approximately 120°C lower between 10 - 30 kb in the "water added" system. In the "water added" system, the "clinopyroxene in" phase boundary can be distinguished from the "phlogopite in" phase boundary, and the extrapolation of the mineral phase boundaries to higher pressures may intersect the liquidus between 55 and 60 kb, indicating a possible multiple saturation point of olivine + clinopyroxene + phlogopite and possibly spinel. Another difference between the two systems is the apparent shift of the "spinel in" phase boundary in the "water added" system to lower pressures between 10 and 20 kb, instead of 20 and 30 kb. All the minerals present in the "water added" system are present in the "no added volatile" system, with the exception of armalcolite at 10 kb and 1100°C.

4.3 "Fluorine Added" System

The experimental results of the "fluorine added" system are listed in Table 6, and plotted in Figure 7. The "fluorine added" system liquidus at 20 kb occurs between 1300 and 1400°C, with olivine as the liquidus phase. With decreasing temperature from the liquidus at 20 kb, spinel is the second phase to crystallize, then phlogopite, followed by clinopyroxene. The low-temperature and low-pressure phase assemblage in the "fluorine added" system is olivine + clinopyroxene + phlogopite + spinel + perovskite + apatite + armalcolite + liquid. Due to the limited number of experiments in the "fluorine added" system, it is unreasonable to extrapolate the phase boundaries to higher pressures.

The "fluorine added" system is similar to the "water added" system in that the "phlogopite in" phase boundary may be occurring at approximately the same temperature at 10, 20 and 30 kb, and occurs at a higher temperature than the "clinopyroxene in" phase boundary. Like the "water added" system, armalcolite is a stable low-temperature and low-pressure mineral phase, but occurs at 1000°C (Figure 7) instead of 1100°C (Figure 6). There does not appear to be any direct correlation between the "fluorine added" and the "no added volatile" system.

Table 6: Results from the "fluorine added" experimental system.

Charge #	Cap	Pres	Temp	Time	Mineralogy
FPC 1	Pt_{Fe}	20	1400	5	quench liquid
FPC 2	Pt_{Fe}	20	1300	20	$ol_{95.8}$
FPC 3	$Ag_{50}Pd_{50}$	20	1200	120	$ol_{94.7}$
FPC 4	$Ag_{50}Pd_{50}$	20	1100	300	$ol_{93.2}$, $ph_{89.0}$, sp_{mag}
FPC 6	$Ag_{50}Pd_{50}$	10	1000	360	$ol_{91.0}$, $cpx_{93.0}$, $ph_{84.2}$, sp_{trans}, pv, ap, arm
FPC 7	$Ag_{50}Pd_{50}$	10	1100	300	$ol_{91.5}$, sp_{trans}
FPC 8	$Ag_{50}Pd_{50}$	20	1000	300	$ol_{90.8}$, $cpx_{90.7}$, $ph_{90.2}$, $sp_{ulvo-mag}$
FPC 9	$Ag_{50}Pd_{50}$	30	1200	180	$ol_{94.6}$, $ph_{90.5}$, sp_{mag}
FPC 10	$Ag_{50}Pd_{50}$	30	1100	180	$ol_{92.8}$, $cpx_{92.1}$, $ph_{90.3}$, $sp_{ulvo-mag}$

ol = olivine; cpx = clinopyroxene; ph = phlogopite; sp = spinel; chr = chromite; mag = magnetite; ulvo-mag = ulvospinel-magnetite; trans = transitional; pv = perovskite; ap = apatite; arm = armalcolite; Cap = capsule; Pres = pressure in kilobars; Temp = temperature in degrees Celsius; Time = minutes; Number after mineral symbol is the average Mg number for that mineral.

FIGURE 7: Pressure-temperature diagram for phase relations in the Prairie Creek olivine lamproite, sample PC-30, under "fluorine added" conditions. Solid lines represent experimentally determined boundary curves; dashed lines inferred boundary curves.

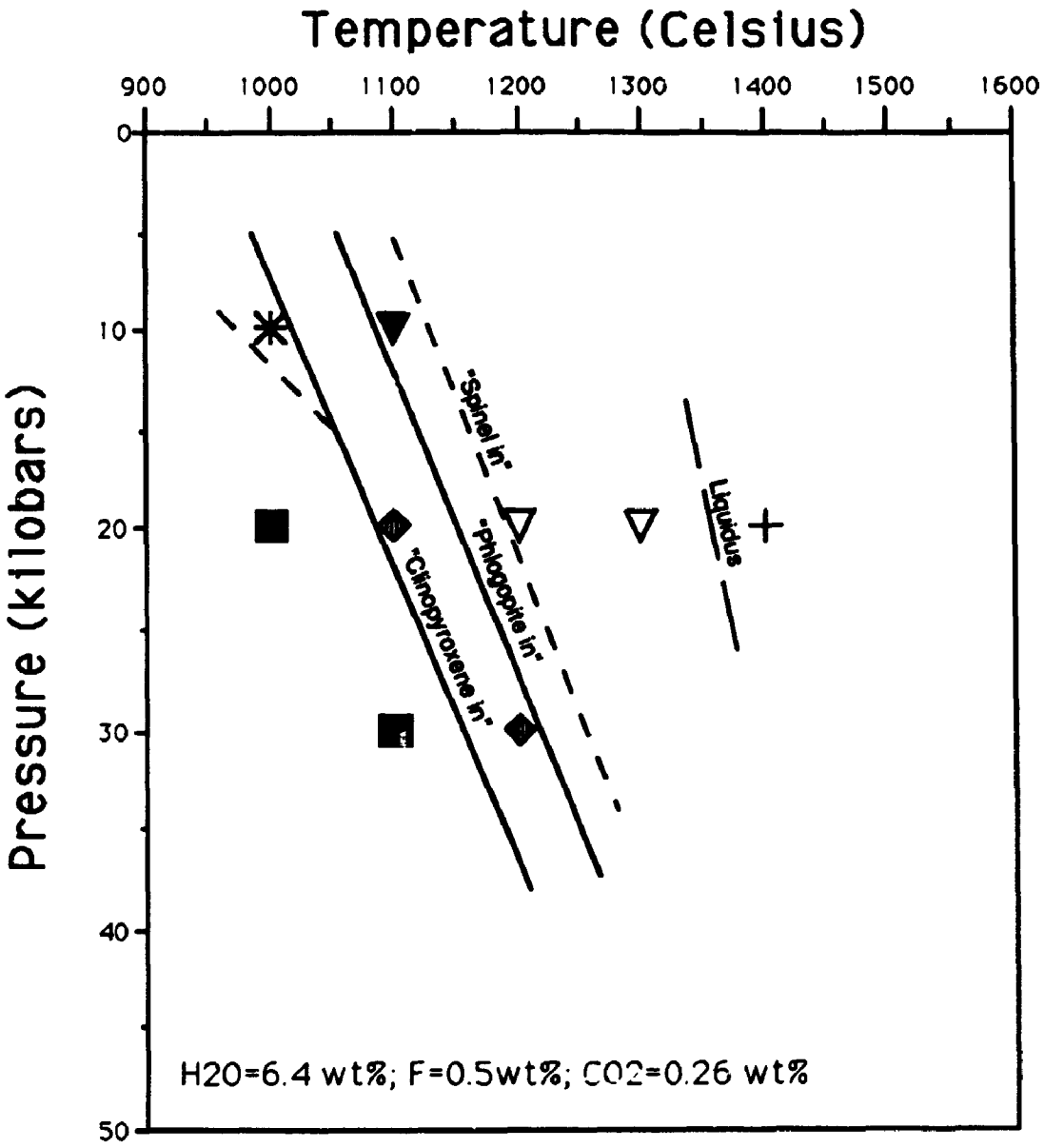

+ Liquid
▽ Olivine + Liquid
▼ Olivine + Spinel + Liquid
◆ Olivine + Phlogopite + Spinel + Liquid
■ Olivine + Spinel + Clinopyroxene + Phlogopite + Liquid
✳ Olivine + Spinel + Clinopyroxene + Phlogopite + Perovskite + Apatite + Armalcolite + Liquid

CHAPTER 5

MINERAL CHEMISTRY

5.0 Introductory Statement

The petrogenetic model of the Prairie Creek olivine lamproite, presented in this study, is based primarily on the paragenetic sequence and mineral chemistry of olivine, clinopyroxene, phlogopite, spinel and potassium richterite from the three facies of the Prairie Creek intrusion, the two types of cognate xenoliths, and the three suprasolidus experimental systems. The paragenetic sequence of the Prairie Creek intrusion has been described in Chapter 2, and the suprasolidus experiments of the HYP facies in Chapter 4. In this chapter, the chemistry of each mineral from the different facies of the Prairie Creek intrusion and the experimental systems are compared and contrasted.

The presentation of mineral chemistry from several different rocks of the Prairie Creek intrusion and experimental systems was simplified by dividing the mineral analyses from different sources into a series of variation diagrams. The elements were selected for the axis of each variation diagram, based on their ability to show variation in the chemical composition of the minerals in each of the different rocks of the Prairie Creek intrusion, and the chemical composition of the minerals under different experimental conditions. The chemical variation of the minerals as a function of elemental partitioning models and conditions of crystallization was then investigated. Each section concludes by comparing the results from the present study to the mineral chemistry of other olivine lamproites.

At the beginning of each section, representative analyses are presented in table form. The remaining analyses are listed in Appendix 5.

5.1 Olivine

Olivine in olivine lamproites occurs either as small euhedral or large anhedral grains (Scott-Smith and Skinner 1984a; Jaques et al. 1984a; Mitchell 1985). The interpretation of their origin as either phenocrystic or xenocrystic is critical to evaluating whether olivine lamproites are primitive or differentiated magma compositions. Chemically, these two types of olivine are indistinguishable (Scott-Smith and Skinner 1984a; Jaques et al. 1984a; Mitchell 1985). Based on texture and the lack of evidence to support either a xenocrystic or phenocrystic origin, the small euhedral olivines (SEO) are considered to be phenocrystic, and the large anhedral olivine grains (LAO) are considered to be macrocrystic. Chemically, a limited amount of normal and reverse zoning of Fe and Mg occurs in both the LAO and SEO in the HYP facies. Olivine analyses from the experimental systems have Fe and Mg values similar to the LAO and SEO, but the olivine analyses from the experimental systems range to higher values of Mg (Table 7). The experimental conditions for the olivine which has the lowest Fe values represent conditions in which Fe is most likely to be absorbed from the sample to the capsule (Chapter 3). As a result, the lower Fe values in the olivine from the experimental system may be a function of the experimental conditions. Based solely on this composition, the LAO appear to be phenocrysts within the HYP facies, however, their origin as xenocrysts can not be ruled out, due to their compositional similarity to olivines typically in mantle rocks from which the Prairie Creek magma originated.

TABLE 7: Representative olivine compositions from the Prairie Creek hypabyssal facies and suprasolidus experiments.

	Large Anhedral Olivine				Small Euhedral Olivine				Experimental Olivine		
	102c	102e	106c	106e	107c	107e	108c	108e	10':1000°	20':1240°	40':1460°
SiO2	40.59	41.11	40.99	41.36	40.49	41.08	41.50	40.74	39.71	40.64	41.07
TiO2	0.02	bld	0.02	bld	0.04	0.02	0.07	0.04	0.03	0.09	0.03
Cr2O3	bld	0.04	0.06	bld	bld	0.02	0.03	0.12	0.02	bld	0.15
FeO*	8.59	8.66	8.30	8.96	8.38	8.51	8.95	8.77	8.50	6.52	4.60
MnO	0.08	0.14	0.14	0.11	0.11	0.12	0.19	0.18	0.15	0.19	0.22
MgO	50.26	49.60	50.42	49.47	50.07	49.29	48.88	49.21	51.18	51.96	53.83
CaO	0.05	0.03	0.06	0.13	0.06	0.26	0.14	0.15	0.10	0.07	0.08
K2O	0.03	0.03	0.02	0.01	0.02	0.04	0.01	0.05	bld	bld	bld
NiO	0.54	0.42	0.38	0.40	0.43	0.40	0.36	0.42	0.36	nd	nd
Total	100.16	100.03	100.39	100.44	99.60	99.74	100.13	99.68	100.05	99.47	99.98
Mg num.	91.3	91.1	91.5	90.8	91.4	91.2	90.7	90.9	91.5	93.4	95.4
Structural formula calculations based on 4 oxygens											
Si	0.991	1.003	0.996	1.006	1.012	0.999	0.992	1.005	0.971	0.988	0.985
Ti	0.000	0.000	0.000	0.000	0.001	0.001	0.001	0.000	0.001	0.002	0.000
Cr	0.000	0.001	0.001	0.000	0.001	0.002	0.000	0.000	0.000	0.000	0.003
Fe	0.175	0.177	0.169	0.182	0.182	0.180	0.172	0.174	0.174	0.133	0.092
Mn	0.002	0.003	0.003	0.002	0.004	0.004	0.002	0.002	0.003	0.004	0.004
Mg	1.829	1.804	1.826	1.793	1.776	1.800	1.829	1.797	1.867	1.882	1.925
Ca	0.001	0.001	0.002	0.003	0.004	0.004	0.002	0.007	0.003	0.002	0.002
K	0.001	0.001	0.001	0.000	0.000	0.002	0.001	0.001	0.000	0.000	0.000
Ni	0.011	0.008	0.007	0.008	0.007	0.008	0.008	0.008	0.007	0.000	0.000
Sum	3.010	2.998	3.005	2.994	2.987	3.000	3.007	2.994	3.026	3.011	3.011

Mg num. =100Mg/(Mg+Fe); * Total Fe calculated as FeO; c = core analysis; e = edge analysis; ' kilobars; ° temperature in degrees Celsius; nd = not determined; bld = below detection limits .

5.2 Clinopyroxene

A Ti/Al greater than 5 for clinopyroxenes in lamproites appears to be unique. A reason for this is the direct substitution of Ti for Si in the tetrahedral site (Cundari and Salviulo 1989), instead of the coupled substitution $^{VI}Ti + 2^{IV}Al = {}^{VI}Mg + 2^{IV}Si$ (Thompson 1972), which forms the hypothetical "titan-pyroxene molecule" $CaTiAl_2O_6$ (Yagi and Onuma 1967). In this section, clinopyroxene compositions from the HYP facies, diopside-richterite xenoliths, and the experiments are described and compared.

Clinopyroxene analyses from the intrusion (Table 8) are grouped into five different subdivisions according to their mode of occurrence: hypabyssal facies (HYP); diopside-richterite cognate xenolith (DRX); corona rim 1 (CR1); corona rim 2 (CR2); and corona rim 3 (CR3). The composition of clinopyroxene in each of these modes is diopside, with the exception of three analyses which are Cr-diopsides. Analyses from the experiments are subdivided arbitrarily into two groups based on composition and pressure; those that occur above 25 kb, high pressure augite (HPA); and those that occur below 25 kb, low pressure diopside (LPD).

5.2.1 Diopside analyses from the hypabyssal facies (HYP) and the diopside-richterite cognate xenoliths (DRX).

A variation diagram with HYP and DRX is plotted in Figure 8. The data form a single continuous trend of increasing Al and Fe, decreasing Mg and constant Ca, with increasing Ti. The diopsides in the DRX have lower Ti, Al and Fe and higher Mg compared to those in the HYP. Diopsides in the DRX have Ti less than 0.04 and those in the HYP have Ti greater than ~ 12 formula units. The three Cr-diopside analyses (two from a single columnar DRX and one from

TABLE 3: Representative clinopyroxene analyses from the hypabyssal facies, cognate xenoliths, and the three experimental systems.

	Hypabyssal facies		Diopside-richterite cognate xenoliths					Experimental systems			
	HYP	HYP	DRX	DRX	CR1	CR2	CR3	LPD	LPD	HPA	HPA
SiO2	54.84	53.18	53.99	54.70	54.14	53.82	52.71	52.57	51.72	53.31	53.44
TiO2	1.18	2.15	0.96	0.41	0.41	1.06	1.40	1.15	2.04	0.43	0.36
Al2O3	0.18	0.38	0.06	0.04	0.15	0.11	0.21	0.15	0.30	1.00	1.50
Cr2O3	0.25	0.11	0.21	0.33	0.34	0.46	0.17	0.28	0.23	0.69	0.29
FeO*	2.56	3.44	0.02	0.08	1.98	2.26	3.58	2.96	3.15	3.49	3.29
MnO	0.12	0.19	2.54	2.46	0.15	bld	bld	0.16	0.11	0.18	0.11
MgO	16.36	15.83	16.89	16.58	17.16	16.72	16.20	16.46	16.70	19.09	20.66
CaO	24.29	24.26	25.18	25.23	24.93	24.73	24.33	25.17	24.69	20.49	19.25
K2O	bld	bld	0.02	0.02	bld	0.05	0.10	bld	0.13	0.06	0.07
Na2O	0.41	0.44	0.43	0.44	0.53	0.44	0.95	0.39	0.60	0.46	0.14
Total	100.19	99.98	100.30	100.29	99.79	99.65	99.65	99.29	99.67	99.20	99.11
Mg num.	91.93	89.13	92.22	92.32	93.92	92.95	88.97	90.84	90.43	90.70	91.80
Structural formula calculations based on 6 oxygens											
Si	1.993	1.952	1.969	1.992	1.979	1.972	1.949	1.948	1.915	1.953	1.945
IV Al	0.007	0.016	0.003	0.002	0.006	0.005	0.009	0.007	0.013	0.043	0.055
VI Al	0.001	0.000	0.000	0.000	0.000	0.000	0.000	0.000	0.000	0.000	0.009
Ti	0.032	0.059	0.026	0.011	0.011	0.029	0.039	0.032	0.057	0.012	0.010
Cr	0.007	0.003	0.006	0.009	0.010	0.013	0.005	0.008	0.007	0.020	0.008
Fe	0.078	0.106	0.077	0.075	0.061	0.069	0.111	0.092	0.098	0.107	0.100
Mn	0.004	0.006	0.002	0.002	0.005	0.000	0.000	0.005	0.003	0.006	0.003
Mg	0.886	0.866	0.918	0.900	0.935	0.913	0.893	0.909	0.922	1.042	1.121
Ca	0.946	0.954	0.984	0.984	0.976	0.971	0.964	0.999	0.979	0.804	0.751
K	0.000	0.000	0.001	0.001	0.000	0.002	0.005	0.000	0.006	0.003	0.003
Na	0.029	0.031	0.030	0.031	0.038	0.031	0.068	0.028	0.043	0.033	0.010
Total	3.983	3.993	4.016	4.007	4.021	4.005	4.043	4.028	4.043	4.023	4.015

Mg num. = 100Mg/(Mg+Fe), *FeO is total Fe; bld=below detection limit; HYP-cpx microphenocrysts from the hypabyssal rock;
DRX = diopside-richterite cognate xenolith; CR1= corona rim 1; CR2 = corona rim 2; CR3 = corona rim 3;
HPA-high pressure augite (>25 kb); LPD-low pressure diopside (<25 kb).

FIGURE 8: Variation diagram of diopside analyses from the hypabyssal facies (✖ HYP) and the diopside-richterite cognate xenoliths (▲ DRX). The HYP and DRX analyses form a single compositional trend, with those of the DRX. The DRX have lower values of Ti, Al, and Fe, and the DRX Cr-diopsides have a much lower Ti value than the other analyses. Analyses are plotted as atomic formula units based on six oxygens.

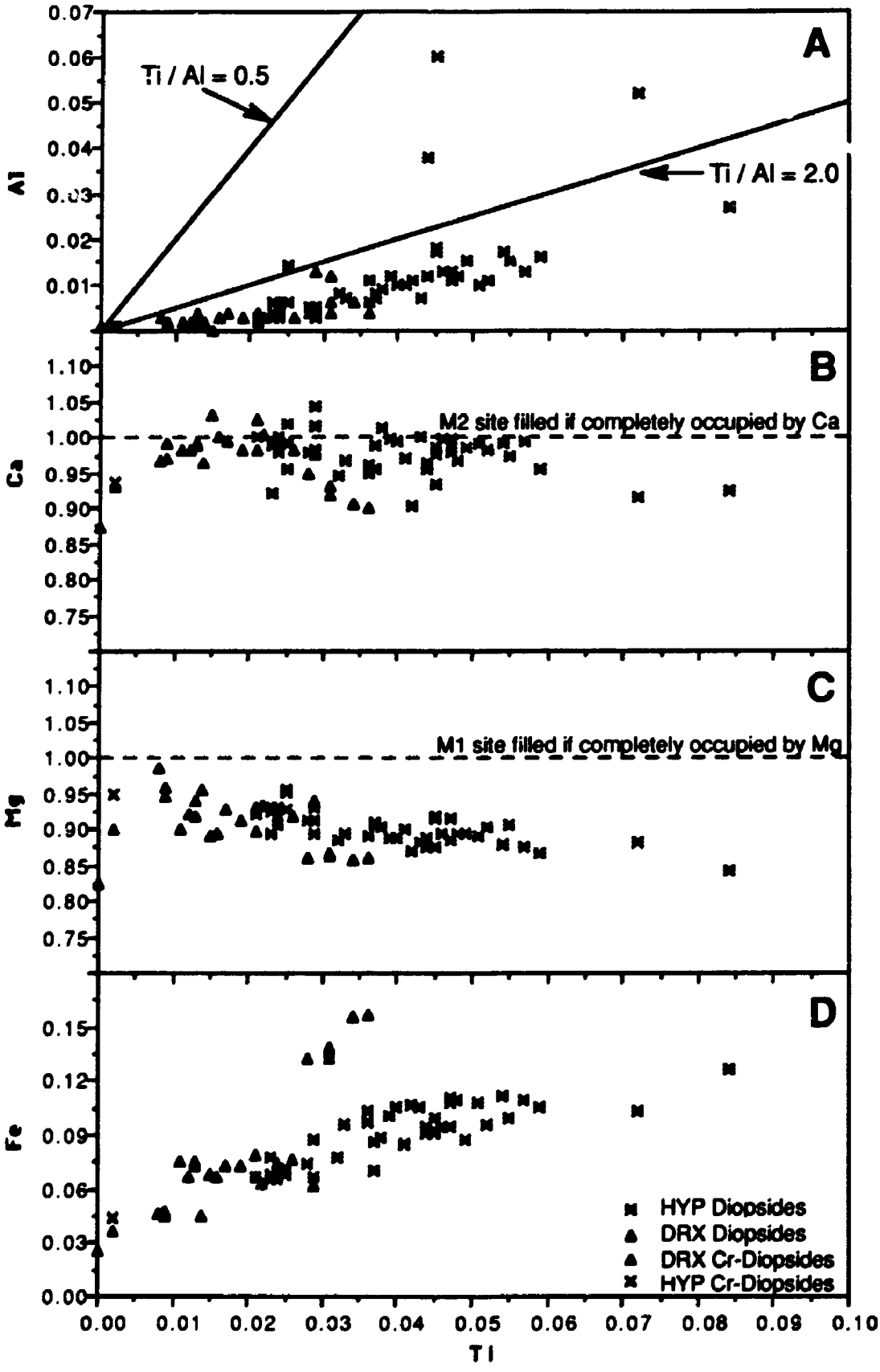
A
Ti / Al = 0.5
Ti / Al = 2.0
Al
B
M2 site filled if completely occupied by Ca
Ca
C
M1 site filled if completely occupied by Mg
Mg
D
Fe
HYP Diopsides
DRX Diopsides
DRX Cr-Diopsides
HYP Cr-Diopsides
Ti

the HYP) have significantly lower Ti than the other analyses, and are not considered part of the overall trend. All the analyses plotted in Figure 8, with the exception of a few points, have a Ti/Al value greater than 2.0. This ratio is greater than the maximum Ti/Al value of 0.5 for the presence of Ti within the diopside crystal structure as the hypothetical "titan-pyroxene molecule" $CaTiAl_2O_6$ (Yagi and Onuma 1967; Cundari and Salviulo 1989). In Figure 8B, data that plot along the dotted line where Ca = 1.0 indicate that the M2 site of the diopsides in both the HYP and DRX are predominantly filled with Ca. In Figure 8C, those that plot along the dotted line where Mg = 1.0 indicate that the M1 sites are predominantly filled with Mg. In each case, the deficiency calculated to be in the M1 site is approximately equal to that of the corresponding Fe value.

The HYP diopsides are not compositionally zoned from core to margin. In contrast, the diopsides in the DRX are weakly zoned, with higher amounts of Ti, and slightly lower Mg number at the margin than at the core. Six analyses from a single round DRX have Fe values greater than 0.12 (Figure 8D). These are higher than any other Fe values from the HYP or DRX. The two Cr-diopside analyses from a columnar DRX, also has diopsides which are not Cr rich.

5.2.2 Diopside analyses from the corona rim 1 (CR1), corona rim 2 (CR2), and corona rim 3 (CR3).

A variation diagram of diopside analyses from the CR1, CR2 and CR3 is plotted in Figure 9 and compared with fields of HYP and DRX analyses. The CR1, CR2 and CR3 data form a single continuous trend of increasing Al and Fe, decreasing Mg and constant Ca with increasing Ti. These results overlie precisely the distribution of the diopsides from HYP and DRX, with the exception

FIGURE 9: Variation diagram of diopside analyses from the three coronas around the diopside-richterite cognate xenoliths. The analyses were obtained from the corona rim 1 (+ CR1), corona rim 2 (■ CR2) and corona rim 3 (▪ CR3). The elements plotted and the axes scale are identical to Figure 8. Overlaid on the diagram is the range of HYP diopside ( ) and DRX diopside ( ) analyses. The CR1analyses are similar to the DRX analyses, and the CR2 and CR3 analyses are similar to the HYP analyses. The CR1 Cr-diopside analyses occur with the DRX Cr-diopside analyses (Figure 10).

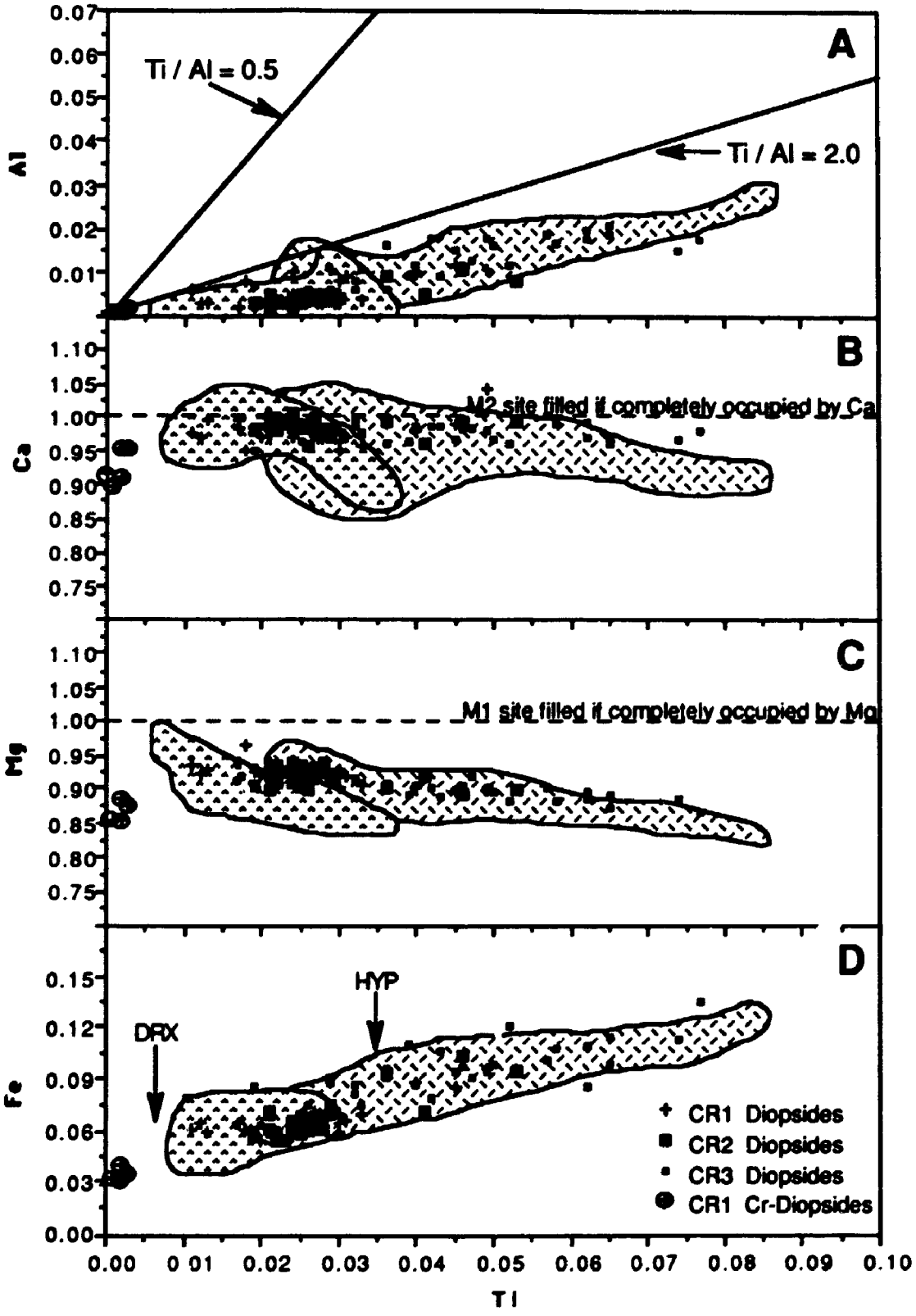
A
Ti / Al = 0.5
Ti / Al = 2.0
Al
B
M2 site filled if completely occupied by Ca
Ca
C
M1 site filled if completely occupied by Mg
Mg
D
HYP
DRX
Fe
CR1 Diopsides
CR2 Diopsides
CR3 Diopsides
CR1 Cr-Diopsides
Ti

of five analyses which are Cr-diopsides. These CR1 Cr-diopsides surround the columnar DRX with Cr-diopside. The CR1 analyses have the lowest Ti, Al and Fe of the three corona rims, and have a similar range of chemical results to the DRX. The lower-Ti CR1 values are located near the transition from the DRX to the CR1, and the higher Ti values are located near the transition from the CR1 to the CR2. The Ti values of diopside from the CR2 occur between 0.018 and 0.055 atoms per formula unit. These values indicate a transitional composition between the diopsides from the DRX and HYP. The CR3 analyses are identical to the HYP analyses, in that Ti concentrations are between 0.02 and 0.08 atoms per formula unit. All the corona data in Figure 9 plot below a Ti/Al value of 2, Ca values are almost equal to one, and Mg decreases as Fe increases.

5.2.3 Diopside and augite analyses from the experiments: diopsides from pressures less than 25 + 5 kb (LPD), and augites from pressures greater than 25 + 5 kb (HPA).

The LPD analyses also define a compositional trend of increasing Al and Fe with decreasing Mg and constant Ca, with increasing Ti (Figure 10). This trend is similar to that described for diopsides in Figures 8 and 9 from the HYP facies, which again has been superimposed on the diagram to facilitate comparison. The LPD differ from the DRX and CR1 diopsides by the absence of Ti values less than 0.015. They also differ from the HYP and CR3 by the absence of Ti values greater than 0.06. However, there is no significant difference between the LPD and CR2 diopsides. The LPD have a Ti/Al greater than 2, Ca almost equal to one, and Mg decreases as Fe increases, these concentrations are analogous to those presented in Figures 8 and 9.

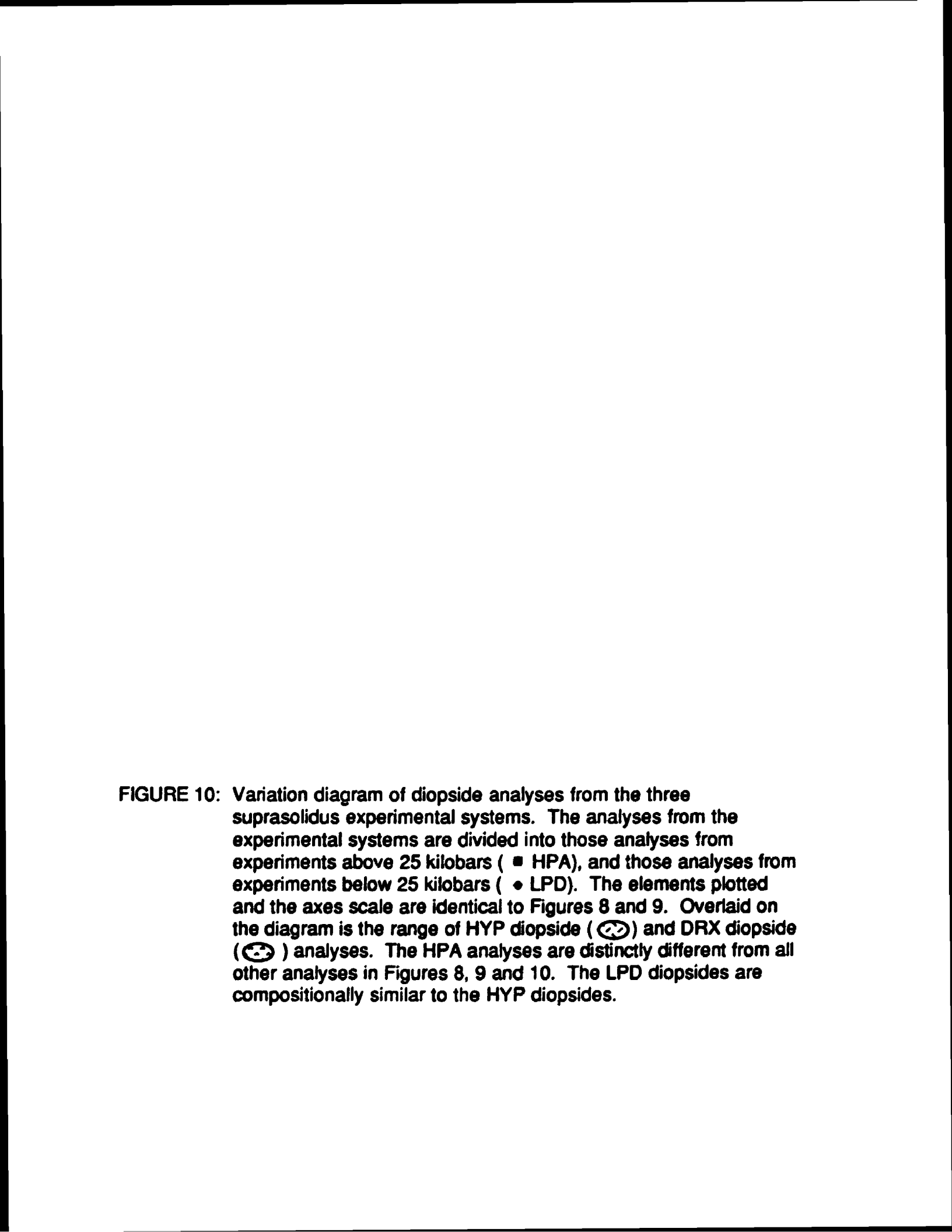

FIGURE 10: Variation diagram of diopside analyses from the three suprasolidus experimental systems. The analyses from the experimental systems are divided into those analyses from experiments above 25 kilobars (■ HPA), and those analyses from experiments below 25 kilobars (• LPD). The elements plotted and the axes scale are identical to Figures 8 and 9. Overlaid on the diagram is the range of HYP diopside ( ) and DRX diopside ( ) analyses. The HPA analyses are distinctly different from all other analyses in Figures 8, 9 and 10. The LPD diopsides are compositionally similar to the HYP diopsides.

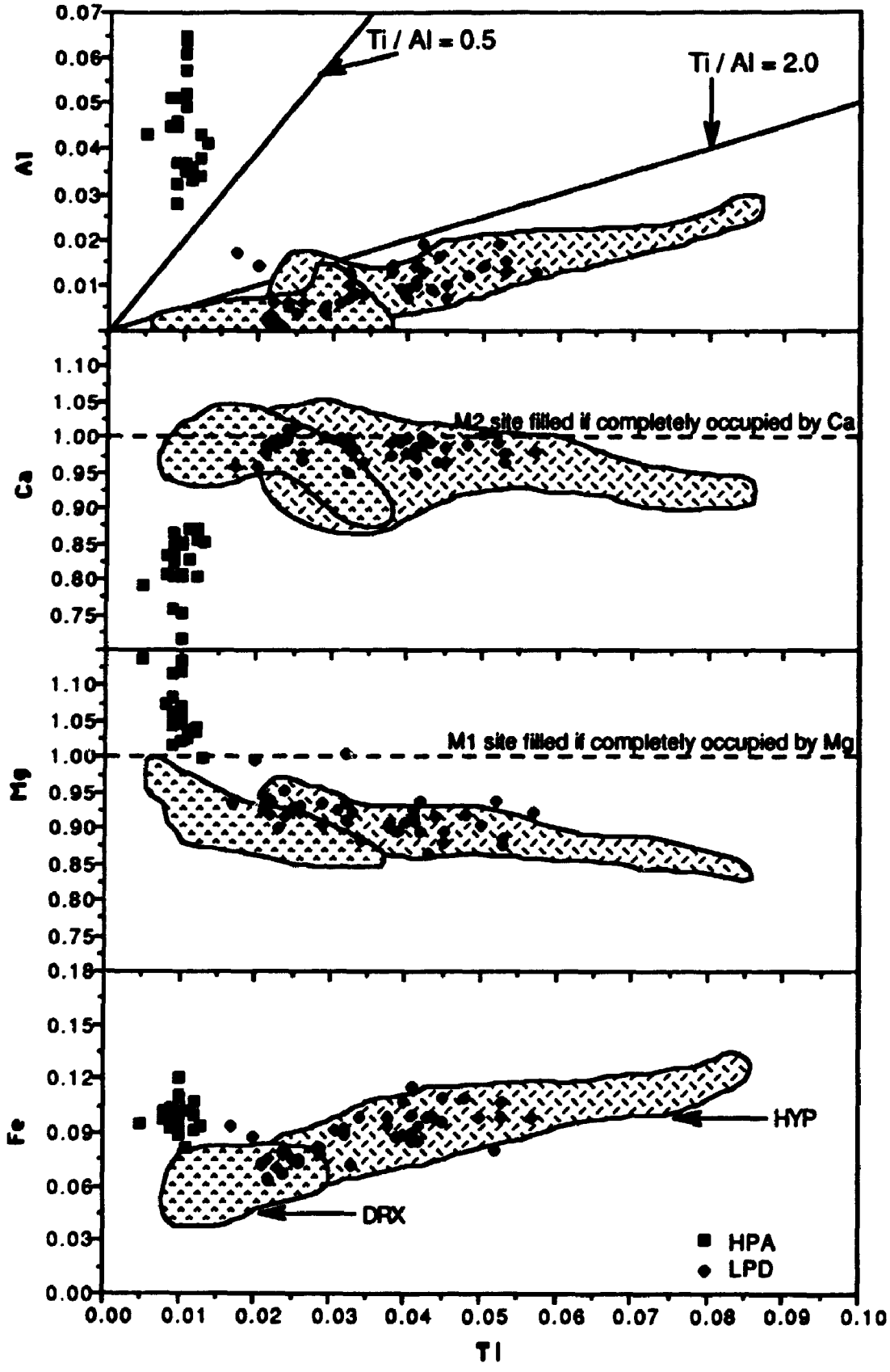
Ti / Al = 0.5
Ti / Al = 2.0
Al
Ca
M2 site filled if completely occupied by Ca
Mg
M1 site filled if completely occupied by Mg
Fe
HYP
DRX
HPA
LPD
Ti

The HPA (Figure 10) differ from all other diopsides analyzed in that their Al, Mg and Fe increase and Ca decreases, with a constant Ti, and Al/Ti less than 0.5. The HPA Mg values are greater than one and Ca values are less than one. This relationship is a result of the solid solution between diopside and augite, whereupon, the substitution of Mg into the M2 site for Ca, produces augite.

5.2.4 Elemental substitution in the diopside and augite.

As is typical of lamproite clinopyroxenes (Mitchell 1985), Al + Si concentrations are insufficient to fill the tetrahedral site ($Si + Al^{iv} < 2$) (Figure 11). The tetrahedral vacancy in the augites is constant with decreasing Si and increasing Al, whereas, the tetrahedral site vacancy in the diopsides increases with decreasing Si and slightly increasing Al.

The tetrahedral site vacancy in both the augite and the diopside can be balanced by substituting either Fe^{3+} or Ti^{4+}, in addition to Al^{3+}, for Si^{4+}. Owing to the inability of the electron microprobe to differentiate between Fe^{2+} and Fe^{3+}, and the absence of Mossbauer data, Fe^{3+} is estimated by balancing the charge of the structural formula (Barton 1979; Cameron and Papike 1980). To determine the charge balance, $Na + {}^{IV}Al$ is plotted against ${}^{VI}Al + 2Ti + Cr$ according to Cameron and Papike (1980) (Figure 12). Analyses that plot above the charge balance line indicate a charge deficiency, and require the presence of Fe^{3+} to balance the charge. Those that plot below the line have a charge excess, and do not require Fe^{3+} for a balanced charge. The HPA and 15 diopside analyses, mainly from the columnar DRX with Cr-diopside, have a charge deficiency. All other diopsides have a charge excess.

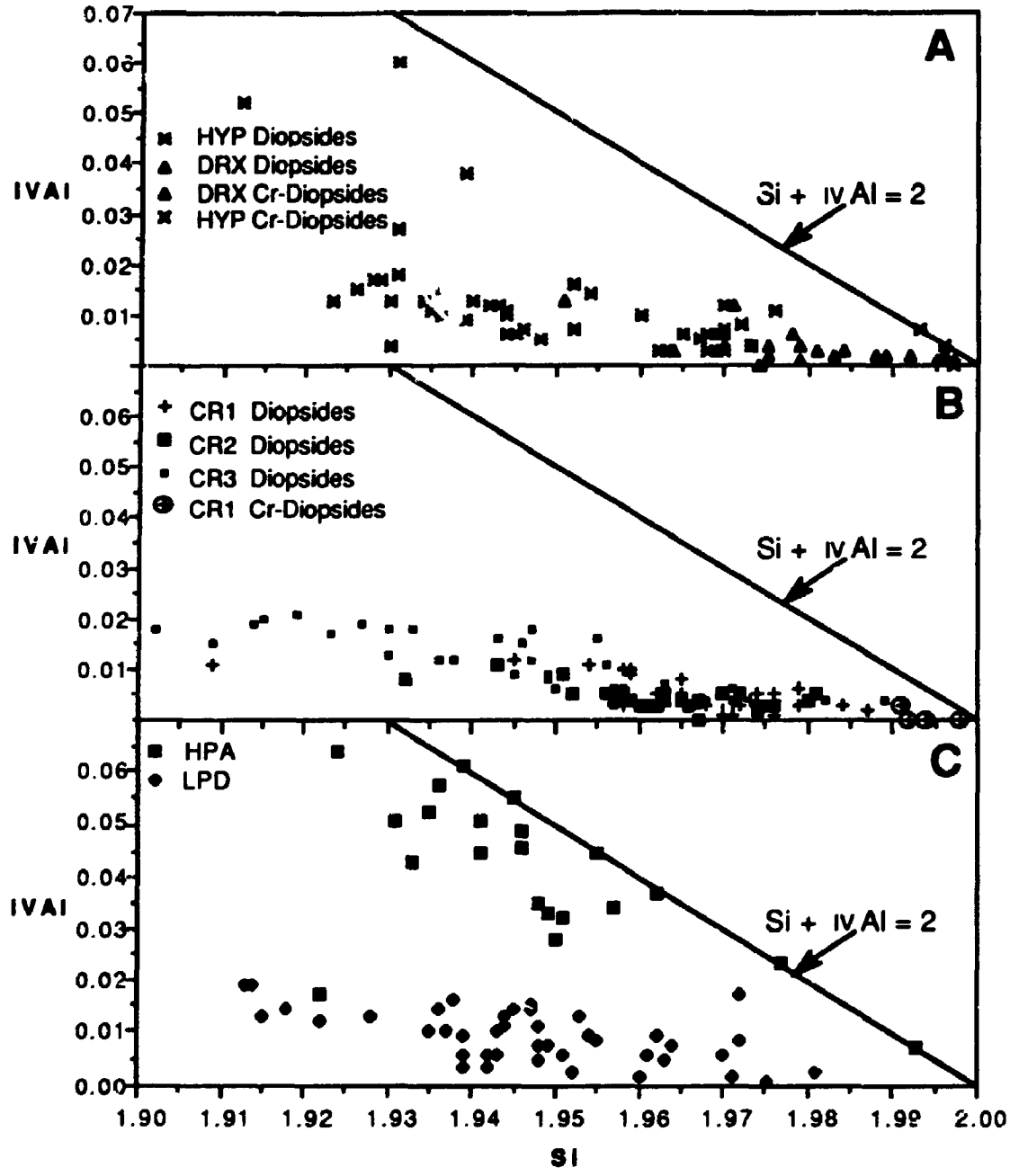

FIGURE 11. A series of three diagrams demonstrating the variation of ^{IV}Al relative to Si for all the diopside and augite analyses. In all but 11 analyses (7 of which are HPA), ^{IV}Al is insufficient to fill the tetrahedral site vacancy. Only the HPA analyses form a trend parallel to the Si + IVAl =2 line.

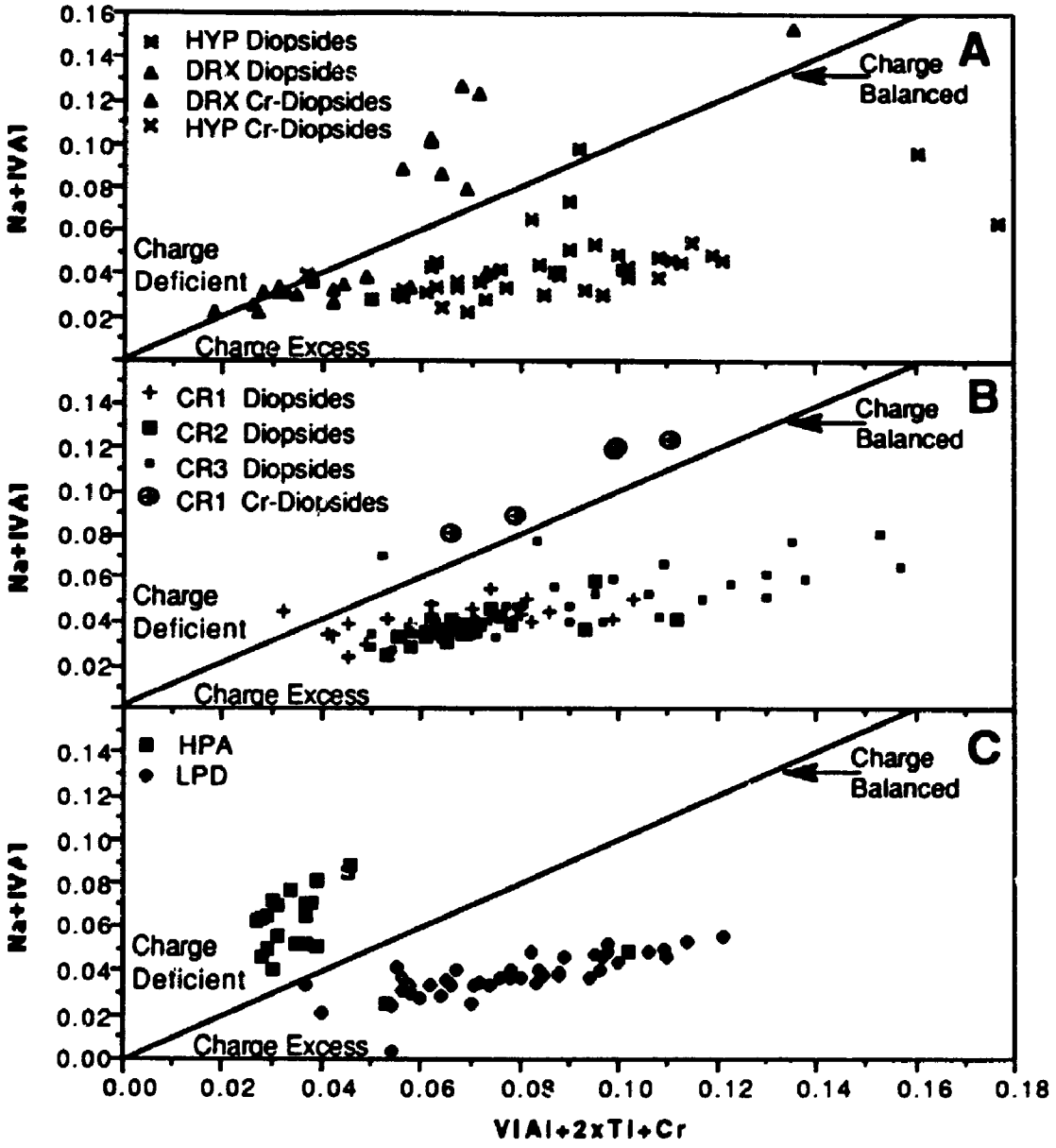

FIGURE 12: Three diagrams demonstrating the charge balance of clinopyroxene analyses. The LPD and most of the DRX diopside analyses have a charge deficiency, while the remaining analyses have a charge excess. Analyses with a charge deficient are more likely to contain Fe^{3+} (Cameron and Papike 1980)

The HPA are characterized by Ti/Al values less than 0.5 (Figure 10), a charge deficiency (Figure 12), and Ti values which do not correlate with an increase in the tetrahedral site vacancy (Figure 13). Based on these results, it is assumed that Fe^{3+} is preferentially substituting into the tetrahedral site, and Ti^{4+} is substituting into the octahedral site according to the coupled substitution $^{VI}Ti + 2^{IV}Al = {}^{VI}Mg + 2^{IV}Si$ (Thompson 1972), forming the "titan-pyroxene molecule", $CaTiAl_2O_6$ (Yagi and Onuma 1967).

All diopsides are characterized by Ti/Al values greater than 0.5 (Figure 8, 9 and 10), a charge excess (Figure 12), and a marginally increased tetrahedral site vacancy proportional to decreasing Si and increasing Ti concentrations (Figure 13). These results are explained by the substitution of Ti^{4+} for Si^{4+} into the tetrahedral site at a ratio of one to one (Cundari and Salviulo 1989), instead of the Ti^{4+} substitution into the octahedral site, as characterized by the HPA. The diopsides in the DRX with the charge deficiencies probably follow the same substitution mechanism as the other diopsides with regards to Ti, but they may represent diopside analyses with a greater abundance of Fe^{3+}.

Although Fe^{3+} may not be the preferred element of substitution into the tetrahedral site, it is not excluded from being an important element filling the tetrahedral vacancy. In Figure 14, Al + Ti versus Si is plotted for all the diopside analyses. Several of the values plot below the filled tetrahedral site line of Si + Al + Ti = 2, presumably requiring Fe^{3+} to balance the tetrahedral site of the diopsides. As a result, the order of preference for the substitution of elements into the tetrahedral site is $Al^{3+} > Ti^{4+} > Fe^{3+}$ for the diopsides, and $Al^{3+} > Fe^{3+} > Ti^{4+}$ for the augites.

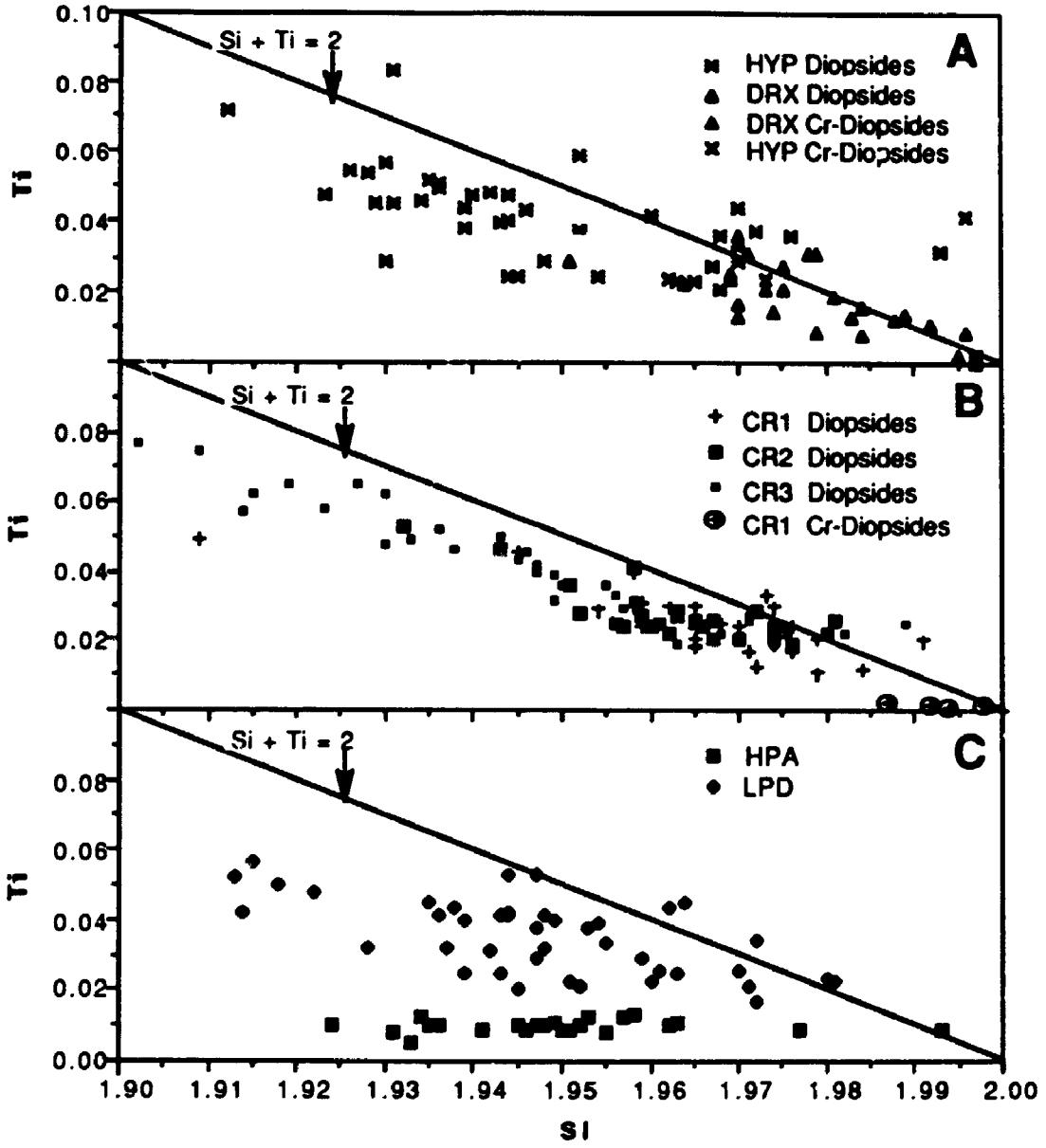

FIGURE 13: Three diagrams demonstrating the variation of Ti relative to Si for all the clinopyroxene analyses. The line Ti + Si = 2 represents a balanced tetrahedral site if Ti were substituting directly for Si at a ratio of one to one into the tetrahedral site. All the diopside analyses are parallel the Si + Ti = line, whereas, the HPA analyses form a trend which is not related to the line.

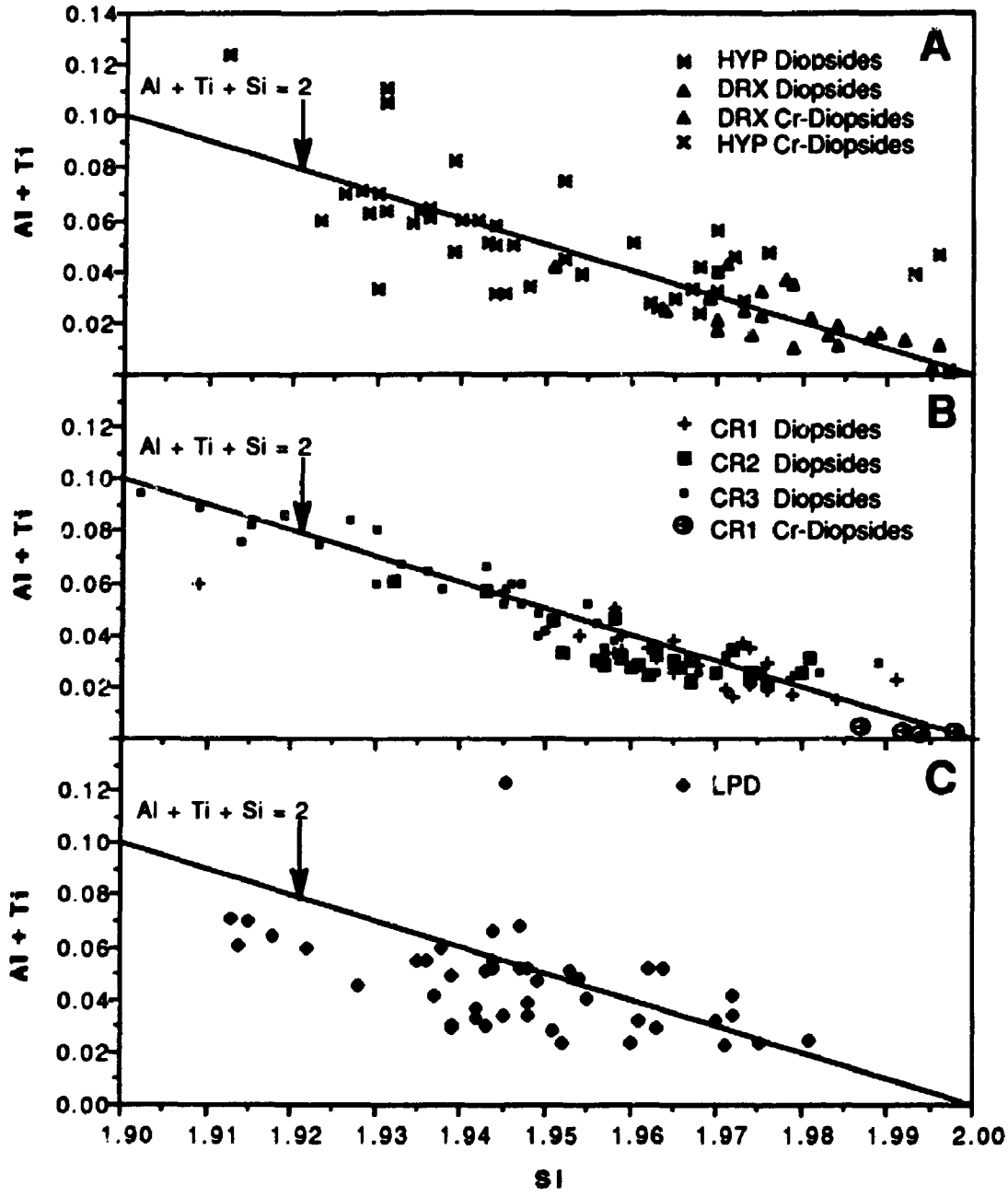

FIGURE 14: Three diagrams demonstrating the variation Al + Ti relative to Si for diopsides only. The analyses follow the line Al + Ti + Si = 2, which represents a filled tetrahedral site if Ti were substituting directly for Si at a ratio of one to one.

5.2.5 Comparison of clinopyroxene analyses from other olivine lamproites.

In Figure 15, the diopside analyses from the Prairie Creek HYP facies are compared tc representative diopside analyses from other olivine lamproite intrusions. The chemical compositions of clinopyroxene in the West Kimberley olivine lamproites from Western Australia (Jaques et al. 1984a; 1986) closely resemble those from the Prairie Creek HYP facies. The diopside analyses from the Kapamba, Zambia, olivine lamproite are variable, and exhibit higher Al values than the majority of the diopsides from the HYP. Diopside analyses from the American Mine (Scott-Smith and Skinner 1984b), an olivine lamproite intrusion located near the Prairie Creek intrusion, are also variable; one analysis exhibits the same Al and Ti values as the HYP, and the other analysis has the highest Al concentrations of all the diopside analyzed. The substitution of Ti into the diopside from West Kimberley and Prairie Creek, appear to be controlled by the direct substitution of Ti for Si. As a result of the analyses from Kapamba and the American Mine having lower Ti/Al values, the substitution of Ti in the diopsides is assumed to be controlled by both the direct substitution of Ti for Si, and the coupled substitution $^{VI}Ti + 2^{IV}Al = {}^{VI}Mg + 2^{IV}Si$.

5.3 Phlogopite

Phlogopite is an important petrogenetic indicator of lamproites, so much so that the chemistry and texture of phlogopite have been used as the basis of a twofold petrogenetic division of the lamproite group of rocks (Mitchell 1985; Mitchell and Bergman 1991). The division is based on classifying the occurrence of phlogopite in lamproites as either "phenocrystal" or "groundmass" (the term groundmass includes poikilitic phlogopites). Lamproites with

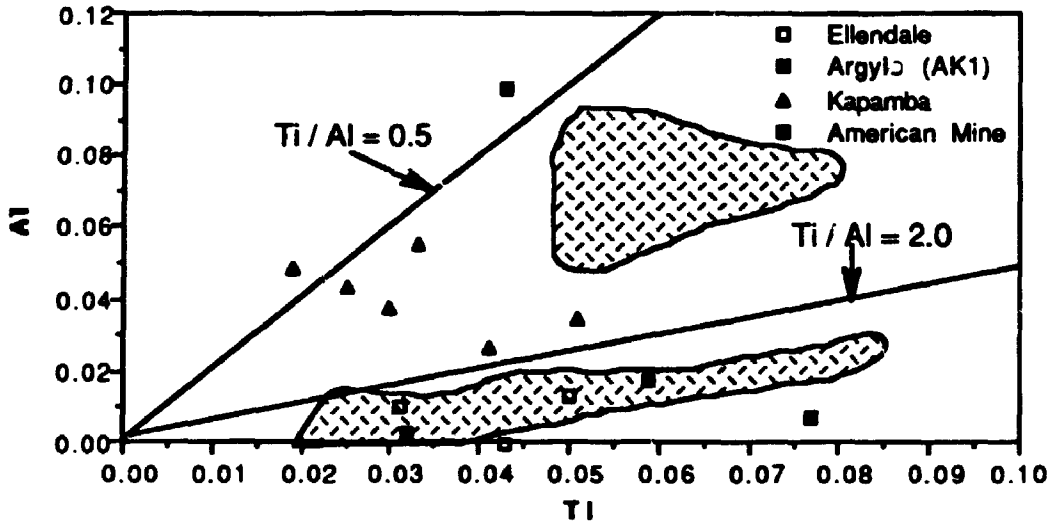

FIGURE 15. The range of diopside compositions from the Prairie Creek hypabyssal facies (◯), compared to diopside compositions from other olivine lamproites. Diopsides from the Argyle (AK1) and Ellendale olivine lamproites are compositionally similar to the diopsides from the Prairie Creek rock. Ellendale analyses from Jaques et al. 1984, Argyle (AK1), Jaques et al. 1989; Kapamba, Scott-Smith et al. 1989; American Mine, Scott-Smith and Skinner 1984b.

phenocrystal phlogopites have been named phlogopite lamproites, and lamproites with groundmass phlogopite have been named madupitic lamproites. Phlogopites with chemical compositions similar to typical lamproite phenocryst and groundmass phlogopites are present in the Prairie Creek intrusion as well as phlogopites similar to those produced in the suprasolidus experiments of the HYP facies of rock. It is the objective of this section to describe the chemical variation of the phlogopite from the Prairie Creek intrusion and suprasolidus experiments, and to compare these results to the phenocrystal and groundmass phlogopite compositions of lamproites.

Phlogopite analyses (Table 9) from the Prairie Creek intrusion are grouped into five different modes of occurrence: tuff and breccia (tuff-breccia), hypabyssal facies (HYP), diopside-richterite cognate xenolith (DRX), corona rim 2 and corona rim 3 (CR2-3), and phlogopite-bearing cognate xenoliths (PBX). The texture of the phlogopites from the tuff-breccia is phenocrystic, whereas the phlogopite from the other four occurrences is poikilitic. Based on the occurrence of experimentally derived phlogopite compositions similar to both the phenocrystic and poikilitic phlogopites, the phlogopites are arbitrarily subdivided according to composition and pressure. In this study, phlogopite compositions similar to the phlogopite phenocrysts occur at pressures greater than 15 ± 5 kb and are called high pressure phlogopite (HPP), and those that are similar to the poikilitic phlogopites occur at pressures less than 15 ± 5 kb and are called low pressure phlogopites (LPP). The results in each of the figures are presented in atomic formula units based on 22 oxygens.

TABLE 9: Representative phlogopite compositions from the tuff, hypabyssal facies, cognate xenoliths, and experimental systems.

	Tuff		Hypabyssal facies		Cognate xenolith				Experimental systems		
	Core	Edge	HYP	HYP	PBX	DBX	CR2	CR3	HPP	LPP	LPP
SiO2	40.22	42.52	42.41	42.56	41.37	42.92	42.91	42.08	41.87	42.29	43.69
TiO2	5.26	6.44	4.40	5.84	4.65	4.05	4.11	4.53	1.97	3.99	4.63
Al2O3	11.34	8.20	7.21	6.65	7.83	6.56	6.07	6.11	12.42	5.84	6.09
Cr2O3	0.42	0.04	0.00	0.05	0.09	0.00	0.00	0.05	0.93	0.02	0.12
FeO*	4.92	7.58	7.73	8.21	7.71	7.16	7.60	8.04	4.79	7.98	7.52
MnO	0.06	0.00	0.00	0.00	0.06	0.00	0.01	0.00	0.07	0.05	0.12
MgO	22.20	20.25	22.80	21.28	22.54	22.97	22.91	22.22	23.72	22.77	22.66
CaO	0.00	0.03	0.05	0.06	0.13	0.05	0.01	0.00	0.12	0.06	0.12
K2O	10.47	10.10	9.78	9.94	10.19	10.09	9.88	10.13	10.08	9.49	9.27
Na2O	0.10	0.15	0.65	0.81	0.51	0.83	0.91	0.82	0.08	0.05	0.11
BaO	0.19	0.13	1.16	0.97	0.73	0.42	0.66	1.08	0.39	1.34	0.95
F	0.49	0.45	4.24	2.99	4.11	4.41	4.40	4.34	0.40	3.42	4.29
Total	95.67	95.89	100.43	99.36	99.92	99.46	99.47	99.4	98.94	97.3	99.57
F=O	0.21	0.19	1.79	1.26	1.73	1.86	1.85	1.83	0.17	1.84	1.81
Total	95.46	95.70	98.64	98.10	98.19	97.60	97.62	97.57	96.67	95.86	97.76
Mg num.	91.93	82.65	84.02	82.21	83.90	85.12	84.31	83.13	89.60	83.57	84.31
Structural formula calculations based on 22 oxygens											
Si	5.754	6.107	5.878	5.979	5.771	5.969	5.988	5.926	5.882	6.054	6.056
IV Al	1.912	1.388	1.178	1.101	1.287	1.075	0.998	1.014	2.056	0.985	0.995
VI Al	0.000	0.000	0.000	0.000	0.000	0.000	0.000	0.000	0.000	0.000	0.000
Ti	0.566	0.696	0.459	0.617	0.488	0.424	0.431	0.480	0.208	0.430	0.483
Cr	0.048	0.005	0.000	0.006	0.010	0.000	0.000	0.006	0.103	0.002	0.013
Fe	0.589	0.910	0.896	0.965	0.899	0.833	0.887	0.947	0.563	0.955	0.872
Mn	0.007	0.000	0.000	0.000	0.007	0.000	0.001	0.000	0.008	0.006	0.014
Mg	4.735	4.336	4.711	4.456	4.688	4.762	4.766	4.665	4.967	4.859	4.682
Ca	0.000	0.005	0.007	0.009	0.019	0.007	0.001	0.000	0.018	0.009	0.018
Ba	0.011	0.007	0.063	0.053	0.040	0.023	0.036	0.060	0.021	0.075	0.052
K	1.911	1.851	1.729	1.781	1.814	1.79	1.759	1.820	1.806	1.733	1.639
Na	0.028	0.042	0.175	0.221	0.138	0.224	0.246	0.224	0.022	0.014	0.030
F	0.222	0.204	1.859	1.328	1.813	1.940	1.942	1.933	0.178	1.548	1.880
Total	15.783	15.551	16.955	16.516	16.974	17.047	17.055	17.075	15.832	16.670	16.734

Mg num. = 100Mg/(Mg+Fe); *FeO is total Fe; key to sample abbreviations in text.

5.3.1 Phlogopite analyses from the tuff and breccia (tuff-breccia), and hypabyssal facies (HYP).

The chemical composition of the phlogopites from the tuff-breccia are indistinguishable and form a single compositional trend of increasing Fe and Mg, decreasing Cr and to some extent Ti, and constant F, with decreasing Al. As a result, they have been grouped together and are considered representative of phenocrystic phlogopites in the Prairie Creek intrusion. The tuff-breccia core analyses are lower in F and Fe, and higher in Ti, Al, Cr and Mg, compared to the tuff-breccia edge analyses (Table 9).

The poikilitic phlogopite analyses from the HYP plot as a single cluster (Figure 16) in all but Figure 16C, which outlines a short trend of increasing Fe with decreasing Al. In Figure 16A and 16E, a few poikilitic phlogopite analyses from the HYP facies, plot separately from the others with higher Ti and lower Mg and F values. These are denoted as "Ti-poik" on the diagram and occur in a sample collected from outcrop of HYP facies exposed to the north-east of the other samples (Figure 3). Compared to the phenocrystic phlogopite, the poikilitic phlogopites from the HYP have lower Ti, Cr and Al, higher Fe and F, and similar Mg.

5.3.2 Phlogopite analyses from the phlogopite-bearing xenolith (PBX), diopside-richterite xenolith (DRX), and the corona rim 2 (CR2) and corona rim 3 (CR3) around the diopside-richterite xenolith.

In Figure 17, the PBX, DRX, CR2 and CR3 phlogopite analyses are plotted. On the same diagram, the elemental distribution of the phenocrystic phlogopite from the tuff-breccia and poikilitic phlogopites from the HYP, are overlain to facilitate comparison. Except for the F, the phlogopite from the PBX

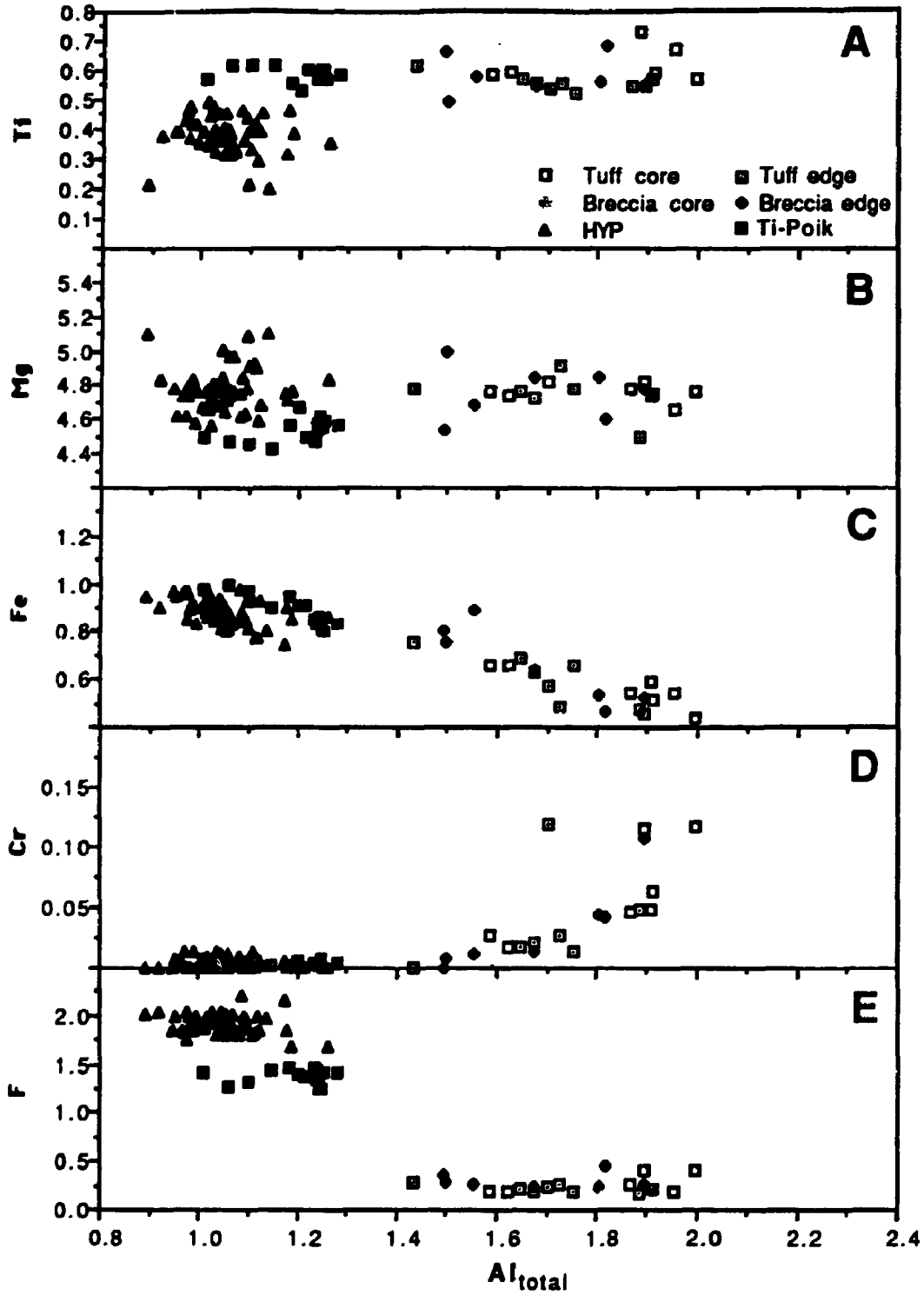

FIGURE 16: Variation diagram of phlogopite analyses from the tuff, breccia and hypabyssal facies (HYP). The Al values >1.4 are phenocrystic phlogopite from the tuff and breccia, and the Al values <1.4 are poikilitic phloogpite from the HYP facies. Ti-poik are phlogopite analyses from the HYP facies that have higher Ti values than the HYP phlogopites.

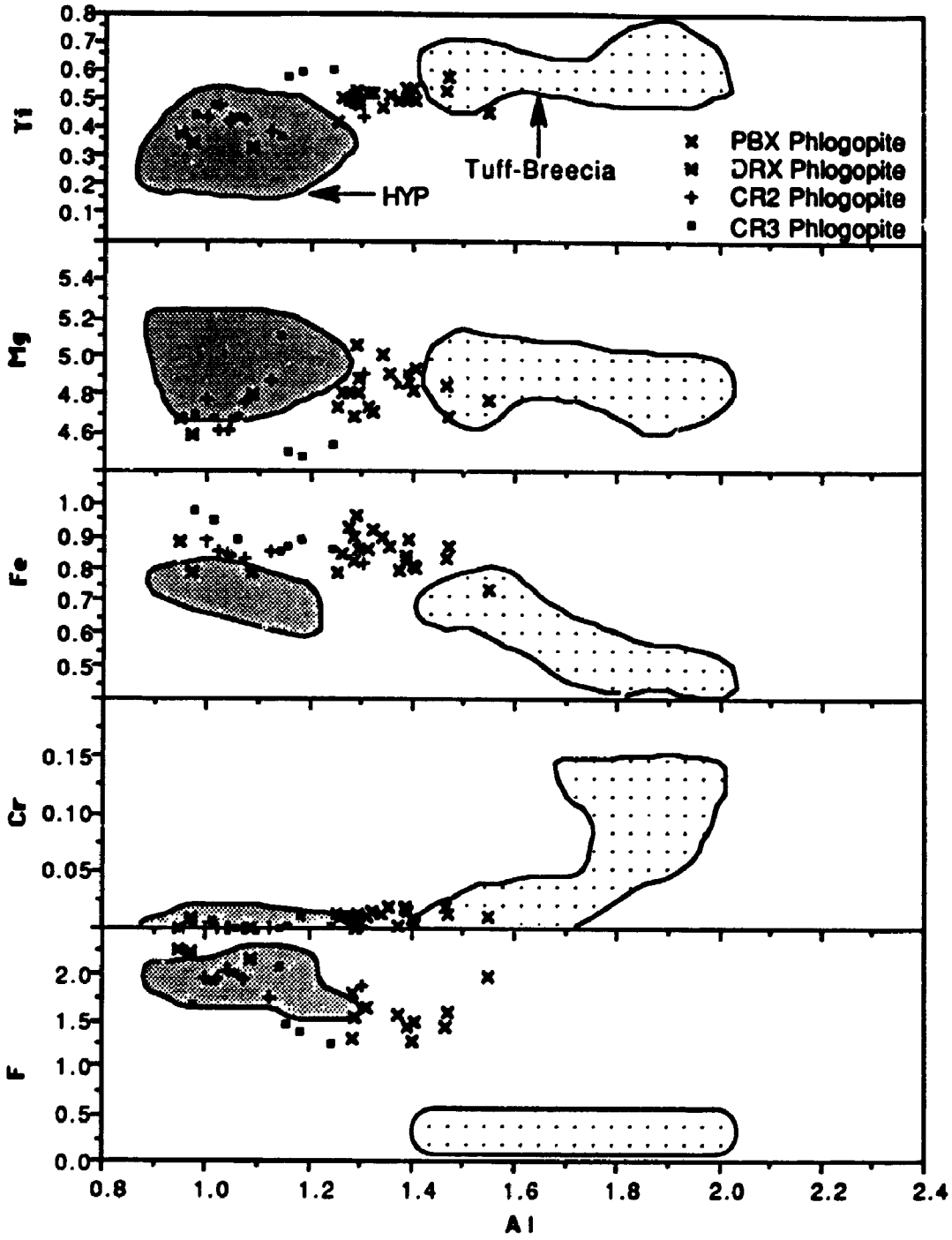

FIGURE 17: Variation diagram of phlogopite analyses from the phlogopite-bearing (PBX) and lenticular diopside-richterite cognate xenoliths (DRX), corona rim 2 (CR2) and corona rim 3 (CR3). The elements plotted and the axes are identical to Figure 22. Overlaid on the diagram are the ranges of phenocrystic phlogopite from the tuff and breccia (▭) and poikilitic from the HYP facies (▭).

plot between the phenocrystic and poikilitic phlogopite data. The higher F values in the PBX are similar to those exhibiting the HYP phlogopite. The phlogopites from the DRX, CR2 and CR3 have lower Al than those in the PBX and tuff-breccia, and are similar in composition to those in the HYP. Three CR3 analyses with higher Ti and lower Mg and F, are similar to the Ti-poik. These analyses are from a corona rim 3 of a DRX hosted in the same HYP sample as the Ti-poik analyses. Owing to the inability to distinguish between the compositions of the CR2 and CR3 phlogopite, they were grouped together and will be referred to as CR2-3. By combining the data plotted in Figures 16 and 17 for the phlogopite analyses from the Prairie Creek rock, a continuous trend of increasing Fe with decreasing Ti and Cr, and constant Mg, with decreasing Al is defined.

5.3.3 Phlogopite analyses from the experiments at pressures greater than 15 + 5 kb, high pressure phlogopite (HPP), and less than 15 + 5 kb, low pressure phlogopite (LPP).

In Figure 18, the LPP and HPP phlogopite analyses from the "no added volatiles", "water added" and "fluorine added" system are plotted and compared with the phlogopite compositional ranges of the tuff-breccia, and HYP facies. The HPP phlogopite analyses plot as a well defined cluster having higher Al, Mg and Cr and lower Ti, Fe and F values than the LPP phlogopite analyses. Compared to the high Al phlogopite analyses from the tuff-breccia, the HPP phlogopite has similar Al, Fe, Cr, and F, higher Mg, lower Ti, and a similar trend of decreasing Al with decreasing Cr.

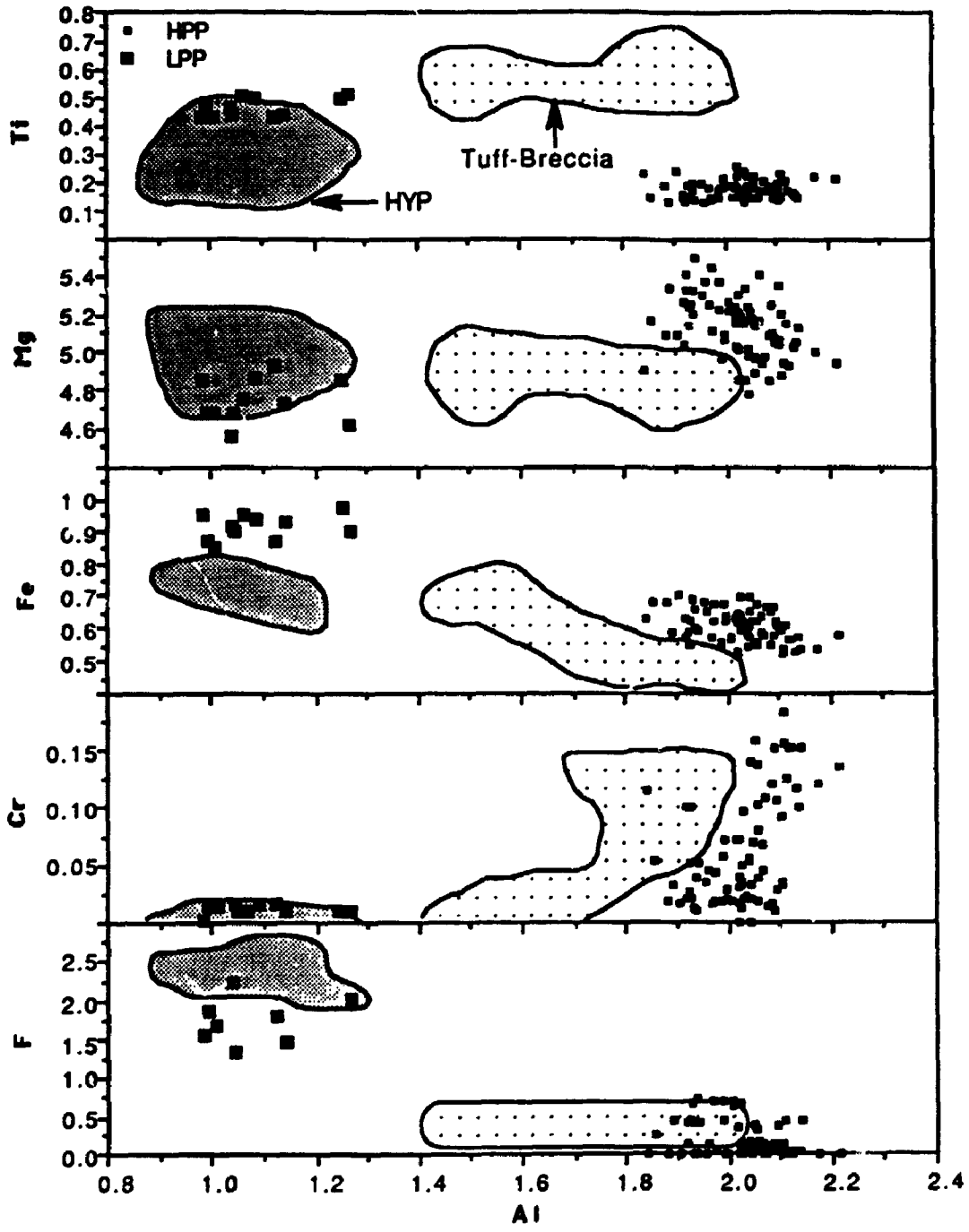

FIGURE 18. Variation diagram of phlogopite analyses from the experimental systems. The elements plotted and the axes are identical to Figure 16 and 17. Overlaid on the diagram are the ranges of phenocrystic phlogopite from the tuff and breccia (⊡) and the poikilitic phlogopite from the HYP facies (◯). The analyses that occur in the experiments above 15 kb (HPP), are similar to the phenocrystic phlogopite compositions, whereas, the phlogopite analyses that occur below 15 kb, are similar to the poikilitic phlogopite analyses.

The LPP are variable in composition, do not consistently follow a discernable trend, and, except for higher Fe and lower F, they are compositionally similar to the phlogopite from the HYP (Figure 18). The change in composition from the HPP to the LPP is characterized by a decrease in Al, Cr, and Mg, and an increase in Fe, F, and Ti. The decrease in Al and Cr, and the increase in Fe and F are the same as the continuous compositional change from the tuff-breccia phlogopite, through to the HYP phlogopite composition.

The HPP analyses vary according to the bulk F content of the experimental systems (Figure 18). In the "fluorine added" system, the HPP exhibits a F composition between 0.25 and 0.75 atoms per formula unit, while the HPP from the "no added volatile" and "water added" systems have less than 0.25 atoms per formula unit of F.

5.3.4 Investigating the elemental substitution mechanisms of phlogopite.

Figure 19 demonstrates that all the phlogopite analyses from the study, with the exception of six HPP, have Si + Al equalling less than 8. The phlogopite from tuff-breccia, and HYP define a trend of decreasing Al and increasing Si with increasing tetrahedral site deficiency. This is opposite to the trends defined by the phlogopite from the PBX and the LPP and HPP, which define a trend of decreasing Al and increasing Si with decreasing tetrahedral site deficiency. The difference between the HPP and LPP in Figure 19C, corresponds to the same trend as that defined in Figure 19A by the phenocrystic phlogopite from the tuff-breccia and the poikilitic phlogopite from HYP. The LPP and HYP phlogopite analyses have the highest Fe, the lowest Al (Figure 16 and 18), and the largest tetrahedral site deficiency (Figure 19). The tuff-breccia and

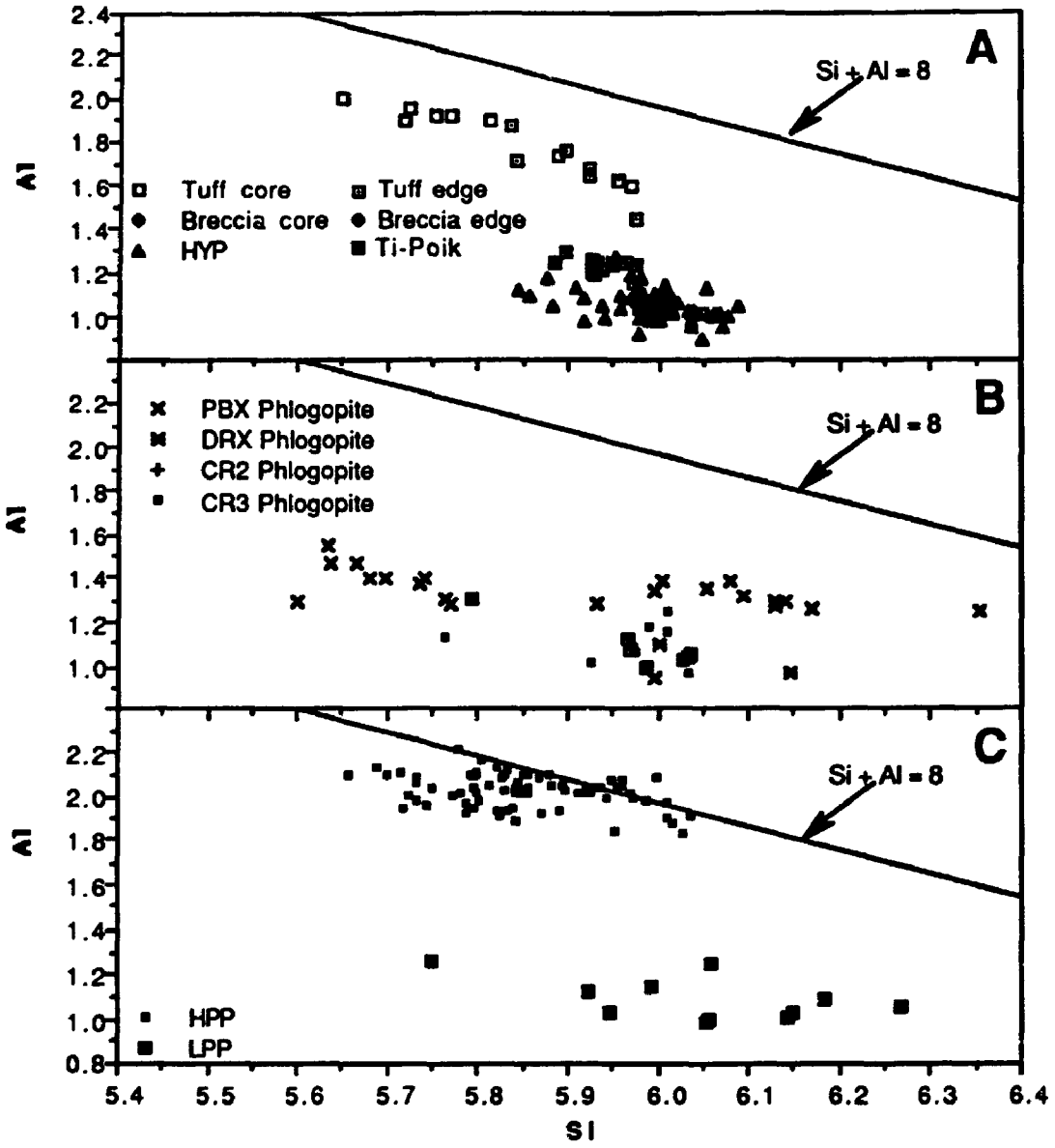

FIGURE 19: Diagram demonstrating the variation of Al relative to Si for all phlogopite analyses. The line Si + Al = 8 represents a balanced tetrahedral site. In all but a few HPP (high pressure phlogopite) analyses, Al values are insufficient to fill the tetrahedral site vacancy.

HPP core analyses have the highest Al, the lowest Fe (Figure 16 and 18) and the least amount of tetrahedral deficiency of all the phlogopites analyzed (Figure 19).

The occupancy of the phlogopite tetrahedral site and the structural position of Ti^{4+} in phlogopite have been discussed in several studies (Forbes and Flower 1974; Wendlandt 1977; Robert 1976; Velde 1979; Mansker et al. 1979; Arima and Edgar 1981; Trønnes et al. 1985; Wagner and Velde 1986; Mitchell and Bergman 1991; Guo and Green 1990). From these studies, the main substitution mechanisms that appear to be reasonable for the Al-deficient phlogopites in lamproites are:

$2\,{}^{VI}Mg^{2+} = {}^{VI}Ti^{4+} + \square$	Forbes and Flower (1974)	(1)
$Mg^{2+} + 2Si^{4+} = Ti + 2\,{}^{IV}Al^{3+}$	Robert (1976)	(2)
${}^{VI}Mg^{2+} + Si^{4+} = Ti^{4+} + {}^{IV}Mg^{2+}$	Wagner and Velde (1986)	(3)
${}^{VI}Mg^{2+} + 2OH^{-} = {}^{VI}Ti^{4+} + 2O^{-}$	Arima and Edgar (1981)	(4)
$Ba+3Ti+4Al+ = 2K+4(Mg,Fe)+4Si$	Guo and Green (1990)	(5)

The correlation of the phlogopite data from the present study to the substitutions (1) and (2) is evaluated in Figures 20 and 21. None of the phlogopite analyses conform to either of the two ideal substitutions, and as a result they are not considered further. The study by Wagner and Velde (1986) would suggest that the positive correlation between Ti and Si + Al + Cr, found to exist in this study and plotted in Figure 22, would mean that substitution (3) is not a feasible substitution mechanism. Substitution (4) can not be evaluated

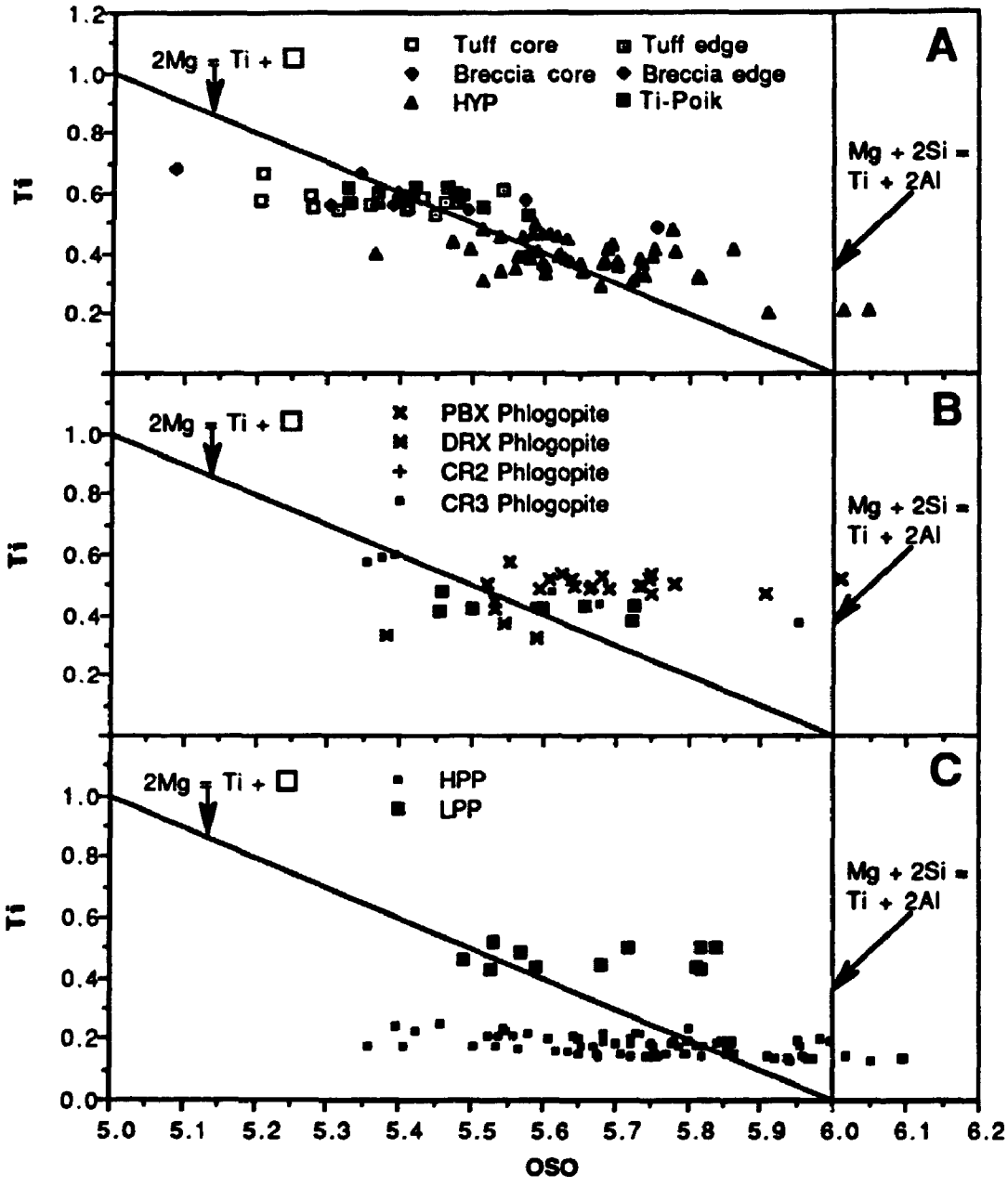

FIGURE 20: Diagram testing the correlation of the phlogopite data to the substitution mechanism $2^{IV}Mg = {}^{VI}Ti + \square$ (1) and $Mg + 2Si = Ti + 2^{IV}Al$ (2). The lack of correlation between the phlgopite data and the lines marking substitution numbers (1) and (2), indicates the chemical variation of the analyses is not a function of either substitution mechanism. OSO = octahedral site occupancy.

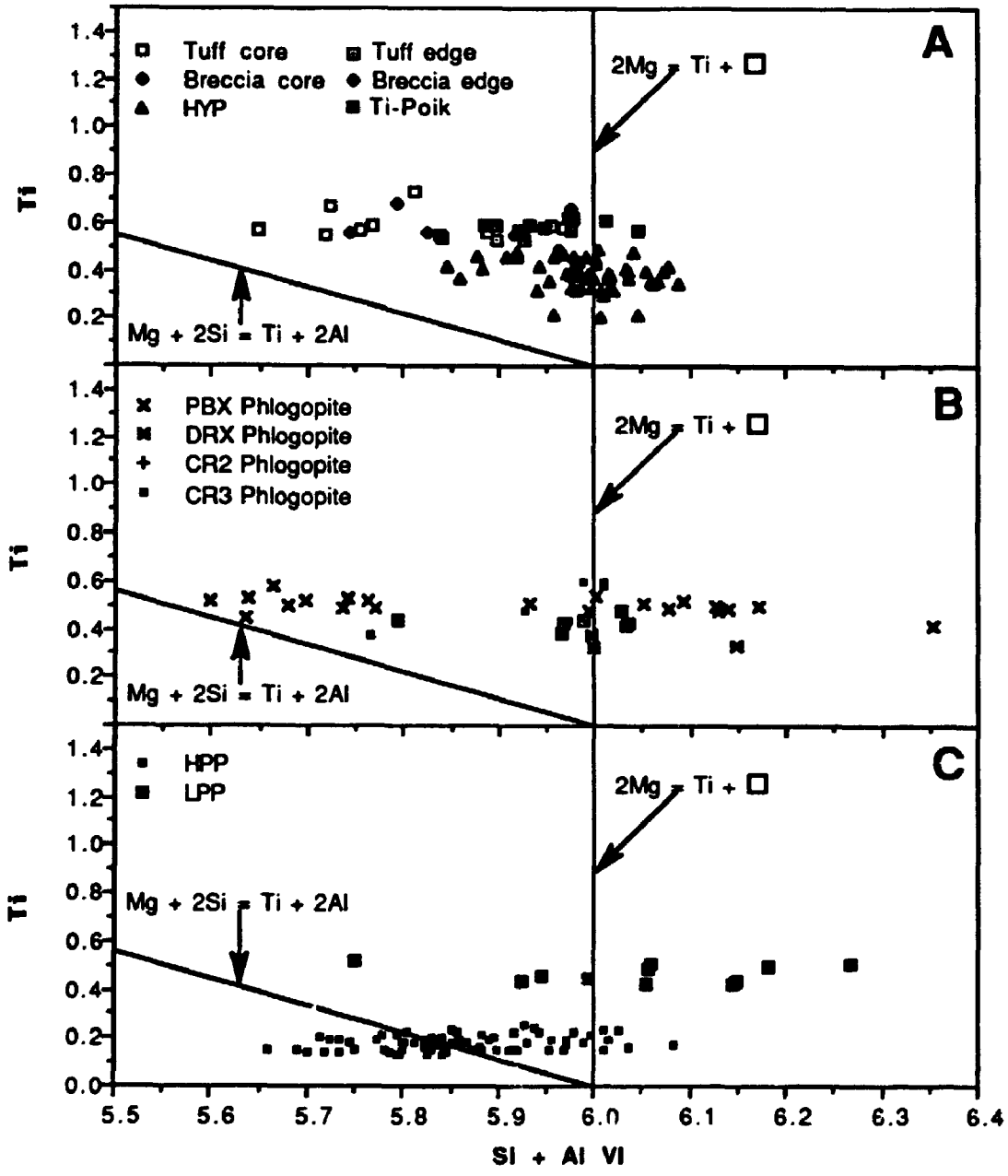

FIGURE 21: Diagram also testing the feasibility of substitution mechanisms (1) and (2). As in Figure 20, the phlogopite analyses do not correlate with either substitution mechanism.

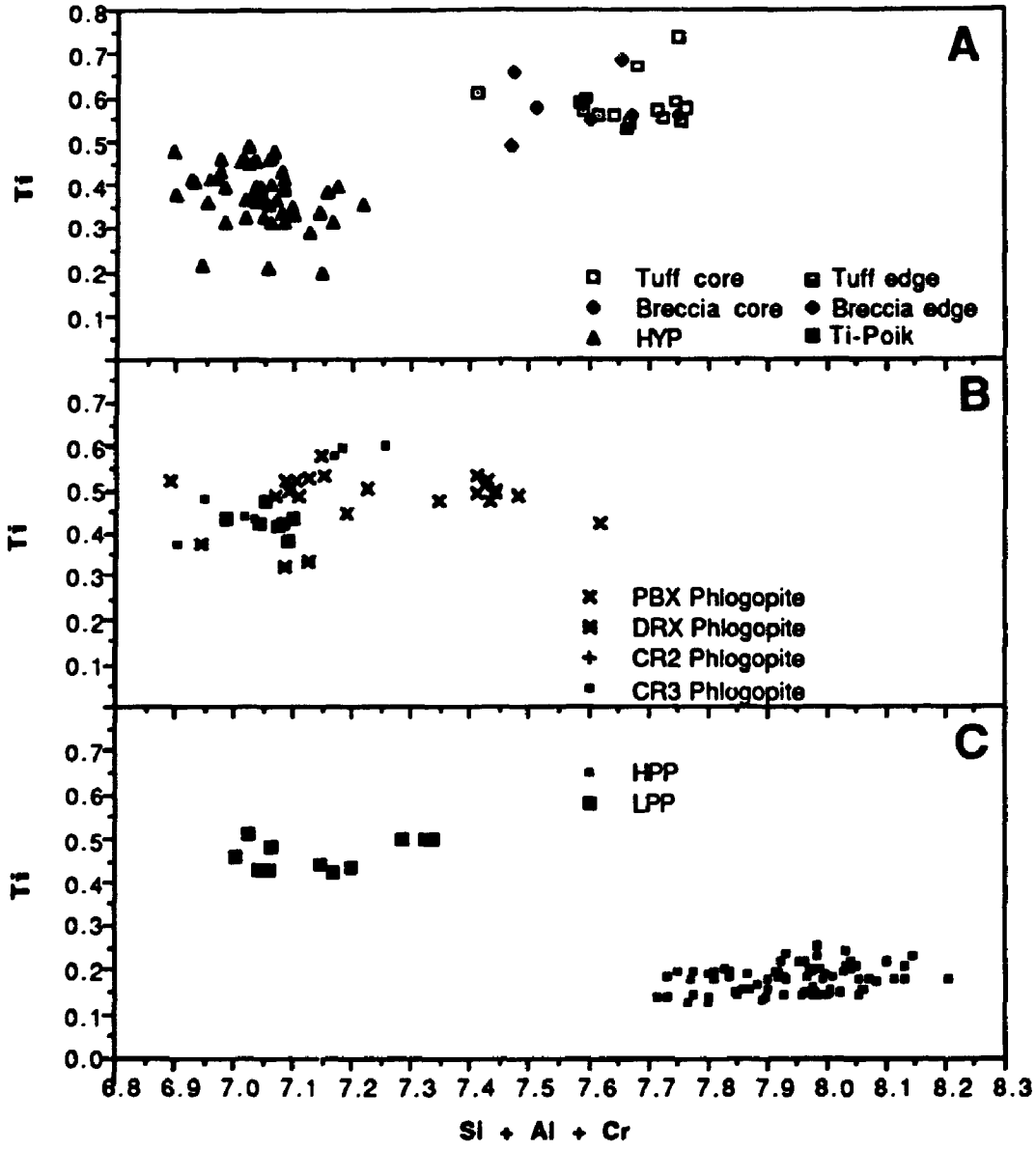

FIGURE 22: Diagram testing the correlation of the phlogopite data to the substitution mechanism VIMg + Si = Ti + IV Mg (3). The variation of phlogopite compositions do not consistantly follow a negative correlation. As a result, it is unlikely substitution (3) can account for the chemical variation of the phlogopite chemistry (Wagner and Velde 1986).

due to the absence of water data for the phlogopite analyses. Phlcgopite analyses from the present study appear to correlate with substitution (5), even though the analyses are not high Ba phlogopites (Figure 23). The LPP and poikilitic phlogopite have a lower Ba + 3Ti + 4Al than the HPP and phenocrystic phlogopite analyses. The poikilitic phlogopite from PBX have Ba + 3Ti + 4Al values between those in the LPP and HPP, and values similar to the poikilitic and LPP phlogopite analyses. The HPP and phenocrystic phlogopite plot in the same relative region as the high pressure phlogopites from Guo and Green (1990). However, owing to the lack of a direct correlation between the data from the present study to the ideal substitution lines in Figure 23, substitution (5) is not considered to model the variation of the phlogopite substitution.

The inability to identify a substitution mechanism tc explain the variations of phlogopite in the present study is considered to be primarily a result of the absence of Fe^{3+} data. A similar conclusion was reached by Mitchell (1981) in trying to model the variation of phlogopite chemistry from the lamproites in West Kimberley, Western Australia. Mitchell (1981) identified a trend of decreasing Al with increasing Fe, and suggested the coupled substitution $3K^{+}_{xii} + 2(Mg,Fe)^{2+}_{vi} + Al^{3+}_{iv} = Ti^{4+}_{vi} + \square_{vi} + \square_{xii} + Fe^{3+}_{iv} + (Ba^{2+},Na^{+})_{xii}$ (modified by Mitchell and Bergman 1991). It is proposed that this substitution may be more reasonable, but can not be fully evaluated in the present study.

The absence of Fe^{3+} data inhibits the identification of the substitution mechanism controlling the variation in chemistry of the phlogopites. This is especially important with respect to the phlogopite from the present study, because Fe and the vacancy in the tetrahedral site increases as Al decreases.

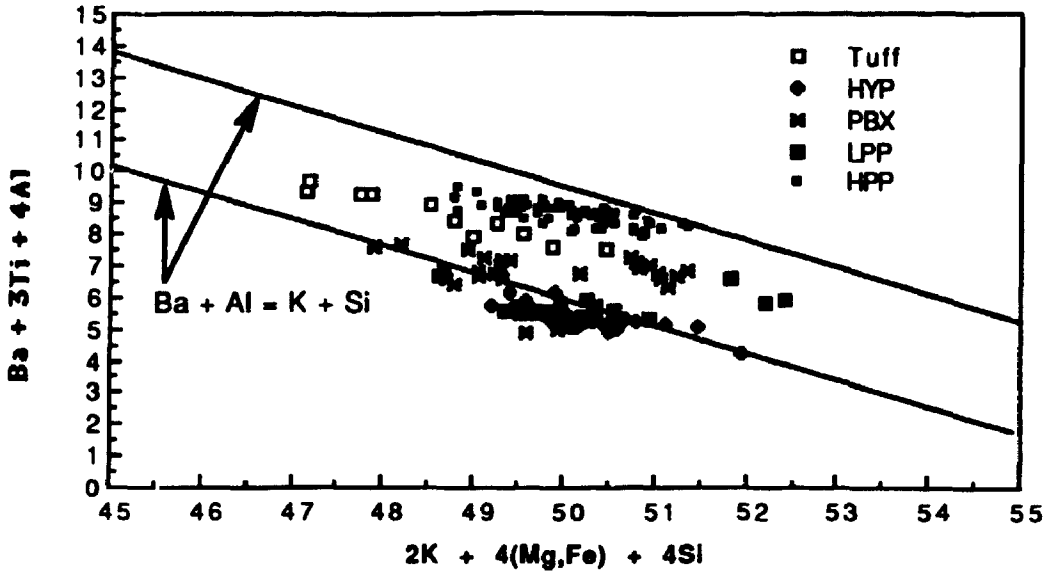

FIGURE 23: Diagram testing the correlation of the phlogopite analyses to substitution mechanism number (5). None of the analyses, nor the differences between the groups, correlate directly with any of the ideal substitution lines marked on the diagram. However, the analyses do appear to have a negative correlation, Ba + 3Ti + 4Al increases as 2K + 4(Mg,Fe) + 4Si decreases. Phlogopite analyses from the tuff, hypabyssal facies (HYP), phlogopite-bearing cognate xenolith (PBX), less than 15 kilobars (LPP), and greater than 15 kilobars (HPP).

The effects of temperature on the chemical composition of the HPP was also investigated. None of the elements in the phlogopite appeared to have a strong correlation with temperature, although Al and Ti decrease sightly as temperature decreases from the liquidus (Figure 24).

5.3.5 Tetraferriphlogopite in the hypabyssal facies

Phlogopite analyses with a high tetraferriphlogopite composition ($K_2(Mg,Fe)_6Si_6Fe_2^{3+}O_{20}(OH)_4$) occur along the outside margins of the poikilitic phlogopite in the HYP and PBX. Phlogopite analyses from both locations are compared to representative phenocrystic and poikilitic phlogopite analyses from the present study in Table 10. The composition of the phlogopites with the high tetraferriphlogopite component differs from the phenocrystic and poikilitic phlogopite by having higher Fe and Na, and lower Al and Ti. The tetraferriphlogopite compositional data represent a low Al and Ti high Fe and F (Figure 25) extension of the trends defined in Figures 16, 17, and 18.

5.2.6 Comparison of phlogopite analyses from other olivine lamproites.

In Figure 26, the phlogopite analyses from the present study are compared to the phenocryst and groundmass phlogopite analyses from other olivine lamproites. Micro-phenocrystic and groundmass phlogopites from the Ellendale olivine lamproite are chemically similar to the phenocryst phlogopite from the tuff and breccia facies of rock in the Prairie Creek intrusion. Analyses of groundmass phlogopite from the Ellendale, Kapamba (Scott-Smith et al. 1989) and Kimberlite Mine (Scott-Smith and Skinner 1984b) olivine lamproites indicate that they are compositionally similar to the poikilitic and tetraferriphlogopites from the Prairie Creek HYP facies. Phlogopite data from

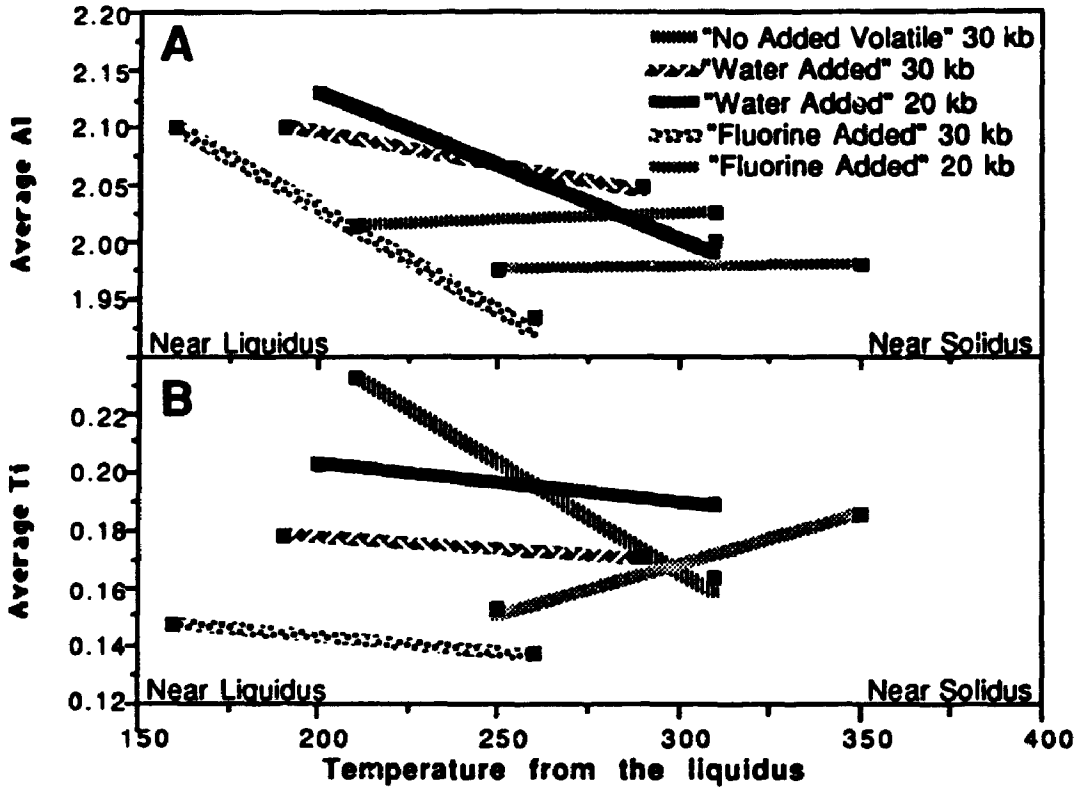

FIGURE 24: Diagram illustrating the change in Al and Ti for the HPP phlogopites as temperature decreases from the liquidus. The diiferent line patterns correspond to different isobaric sections from all three of the experimental systems.

TABLE 10: Comparison of representative tuff and HYP facies phlogopite analyses to the tetraferriphlogopites from the HYP facies.

	Tetraferriphlogopite			Tuff	HYP
SiO2	45.00	44.27	45.45	40.22	42.41
TiO2	1.73	2.05	1.35	5.26	4.40
Al2O3	2.20	3.51	0.60	11.34	7.21
Cr2O3	0.09	bld	0.14	0.42	bld
FeO*	11.60	11.20	15.15	4.92	7.73
MnO	0.02	0.00	0.27	0.06	bld
MgO	22.96	22.76	19.10	22.20	22.80
CaO	0.10	0.09	0.02	0.00	0.05
K2O	9.79	9.91	10.34	10.47	9.78
Na2O	1.76	1.80	2.91	0.10	0.65
BaO	0.72	0.66	nd	0.19	1.16
F	5.45	5.37	nd	0.49	4.24
Total	101.42	101.62	95.33	95.67	100.43
F=O	2.29	2.26		0.21	1.79
Total	99.21	99.36	95.33	95.46	98.64
Mg number	77.92	78.37	69.21	91.93	84.02
Structural formula calculations based on 22 oxygens					
Si	6.280	6.163	6.897	5.754	5.878
Ti	0.182	0.215	0.154	0.566	0.459
Al	0.375	0.576	0.107	1.912	1.178
Cr	0.010	0.000	0.017	0.048	0.000
Mn	0.002	0.000	0.035	0.007	0.000
Fe	1.354	1.304	1.923	0.589	0.896
Mg	4.777	4.723	4.321	4.735	4.711
Ca	0.015	0.013	0.003	0.000	0.007
Ba	0.039	0.036	0.000	0.011	0.063
K	1.743	1.76	2.002	1.911	1.729
Na	0.476	0.486	0.856	0.028	0.175
F	2.405	2.364	0.000	0.222	1.859
Total	17.658	17.640	16.315	15.783	16.955

Mg number = 100Mg/(Mg+Fe); *FeO is total Fe; nd=not determined; bld=below detection.

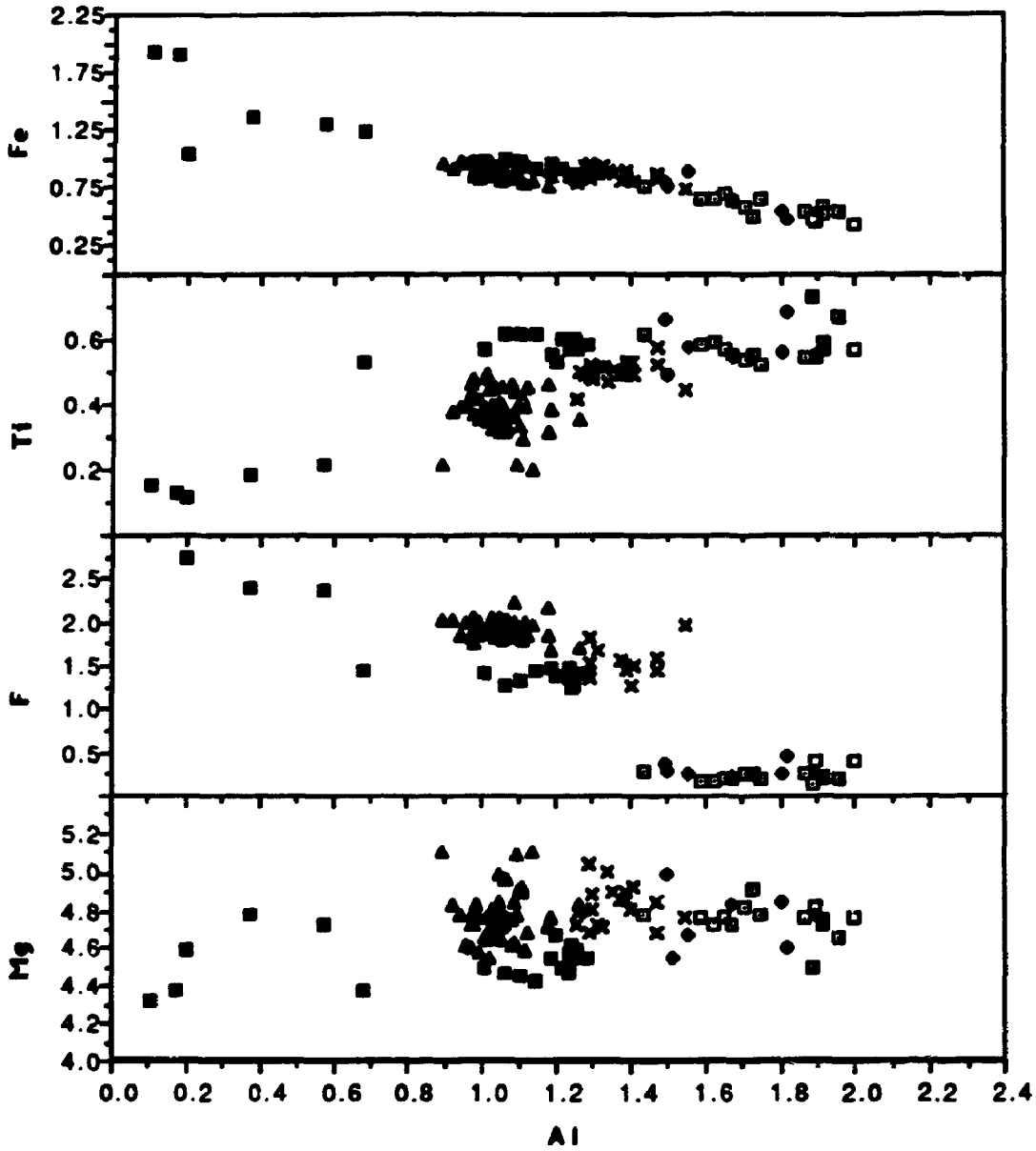

FIGURE 25: Variation diagram comparing the tetraferriphlogopite analyses to analyses from the tuff and breccia, HYP facies, Ti-poik, and PBX. The tetraferriphlogopite analyses are the low Al and high Fe extension of the trend defined by the poikilitic and phenocrystic phlogopite compositions.

- Tuff core
- Tuff edge
- Breccia core
- Breccia edge
- HYP
- Ti-Poik
- PBX
- Tetraferriphlogopite

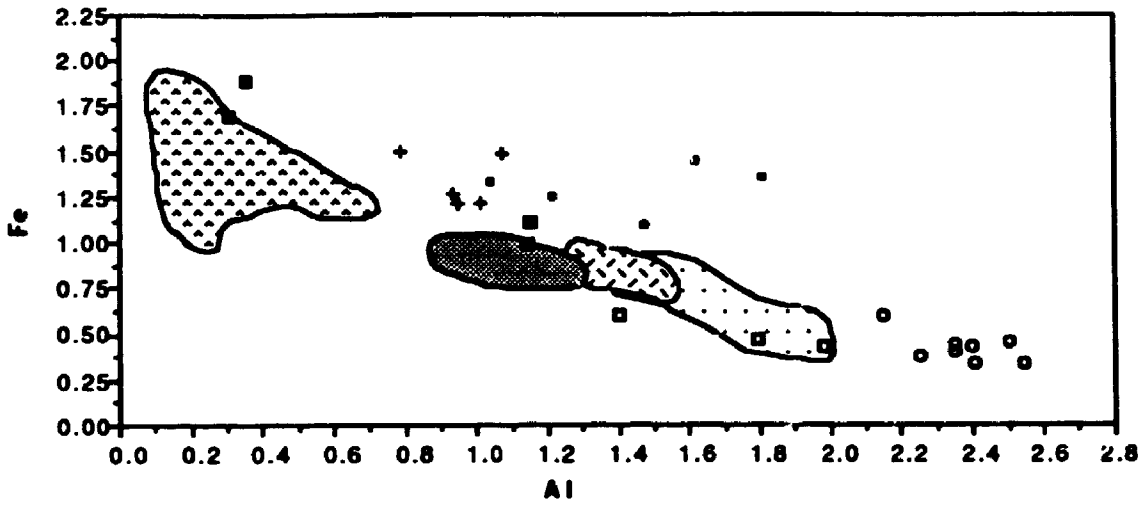

FIGURE 26. Comparison of the Prairie Creek phenocrystic, poikilitic and tetraferriphlogopite compositions compared to phenocrystic and poikilitic (groundmass) phlogopite compositions from other olivine lamproites. Ellendale olivine lamproite is the only olivine lamproite plotted from other locations with both phenocrystic and groundmass compositions. The phlogopite compositions from other olivine lamproite sources are similar.

- Ellendale phenocryst (Jaques et al. 1986)
- Ellendale groundmass (Jaques et al. 1986)
- Argyle groundmass (Jaques et al. 1986)
- Kapamba groundmass (Scott-Smith et al. 1989)
- Kimberlite Mine groundmass (Scott-Smith and Skinner 1984a)
- Synthetic Olivine Lamproite (Foley 1990)

Prairie Creek Phlogopite

- Prairie Creek phenocryst
- Prairie Creek Xenolith poikilitic
- Prairie Creek poikilitic (groundmass)
- Prairie Creek Tetraferriphlogopite

the suprasolidus experiments of the olivine lamproite synthetic composition representative of Western Australia olivine lamproites (Foley 1990) are also plotted in Figure 26. These phlogopites crystallized between 20 and 40 kb, in iron-wüstite buffered experiments, where CH_4 was an important volatile species. The lower Al phlogopites from the synthetic olivine lamproite are compositionally similar to the phenocrystic phlogopite from the Prairie Creek HYP facies, but most of the analyses have a higher Al and lower Fe than the Prairie Creek phlogopite. The phlogopite Al values from the synthetic olivine lamproite are also much higher than those in the HPP from the present study. The phlogopite chemistry plotted from other olivine lamproites in Figure 26, although somewhat variable, is considered to be part of the same Fe and Al trend defined by the phlogopite chemistry from the Prairie Creek intrusion. Based on the results from the experiments of the Prairie Creek HYP facies, the decrease in Al with an increase in Fe could be a function of the crystallization of phlogopite at successively lower pressures.

5.4 Spinel

Spinels occurring in lamproites have been divided into four groups based on their composition (Mitchell 1985). Three of these groups are used to define a compositional trend indicative of spinels that have crystallized from lamproitic magmas (Mitchell 1985). The composition of spinels from the Prairie Creek HYP facies of rock follows such a trend, and to some degree, so do the spinel compositions from the suprasolidus experiments of the HYP facies. In order to determine the genesis of spinels in the Prairie Creek intrusion, the

chemical composition of the spinels from the HYP facies are compared to the those from the experimental charges. The results are then compared to spinel analyses from other olivine lamproites.

Microprobe analyses of spinel from the HYP facies and all three of the experimental systems (Table 11) were obtained. The results are presented in atomic formula units based on four oxygens. Fe^{2+} and Fe^{3+} were calculated from FeO_{Total} based on spinel stoichiometry (Finger 1972).

Owing to the distinct mantling of the spinels in the HYP facies, data is divided into two groups: those taken from the core of the minerals, and those from the margin. The core and margin analyses form a single continuous trend of decreasing Cr with increasing Ti (Figure 27), and increasing Fe^{2+} with increasing and Fe^{3+} (Figure 28). The core data plot along the entire trend and are well defined, whereas the margin data indicate a more variable composition, and except for a few points, occur only with the high Ti and low Cr values. The calculated end member compositions (Table 11) demonstrate that the trend from core to margin is one of decreasing amounts of chromite and increasing amounts of magnetite and ulvöspinel.

The spinel from the "no added volatile", "water added", and "fluorine added" experimental systems are chemically more complex than the spinel from the HYP facies. The analyses are divided into four groups according to their dominant calculated end member composition: "chromite"; "magnetite", "transitional" (between magnetite and ulvöspinel), and "ulvöspinel-magnetite" (Table 11). The field of stability of each mineral group with respect to pressure

TABLE 11: Representative spinel compositions from the experimental systems and the hypabyssal rock.

	Experimental System						Hypabyssal Facies of Rock			
Series:	Ulvospinel-Magnetite		Magnetite	Transitional		Chromite	HYP facies			
	EPC 45	FPC 8	EPC 50	EPC 52	PCW 28	EPC 10	Core	Core	Edge	Edge
TiO2	24.05	33.72	4.95	13.43	16.41	2.60	2.69	3.21	9.50	9.32
Al2O3	0.63	0.53	3.39	5.02	10.09	4.71	0.94	3.37	0.01	0.07
Cr2O3	10.70	2.96	16.97	25.37	32.07	55.70	50.94	45.23	13.74	11.10
FeOT*	57.10	55.50	59.71	41.36	19.53	20.25	37.05	39.46	66.73	70.08
MnO	0.00	0.01	0.47	0.39	0.41	0.32	0.92	0.84	1.18	1.23
MgO	5.88	6.51	9.91	12.61	20.09	13.59	5.04	5.47	3.68	3.90
Total	98.36	99.23	95.4	98.18	98.60	97.17	97.58	97.58	94.84	95.70
FeO	44.55	52.37	20.68	24.99	16.88	13.27	25.46	25.79	32.80	32.60
Fe2O3**	13.95	3.48	43.37	18.19	2.95	7.76	12.88	15.17	37.71	41.65
Total	99.76	99.58	99.74	100.00	98.90	97.95	98.87	99.08	98.62	99.87
Structural formula calculations based on 4 oxygens										
Ti	0.647	0.901	0.129	0.337	0.385	0.066	0.073	0.086	0.267	0.259
Al	0.027	0.022	0.139	0.198	0.371	0.187	0.040	0.142	0.000	0.003
Cr	0.303	0.083	0.467	0.67	0.791	1.484	1.461	1.277	0.406	0.324
Fe2+	1.334	1.556	0.602	0.698	0.440	0.374	0.773	0.409	1.025	1.006
Fe3+	0.376	0.093	1.135	0.457	0.069	0.197	0.352	0.770	1.060	1.156
Mn	0.000	0.000	0.014	0.011	0.011	0.009	0.028	0.025	0.037	0.038
Mg	0.314	0.345	0.514	0.628	0.934	0.683	0.273	0.291	0.205	0.214
Total	3.001	3.000	3.000	2.999	3.001	3.000	3.000	3.000	3.000	3.000
Mole proportion end member calculations										
MgAl2O4	0.88	0.74	4.73	7.00	14.08	6.57	1.31	4.70	0.01	0.10
Mg2TiO4	11.21	12.55	9.94	21.16	32.06	5.22	5.40	6.45	7.32	7.71
Mn2TiO4	0.00	0.02		0.61	0.64				1.84	1.82
Fe2TiO4	51.68	76.87		7.50	0.61				14.53	13.40
MnCr2O4			1.48			1.01	2.89	2.64		
MgCr2O4			17.06			43.44	9.33	4.29		
FeCr2O4	15.76	4.36	3.65	37.36	47.23	30.45	62.26	58.97	20.23	16.35
Fe3O4	20.14	5.09	62.88	26.40	4.17	11.25	18.67	22.06	54.64	60.43

*FeOT is total Fe, **Fe2O3 calculated based on stoichiometry.

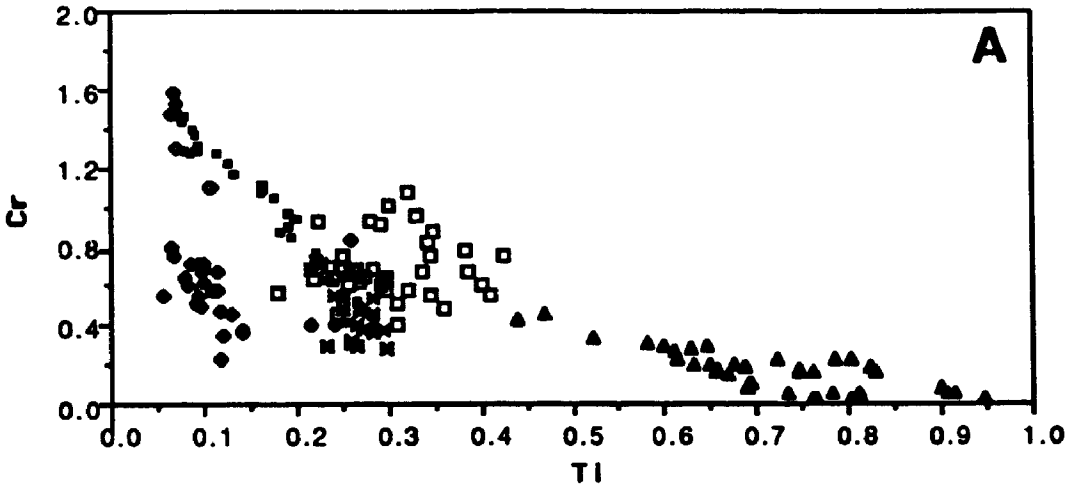

FIGURE 27: Comparison of spinel analyses from the HYP facies and the three experimental systems. The spinel analyses from the experimental systems are divided into four different series based on the dominant end member composition. Except for the transitional series, each series of analyses independantly, as well as a group, define a trend of decreasing Cr with increasing Ti. The chromite series is similar to the HYP core, and the transitional series is similar to the HYP edge

Spinel from the experiments
- ▲ Ulvospinel - Magnetite Series
- ◆ Magnetite Series
- ● Chromite Series
- □ Transitional Series

Spinel from the hypabysal facies
- ▪ HYP Core
- ✖ HYP Edge

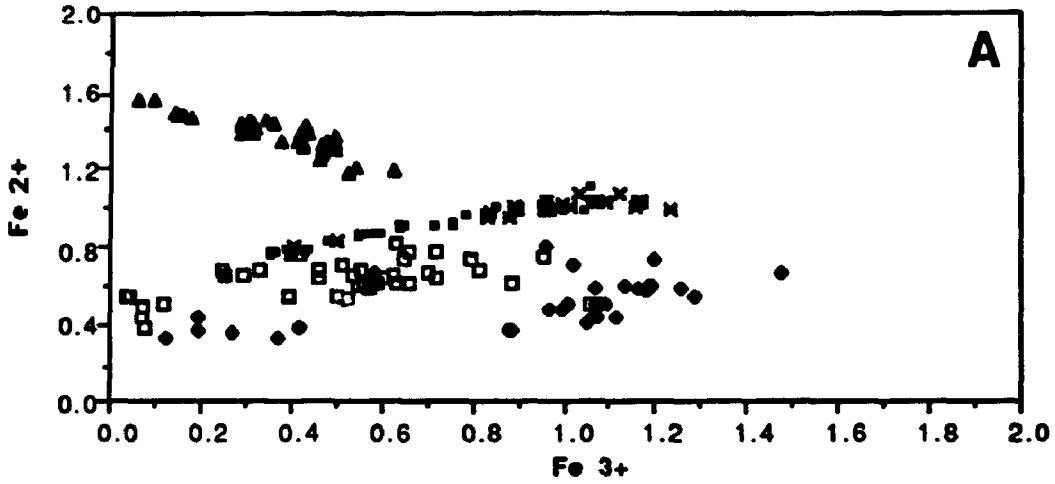

FIGURE 28: Fe^{2+} and Fe^{3+} are calculated based on stoichiometry. All analyses but the ulvospinel - magnetite series define a positive trend. The HYP spinel analyses appear to have slightly higher Fe2+ contents, but the relative increase of Fe2+ to Fe3+ increase is similar.

Spinel from the experiments
- ▲ Ulvospinel - Magnetite Series
- ● Magnetite Series
- ◆ Chromite Series
- □ Transitional Series

Spinel from the hypabysal rock
- • Hypabyssal Core
- ✖ Hypabyssal Edge

and temperature can be outlined for each of the three experimental systems (Figure 29). These fields do not correlate to the silicate phase boundaries described in Figures 5, 6, and 7.

Figure 30 is a plot of the average Cr and Fe^{2+} spinel analyses from each of the experiments versus their temperature from the liquidus. The Cr decreases as temperature increases, and the Fe^{2+} increases as temperature decreases. The relationship of decreasing Cr to increasing Fe^{2+} is the same as the trend defined by the core to margin analyses of spinel from the HYP facies.

The chemical characteristics of each spinel group from the experimental systems are discussed in order of decreasing Cr composition. The chromite series of the experimental system has the highest end member chromite composition of all of the spinels. It defines a trend of decreasing Cr with increasing Ti, (Figure 27) and constant Fe^{2+}, with increasing Fe^{3+} (Figure 28). The Cr, Ti, and Fe^{3+} are similar in amount and relative proportion to the high-Cr core analyses from the spinel in the HYP facies (Figure 27 and 28).

The magnetite series has the highest magnetite end member composition of all the spinel analyses. They plot along the $Fe^{2+}/Fe^{3+} = 0.5$ line, representative of the Fe^{2+}/Fe^{3+} in magnetite (Figure 28). The magnetite series analyses form a short trend of decreasing Cr with increasing Ti, and increasing Fe^{2+} with increasing Fe^{3+}, similar to the trend formed by spinel from the HYP facies and the chromite series. The magnetite series Cr and Fe^{3+} closely resemble the spinel margin analyses from the HYP facies.

FIGURE 29: The distribution of the different spinel compositions within each of the experimental systems as a function of temperature and pressure. The areas of stability are outlined. The silicate phase boundaries are outlined in Figures 5, 6, and 7. The key to the symbols is outlined below.

- + Liquid
- ▲ Olivine + Liquid
- ▲ Olivine + Spinel + Liquid
- ● Olivine + Clinopyroxene + Phlogopite + Liquid
- ■ Olivine + Phlogopite + Liquid
- ■ Olivine + Spinel + Clinopyroxene + Phlogopite + Liquid
- ▣ Olivine + Spinell + Armalcolite+ Liquid
- ✖ Olivine + Spinel + Clinopyroxene + Phlogopite + Perovskite + Apatite + Liquid
- ■ Olivine + Spinel + Clinopyroxene + Perovskite + Liquid
- ◘ Olivine + Spinel + Clinopyroxene + Liquid

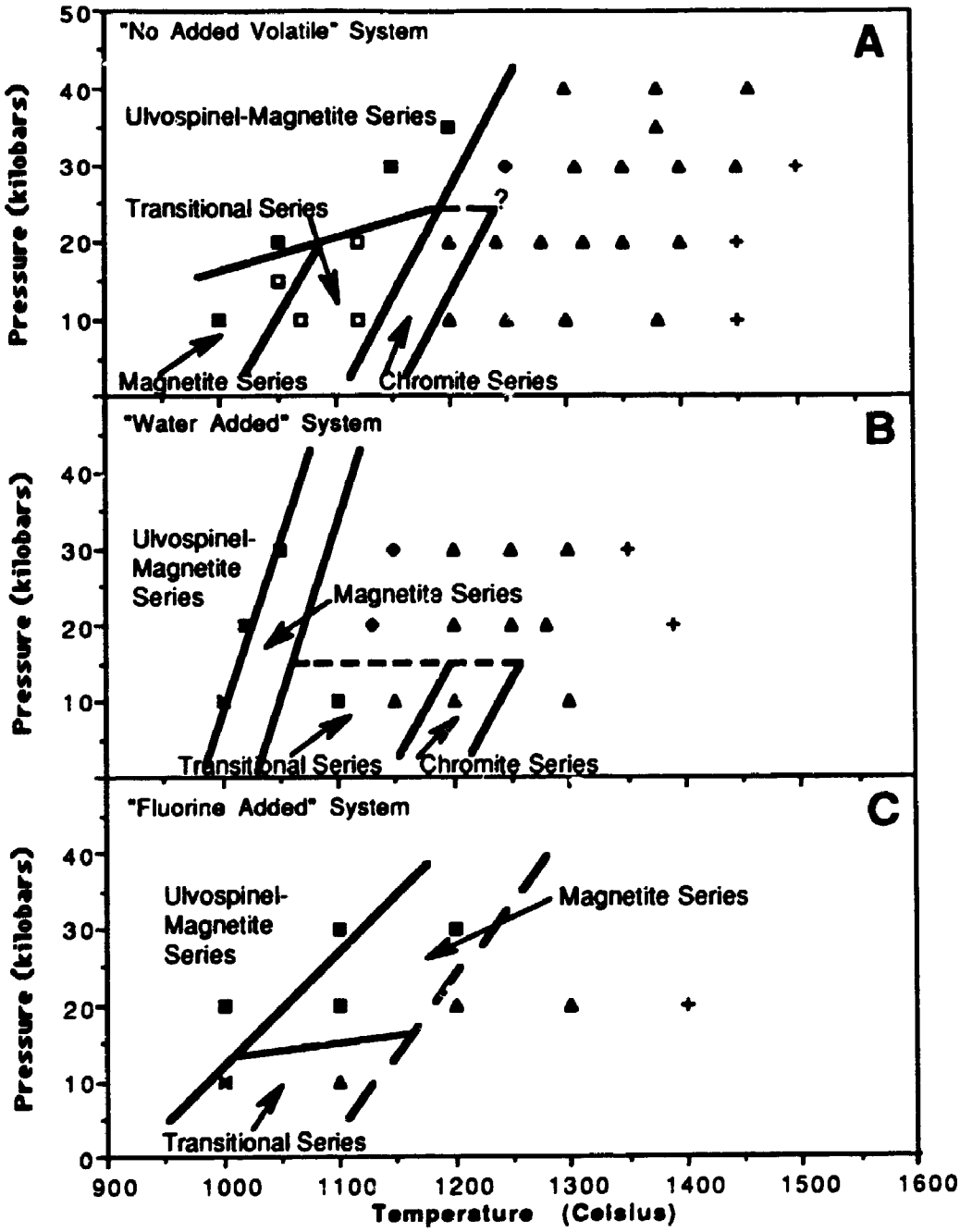
"No Added Volatile" System
A
Ulvospinel-Magnetite Series
Transitional Series
?
Magnetite Series
Chromite Series
"Water Added" System
B
Ulvospinel-
Magnetite
Series
Magnetite Series
Transitional Series
Chromite Series
"Fluorine Added" System
C
Ulvospinel-
Magnetite
Series
Magnetite Series
Transitional Series
Pressure (kilobars)
0
10
20
30
40
50
900
1000
1100
1200
1300
1400
1500
1600
Temperature (Celsius)

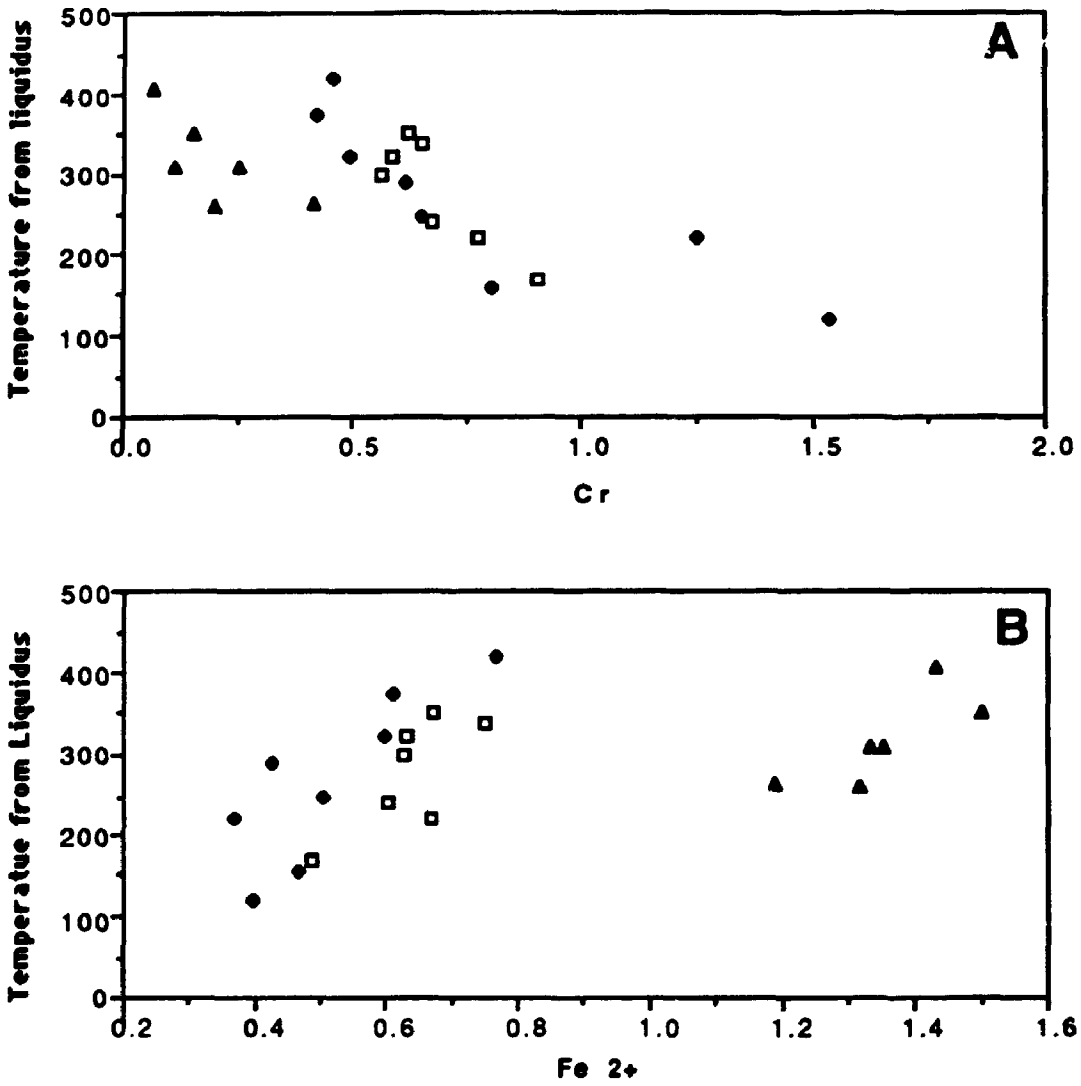

FIGURE 30: Average spinel compositions from each experiment plotted against the temperature from the liquidus of the experiment. Cr appears to be decreasing as the temperature from the liquidus increases, and Fe2+ appears to increase.

- ▲ Ulvospinel - Magnetite Series
- ● Magnetite Series
- ◆ Chromite Series
- □ Transitional Series

The transitional series spinel from the experiments do not form a trend relative to Cr and Ti (Figure 27); however, they do form a well defined trend of increasing Fe^{2+} with increasing Fe^{3+} (Figure 28). The trend in Figure 28 is very similar to that of the spinels from the HYP facies, except the transitional series has lower Fe^{2+} and Fe^{3+} values.

The ulvöspinel-magnetite series of the experimental system form a continuous trend of decreasing Cr with increasing Ti, and increasing Fe^{2+} with decreasing Fe^{3+} (Figure 27 and 28). The decreasing Cr with increasing Ti is analogous to the trends defined by the other spinel analyses; however, the decreasing Fe^{3+} is unique to the ulvöspinel series. This is considered to be a function of the increasing ulvöspinel ($Fe^{2+}TiO_4$) end member composition, while the magnetite ($Fe^{2+}Fe^{3+}{}_2O_4$) end member decreases. The increasing proportion of Fe^{3+} relative to Fe^{2+}, in the other spinels, may be a function of the change in end member composition from chromite ($MgFe^{2+}Cr_2O_4$) to a higher magnetite composition, and in some cases, a higher magnesioferrite ($MgFe^{3+}{}_2O_4$) composition (Appendix 5.4).

In Figure 31A, the spinel analyses are plotted on the front face of a reduced spinel prism. The chromite, magnetite and transitional series of the experimental systems occur as a cluster, having constant Ti/Ti+Cr+Al, with increasing Fe^{2+}/Fe^{2+}+Mg. Owing to the high proportion of ulvöspinel in the ulvöspinel-magnetite series, the analyses plot in the top half of Figure 31A. The ulvöspinel-magnetite series appears to represent an extension of the core to margin trend defined by the spinel analyses from the HYP facies, which have

constant $Fe^{2+}/Fe^{2+}+Mg$ with increasing Ti/Ti+Cr+Al values. The spinel from the HYP facies defines a relatively short trend of increasing Ti/Ti+Cr+Al with increasing $Fe^{2+}/Fe^{2+}+Mg$.

The spinel analyses are also projected onto the front face of the oxidized spinel prism in Figure 31B, where Ti has been replaced by Fe^{3+} at the apex of the prism. The chromite, magnetite, and transitional series plot as a single group of data which increase in $Fe^{2+}/Fe^{2+}+Mg$ with increasing $Fe^{3+}/Fe^{3+}+Al+Cr$. Seven of the transitional series analyses have $Fe^{3+}/Fe^{3+}+Al+Cr$ values separate from the others, and are similar to the chromite series. The ulvöspinel-magnetite form a single linear trend which appears to have a slight decrease in $Fe^{2+}/Fe^{2+}+Mg$ with increasing $Fe^{3+}/Fe^{3+}+Al+Cr$. The trend of the ulvöspinel-magnetite group crosses the core and margin spinel analyses from the HYP facies. Although the slope of the trend defined by these two groups is different, the higher $Fe^{3+}/Fe^{3+}+Al+Cr$ from the HYP facies is similar to that exhibited by the ulvöspinel-magnetite series.

Previous studies examining the composition of spinel from the Prairie Creek HYP facies of rock have indicated a bimodal distribution of analyses based primarily on $Fe^{2+}/Fe^{2+}+Mg$ (Mitchell 1985). Spinel analyses similar to the lower $Fe^{2+}/Fe^{2+}+Mg$ values in the study by Mitchell (1985) are absent in the present study, but are similar in composition to the chromite series from the experiments (Figure 32). The lower $Fe^{2+}/Fe^{2+}+Mg$ values from the HYP facies demonstrate that the composition of spinels from the experiments has a similar trend to that defined by the spinel analyses from the HYP facies.

FIGURE 31A: The spinel analyses from the HYP facies define a relatively short trend of increasing Ti/Ti+Al+Cr with increasing $Fe^{2+}/Fe^{2+}+Mg$. The transitional, magnetite and chromite series have similar Ti/Ti+Al+Cr values as the HYP spinel analyses, but have much lower $Fe^{2+}/Fe^{2+}+Mg$. The ulvospinel-magnetite have similar $Fe^{2+}/Fe^{2+}+Mg$, but higher Ti/Ti+Al+Cr compared to the HYP facies analyses.

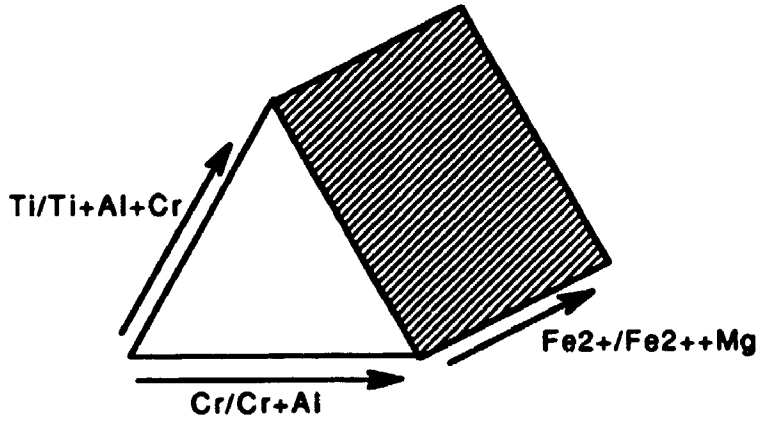

FIGURE 31B: In the oxidized prism, the ulvospinel-magnetite series is similar to the HYP analyses. The other three series have similar to slightly lower $Fe^{3+}/Fe^{3+}+Al+Cr$, and have lower $Fe^{2+}/Fe^{2+}+Mg$. The trend defined by the chromite, magnetite and transitional series spinels is somewhat negative.

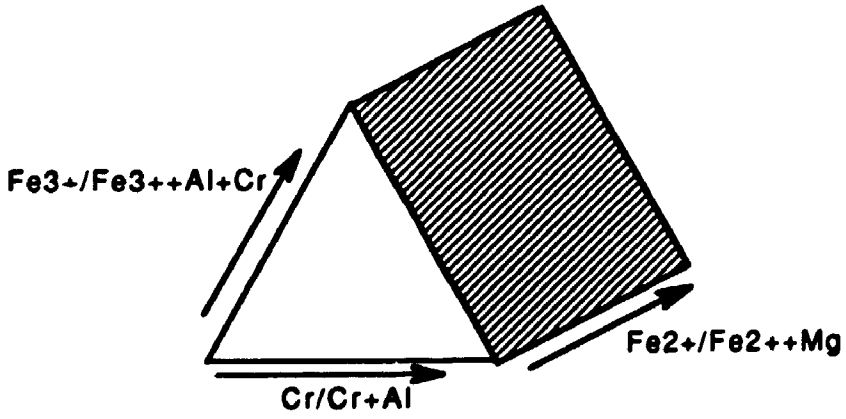

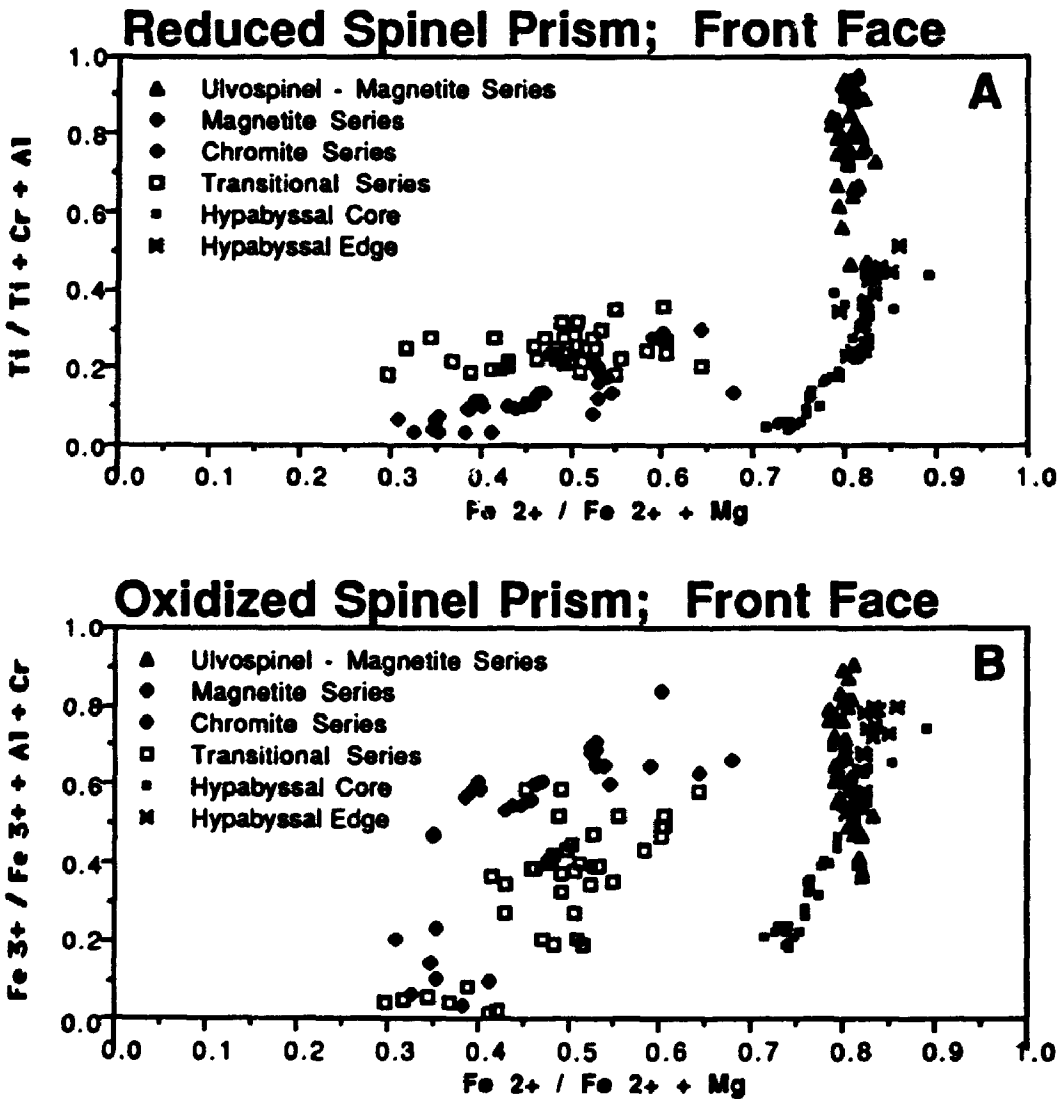
Reduced Spinel Prism; Front Face
A
Ulvospinel - Magnetite Series
Magnetite Series
Chromite Series
Transitional Series
Hypabyssal Core
Hypabyssal Edge
Ti / Ti + Cr + Al
Fe 2+ / Fe 2+ + Mg
Oxidized Spinel Prism; Front Face
B
Ulvospinel - Magnetite Series
Magnetite Series
Chromite Series
Transitional Series
Hypabyssal Core
Hypabyssal Edge
Fe 3+ / Fe 3+ + Al + Cr
Fe 2+ / Fe 2+ + Mg

FIGURE 31:

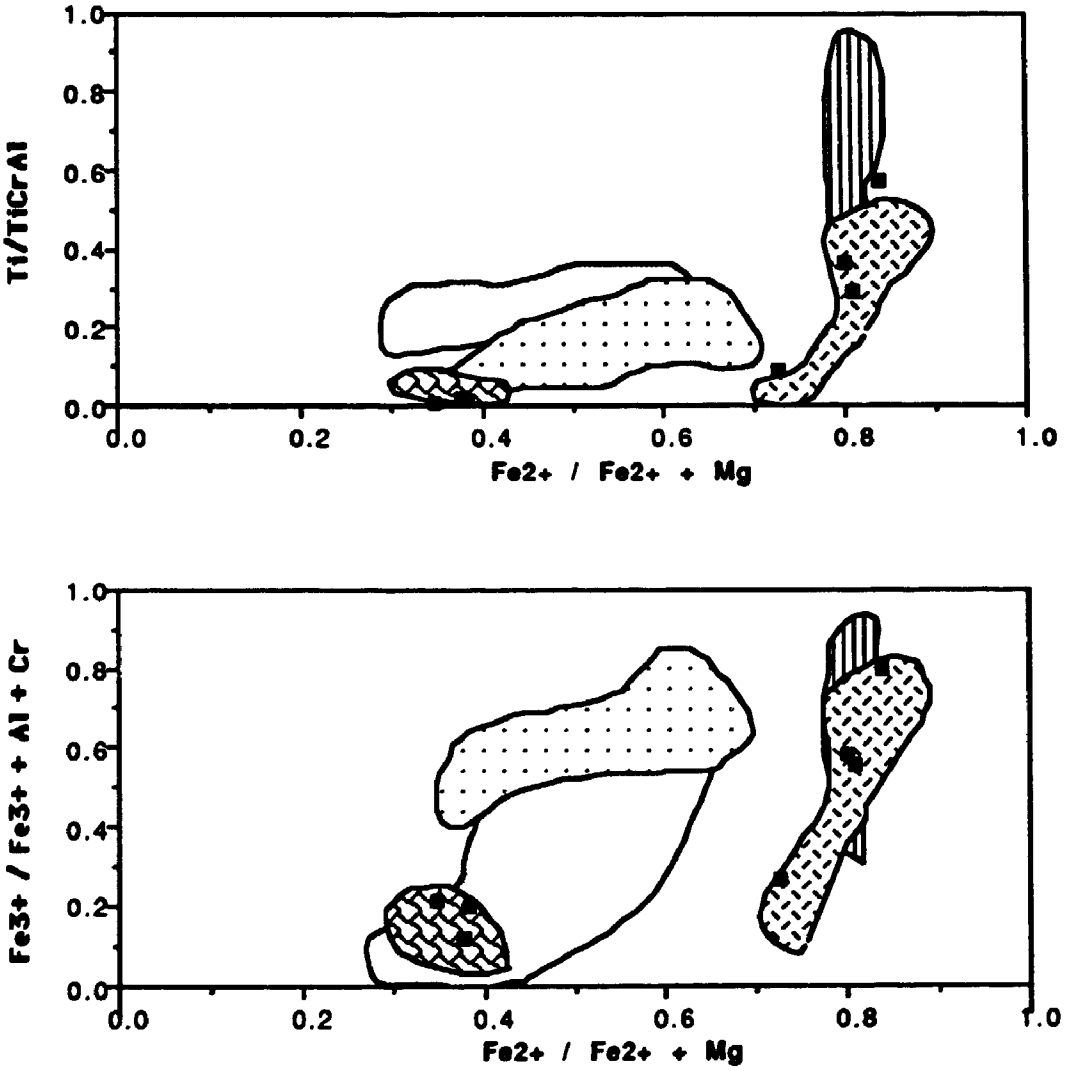

FIGURE 32: Although analyses from the present study do not correspond directly to the chromite series, analyses reported by Mitchell (1985), are compositionally the same. The variation may be a result of spinel compositional variation across the intrusion. The top diagram depicts the front face of the reduced spinel prism, and the bottom diagram depicts the front face of the oxidized prisms.

- HYP facies (Mitchell 1985)
- Ulvospinel - Magnetite Series
- Magnetite Series
- Chromite Series
- Transitional Series
- Hypabyssal Core

With the exception of the magnetite series and many of the transitional series spinel analyses - which have higher $Fe^{3+}/Fe^{3+}+Al+Cr$ values - the trend of decreasing chromite and increasing magnetite and ulvöspinel end members (Figure 31) is similar to the overall range of composition of spinels from lamproites (Figure 33). Within the experiments, the transition of spinel end members from chromite to magnetite-ulvöspinel appears to be a function of spinel crystallization at successively lower temperatures.

5.5 Titan potassic richterite

Amphibole typically occurs in lamproites as Ti-K richterite crystallizing as poikilitic plates paragenetically late in the sequence of crystallization. The Ti-K richterite in lamproites is chemically unique compared to Ti-K richterite compositions from other igneous rocks. Nevertheless, within the lamproite group, the chemical composition of Ti-K richterite varies between regional provinces of lamproites, and between different intrusions from the same province (Mitchell and Bergman 1991). In this section, the chemical composition of Ti-K richterite from the HYP facies and from the columnar and round DRX (Table 12) are compared in order to determine if the composition of the Ti-K richterite in the DRX could be related to an olivine lamproite amphibole composition similar to that of the Prairie Creek HYP facies. The results in each of the figures are presented in atomic formula units based on 23 oxygens.

In Figure 34, the HYP and round DRX Ti-K richterite analyses overlap to form a single continuous trend. The Ti-K richterite in the columnar DRX are slightly different, with lower Ti and Fe, and the higher Mg, Cr, and Ca. Six of the nine analyses are from the same columnar DRX that have Cr-diopsides. The Ti-

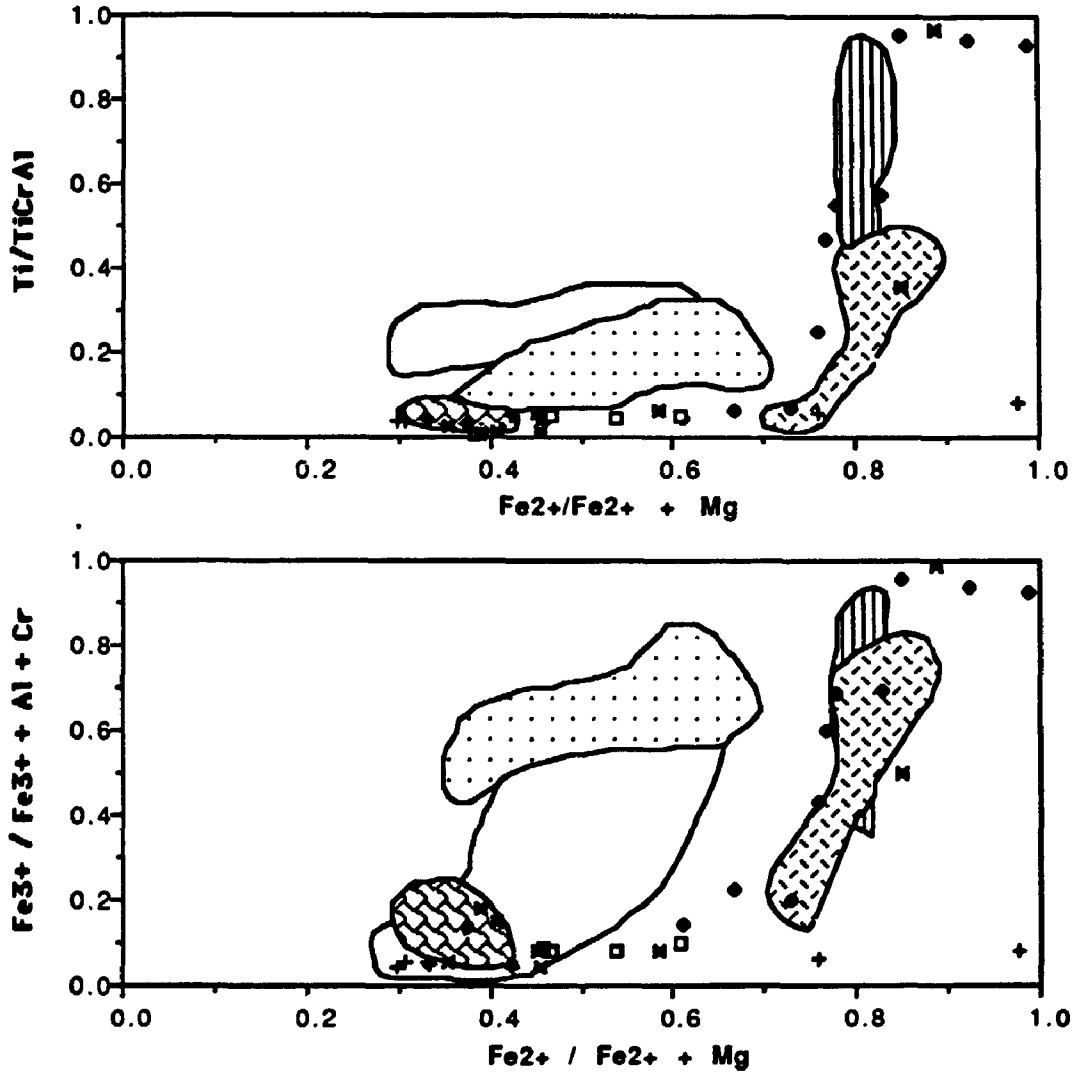

FIGURE 33: Comparison of the spinel analyses from the present study to those from other olivine lamproites. Except for a higher magnesioferrite end member composition in the transitional and magnetite series, the spinel compositions are similar. The top diagram depicts the front face of the reduced spinel prism, and the bottom diagram depicts the front face of the oxidized prisms.

- + Argyle (AK1) (Jaques et al. 1989)
- ✖ Ellendale (Jaques et al. 1984)
- ● Kapamba (Scott-Smith et al. 1989)
- ◘ Kimberlite Mine (Scott-Smith and Skinner 1984)

- Ulvospinel - Magnetite Series
- Magnetite Series
- Chromite Series
- Transitional Series
- Hypabyssal Core

TABLE 12: Representative Ti-K richterite compositions from the hypabyssal facies, and the round and lenticular diopside-richterite cognate xenoliths.

	DRX				HYP facies	
	Columnar		Round			
SiO2	57.35	56.41	51.52	54.71	54.34	54.20
TiO2	0.50	0.31	5.60	3.05	3.49	2.83
Al2O3	0.17	0.04	0.25	0.07	0.57	0.65
Cr2O3	1.05	0.16	0.00	0.23	0.03	0.05
MnO	0.06	0.04	0.15	0.13	0.09	0.12
FeO*	1.38	0.98	6.48	4.42	4.03	3.08
MgO	21.77	22.51	18.81	20.37	20.40	21.97
CaO	6.19	6.76	4.25	4.31	5.95	6.43
K2O	5.11	5.27	5.14	5.12	5.17	4.93
Na2O	4.46	4.08	5.28	5.13	4.26	4.28
F	2.89	3.24	2.51	3.43	2.48	3.05
Total	100.93	99.80	99.99	100.97	100.81	101.59
F≡O	1.22	1.36	1.06	1.44	1.04	1.28
Total	99.71	98.44	98.93	99.53	99.77	100.31
Mg number	96.6	97.6	83.8	89.1	90.0	92.7
Structural formula calculations based on 23 oxygens.						
Si	7.784	7.739	7.292	7.541	7.504	7.407
Al	0.027	0.006	0.042	0.011	0.093	0.105
Ti	0.051	0.032	0.596	0.316	0.362	0.291
Cr	0.113	0.017	0.000	0.025	0.003	0.005
Mn	0.007	0.005	0.018	0.015	0.011	0.014
Fe	0.157	0.112	0.767	0.510	0.465	0.352
Mg	4.405	4.604	3.969	4.186	4.200	4.476
Ca	0.900	0.994	0.645	0.637	0.880	0.941
K	0.885	0.922	0.928	0.900	0.911	0.860
Na	1.174	1.085	1.449	1.371	1.141	1.134
F	1.240	1.406	1.124	1.495	1.083	1.318
Total	16.743	16.922	16.830	17.007	16.653	16.903

Mg number = Mg/(Mg+Fe)x100, *FeO is total Fe

FIGURE 34: Variation diagram of Ti-K richterite analyses from the hypabyssal facies (HYP), and the round diopside-richterite (round DRX) and columnar diopside-richterite (angular DRX) cognate xenoliths. The HYP and round DRX Ti-K richterite analyses overlap to form a continuous trend, with the round DRX compositions being the most evolved. The columnar DRX Ti-K richterite analyses do not directly correlate with this trend.

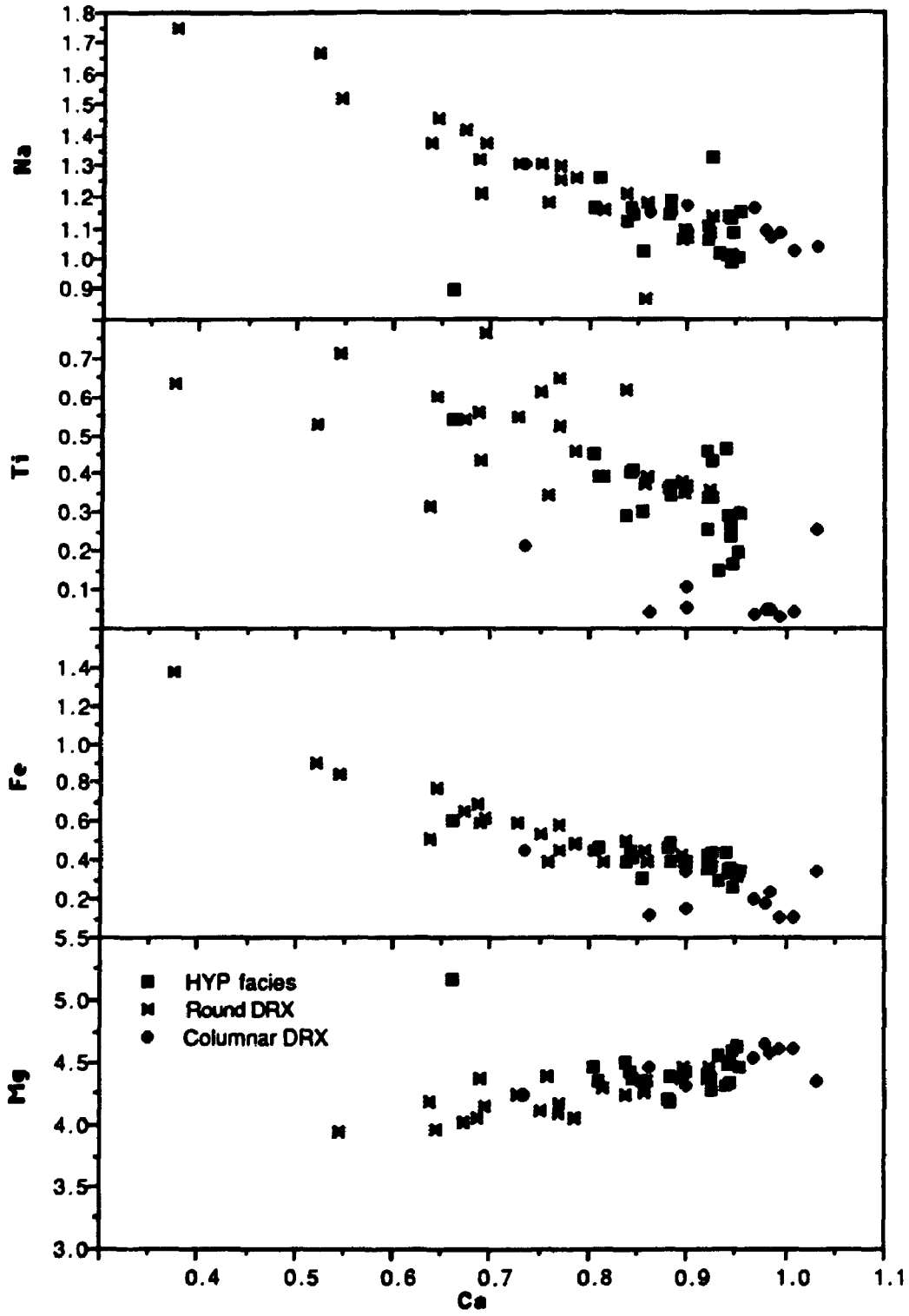
Na
Ti
Fe
Mg
Ca
HYP facies
Round DRX
Columnar DRX

K richterite in the round DRX have the highest Fe, Na, and Ti, and the lowest Mg, Ca and F. The Ti-K richterite analyses from the HYP facies occur between the columnar and round DRX, outlining a trend of increasing Fe, Ti and Na, with decreasing Ca and decreasing Mg with decreasing Ca. The Ti-K richterite from the round and columnar DRX are zoned, The zonation is characterized by a small increase of Ti and Fe, and a decrease of Mg, and Ca.

Typical of Ti-K richterite in lamproites, the tetrahedral sites of all three occurrences of Ti-K richterite are deficient in Si (Figure 35A). The Al in the Ti-K richterite does not increase as Si increases, however, the observed increase in Ti is directly proportional to the decrease in Si (Figure 35B). As a result, Ti^{4+} is considered to be an important tetrahedral vacancy filling element , as well as Al and Fe^{3+} (Thy 1982; Thy et al. 1987) with the remaining vacancy within the tetrahedral site assumed to be filled by Fe^{3+}.

In Figure 36, the Ti-K richterite compositions from the present study are compared to those Ti-K richterite from other olivine lamproites. The Ti-K richterite compositions from the American Mine (Scott-Smith and Skinner 1984) and Ellendale (Jaques et a. 1984) olivine lamproites are similar to the columnar DRX and the high Ca Ti-K richterite compositions from the HYP facies. The Ti-K richterite from Kapamba (Scott-Smith et al. 1989) are variable and do not correlate with the Ti-K richterite analyses from the other olivine lamproites plotted on the diagram. Ti-K richterite analyses are absent in the experiments from the present study.

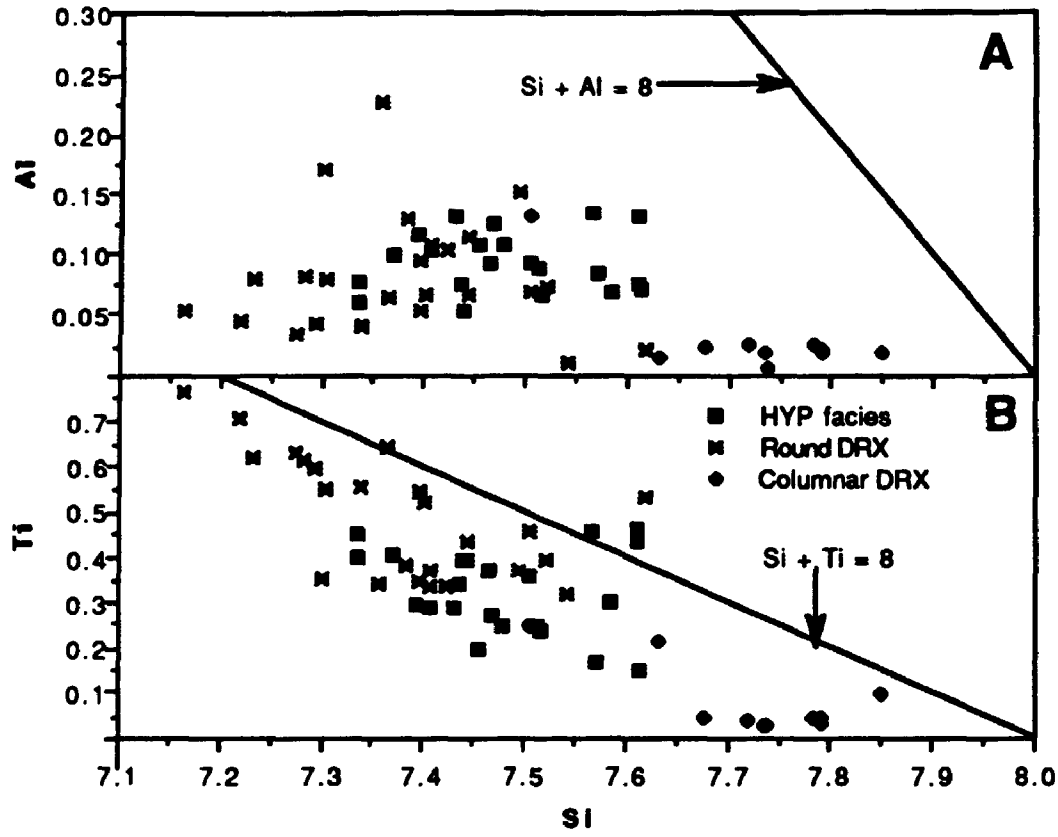

FIGURE 35: Diagram demonstrating the correlation between Al and Ti to the tetrahedral site occurpancy of the Ti-K richterite, indicated by the Si + Al = 8 line. Ti increases proportionately to decreasing Si, whereas there is no correlation of the Al values.

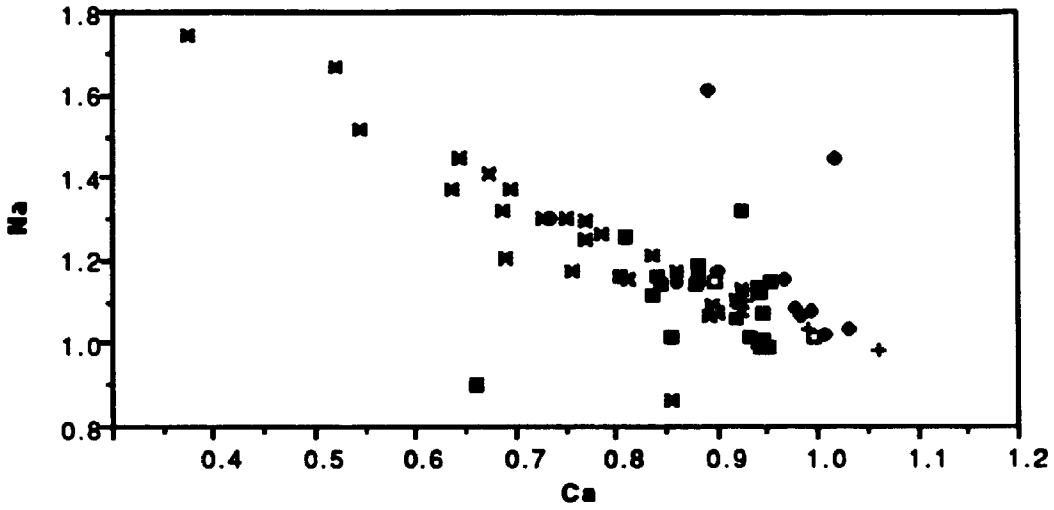

FIGURE 36: Comparison of the Ti-K richterite analyses from the present study to those from other olivine lamproites. The Ti-K richterite values from the American mine (Prairie Creek area) and Ellendale (Western Australia), are similar to the HYP analyses. The Kapamba differ form the other analyses by having much higher Ca values.

- ■ Hypabyssal (HYP)
- ✖ Round DRX
- ● Columnar DRX
- □ American Mine (Scott-Smith and Skinner 1989b)
- + Elendale (Jaques et al. 1985)
- ● Kapamba (Scott-Smith et al. 1989)

5.6 Accessory Minerals and Devitrified Glass

The accessory minerals were not investigated in as much detail as olivine, clinopyroxene, phlogopite, spinel and potassium richterite. This section briefly presents the chemical analyses from the present study for armalcolite ($(Fe,Mg)Ti_4O_{10}$), shcherbakovite-like mineral ($(Na,K)(Ba,K)Ti_2Si_4O_{14}$), wadeite ($K_4Zr_2Si_6O_{18}$), unidentified K-Al phase, and devitrified glass. Analyses for apatite, perovskite, and priderite are reported in Scott-Smith and Skinner (1984) and Mitchell and Lewis (1983).

Armalcolite is present with olivine and spinel in the "water added" 10 kb and 1100°C and "fluorine added" 10 kb and 1000°C experiments. In Table 13, analyses of armalcolite from both of the systems are compared to the composition of armalcolite from the Smoky Butte phlogopite lamproite (Velde et al. 1975; Mitchell et al. 1987).

Unidentified shcherbakovite-like mineral analyses have not been reported prior to this study. They are restricted to the corona rim 2 of the lenticular diopside-richterite cognate xenoliths. In Table 14, their composition is compared to titanosilicates which have been documented to occur in other lamproites (Prider 1965; Mitchell and Bergman 1991).

Analyses of the unidentified K-Al silicate phase were obtained from the small irregular shaped inclusions in the microphenocryst clinopyroxene in the HYP facies, as well as the clinopyroxene from the corona rim 1, corona rim 2, and corona rim 3 of the diopside-richterite cognate xenoliths. Owing to their small size (less than 5um) analyses without contamination clinopyroxene were difficult to obtain. Originally the analyses were interpreted as leucite inclusions

TABLE 13: Representative armalcolite analyses from "water added" and "fluorine added" experimental system compared to those from the Smoky Butte lamproite.

	PCW 6	FPC 6	74A1*	73A8*
TiO2	63.49	60.80	60.33	69.02
Al2O3	1.53	1.11	0.02	0.47
Cr2O3	1.08	0.49	0.82	0.43
MnO	0.06	0.00	0.33	0.15
FeO*	18.57	25.99	28.97	19.66
MgO	10.99	8.76	8.65	9.39
Total	95.72	97.15	99.12	99.12

*FeO is total Fe; * from Wagner and Velde (1986).

Table 14: Representative analyses of shcherbakovite from Prairie Creek and Western Australia.

	PC 22	PC 22	A	B
SiO2	31.42	30.55	40.72	41.05
TiO2	30.28	28.73	24.36	24.06
Al2O3	0.03	0.02	nd	nd
Cr2O3	0.00	0.03	nd	nd
MnO	0.31	0.22	nd	nd
FeO*	2.50	2.58	1.79	1.48
MgO	2.93	3.09	0.56	0.51
CaO	1.47	1.18	3.01	3.04
BaO	16.22	18.89	14.14	13.57
K2O	4.97	4.09	3.77	4.32
Na2O	8.23	7.89	11.19	10.99
F	0.66	1.07	nd	nd
Total	99.02	98.34	99.54	99.02

*FeO is total Fe; A and B are analyses of shcherbakovite from Walgidee Hills, Western Australia. A from Jaques et al. 1986; B from Mitchell (1985)
nd = not determined

(Walker and Edgar 1986), however, further analyses demonstrated a non-stoichiometric structural formula, and a substantial chemical variability, especially with the K_2O and Al_2O_3 wt. % values (Table 15).

TABLE 15: Representative analyses of K-Al silicate inclusions in clinopyroxene.

	PC 30	PC 30	PC 30	PC 30
SiO2	44.33	49.10	42.81	45.82
Al2O3	16.93	5.94	20.38	17.75
FeO*	6.02	8.05	5.65	6.65
MgO	3.79	12.06	2.80	3.67
CaO	0.55	0.09	0.87	0.34
K2O	27.38	24.39	26.70	26.91
Na2O	0.73	1.16	0.60	0.50
Total	99.73	100.79	99.81	101.64

* FeO as total Fe

CHAPTER 6

DISCUSSION

6.0 Introductory Statement

The petrogenetic model proposed here for the Prairie Creek intrusion, focuses on the phase relations and mineral chemistry of the tuff, breccia, and HYP facies, and cognate xenoliths. In addition, suprasolidus experimental results of the HYP facies are compared and contrasted with phase relations and mineral chemistry in the intrusion, in an attempt to model the conditions of crystallization in nature. The proposed petrogenetic model is then placed in the context of other published petrogenetic studies on olivine lamproites, particularly those from Zambia and Western Australia.

6.1 Petrogenetic Model

The petrogenetic model for the Prairie Creek olivine lamproite begins with a brief discussion of the possible depths of origin and mode of ascent for the Prairie Creek magma, followed by discussion of the source rock composition, and origin of large anhedral olivine grains. This section also includes an outline of the possible effects of the ascent on the petrogenesis of the rock, proposes two different paragenetic sequences developed within the magma column, and discusses the formation of the cognate xenoliths and their relationship to the petrogenesis of the intrusion.

6.1.1 Depth of Origin and Magma Ascent

In both kimberlites and lamproites, diamonds are considered to be xenocrystic, having been incorporated into the ascending magma by the disaggregation of mantle rocks during ascent (Boyd and Finnerty 1980; Meyer 1985; Hall and Smith 1985; Jaques et al.1990). In the Prairie Creek olivine lamproite, diamonds are hosted in the tuff, breccia and HYP facies (Miser and Ross 1923). At present, the only indication that the Prairie Creek olivine lamproite originated from mantle pressures is the occurrence of diamond, and the limited occurrence of pyrope and chrome diopside from heavy mineral concentrates (Bolivar and Steele 1976). Diamond xenocrysts within lamproites are considered to have originated from similar depths as diamonds hosted in kimberlites (Hall and Smith 1985; Jaques et al. 1990). Based on the presence of diamond, a pressure of origin for the olivine lamproite magma is considered to be greater than 50 kb. This pressure represents the minimum pressure for diamond to occur as the stable polymorph of carbon within the mantle (Kennedy and Kennedy 1976), based on the calculated temperature of an average continental geothermal gradient (Boyd and Nixon 1973; Ellis and Green 1979; Lindsley and Dixon 1976; MacGregor 1974; Wells 1977) being greater than that of the solidus of a typical mantle rock (Meyer 1985). For the diamonds to have been incorporated into the Prairie Creek magma as xenocrysts, the magma must have begun its ascent from pressures not less than 50 kb.

The rate of ascent, and to some extent, the oxidation state of the magma control the preservation of diamonds within the magma at pressures less than the conversion of diamond to graphite (Boyd and Finnerty 1980; Meyer 1985; Foley 1985; Foley et al. 1986). The occurrence of diamonds in a rock does not directly indicate the rate of magma ascent. The activation energy of the reaction

diamond to graphite below the diamond - graphite transition within an ascending lamproitic magma is not known. However, a relatively short time of ascent and magma cooling must have occurred in order that the diamond not retrograde to graphite.

The model for magma ascent from greater than 50 kb must take into consideration the limited time that diamond can occur in a magma at pressures below its stability. At the present, the only well accepted model for such an ascent from high pressures is the buoyancy-driven magma fracture (BDMF) model (Anderson 1979; Artyushov and Sobolev 1984; Harris 1985; Spera 1984, 1987; Bailey 1985; Spence and Turcotte 1985, 1990; Spence et al. 1987). In order to keep the magma from solidifying during ascent in a BDMF, a minimum ascent rate, loss of heat, and a limited time for crystallization are required (Anderson 1979; Spera 1985; Spence and Turcotte 1985, 1990). These requirements correlate with the requirements for the preservation of diamonds during transport from their environment of stability to the surface of the continental crust. Estimates of ascent velocities range from 10 to 30 metres per second (Anderson 1979; Spence and Turcotte 1985).

If the magma ascends through a BDMF, it has been proposed that pressure and temperature gradients develop within the magma column (Anderson 1979; Spence and Turcotte 1985, 1990; Spence et al. 1987). These gradients may cause the lower density elements, in particular volatiles, to diffuse to the top of the magma column, where the pressure and temperature are the lowest. When the magma reaches lower pressures, the temperature gradient within the magma column would become greater, and the density and solubility of the volatiles would decrease dramatically. As a result, the "driving

force" for the segregation of the volatiles to the top of the magma column would become progressively greater during ascent (Spence and Turcotte 1990; Spence et al. 1987). Such a migration of volatiles within the magma column will affect the petrogenesis of the ascending magma.

6.1.2 Source rock composition, origin of large anhedral olivine (LAO) and the beginning of ascent.

Based on mica harzburgite as a source rock composition for lamproites, the experiments in the present study should have revealed a multiple saturation point above 50 kb of olivine, orthopyroxene and mica (Foley 1989). Although a well defined multiple saturation point with orthopyroxene as a liquidus phase was not observed in the three experimental systems, a mica-harzburgite can not be ruled out as a possible source rock for the Prairie Creek HYP facies, as discussed below.

Experiments undertaken on a simplified mica-harzburgite system (Gupta and Green 1988) have demonstrated that the liquidus in equilibrium with a mica-harzburgite at 28 kb could be strongly influenced by pressure and H_2O/CO_2. At relatively low pressures with high H_2O/CO_2, the liquid most likely to be in equilibrium with the mica-harzburgite is hypersthene normative, whereas, at high pressures with low H_2O/CO_2, the liquid in equilibrium with the mica-harzburgite is not hypersthene normative. As a result, partial melting of similar source compositions could yield both a hypersthene normative lamproitic liquid with orthopyroxene as a liquidus phase (Foley 1989), and a SiO_2 undersaturated liquid without orthopyroxene. In the present study, the absence of both a multiple saturation point and orthopyroxene as a liquidus phase could be due to the fact that the highest pressure studied was only 40 kb

and the HYP facies is not hypersthene normative. As a result, it cannot be conclusively shown whether or not the Prairie Creek olivine lamproite may have been in equilibrium with a mica-harzburgite source rock.

After magma formation, crystallization of large anhedral olivine (LAO) as a phenocryst phase or incorporation of olivine as a xenocryst must have taken place. The size and homogeneous composition of LAO is considered to indicate that it crystallized in a stable igneous environment, atypical of the environment present during ascent and eruption of the Prairie Creek magma. If the LAO had originated during ascent from the accumulation of olivine through crystal settling processes, or the disaggregation of olivine rich mantle rocks, it is unlikely that it would have had sufficient time to equilibrate with the ascending magma Without time to equilibrate, the LAO would most likely be zoned, and not have an identical chemical composition to the small euhedral olivine (SEO) phenocrysts, which crystallized during the later stages of eruption. It is assumed that the most feasible explanation for the lack of compositional variation of LAO, and its compositional similarity with the SEO, can be explained by the occurrence of both the LAO and SEO in equilibrium with the olivine lamproite magma.

The LAO serrate margins have been interpreted to suggest that they are xenocrysts: a texture indicative of a reaction relationship between the olivine and a more siliceous lamproitic magma (Mitchell 1985; Mitchell and Bergman 1991). As discussed previously, the addition of xenocrystic olivine would have had to occur prior to ascent. At these conditions, olivine (Figure 5 and 6) or orthopyroxene (Foley 1989) is the stable liquidus mineral in olivine lamproites. If olivine was the liquidus phase, xenocrystic or phenocrystic olivine could not

react with the liquid to form a serrate boundary. If orthopyroxene was the liquidus phase, xenocrystic olivine with a serrate boundary and orthopyroxene phenocrysts, or orthopyroxene with a serrate boundary rimmed by olivine without a serrate boundary, would occur in the Prairie Creek rock; neither of these relationships was observed. On the basis of the absence of these textures, it is considered unlikely that the LAO reacted with the magma at high pressures, whether the olivine is phenocrystic or xenocrystic. Another constraint on the conditions for the reaction of the LAO with the magma is that, based on their identical chemical compositions, the olivine must have stopped reacting with the magma before the crystallization of the SEO phenocrysts. The only other possible time the LAO could have reacted with the Prairie Creek magma is during ascent of the magma from high pressures to the surface, prior to the crystallization of the SEO phenocrysts.

Reaction of the LAO with the magma could have occurred during ascent if the temperature of the magma had not decreased rapidly during the initial stages of ascent. It may also have occurred if the abundances of H_2O and/or F increased within the olivine lamproite magma. Both of these processes could result from the rapid transport of the magma within a buoyancy-driven magma fracture (BDMF). A combination of the positive slope of the liquidus phase boundary and the decrease in the liquidus by up to 100°C with the addition of either H_2O or F as indicated by the experimental results (Figure 5 and 6) suggests that it is possible that the magma could cross the liquidus boundary during ascent (Figure 37). As a result, the development of a serrate boundary around LAO through a reaction relationship during ascent of the Prairie Creek magma is considered possible.

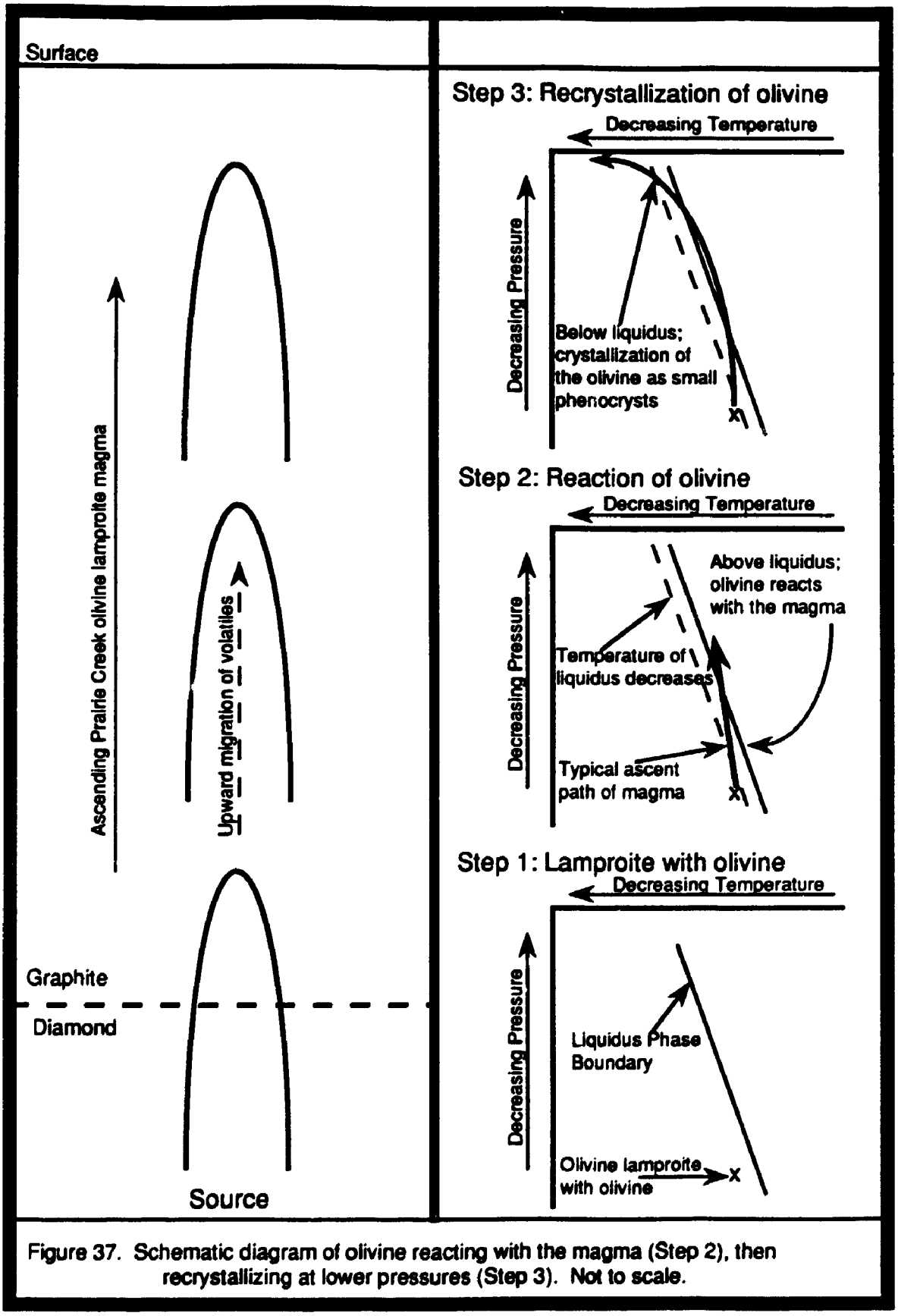

Figure 37. Schematic diagram of olivine reacting with the magma (Step 2), then recrystallizing at lower pressures (Step 3). Not to scale.

As the magma ascended through a BDMF to lower pressures, the magma would begin to cool rapidly due to the higher temperature gradient between the magma and its host. When the temperature of the magma became less than that of the liquidus temperature, olivine would again become the stable liquidus phase in the magma (Figure 37). It is my interpretation that this second generation of olivine crystallization is represented in the study samples by the SEO phenocrysts. Owing to the rapid change in temperature during the later stages of the eruption sequence, the SEO could have crystallized in a supercooled magma. If so, this would result in the homogeneous nucleation of the SEO phenocrysts throughout the magma, instead of heterogeneous nucleation around the LAO.

6.1.3 Ascent and volatile migration

The proposed migration of volatiles upward within the magma column during ascent could also cause the development of different paragenetic sequences. Based on the relative stability of phlogopite, and clinopyroxene, two different paragenetic sequences are present within the Prairie Creek intrusion: phlogopite without clinopyroxene in the tuff and breccia (Chapter 2.2.1 and 2.2.2); and clinopyroxene before phlogopite in the HYP magma (Chapter 2.2.3). In the experiments, the addition of H_2O and F resulted in a change in the paragenetic sequence from clinopyroxene crystallizing before phlogopite (Figure 5), to clinopyroxene crystallization after phlogopite (Figure 6). If the addition of volatiles in the experiments is a reasonable approximation of the increase of volatiles within the magma column during ascent, and if added volatiles are excluded, the composition of the HYP magma may be similar to that of the tuff and breccia magma prior to their explosive eruption. As a result, the differences in paragenetic sequence between the tuff - breccia and

HYP facies of rock are considered to be a result of higher H2O and/or F in the tuff-breccia than in the HYP facies. Based on this consideration, the "no added volatile" system is assumed to be paragenetically similar to the HYP facies, and the "water added" and "fluorine added" systems are paragenetically similar to the tuff and breccia.

In addition to the differences in paragenetic sequences between the HYP facies and the tuff and breccia, the phlogopites differ in texture and composition. Phenocryst phlogopites occurring in the tuff and breccia have relatively higher Al, Cr and lower Fe and F than the poikilitic phlogopites of the HYP facies. This relationship between the phlogopites in the Prairie Creek olivine lamproite has previously been interpreted to be a function of the phenocryst phlogopite crystallizing from a less evolved magma composition than that of the poikilitic phlogopite (Scott-Smith and Skinner 1984a; Mitchell 1985). However, based on the compositional correlation between the phenocryst phlogopite and the HPP from the experiments at pressures greater than 15 kb (Figure 18), it is not considered necessary for the phenocryst phlogopite to have originated from a magma composition less evolved than that of the HYP facies. Based on the experiments in this study, the tuff and breccia are assumed to have begun crystallizing phlogopite at pressures greater than 15 kb with higher H_2O and/or F than phlogopite in the HYP facies. In the HYP facies, the poikilitic phlogopite is assumed to have begun crystallization at pressures less than 15 kb, with a relatively low H_2O and/or F (Figure 38). The pressure constraints for the crystallization of the phlogopite are not considered to represent the actual pressure of crystallization, but rather, the relative pressure of crystallization for the phlogopite in the Prairie Creek intrusion.

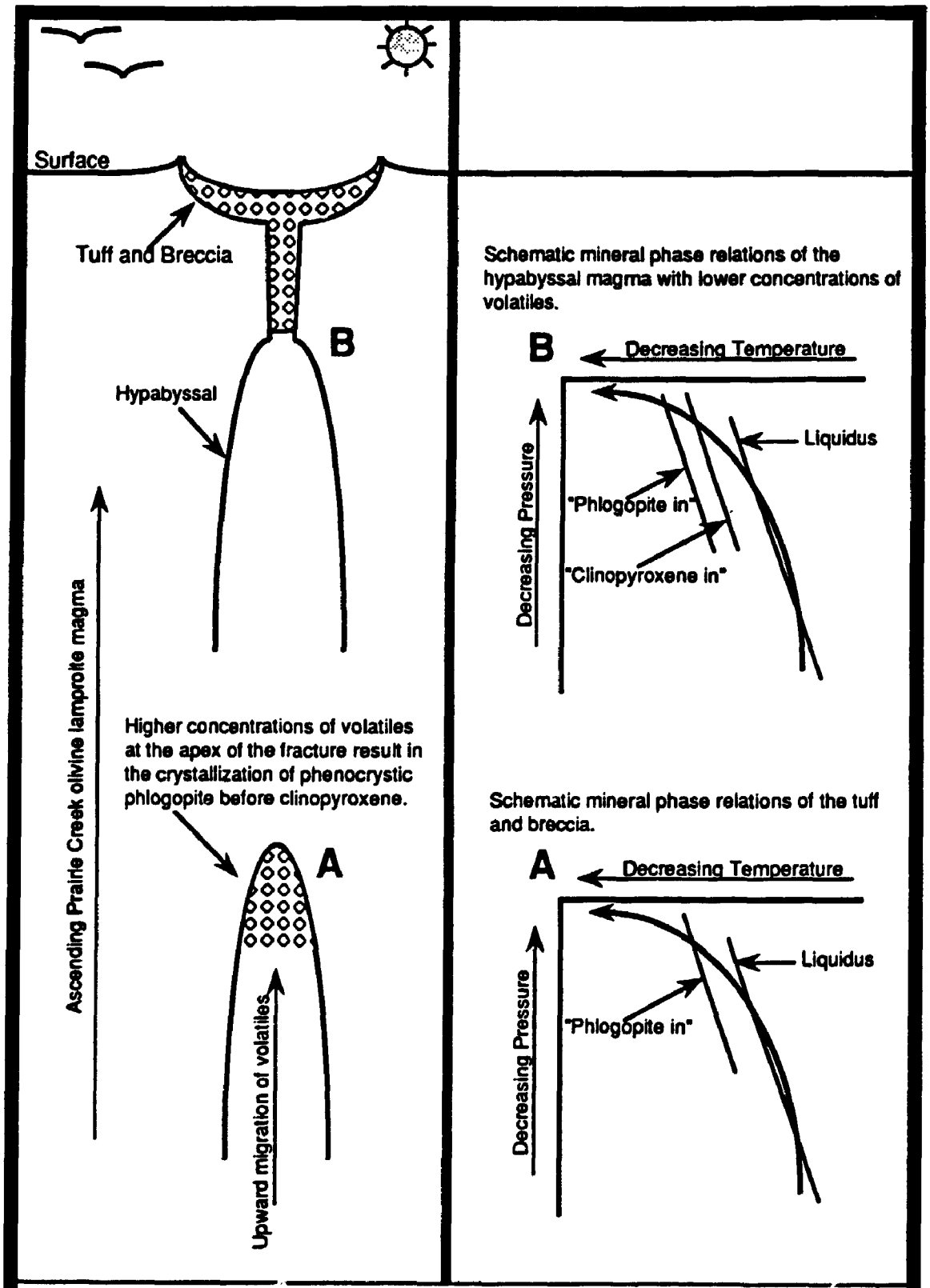

Figure 38: Schematic diagram of phlogopite and clinopyroxene crystallization in the tuff, breccia and hypabyssal rock. Not to scale.

The pressure and temperature conditions at which the olivine lamproite magma became distinctly zoned vertically within the ascending magma column can not be determined. However, a significant difference in volatile content between the HYP facies and the tuff and breccia must have existed prior to the crystallization of the phenocryst phlogopite in the tuff and breccia, and the crystallization of clinopyroxene in the HYP facies. The subsequent petrogenesis of the different paragenetic sequences within the Prairie Creek lamproite magma is discussed separately.

6.1.4 Petrogenesis of the tuff and breccia

The majority of the tuff and breccia consists of serpentinized olivine and groundmass. The groundmass is a result of the emplacement and rapid quenching of the magma. Rapid quenching may explain the absence of minerals not closely associated with the liquidus, such as clinopyroxene. The modal percent variation of phlogopite and olivine within and between the tuff and breccia may be the result of density sorting due either to an epiclastic detrital (Scott-Smith and Skinner 1984a), or a base surge - pyroclastic (Mitchell and Bergman 1991) origin.

Complete serpentinization of the LAO and SEO and the absence of low temperature minerals have left phlogopite phenocrysts as the only mineral that can be analyzed and, therefore, used for petrogenetic analysis of the tuff and breccia. The chemical composition of the phlogopite phenocrysts in the tuff and breccia evolved from higher Al and Cr to higher Fe and F, from core to margin. As discussed earlier (Chapter 5.3), the core compositions are similar to the HPP

from the experiments, which crystallized at pressures greater than 15 kb. After the crystallization of the lower Al phlogopite margins, the paragenetic sequence of the tuff and breccia is unclear, due to the volcanoclastic origin of these rocks.

In the tuff and breccia, rounded apatite-filled vesicles crystallize during the early stages of tuff formation. In the "water added" and "fluorine added" experimental systems, apatite crystallizes only at low-temperature and low-pressures. This may suggest that increased H_2O and/or F influenced the stability of apatite within the tuff, but due to the absence of experiments below 10 kb, the volatile abundance can not be demonstrated to be the sole influence on apatite stability.

6.1.5 Petrogenesis of the hypabyssal (HYP) facies

After the crystallization of the SEO, the paragenetic sequence of the HYP facies is; spinel - clinopyroxene - perovskite - apatite - phlogopite - Ti-K richterite - priderite - wadeite - perovskite. Petrographically, the onset of spinel and clinopyroxene crystallization in the HYP magma can not be worked out through thin section investigations. However, interpolation of the results of the "no added volatile" system indicates chromite would be the next phase to crystallize after SEO. The composition of spinel within the HYP facies changes from chromite at its core, to a high-Ti magnetite composition at its margin. Both the experimental systems and the rock exhibit a trend of decreasing Cr and increasing Ti. The change in composition in the experimental systems appears to be a function of temperature and/or the degree of crystallization. The "low temperature" ulvospinel composition is present in the low temperature "no

added volatile" experiments, but is absent in the HYP facies. This may be a function of the quenching of the Prairie Creek magma with 27 percent remaining liquid (Table 1), at a temperature or degree of crystallization in which ulvospinel had not yet become a stable phase.

Soon after the crystallization of chromite, clinopyroxene became a stable phase, crystallizing as small euhedral microphenocrysts within the HYP magma. These clinopyroxenes are typical of lamproite clinopyroxenes, which are unique to the lamproite group due to their abundant tetrahedrally coordinated Ti (Cundari and Salviulo 1989). Clinopyroxene with tetrahedrally coordinated Ti occur in all three experimental systems at pressures less than 30 kb (Chapter 5.2). At pressures greater than 20 kb, Ti appears to be located in the octahedral site, possibly having been incorporated into the clinopyroxene structure by the $^{VI}Ti + 2^{IV}Al = {}^{VI}Mg + 2^{IV}Si$ coupled substitution (Thompson 1972) (Chapter 5.2). As a result, with a typical ascent path, clinopyroxene with tetrahedrally coordinated Ti should be the only clinopyroxene present in the Prairie Creek olivine lamproite.

Perovskite and apatite crystallized contemporaneously with, or soon after, the crystallization of the clinopyroxene within the HYP magma. In the "no added volatile" experimental system, the incoming of perovskite occurs after the incoming of clinopyroxene, and is present only at low temperatures and 10 kb (Figure 5). Apatite did not occur in the "no added volatile" experimental system, but is present also at low temperatures and at 10 kb in the "water added" and "fluorine added" systems. Based on a typical ascent path within the experimental systems, perovskite and apatite would not become stable phases in the HYP magma until it reached pressures less than 10 kb, and did not

crystallize until after the onset of clinopyroxene crystallization. The presence of apatite may be indicative of higher volatile concentrations greater than the "no added volatile" experimental system, occurring during the late stage crystallization of the HYP facies. This speculation was not confirmed by this study, as experiments below 10 kb were not performed.

Poikilitic phlogopite crystallized as a stable phase after the crystallization of olivine, chromite, clinopyroxene, perovskite and apatite. Inclusions of devitrified glass or gas vesicles are present within the poikilitic phlogopite. The poikilitic texture, the abundance of inclusions, and the parallel alignment of clinopyroxene around the LAO and SEO indicate that the poikilitic phlogopite rapidly crystallized late in the paragenetic sequence of the HYP facies.

Although the poikilitic phlogopites are not distinctly zoned, they are mantled by a relatively high Fe, Na and F and low Ti and Al composition (Figure 25). This change in composition may follow the solid solution of phlogopite between octahedral site deficient Ti-phlogopite ($K_2(Mg,Fe)_4TiSi_6Al_2O_{20}(OH,F)_4$) to tetraferriphlogopite ($K_2(Mg,Fe)_6Si_6Fe_2O_{20}(OH,F)_4$). As the tetraferriphlogopite component in the poikilitic phlogopite increases, the phlogopite becomes peralkaline, Ti decreases, and F increases. A similar trend, with the exception of Ti, can be defined between the chemical composition of the HPP and LPP (Figure 18). As a result, the change from octahedral site deficient Ti-phlogopite to tetraferriphlogopite within the Prairie Creek HYP facies may be a function of pressure. Previous studies have suggested that the chemical evolution of phlogopites in lamproites to tetraferriphlogopite occurred in an oxidized lamproitic magma (Mitchell 1981, 1985; Foley 1987). The oxidation of the

lamproitic magma occurs during ascent by the migration of H^+ out of the magma (Foley 1985; Foley et al. 1986; Kadik and Lukanin 1985a; 1985b). It follows that during ascent, the oxidation of the magma would progressively increase as pressure decreased. Therefore, although the change from high-Al phenocrystic phlogopites to low-Al poikilitic tetraferriphlogopite may occur because of pressure, oxygen fugacity within the magma may also play an important role.

Most of the variations in elemental abundance of the phlogopite compositions in the Prairie Creek intrusion occur as a continuum. However, the F contents of the phenocryst and poikilitic phlogopites are distinctly different, with significantly higher F in the latter (Figure 16). Such a difference could be explained by the HYP facies having a higher abundance of F during poikilitic phlogopite crystallization than the tuff and breccia had during the phenocrystic phlogopite crystallization. By contrast, HPP have F concentrations much less than the LPP in the "water added" and "fluorine added" systems (Figure 18). These results are considered to demonstrate that the F concentrations in the phlogopites were not controlled by the bulk F in the magma, and that the compositional change from low to high F occurs in conjunction with the increase in the tetraferriphlogopite component of the phlogopites, both in the HYP facies and in the experimental systems. It may also indicate that the change in phlogopite composition occurs abruptly at a specific condition within the magma.

Substitution mechanisms which other authors have proposed for phlogopites that have crystallized from lamproitic magmas (Arima and Edgar 1981; Wagner and Velde 1986; Guo and Green 1990) do not fully explain the variation from the octahedral site deficient Ti-phlogopite to tetraferriphlogopite.

Although the data from the present study closely follow the coupled substitution $Ba^{2+} + 3Ti^{4+} + 4Al^{3+} = 2K^{+} + 4(Mg^{2+} + Fe^{2+}) + 4Si^{4+}$ (Guo and Green 1990), the absence of Fe^{3+} data may explain why the phlogopite chemistry from the present study does not follow the proposed substitution mechanism. The modified phlogopite substitution of Mitchell (1981), $3K^{+} + 2(Mg,Fe)^{2+} + Al^{3+} = Ti^{4+}_{vi} + \square_{vi} + \square_{vii} + Fe^{3+}_{iv} + (Ba^{2+},Na^{+})$ put forward to explain the compositional variation of increasing Fe and decreasing Al in phlogopites from lamproites in West Kimberley, Western Australia (Mitchell and Bergman 1991) may explain the phlogopite compositional variation in the present study because it takes into consideration the decreasing Al and an increasing Fe^{3+}. However, due to the absence of Fe^{3+} data, the substitution mechanism in the phlogopites from the Prairie Creek intrusion can not be determined.

The most significant compositional difference between the phlogopites from the Prairie Creek intrusion and those in the experiments is the lower-Ti values in the HPP as compared to the phenocrystic phlogopite and LPP. The compositional difference is considered to be a function of the composition of the spinels which were crystallizing contemporaneously with the phlogopite. The phenocryst phlogopites do not appear to have crystallized in the presence of a high-Ti spinel phase, whereas the HPP are present with Ti bearing spinels. This is considered to explain why the HPP have lower-Ti values than the phenocryst phlogopite. However, the Ti in phlogopite is not simply a function of the pressure or absence of Ti-bearing spinel. The LPP, which are also in equilibrium with high-Ti spinels and relatively high-Ti diopside, have a higher-Ti value than that of the HPP (Table 8 and 9). As a result, it seems likely that the

substitution mechanism controlling the Ti in phlogopites at low pressures has a greater influence on the occurrence of Ti in the phlogopite than does the bulk Ti content of the liquid.

Although the paragenetic sequence of the "no added volatile" system best resembles that of the HYP facies, phlogopite is not a stable mineral phase at 10 kb in the experimental system. However, LPP, which is compositionally similar to the poikilitic phlogopite, is present in the "water added" and "fluorine added" systems. Assuming the ascent rate is the "driving force" for volatile migration, and although the HYP facies began crystallizing with a relatively low volatile abundance, late stage crystallization of phlogopite may have been influenced by an increase in the abundance of volatiles. These results could indicate that LPP is not stable within the HYP facies at low pressures unless the rock has a higher concentration of H_2O or F.

With decreasing pressure and temperature, poikilitic phlogopite within the HYP facies appears to be replaced by Ti-K richterite as the stable hydrous phase; Ti-K richterite crystallized in the form of minute euhedral grains in the groundmass and along the grain boundaries of the poikilitic phlogopite. Ti-K richterite is the only major phase present in the rock which is not present in the experimental systems. This may be a result of the experimental conditions, or the absence of experimental results from below 10 kb. In other suprasolidus experiments on lamproites, Ti-K richterite appears as a stable hydrous phase joining phlogopite at pressures less than 10 kb (Barton and Hamilton 1978).

Prior to the intrusion and quenching of the HYP facies, wadeite, priderite and shcherbakovite-like mineral crystallized from the HYP magma. Wadeite and the shcherbakovite-like mineral are poikilitic, occurring as irregular patches throughout the HYP facies, while priderite occurs as parallel, aligned columns with variable lengths. These minerals are indicative of lamproites (Jaques et al. 1984a; Mitchell 1985; Bergman 1987; Mitchell and Bergman 1991), and are present in both low SiO_2 and high SiO_2 lamproites. Due to their textures, crystallization prior to the quenching of the magma, and their lack of dependence on the SiO_2 content of the lamproitic magma, it is assumed that these minerals crystallized rapidly from a supercooled magma.

6.1.6 Petrogenesis of the cognate xenoliths

The chemical variation of diopside, Ti-K richterite and phlogopite within the diopside-richterite (DRX) and phlogopite-bearing (PBX) cognate xenoliths, with the exception of the columnar DRX, has been demonstrated in this study to be part of the same compositional continuum as the equivalent minerals within the Prairie Creek intrusion. This suggests that not only are these xenoliths cognate, but that they crystallized from a magma with a similar composition and under similar conditions to that of the HYP facies. Based on this possibility, their genesis is evaluated in light of the petrogenetic model proposed for the Prairie Creek olivine lamproite.

The PBX consist mainly of poikilitic phlogopite. The PBX phlogopite is transitional in composition between the phenocrystic phlogopite from the tuff and breccia, and the poikilitic phlogopite from the HYP facies. The only exception is F, which is similar to the poikilitic phlogopite in the HYP facies. Based on the experimental results of the HYP facies, the absence of

clinopyroxene in the PBX would suggest that the magma from which phlogopite crystallized would have had a higher abundance of either H_2O and/or F. Comparing these results to the petrogenetic model for the Prairie Creek intrusion, it would appear that the PBX petrogenesis may be similar to that of the tuff and breccia. If the PBX xenoliths are directly related to the Prairie Creek intrusion, it is hypothesized that they represent tuff - breccia magma plated along the conduit wall, which was subsequently incorporated during ascent by the HYP magma.

If the composition of phlogopite in the Prairie Creek magma is controlled by pressure and oxygen fugacity, then the transitional composition of the PBX phlogopite could be indicative of conditions of crystallization intermediate between the poikilitic and phenocrystic phlogopite. Although the composition of phlogopite in the PBX is transitional, if F is an indication of a change from octahedral site deficient Ti-phlogopite to tetraferriphlogopite, then phlogopite likely crystallized at pressures less than the pressures and oxygen fugacity from which the phenocryst phlogopites crystallized.

The DRX are distinguished from the PBX by having abundant diopside and Ti-K richterite, and a well-developed diopside-phlogopite bearing corona. Assuming the DRX originated from a magma with a similar composition to the HYP facies, then the appearance of diopside before phlogopite indicates that diopside crystallization occurred at a relatively lower H2O and/or F content than the crystallization of phlogopite in the PBX. The occurrence of phlogopite similar to the LPP only in the lenticular DRX, and Ti-K richterite in the round and columnar DRX. may indicate that the lenticular, columnar and round xenoliths crystallized at a relatively lower pressure than the PBX. The mineralogical

change from phlogopite bearing lenticular DRX to Ti-K richterite bearing round and columnar xenoliths may be a result of different conditions of crystallization, and possibly in the case of the columnar DRX, a mantle origin (F. E. Llyod 1991, personal communication). Mineral compositions within the columnar DRX similar to those in the round and lenticular DRX, are considered to be the result of lamproitic magma infiltrating and reacting with the Cr-diopside bearing mantle xenolith.

The inclusion of DRX into the HYP facies, resulted in a reaction with the HYP magma producing a corona, which is divided into three zones. The mineral chemistry of clinopyroxene across the corona, is transitional between the diopside in the corona, and the diopside in the HYP facies. The phlogopite in the corona (CR2-3), is compositionally identical to that of the poikilitic phlogopite in the HYP facies. In addition to the corona around each of the DRX, the minerals within the xenolith appear to grow inward from the margin of the xenolith. This may indicate that at the time of incorporation, the xenoliths may not have been completely crystallized. If this were the case, then the non-psuedomorphing secondary minerals in the xenoliths originated from the devitrification of glass.

The incorporation of the DRX, and its reaction with the HYP magma, influenced the composition of the surrounding magma. Evidence for this is the absence of olivine in the corona rim 1 and 2, and the absence of perovskite in corona rim 3. The absence of corroded perovskite in what appears as typical HYP facies is considered to suggest that the perovskite had not yet crystallized in the HYP magma at the time the DRX were included.

6.2 Petrogenetic comparison of the Prairie Creek olivine lamproite to other olivine and phlogopite lamproites

Recent studies have demonstrated that lamproites represent a distinct group of rocks (Scott-Smith and Skinner 1984a; Mitchell 1985; Bergman 1987; Foley et al. 1987; Foley 1987; and Mitchell and Bergman 1991), and that within the lamproite group of rocks, there are inter- and intra-provincial variations in whole rock and mineral chemistry which characterize each suite and occurrence of lamproite (Mitchell and Bergman 1991). Although these variations show lamproite occurrences are distinctly different, there are paragenetic and mineral chemical characteristics that are consistent throughout the lamproite group (Mitchell 1985; Scott-Smith and Skinner 1984a; Bergman 1987; Foley et al. 1987; Mitchell and Bergman 1991). The objective of this petrogenetic comparison is to determine if the paragenetic and mineral chemistry variation within the Prairie Creek olivine lamproite magma during ascent could be indicative of important petrogenetic factors of the lamproite group of rocks.

The comparison of the results from the present study to the petrogenes of other lamproites presented in other studies is limited by the variation in whole rock composition of lamproites, the absence of comparable experimental studies, and the number of potential variables influencing mineral compositions and stabilities which were not controlled in the experiments (for example oxygen fugacity). Nevertheless, because the Prairie Creek intrusion is

representative of a lamproite magma composition, it is considered reasonable to compare the petrogenetic results from the present study to results from other lamproite studies.

The comparative petrogenesis begins with a brief outline of the common geological characteristics of lamproites, and then compares the petrogenesis of olivine, spinel, and phlogopite within the Prairie Creek olivine lamproite to their petrogeneses in other lamproites. The comparison focuses mainly on lamproites from Western Australia because of the availability of comprehensive petrogenetic studies (Wade and Prider 1960; Atkinson et al. 1984; Jaques et al. 1984, 1986, 1989; Mitchell 1981, 1985; Mitchell and Bergman 1991; Foley 1989)) and the compositional similarities of the Ellendale and Argyle olivine lamproites with the Prairie Creek olivine lamproite (Table 2).

6.2.1 Common characteristics of lamproites

The research on diamonds in olivine lamproites from North America, Africa and Western Australia demonstrates that they are derived from a deep-seated mantle source. Although diamonds appear to be more prevalent in olivine lamproites, diamonds are also reported to occur in the more siliceous "phlogopite lamproites" in West Kimberley, Western Australia (Jaques et al. 1984a; Atkinson et al. 1984), indicating a depth of origin in excess of 50 kb. Spatially, the olivine lamproites can occur with or separate from the "phlogopite lamproite" (Jaques et al. 1984; Foley 1989; Mitchell and Bergman 1991). Both types of lamproites are located at the margins of stable continental cratons, and chemical and experimental studies have suggested that they both have

originated by the partial melting of a depleted enriched mantle composition, considered to be represented by a mica-harzburgite (Jaques et al. 1984a; Foley 1989).

Owing to the deep-seated origin and occurrence of diamonds in lamproites, it is assumed that the buoyancy-driven magma fracture (BDMF) model is a common model of ascent for all lamproites. If this is the case, the paragenetic sequence of the lamproite group of rocks could be influenced by the transport of the magma from its source to the surface.

6.2.2 Genesis of olivine.

In all olivine-bearing lamproites, olivine occurs as two texturally distinct varieties: anhedral macrocrysts and subhedral - euhedral phenocrysts or microphenocrysts (Mitchell 1985; Mitchell and Bergman 1991). In the Prairie Creek intrusion, the olivine size and texture, the serrate margin around the LAO, and the lack of compositional difference between the two sizes of olivine are typical of what is observed in other olivine lamproites (Scott-Smith and Skinner 1984a; Cullers et al. 1985; Jaques et al. 1984a; Mitchell 1985; Scott-Smith et al. 1989; Mitchell and Bergman 1991). These textural and chemical similarities of olivine from the present study to olivine from other olivine lamproites with a similar whole rock composition, such as the Ellendale and Argyle olivine lamproites, may indicate a common petrogenesis. If this were the case, it could be assumed that: olivine lamproite magmas are in equilibrium with olivine prior to ascent, these olivines react with the magma during ascent, and there is a second generation of olivine crystallization at lower pressures compositionally similar to the LAO.

Compositional differences between the two sizes of olivine do occur in olivine lamproites and phlogopite lamproites with lower modal abundances of olivine, for example the Kapamba olivine lamproite (Scott-Smith et al. 1989), and phlogopite lamproites from West Kimberley (Jaques et al. 1984a, 1986)). The olivine compositional differences are characterized by decreasing Mg number from core to margin of the SEO, with Mg number at the margin being greater than 10 units lower than the Mg number of the LAO. Although this relationship may be indicative of olivine fractionation, such a process can not explain the variation of whole rock compositions between the lamproites with high modal abundances of olivine and those of the lamproite group with low olivine modal abundances (Jaques et al. 1984a; Mitchell and Bergman 1991). As a result, the petrogenetic relationship between the olivine lamproites and the phlogopite lamproites is considered to be more complicated than the simple subtraction or addition of olivine from a lamproitic magma.

6.2.3 Genesis of Spinel.

Spinel occurs in lamproites that typically contain greater than eight modal % olivine (Jaques et al. 1986). Texturally, the spinel occurs as small euhedra within the groundmass or glass, crystallizing after or during SEO phenocryst crystallization and before the poikilitic phlogopite. Based on their composition, the spinels are divided into three main groups which define a compositional trend from chromite to ulvospinel-magnetite end members (Figure 31A). The experimental results from the present study indicate that such a trend may either be a result of crystallization during decreasing temperature or the increasing degree of crystallization in the magma (Chapter 5.4). If this were the case, lamproites which quenched early in the crystallization sequence would be less likely to have ulvospinel-magnetite than lamproites which have a

longer period of crystallization to lower temperatures. The occurrence of ulvospinel-magnetite in the Kapamba olivine lamproite with less than 16 modal % glass (Scott-Smith et al. 1989), and its absence in the Prairie Creek olivine lamproite with greater than 25 modal % glass, may by indicative of such a process. As a result, the composition of spinel in lamproites is considered to be indicative of spinel crystallization at successively lower temperatures.

6.2.4 Genesis of phlogopite.

In the lamproite group of rocks, the habit of phlogopite has been used as a petrogenetic indicator (Mitchell 1985; Mitchell and Bergman 1991). Lamproites containing high-Al phenocrystic phlogopite are called "phlogopite lamproite", low-Al poikilitic phlogopite are called "madupitic lamproite" and high-Al phenocryst phlogopite rimmed by low-Al poikilitic phlogopite are called "transitional madupitic lamproite". The "phlogopite lamproites" are interpreted to be representative of primitive lamproite compositions, and the madupitic lamproites are considered to be differentiated magma compositions derived from the "phlogopite lamproite". Based on this classification, the tuff-breccia of the Prairie Creek rock would be an olivine "phlogopite lamproite", and the HYP facies an olivine "madupitic lamproite". As demonstrated earlier (Chapter 5.3), the compositional difference between the phlogopites in the tuff-breccia and those in the HYP facies may be a function of the pressure and oxygen fugacity at which the phlogopite crystallized. If pressure and oxygen fugacity are the factors which control the composition of phlogopite, and the conditions of crystallization determine whether the phlogopite is an early phenocrystic phase or a late poikilitic phase, then phlogopite habit and compositions can not be used to interpret whether a lamproite is primitive or differentiated.

The near-liquidus occurrence of phlogopite in "phlogopite lamproites" (Foley 1989) is considered to indicate that high-Al phenocryst phlogopite is most likely to occur in the "phlogopite lamproites". The occurrence of high-Al phenocrystic or low-Al poikilitic phlogopite in olivine lamproites depends on the pressure at which phlogopite is a stable mineral phase in the olivine lamproite magma. For instance, in the Prairie Creek olivine lamproite, it is proposed that higher H2O and/or F contents at the top of the magma column increased the stability of phlogopite at high pressures, resulting in the crystallization of high-Al phenocrystic phlogopite at the top of the magma column; whereas, lower in the magma column where H2O and/or F contents were much lower, phlogopite did not become a stable phase until lower pressures, resulting in its crystallization as a low-Al poikilitic phlogopite. The occurrence of both high-Al phenocrystic and low-Al poikilitic phlogopite also occurs in the Ellendale olivine lamproite of West Kimberley (Jaques et al. 1984a, 1986), but only low-Al poikilitic phlogopite occurs in the Argyle olivine lamproite (Jaques et al. 1989). The phlogopite characteristics of the "transitional madupitic lamproites" is interpreted to be a result of continuous phlogopite crystallization from high to low pressures, resulting in high-Al phenocrystic phlogopite being rimmed by low-Al poikilitic phlogopite.

Conditions other than pressure have been suggested to explain the differences between the high-Al phenocrystic phlogopite and the low-Al poikilitic phlogopite. Foley (1990) considered the absence of low-Al phlogopite compositions in high pressure experiments on olivine lamproites and phlogopite lamproites to be a function of a high H_2O content. However, none of the experiments in his study were undertaken below 20 kb, and the oxygen fugacity (buffered at iron-wustite) is much lower than what would be expected

for phlogopite crystallization in lamproites at low pressures. If the substitution of Fe^{3+} is important for the occurrence of low-Al phlogopites, then an oxygen fugacity where very little Fe^{3+} is present would not be conducive to the crystallization of low-Al phlogopite. Such an interpretation further supports the importance of oxygen fugacity for the occurrence of tetraferriphlogopite in the crystallization sequence of lamproites at low pressures. In addition, the occurrence of low-Al phlogopite in the "fluorine added" experiments also decreases the importance of the abundance of water in controlling the Al content of the phlogopites.

CHAPTER 7

CONCLUSIONS

The Prairie Creek olivine lamproite magma, in equilibrium with olivine, began its ascent from pressures greater than 50 kb. The magma ascended through a buoyancy-driven magma fracture to the surface. During ascent, diamonds and a few mantle rocks were incorporated into the magma from the surrounding mantle. As the magma was transported further upward, a pressure and temperature gradient developed within the fracture. This gradient was the "driving force" for the migration of volatiles to the apex of the fracture. The higher concentrations of volatiles, and rapidly reduced pressure, combined to cause the temperature of the liquidus phase boundary to decrease, and become less than the temperature of the magma. This caused the resorption of olivine, producing a serrate margin around the olivine grains. At lower pressures, the temperature began to decrease more rapidly, becoming less than the liquidus temperature. The second generation of olivine crystallization as a liquidus phase within the intrusion is represented by the small euhedral olivine phenocrysts. The apparent homogeneous nucleation of olivine within the magma, instead of heterogeneous nucleation of olivine around the previously crystallized LAO grains, may suggest that the magma was supercooled during the crystallization of the small euhedral olivine phenocrysts.

The redistribution of volatiles toward the top of the magma filled fracture also influenced the stability of phlogopite and clinopyroxene. The higher concentrations of H_2O and possibly F, resulted in phlogopite crystallizing

without clinopyroxene. This paragenetic sequence occurs in the tuff and breccia, which are the explosively erupted magma of the Prairie Creek intrusion. The absence of clinopyroxene after the crystallization of phlogopite and other lower temperature minerals in the tuff - breccia is considered to be a result of the rapid quenching of the magma. The magma with relatively lower concentrations of H_2O and/or F, located below the volatile-enriched composition within the magma fracture, ascended more slowly and intruded the tuff and breccia. This magma is represented by the HYP facies, which paragenetically differs from the tuff - breccia by having clinopyroxene crystallizing before phlogopite.

The different relative conditions of phlogopite crystallization within the magma filled fracture resulted in compositionally and texturally different phlogopites. The phenocryst phlogopite in the tuff - breccia crystallized at relatively higher pressures than the poikilitic phlogopite in the HYP facies. The change in composition from phenocrystic to poikilitic, as well as the compositional evolution of the poikilitic phlogopite, appears to be a result of a change from an octahedral site deficient Ti-phlogopite to a tetraferriphlogopite end member. The compositional evolution to tetraferriphlogopite may also be influenced by the oxidation state of the lamproitic magma during ascent, which is assumed to increase as pressure decreases. Although the compositional change in phlogopite end members is a continuum, specific conditions of crystallization may appear as limits of stability for each end member within the ascending olivine lamproite liquid.

The chemical compositions of clinopyroxene and spinel in the HYP facies are also considered to be controlled by their conditions of crystallization. The occurrence of diopside in the HYP facies with Ti substituting one-to-one for Si in the tetrahedral site may be a result of clinopyroxene crystallization occurring at pressures less than 30 kb in a Al_2O_3 poor lamproitic magma. Unlike clinopyroxene and phlogopite, which are influenced by pressure, the composition of spinel appears to have been mainly controlled by temperature. The compositional change from chromite cores to Ti-magnetite rims is considered to be a function of spinel crystallization with decreasing temperature, or a function of the degree of crystallization within the magma.

Phlogopite-bearing and diopside-richterite cognate xenoliths were incorporated into the HYP magma before the crystallization of perovskite. The mineral phase relations and chemistry of these xenoliths follow the same paragenetic sequence of the tuff - breccia and HYP magma, and their genesis may have been similarly influenced by pressure, temperature and volatiles. Based on the cognate xenoliths' variable mineralogy and change in mineral chemistry similar to that observed in the Prairie Creek intrusion, the xenoliths are considered to represent remnant magma from within the conduit used by the tuff - breccia magma. Owing to the change in phase relations and mineral chemistry, the liquid is assumed to have been incorporated into the ascending HYP magma at successively lower pressures and temperatures. The PBX may have been incorporated at higher pressures than the DRX. This order of inclusion is based on the influence of volatiles on the relative stability of phlogopite and clinopyroxene, and the chemical composition of the phlogopite. The three types of DRX when incorporated reacted with the liquid and formed a clinopyroxene-phlogopite dominated corona which has been subdivided into

three distinct coronas. The chemical change of the corona is transitional between the chemical composition of the minerals in xenoliths and the minerals in the HYP facies.

Before the HYP magma was quenched to glass as it intruded the tuff - breccia Ti-K richterite, wadeite, priderite, and shcherbakovite-like mineral crystallized from the magma. The glass was subsequently devitrified and the olivine serpentinized.

Comparison of the results of the present study to olivine lamproites from Zambia and Western Australia indicates that the common petrogenetic relationships of lamproitic magma are: two generations of compositionally similar olivine, a change in spinel composition from chromite to ulvospinel-magnetite with decreasing temperature, and a change in phlogopite composition from octahedral site deficient Ti-phlogopite (phenocrystic phlogopite) to tetraferriphlogopite (poikilitic phlogopite) as a function of pressure. If these important petrogenetic characteristics of lamproitic magmas are controlled by its ascent in a BDMF, then in order to determine the relationship between olivine lamproites and higher-SiO_2 phlogopite lamproites, the effects of crystallization of lamproitic magmas within a BDMF must be determined. It is also suggested that unraveling the effects of ascent on the petrogenesis of the lamproites is necessary to determine which of the lamproite compositions are primitive magmas.

APPENDIX 1

Sample Preparation

Sample PC-30 was prepared into a powder by a preliminary crushing to less than 5 mm. These fragments were then examined under a binocular microscope. Pieces without xenoliths, or abnormally large olivine grains, were chosen as representative of the sample. The selected pieces were then crushed to less than 1 mm, placed in a mortar and pestle with acetone, and ground for 2.5 hours. The grinding process occurred in the following sequence, 0.5 hours by hand, 1.5 hours by automatic mortar and pestle, and 0.5 hours by hand. After the grinding was complete, the acetone was left to evaporate and a small portion of the sample was tested with a sieve to make sure it was less than -200 mesh. The less than -200 mesh sample was then dried for 24 hours at 110^{o}C. The prepared sample was stored for the duration of the study in a desiccator.

APPENDIX 2

Capsule preparation

The capsule charges were prepared by placing the powdered rock of PC-30 into Fe soaked platinum above 1225°C, and $Ag_{50}Pd_{50}$ alloy below 1225°C. Both capsule types were 7 mm long, with a 1 mm outside diameter. Before use, all capsules were cleaned by soaking in boiling 20% HCl solution for several hours, and then bombarded with ultrasound for two hours.

The suitable prepared capsule was then crimped and welded at one end. The Pt_{Fe} was welded in a normal atmosphere, whereas $Ag_{50}Pd_{50}$ was welded with a N_2 atmosphere to prevent oxidation. After welding the $Ag_{50}Pd_{50}$, the capsule was annealed with a flame of a Bunsen burner for one minute, in order to volatilize impurities. Approximately 7 milligrams of sample was then placed in the capsule. The open end of the capsule was then cleaned and crimped, and a small piece was cut off to expose a fresh metal surface. The capsule and contents were weighted, and a wet tissue was wrapped around the welded end of the capsule. (The tissue decreased the heating of the sample, and reduced the risk of the volatiles within the sample to escape while welding.) After welding, the sealed capsule was weighted and placed in an oven at 110°C for 0.5 hours, whereupon, the capsule was taken out and weighted. If there was not a weight difference, the capsule was squeezed in an encapsulator, in order to fit in the high pressure cell assembly of the piston cylinder. The capsule was again dried and weighted to make sure a hole was not made during the encapsulation process.

After the completion of each experiment, the capsule was cleaned of foreign material and weighted. It was then pierced with a small sharp steel rod, dried at 110°C for 2 hours and reweighed. If there was a significant weight difference, volatiles were assumed to have been sealed in the charge during the experiment. One end of the charge was then cut off, allowing the material within the capsule to be extracted as a disaggregated powder. The powder was then placed into small glass vial plugged with a cork.

Capsule preparation for experiments in the "no water added" system, were completed based on the standard technique outlined above. The differences in capsule preparation for the "water added" and "fluorine added" systems are outlined below.

The "water added" system was undertaken by increasing the weight percent water of PC-30 to 15. This was accomplished by adding deionized water with a microsyringe into the bottom of an empty capsule with one end welded shut. The capsule weight was subtracted from the capsule + water weight, and the amount of sample necessary to represent 91.4 wt % of the charge was calculated, and then added. Once the appropriate amount of PC-30 and deionized water were in the capsule, it was welded closed using the standard technique above. After welding, it was weighted to make sure the water did not escape during the welding process.

The "fluorine added" system was undertaken by increasing the fluorine content in PC-30 from 0.17 wt% to 0.5 wt% by the addition of a less than -200 mesh powder of 98% pure LiF. A homogeneous sample was prepared by mixing a total of 0.451 wt% LiF with PC-30 in a mortar and pestle for 0.5 hours.

An experimental charge of LiF + PC-30 was prepared using the standard capsule preparation technique.

APPENDIX 3

Procedure for Fe^{2+} soaked platinum capsule

Fifteen platinum capsules were placed into a platinum crucible. A homogeneous mixture of 3 grams of sodium metasilicate with 8.5 wt % Fe sponge, was then placed into the crucible, making sure to cover all the capsules. The amount of Fe was determined based on the iron content of the sample which would be in contract with the capsule. The platinum crucible was then placed in a furnace set at 1200°C, with a nitrogen gas atmosphere. The nitrogen gas inhibited the oxidation of the Fe sponge to Fe^{3+}. After 24 hours, the sample was then quenched in water. The capsules were liberated from the quenched glass by placing the crucible and its contents in hot agitated water for approximately 12 to 24 hours. To ensure all foreign material had been removed from the capsule, after the dissolution of the glass, the platinum capsules were soaked in hot 20 percent HCl for several hours, and then bombarded with ultrasound for two hours. The capsule charges were then prepared according the procedure outlined in Appendix 2.

APPENDIX 4

Electron microprobe operating conditions

Mineral compositions were determined from carbon coated polished thin sections of the rock, and disaggregated experimental run products embedded in epoxy mounted on polished 25 mm diameter glass slides. Analyses at the start of the study were obtained using a Materials Analysis Company (MAC) model 400 electron microprobe with three spectrometers, and a KRISEL CONTROL automation system. After the second year of the study, analyses were obtained from the JEOL JXA-8600 electron microprobe equipped with four spectrometers, energy dispersive system, and a TRACOR NORTHERN 5500 automation system. Matrix corrections on the MAC were made by using the procedure of Colby (1971) (Majic IV), on a PDP 11/05 computer. Corrections for the JEOL data was completed using the TRACOR NORTHERN "Zaf" program. Both machines were operated at an excitation voltage of 15 kv and a sample current of 250 mA. Beam size was approximately 3 to 5 microns in diameter and count times of 10 seconds or 10,000 counts. Analyzed abundances are within three percent of the amount present, and the limit of detection is approximately 0.05 percent.

APPENDIX 5

5.1 Olivine

Olivine analyses: Large anhedral olivine (LAO)

	PC 30	PC 30a	PC 30	PC 30	PC 30	PC 30	PC 30	PC 30	PC 29b	PC 30	PC 30b	PC 30b	PC 30
	Core	Core	Core	Core	Core	Core	Core	Core	Core	Core	Core	Core	Core
SiO2	40.59	40.99	40.96	41.06	40.53	41.57	41.25	41.02	41.30	40.90	41.22	40.77	41.28
TiO2	0.02	0.02	0.02	0.00	0.00	0.00	0.01	0.00	0.00	0.02	0.00	0.04	0.11
Cr2O3	0.00	0.06	0.00	0.02	0.00	0.04	0.05	0.02	0.08	0.01	0.00	0.00	0.02
FeO	8.59	8.30	8.27	8.29	8.19	8.21	8.75	8.30	8.10	8.29	8.53	8.08	8.69
MnO	0.08	0.14	0.09	0.11	0.08	0.13	0.08	0.19	0.00	0.13	0.18	0.16	0.22
MgO	50.26	50.42	49.46	49.73	50.01	50.07	48.97	49.52	50.86	49.93	50.23	51.27	48.64
CaO	0.05	0.06	0.04	0.03	0.04	0.04	0.10	0.10	0.06	0.06	0.08	0.07	0.07
NiO	0.54	0.38	0.46	0.52	0.42	0.43	0.44	0.35	0.32	0.43	0.37	0.40	0.34
Total	100.13	100.37	99.30	99.76	99.27	100.49	99.65	99.50	100.72	99.77	100.61	100.79	99.37
Mg #	91.3	91.6	91.4	91.5	91.6	91.6	90.9	91.4	91.8	91.5	91.3	91.9	90.9
Structural formula calculations based on 4 oxygens													
Si	0.991	0.996	1.004	1.003	0.995	1.007	1.010	1.004	0.997	0.999	0.999	0.986	1.012
Ti	0.000	0.000	0.000	0.000	0.000	0.000	0.000	0.000	0.000	0.000	0.000	0.001	0.002
Cr	0.000	0.001	0.000	0.000	0.000	0.001	0.001	0.000	0.002	0.000	0.000	0.000	0.000
Fe	0.175	0.169	0.170	0.169	0.168	0.166	0.179	0.170	0.164	0.169	0.173	0.163	0.178
Mn	0.002	0.003	0.002	0.002	0.002	0.003	0.002	0.004	0.000	0.003	0.004	0.003	0.005
Mg	1.829	1.826	1.808	1.811	1.830	1.807	1.787	1.807	1.831	1.818	1.815	1.849	1.777
Ca	0.001	0.002	0.001	0.001	0.001	0.001	0.003	0.003	0.002	0.002	0.002	0.002	0.002
Ni	0.011	0.007	0.009	0.010	0.008	0.008	0.009	0.007	0.006	0.008	0.007	0.008	0.007
Total	3.009	3.004	2.994	2.996	3.004	2.993	2.991	2.995	3.002	2.999	3.000	3.012	2.983

Olivine analyses: Large anhedral olivine (LAO)

	PC 30 Core	PC 30 Core	PC 30 Core	PC 30 Core	PC 30 Core	PC 30 Core	PC 30 Core	PC 30 Core	PC29e Core	PC 30a Edge	PC 30 Edge	PC 30 Edge	PC 30 Edge
SiO2	41.58	40.70	42.02	41.11	40.80	41.23	41.31	40.21	41.62	41.36	41.11	40.91	40.43
TiO2	0.05	0.07	0.04	0.04	0.07	0.00	0.02	0.00	0.03	0.00	0.00	0.02	0.03
Cr2O3	0.00	0.00	0.00	0.00	0.00	0.00	0.09	0.00	0.00	0.00	0.04	0.09	0.10
FeO	9.43	9.85	9.33	8.82	8.81	7.70	7.85	8.21	7.75	8.96	8.66	8.52	8.85
MnO	0.21	0.10	0.14	0.13	0.13	0.00	0.03	0.05	0.00	0.11	0.14	0.18	0.13
MgO	48.71	48.46	48.83	49.31	49.23	51.72	51.31	50.86	50.54	49.47	49.60	50.14	49.78
CaO	0.12	0.12	0.10	0.06	0.08	0.03	0.04	0.04	0.09	0.13	0.03	0.16	0.05
NiO	0.52	0.27	0.43	0.24	0.36	0.27	0.29	0.30	0.30	0.40	0.42	0.52	0.52
Total	100.62	99.57	100.89	99.71	99.48	100.95	100.94	99.67	100.33	100.43	100.00	100.54	99.89
Mg #	90.2	89.8	90.3	90.9	90.9	92.3	92.1	91.7	92.1	90.8	91.1	91.3	90.9
Structural formula calculations based on 4 oxygens													
Si	1.011	1.002	1.017	1.006	1.002	0.992	0.995	0.984	1.006	1.006	1.003	0.994	0.991
Ti	0.001	0.001	0.001	0.001	0.001	0.000	0.000	0.000	0.001	0.000	0.000	0.000	0.001
Cr	0.000	0.000	0.000	0.000	0.000	0.000	0.002	0.000	0.000	0.000	0.001	0.002	0.002
Fe	0.192	0.203	0.189	0.180	0.181	0.155	0.158	0.168	0.157	0.182	0.177	0.173	0.181
Mn	0.004	0.002	0.003	0.003	0.003	0.000	0.001	0.001	0.000	0.002	0.003	0.004	0.003
Mg	1.766	1.779	1.762	1.798	1.802	1.855	1.842	1.855	1.821	1.793	1.804	1.817	1.818
Ca	0.003	0.003	0.003	0.002	0.002	0.001	0.001	0.001	0.002	0.003	0.001	0.004	0.001
Ni	0.010	0.005	0.008	0.005	0.007	0.005	0.006	0.006	0.006	0.008	0.008	0.010	0.010
Total	2.987	2.995	2.983	2.995	2.998	3.008	3.005	3.015	2.993	2.994	2.997	3.004	3.007

Olivine analyses: Large anhedral olivine (LAO)

	PC 30a	PC 30a	PC 30	PC 30	PC 29b	PC 30	PC 30	PC 30	PC 30	PC 30	PC 30	PC 25	PC 25
	Edge	Edge	Edge	Edge	Edge	Edge	Edge	Edge	Edge	Edge	Edge	Edge	Edge
SiO2	40.71	40.73	40.92	40.05	40.61	40.48	41.86	40.82	41.03	41.47	40.53	39.41	39.65
TiO2	0.01	0.00	0.01	0.00	0.05	0.07	0.04	0.05	0.04	0.13	0.03	0.02	0.02
Cr2O3	0.08	0.05	0.01	0.07	0.00	0.00	0.01	0.00	0.04	0.12	0.00	0.05	0.13
FeO	8.46	7.99	9.69	8.67	9.42	9.09	9.02	9.58	9.37	8.88	8.98	9.19	9.70
MnO	0.13	0.07	0.28	0.04	0.25	0.14	0.16	0.14	0.19	0.13	0.10	0.00	0.02
MgO	49.41	50.55	49.02	51.18	49.47	49.17	48.76	48.53	48.29	49.11	50.25	50.79	50.38
CaO	0.09	0.08	0.46	0.04	0.52	0.08	0.21	0.37	0.25	0.21	0.22	0.11	0.07
NiO	0.48	0.55	0.32	0.34	0.17	0.38	0.20	0.33	0.33	0.21	0.33	0.31	0.27
Total	99.37	100.02	100.71	100.39	100.49	99.41	100.29	99.82	99.54	100.26	100.44	99.88	100.24
Mg #	91.2	91.9	90.0	90.0	90.4	90.6	90.6	90.0	90.2	90.8	90.9	90.8	90.3
Structural formula calculations based on 4 oxygens													
Si	1.000	0.992	0.998	0.976	0.991	0.997	1.017	1.003	1.009	1.009	0.987	0.969	0.972
Ti	0.000	0.000	0.000	0.000	0.001	0.001	0.001	0.001	0.001	0.002	0.001	0.000	0.000
Cr	0.002	0.001	0.000	0.001	0.000	0.000	0.001	0.000	0.001	0.002	0.000	0.001	0.003
Fe	0.174	0.163	0.198	0.177	0.192	0.187	0.183	0.197	0.193	0.181	0.183	0.189	0.199
Mn	0.003	0.001	0.006	0.001	0.005	0.003	0.003	0.003	0.004	0.003	0.002	0.000	0.000
Mg	1.809	1.836	1.782	1.859	1.800	1.805	1.767	1.777	1.770	1.781	1.824	1.861	1.842
Ca	0.002	0.002	0.012	0.001	0.014	0.002	0.005	0.010	0.007	0.005	0.006	0.003	0.002
Ni	0.009	0.011	0.006	0.007	0.003	0.008	0.004	0.007	0.007	0.004	0.006	0.006	0.005
Total	2.999	3.006	3.002	3.022	3.006	3.003	2.981	2.998	2.992	2.987	3.009	3.029	3.023

Olivine analyses: LAQ		Olivine analyses: Small euhedral olivine (SEO)										
	PC 30	PC 30a	PC 30	PC 29b	PC 30	PC 30	PC 30	PC 30	PC 30a	PC 30b	PC 30a	PC30b
	Edge	Core	Core	Core	Edge	Edge	Edge	Core	Edge	Core	Edge	Edge
SIO2	40.54	40.63	41.23	40.21	41.11	41.40	40.72	41.50	40.74	40.49	41.08	40.84
TIO2	0.00	0.03	0.04	0.02	0.00	0.04	0.03	0.04	0.04	0.04	0.02	0.05
Cr2O3	0.00	0.00	0.04	0.07	0.02	0.08	0.06	0.03	0.12	0.00	0.02	0.00
FeO	8.75	8.17	9.15	9.13	8.12	8.47	9.50	8.95	8.77	8.38	8.51	8.51
MnO	0.18	0.10	0.09	0.00	0.19	0.10	0.10	0.19	0.18	0.11	0.12	0.13
MgO	49.79	49.67	49.29	50.17	49.75	49.89	49.79	48.88	49.21	50.07	49.29	50.30
CaO	0.27	0.06	0.15	0.06	0.04	0.13	0.11	0.14	0.15	0.06	0.26	0.07
NiO	0.40	0.40	0.38	0.31	0.46	0.50	0.36	0.36	0.42	0.43	0.40	0.42
Total	99.93	99.06	100.37	99.97	99.69	100.61	100.67	100.09	99.63	99.58	99.70	100.32
Mg #	91.0	91.6	90.6	90.7	91.6	91.3	90.3	90.7	90.9	91.4	91.2	91.3
Structural formula calculations based on 4 oxygens												
Si	0.992	0.999	1.004	0.985	1.004	1.003	0.992	1.012	0.999	0.992	1.005	0.994
Ti	0.000	0.001	0.001	0.000	0.000	0.001	0.001	0.001	0.001	0.001	0.000	0.001
Cr	0.000	0.000	0.001	0.001	0.000	0.002	0.001	0.001	0.002	0.000	0.000	0.000
Fe	0.179	0.168	0.186	0.187	0.166	0.172	0.194	0.182	0.180	0.172	0.174	0.173
Mn	0.004	0.002	0.002	0.000	0.004	0.002	0.002	0.004	0.004	0.002	0.002	0.003
Mg	1.817	1.821	1.790	1.832	1.811	1.802	1.808	1.776	1.800	1.829	1.797	1.824
Ca	0.007	0.002	0.004	0.002	0.001	0.003	0.003	0.004	0.004	0.002	0.007	0.002
Ni	0.008	0.008	0.007	0.006	0.009	0.010	0.007	0.007	0.008	0.008	0.008	0.008
Total	3.007	3.001	2.995	3.013	2.995	2.995	3.008	2.987	2.998	3.006	2.993	3.005

Olivine analyses: "No added volatile" system

	EPC 2	EPC 2	EPC 2	EPC 2	EPC 3	EPC 3	EPC 3	EPC 3	EPC 4	EPC 4	EPC 4	EPC 4
kilobars	20	20	20	20	30	30	30	30	30	30	30	30
Celsius	1350	1350	1350	1350	1450	1450	1450	1450	1400	1400	1400	1400
minutes	10	10	10	10	10	10	10	10	10	10	10	10
SIO2	42.87	42.40	42.83	42.77	42.84	42.00	42.09	41.67	42.82	41.92	41.72	42.64
TIO2	0.01	0.03	0.06	0.01	0.05	0.08	0.11	0.07	0.02	0.02	0.00	0.00
Cr203	0.11	0.11	0.02	0.13	0.04	0.07	0.09	0.03	0.16	0.13	0.06	0.06
FeO	4.54	4.47	4.38	4.21	5.34	5.26	5.14	5.04	5.57	5.58	5.69	5.47
MnO	0.09	0.07	0.09	0.08	0.04	0.06	0.08	0.05	0.08	0.11	0.06	0.14
MgO	52.07	52.24	52.47	52.33	51.58	51.87	51.94	52.74	50.67	51.44	53.11	51.35
CaO	0.11	0.15	0.19	0.14	0.18	0.17	0.19	0.21	0.14	0.16	0.13	0.16
NiO	0.33	0.39	0.14	0.30	0.07	0.18	0.11	0.12	0.38	0.25	nd	0.24
Total	100.13	99.86	100.18	99.97	100.14	99.69	99.75	99.93	99.84	99.61	100.77	100.06
Mg #	95.3	95.4	95.5	95.7	94.5	94.6	94.7	94.9	94.2	94.2	94.3	94.3
Structural formula calculations based on 4 oxygens												
Si	1.022	1.015	1.019	1.020	1.023	1.010	1.010	0.999	1.028	1.011	0.995	1.021
Ti	0.000	0.001	0.001	0.000	0.001	0.001	0.002	0.001	0.000	0.000	0.000	0.000
Cr	0.002	0.002	0.000	0.002	0.001	0.001	0.002	0.001	0.003	0.002	0.001	0.001
Mn	0.002	0.001	0.002	0.002	0.001	0.001	0.002	0.001	0.002	0.002	0.001	0.003
Fe	0.091	0.089	0.087	0.084	0.107	0.106	0.103	0.101	0.112	0.113	0.114	0.110
Mg	1.850	1.864	1.862	1.861	1.836	1.859	1.858	1.886	1.814	1.850	1.889	1.834
Ca	0.003	0.004	0.005	0.004	0.005	0.004	0.005	0.005	0.004	0.004	0.003	0.004
Ni	0.006	0.008	0.003	0.006	0.001	0.003	0.002	0.002	0.007	0.005	0.000	0.005
Total	2.976	2.984	2.979	2.979	2.975	2.985	2.984	2.996	2.970	2.987	3.003	2.978

nd = not determined

Olivine analyses: "No added volatile" system

	EPC 7	EPC 7	EPC 7	EPC 8	EPC 8	EPC 10	EPC 10	EPC 11	EPC 11	EPC 11	EPC 11	EPC 11
kilobars	30	30	30	10	10	20	20	20	20	20	20	20
Celsius	1250	1250	1250	1250	1250	1200	1200	1280	1280	1280	1280	1280
minutes	30	30	30	30	30	45	45	30	30	30	30	30
SiO2	41.59	42.59	42.54	41.42	42.24	41.11	40.68	40.54	40.70	40.76	41.40	41.31
TiO2	0.01	0.05	0.04	0.02	0.02	0.02	0.07	0.07	0.08	0.09	0.05	0.06
Cr2O3	0.02	0.00	0.12	0.04	0.07	0.00	0.13	0.13	0.08	0.08	0.09	0.09
FeO	7.54	7.20	6.91	6.34	6.39	7.34	7.55	6.49	5.92	5.94	5.45	5.30
MnO	0.14	0.13	0.13	0.16	0.05	0.01	0.12	0.13	0.15	0.07	0.09	0.01
MgO	50.21	50.04	50.33	51.63	50.85	51.15	51.47	51.56	51.94	52.19	52.47	52.93
CaO	0.07	0.13	0.11	0.07	0.29	0.16	0.17	0.12	0.13	0.10	0.11	0.10
NiO	0.36	0.37	0.29	nd	0.37	0.32	0.23	nd	nd	nd	nd	nd
Total	99.94	100.51	100.47	99.68	100.28	100.11	100.42	99.04	99.00	99.23	99.66	99.80
Mg #	92.2	92.5	92.8	93.6	93.4	92.5	92.4	93.4	94.0	94.0	94.5	94.7
Structural formula calculations based on 4 oxygens												
Si	1.009	1.024	1.022	1.002	1.015	0.996	0.985	0.989	0.991	0.990	0.998	0.994
Ti	0.000	0.001	0.001	0.000	0.000	0.000	0.001	0.001	0.001	0.002	0.001	0.001
Cr	0.000	0.000	0.002	0.001	0.001	0.000	0.002	0.003	0.002	0.002	0.002	0.002
Mn	0.003	0.003	0.003	0.003	0.001	0.000	0.002	0.003	0.003	0.001	0.002	0.000
Fe	0.153	0.145	0.139	0.128	0.128	0.149	0.153	0.132	0.121	0.121	0.110	0.107
Mg	1.816	1.793	1.802	1.861	1.822	1.847	1.857	1.876	1.885	1.889	1.885	1.898
Ca	0.002	0.003	0.003	0.002	0.007	0.004	0.004	0.003	0.003	0.003	0.003	0.003
Ni	0.007	0.007	0.006	0.000	0.007	0.006	0.004	0.000	0.000	0.000	0.000	0.000
Total	2.990	2.976	2.978	2.997	2.981	3.002	3.008	3.007	3.006	3.008	3.001	3.005

nd = not determined

Olivine analyses: "No added volatile" system

	EPC 16	EPC 19	EPC 19	EPC 19	EPC 22	EPC 22	EPC 25	EPC 25	EPC 25	EPC 33	EPC 33	EPC 33
kilobars	10	30	30	30	10	10	10	10	10	20	20	20
Celsius	1300	1310	1310	1310	1380	1380	1120	1120	1120	1315	1315	1315
minutes	20	20	20	20	10	10	240	240	240	5	5	5
SiO2	42.15	41.07	40.72	41.00	41.20	41.17	40.98	40.46	41.01	40.17	41.31	41.40
TiO2	0.15	0.18	0.43	0.24	0.05	0.05	0.05	0.06	0.07	0.05	0.02	0.04
Cr203	0.13	0.13	0.17	0.21	0.27	0.20	0.02	0.00	0.13	0.20	0.07	0.13
FeO	4.75	6.45	6.20	6.10	4.67	3.48	7.93	7.58	7.79	5.78	5.28	4.95
MnO	0.05	0.24	0.13	0.20	0.19	0.20	0.16	0.12	0.11	0.19	0.08	0.08
MgO	52.23	52.39	52.10	52.06	54.14	54.79	50.15	51.17	51.37	52.50	52.59	53.25
CaO	0.22	0.11	0.17	0.09	0.12	0.09	0.06	0.07	0.08	0.13	0.04	0.07
NiO	0.43	0.33	0.42	0.29	nd	nd	nd	nd	nd	nd	nd	nd
Total	100.11	100.90	100.34	100.19	100.64	99.98	99.35	99.46	100.56	99.02	99.39	99.92
Mg #	95.1	93.6	93.7	93.8	95.4	96.6	91.9	92.3	92.2	94.2	94.7	95.1
Structural formula calculations based on 4 oxygens												
Si	1.009	0.986	0.982	0.988	0.982	0.982	1.001	0.987	0.990	0.979	0.997	0.993
Ti	0.003	0.003	0.008	0.004	0.001	0.001	0.001	0.001	0.001	0.001	0.000	0.001
Cr	0.002	0.002	0.003	0.004	0.005	0.004	0.000	0.000	0.002	0.004	0.001	0.002
Mn	0.001	0.005	0.003	0.004	0.004	0.004	0.003	0.002	0.002	0.004	0.002	0.002
Fe	0.095	0.129	0.125	0.123	0.093	0.069	0.162	0.155	0.157	0.118	0.107	0.099
Mg	1.863	1.875	1.874	1.871	1.924	1.949	1.826	1.860	1.848	1.907	1.893	1.905
Ca	0.006	0.003	0.004	0.002	0.003	0.002	0.002	0.002	0.002	0.003	0.001	0.002
Ni	0.008	0.006	0.008	0.006	0.000	0.000	0.000	0.000	0.000	0.000	0.000	0.000
Total	2.987	3.009	3.007	3.002	3.012	3.011	2.995	3.007	3.002	3.016	3.001	3.004

nd = not determined

Olivine analyses; "No added volatile" system

	EPC 34	EPC 34	EPC 34	EPC 34	EPC 34	EPC 37	EPC 37	EPC 41	EPC 41	EPC 41	EPC 41	EPC41
kilobars	10	10	10	10	10	20	20	40	40	40	40	40
Celsius	1200	1200	1200	1200	1200	1240	1240	1460	1460	1460	1460	1460
minutes	30	30	30	30	30	30	30	10	10		10	10
SiO2	40.41	40.29	40.52	40.52	40.82	40.64	41.02	41.72	40.74	41.07	42.23	41.54
TiO2	0.06	0.09	0.05	0.05	0.05	0.09	0.02	0.06	0.04	0.03	0.00	0.03
Cr2O3	0.00	0.04	0.20	0.02	0.08	0.00	0.09	0.10	0.13	0.15	0.00	0.19
FeO	8.15	7.68	7.10	6.92	6.86	6.52	6.00	5.87	5.27	4.60	4.52	4.42
MnO	0.19	0.10	0.11	0.14	0.10	0.19	0.11	0.21	0.14	0.22	0.14	0.17
MgO	50.24	50.64	50.92	51.59	51.20	51.96	52.79	52.40	53.38	53.83	53.84	53.93
CaO	0.19	0.16	0.26	0.16	0.22	0.07	0.07	0.11	0.09	0.08	0.08	0.08
NiO	nd	nd	nd	nd	nd	nd	nd	nd	nd	nd	nd	nd
Total	99.24	99.00	99.16	99.40	99.33	99.47	100.10	100.47	99.79	99.98	100.81	100.36
Mg #	91.7	92.1	92.8	93.0	93.0	93.4	94.0	94.1	94.8	95.4	95.5	95.6
Structural formula calculations based on 4 oxygens												
Si	0.991	0.988	0.991	0.987	0.994	0.988	0.988	0.993	0.982	0.985	1.001	0.991
Ti	0.001	0.002	0.001	0.001	0.001	0.002	0.000	0.001	0.001	0.001	0.000	0.001
Cr	0.000	0.001	0.004	0.000	0.002	0.000	0.002	0.002	0.002	0.003	0.000	0.004
Mn	0.004	0.002	0.002	0.003	0.002	0.004	0.002	0.004	0.003	0.004	0.003	0.003
Fe	0.167	0.158	0.145	0.141	0.140	0.133	0.121	0.117	0.106	0.092	0.090	0.088
Mg	1.837	1.852	1.856	1.873	1.859	1.882	1.895	1.869	1.918	1.925	1.903	1.917
Ca	0.005	0.004	0.007	0.004	0.006	0.002	0.002	0.003	0.002	0.002	0.002	0.002
Ni	0.000	0.000	0.000	0.000	0.000	0.000	0.000	0.000	0.000	0.000	0.000	0.000
Total	3.005	3.007	3.006	3.009	3.004	3.011	3.010	2.994	3.014	3.012	2.999	3.006

nd = not determined

Olivine analyses: "No added volatile" system

	EPC 41	EPC 42	EPC 42	EPC 42	EPC 43	EPC 43	EPC 43	EPC 43	EPC 43	EPC 43	EPC 45	EPC 45
kilobars	40	35	35	35	20	20	20	20	20	20	30	30
Celsius	1460	1380	1380	1380	1050	1050	1050	1050	1050	1050	1150	1150
minutes	10	15	15	15	240	240	240	240	240	240	180	180
SiO2	41.40	41.13	41.09	41.37	40.76	40.66	41.14	40.34	40.48	40.65	41.61	41.88
TiO2	0.08	0.03	0.05	0.05	0.05	0.00	0.05	0.06	0.07	0.00	0.08	0.05
Cr203	0.16	0.15	0.11	0.27	0.00	0.03	0.00	0.00	0.00	0.00	0.02	0.01
FeO	4.28	5.87	4.59	4.51	8.15	8.76	8.81	7.89	7.08	8.70	7.36	7.30
MnO	0.17	0.21	0.20	0.14	0.22	0.14	0.23	0.18	0.21	0.14	0.25	0.18
MgO	53.79	52.34	53.46	53.64	51.68	50.66	49.84	51.70	52.13	50.67	51.15	51.16
CaO	0.11	0.07	0.09	0.09	0.07	0.05	0.07	0.12	0.12	0.04	0.10	0.11
NiO	nd	nd	nd	nd	nd	nd	nd	nd	nd	nd	nd	nd
Total	99.99	99.80	99.59	100.07	100.93	100.30	100.14	100.29	100.09	100.20	100.57	100.69
Mg #	95.7	[illegible] 1	95.4	95.5	91.9	91.2	91.0	92.1	92.9	91.2	92.5	92.6
Structural formula calculations based on 4 oxygens												
Si	0.990	0.993	0.989	0.990	0.984	0.989	1.001	0.980	0.981	0.990	1.002	1.006
Ti	0.001	0.001	0.001	0.001	0.001	0.000	0.001	0.001	0.001	0.000	0.001	0.001
Cr	0.003	0.003	0.002	0.005	0.000	0.001	0.000	0.000	0.000	0.000	0.000	0.000
Mn	0.003	0.004	0.004	0.003	0.004	0.003	0.005	0.004	0.004	0.003	0.005	0.004
Fe	0.086	0.118	0.092	0.090	0.165	0.178	0.179	0.160	0.144	0.177	0.148	0.147
Mg	1.918	1.883	1.917	1.914	1.860	1.837	1.809	1.872	1.884	1.839	1.836	1.832
Ca	0.003	0.002	0.002	0.002	0.002	0.001	0.002	0.003	0.003	0.001	0.003	0.003
Ni	0.000	0.000	0.000	0.000	0.000	0.000	0.000	0.000	0.000	0.000	0.000	0.000
Total	3.004	3.004	3.007	3.005	3.016	3.009	2.997	3.020	3.017	3.010	2.995	2.993

nd = not determined

Olivine analyses; "No added volatile" system

	EPC 45	EPC 45	EPC 50	EPC 51	EPC 51	EPC 54	EPC 54	EPC 55	EPC 56	EPC 56	EPC 59	EPC 59
kilobars	30	30	15	10	10	20	20	40	40	40	20	20
Celsius	1150	1150	1050	1000	1000	1400	1400	1300	1380	1380	1120	1120
minutes	180	180	360	420	420	5	5	20	10	10	180	180
SiO2	41.65	41.16	40.52	39.71	41.44	41.38	41.71	41.34	41.35	41.74	40.25	40.83
TiO2	0.05	0.09	0.09	0.03	0.00	0.04	0.07	0.04	0.04	0.04	0.12	0.07
Cr2O3	0.02	0.00	0.12	0.02	0.01	0.00	0.05	0.05	0.11	0.07	0.06	0.13
FeO	7.66	7.19	7.85	8.50	8.26	3.78	3.32	6.75	5.36	5.20	7.82	7.36
MnO	0.15	0.21	0.30	0.15	0.20	0.10	0.07	0.10	0.07	0.10	0.27	0.25
MgO	51.01	51.30	51.48	51.18	50.16	54.45	54.68	51.10	52.89	52.07	51.01	51.20
CaO	0.12	0.09	0.14	0.10	0.10	0.10	0.08	0.12	0.10	0.08	0.14	0.17
NiO	nd	nd	0.24	0.36	0.33	0.28	0.31	0.42	0.39	0.39	0.34	0.31
Total	100.66	100.04	100.74	100.05	100.50	100.13	100.29	99.92	100.31	99.69	100.01	100.32
Mg #	92.2	92.7	92.1	91.5	91.6	96.3	96.7	93.1	94.6	94.7	92.1	92.5
Structural formula calculations based on 4 oxygens												
Si	1.003	0.996	0.981	0.971	1.003	0.988	0.991	1.001	0.992	1.005	0.982	0.989
Ti	0.001	0.002	0.002	0.001	0.000	0.001	0.001	0.001	0.001	0.001	0.002	0.001
Cr	0.000	0.000	0.002	0.000	0.000	0.000	0.001	0.001	0.002	0.001	0.001	0.002
Mn	0.003	0.004	0.006	0.003	0.004	0.002	0.001	0.002	0.001	0.002	0.006	0.005
Fe	0.154	0.146	0.159	0.174	0.167	0.075	0.066	0.137	0.108	0.105	0.159	0.149
Mg	1.831	1.852	1.857	1.867	1.810	1.937	1.937	1.844	1.892	1.869	1.854	1.850
Ca	0.003	0.002	0.004	0.003	0.003	0.003	0.002	0.003	0.003	0.002	0.004	0.004
Ni	0.000	0.000	0.005	0.007	0.006	0.005	0.006	0.008	0.008	0.007	0.007	0.006
Total	2.995	3.002	3.016	3.026	2.993	3.011	3.005	2.997	3.007	2.992	3.015	3.006

nd = not determined

Olivine analyses: "No added volatile" system

	EPC 59	EPC 59	EPC 59	EPC 59	EPC 59	EPC 60	EPC 60	EPC 60	EPC 60	EPC 60
kilobars	20	20	20	20	20	35	35	35	35	35
Celsius	1120	1120	1120	1120	1120	1200	1200	1200	1200	1200
minutes	180	180	180	180	180	180	180	180	180	180
SiO2	40.93	40.40	40.48	40.99	41.14	41.00	40.75	41.14	40.46	40.95
TiO2	0.10	0.09	0.09	0.07	0.09	0.08	0.08	0.05	0.03	0.06
Cr203	0.09	0.02	0.07	0.06	0.04	0.06	0.12	0.15	0.13	0.06
FeO	7.78	7.57	7.32	7.58	7.40	5.80	5.85	5.50	5.93	5.40
MnO	0.19	0.25	0.21	0.18	0.20	0.21	0.18	0.19	0.14	0.16
MgO	51.20	50.93	52.06	50.90	51.32	52.93	52.37	52.81	52.15	53.29
CaO	0.12	0.17	0.17	0.12	0.22	0.07	0.06	0.05	0.05	0.08
NiO	0.34	0.28	0.33	0.33	0.31	0.37	0.41	0.36	0.35	0.36
Total	100.75	99.71	100.73	100.23	100.72	100.52	99.82	100.25	99.24	100.36
Mg #	92.2	92.3	92.7	92.3	92.5	94.2	94.1	94.5	94.0	94.6
Structural formula calculations based on 4 oxygens										
Si	0.989	0.986	0.978	0.994	0.992	0.985	0.986	0.989	0.985	0.984
Ti	0.002	0.002	0.002	0.001	0.002	0.001	0.001	0.001	0.001	0.001
Cr	0.002	0.000	0.001	0.001	0.001	0.001	0.002	0.003	0.003	0.001
Mn	0.004	0.005	0.004	0.004	0.004	0.004	0.004	0.004	0.003	0.003
Fe	0.157	0.155	0.148	0.154	0.149	0.117	0.118	0.111	0.121	0.108
Mg	1.844	1.853	1.875	1.840	1.844	1.895	1.890	1.893	1.893	1.908
Ca	0.003	0.004	0.004	0.003	0.006	0.002	0.002	0.001	0.001	0.002
Ni	0.007	0.005	0.006	0.006	0.006	0.007	0.008	0.007	0.007	0.007
Total	3.008	3.010	3.018	3.003	3.004	3.012	3.011	3.009	3.014	3.014

nd = not determined

Olivine analyses: "Water added" system

	PCW 5	PCW 5	PCW 5	PCW 5	PCW 6	PCW 6	PCW 6	PCW 6	PCW 13	PCW 13	PCW 13	PCW 13
kilobars	20	20	20	20	10	10	10	10	20	20	20	20
Celsius	1200	1200	1200	1200	1100	1100	1100	1100	1280	1280	1280	1280
minutes	180	180	180	180	360	360	360	360	30	30	30	30
SiO2	42.01	41.66	41.51	41.20	41.21	41.05	41.10	40.84	42.56	42.34	42.09	42.54
TiO2	0.03	0.06	0.06	0.06	0.02	0.02	0.01	0.04	0.05	0.06	0.05	0.06
Cr203	0.07	0.00	0.19	0.14	0.12	0.00	0.05	0.06	0.18	0.11	0.09	0.17
FeO	5.22	5.28	5.87	5.49	8.22	8.54	7.73	7.85	4.78	4.72	3.71	3.56
MnO	0.16	0.18	0.15	0.05	0.16	0.13	0.12	0.16	0.16	0.14	0.28	0.13
MgO	51.73	52.73	52.04	52.75	49.46	49.82	49.86	51.08	52.68	52.31	53.14	53.85
CaO	0.10	0.08	0.07	0.11	0.04	0.05	0.05	0.12	0.06	0.09	0.07	0.07
NiO	0.49	0.34	0.39	0.50	0.33	0.40	0.45	0.33	0.29	0.39	0.05	0.18
Total	99.81	100.33	100.28	100.30	99.56	100.01	99.37	100.48	100.76	100.16	99.48	100.56
Mg #	94.6	94.7	94.1	94.5	91.5	91.2	92.0	92.1	95.2	95.2	96.2	96.4
Structural formula calculations based on 4 oxygens												
Si	1.009	0.997	0.998	0.990	1.007	1.001	1.005	0.990	1.011	1.012	1.008	1.007
Ti	0.001	0.001	0.001	0.001	0.000	0.000	0.000	0.001	0.001	0.001	0.001	0.001
Cr	0.001	0.000	0.004	0.003	0.002	0.000	0.001	0.001	0.003	0.002	0.002	0.003
Mn	0.003	0.004	0.003	0.001	0.003	0.003	0.002	0.003	0.003	0.003	0.006	0.003
Fe	0.105	0.106	0.118	0.110	0.168	0.174	0.158	0.159	0.095	0.094	0.074	0.070
Mg	1.853	1.882	1.865	1.889	1.802	1.811	1.817	1.845	1.866	1.864	1.897	1.900
Ca	0.003	0.002	0.002	0.003	0.001	0.001	0.001	0.003	0.002	0.002	0.002	0.002
Ni	0.009	0.007	0.008	0.01	0.006	0.008	0.009	0.006	0.006	0.007	0.001	0.003
Total	2.984	2.999	2.999	3.007	2.989	2.998	2.993	3.008	2.987	2.985	2.991	2.989

nd = not determined

Olivine analyses: "Water added" system

	PCW 14	PCW 14	PCW 14	PCW 23	PCW 23	PCW 23	PCW 23	PCW 23	PCW 25	PCW 25	PCW 25	PCW 25
kilobars	10	10	10	30	30	30	30	30	10	10	10	10
Celsius	1300	1300	1300	1300	1300	1300	1300	1300	1200	1200	1200	1200
minutes	30	30	30	15	15	15	15	15	90	90	90	90
SiO2	41.69	41.45	42.08	40.99	40.59	41.31	41.74	40.73	41.14	40.61	40.87	41.21
TiO2	0.05	0.07	0.08	0.06	0.05	0.01	0.02	0.01	0.07	0.16	0.12	0.17
Cr2O3	0.2	0.22	0.17	0.00	0.03	0.04	0.00	0.12	0.18	0.04	0.03	0.00
FeO	6.46	6.29	5.15	4.93	4.46	4.43	4.43	4.36	7.59	7.35	7.17	6.24
MnO	0.14	0.14	0.08	0.06	0.03	0.02	0.03	0.11	0.28	0.13	0.05	0.08
MgO	51.31	50.96	51.95	53.10	53.82	53.68	54.06	53.86	50.97	50.73	51.64	51.01
CaO	0.29	0.27	0.23	0.06	0.06	0.05	0.07	0.07	0.17	0.24	0.15	0.19
NiO	0.36	0.36	0.44	nd	nd	nd	nd	nd	nd	nd	nd	nd
Total	100.51	99.76	100.18	99.20	99.04	99.54	100.35	99.26	100.40	99.26	100.03	98.90
Mg #	93.4	93.5	94.7	95.1	95.6	95.6	95.6	95.7	92.3	92.5	92.8	93.6
Structural formula calculations based on 4 oxygens												
Si	1.003	1.004	1.008	0.991	0.982	0.992	0.994	0.983	0.995	0.991	0.989	1.002
Ti	0.001	0.001	0.001	0.001	0.001	0.000	0.000	0.000	0.001	0.003	0.002	0.003
Cr	0.004	0.004	0.003	0.000	0.001	0.001	0.000	0.002	0.003	0.001	0.001	0.000
Mn	0.003	0.003	0.002	0.001	0.001	0.000	0.001	0.002	0.006	0.003	0.001	0.002
Fe	0.130	0.127	0.103	0.100	0.090	0.089	0.088	0.088	0.153	0.150	0.145	0.127
Mg	1.840	1.840	1.856	1.913	1.941	1.922	1.920	1.938	1.837	1.845	1.863	1.849
Ca	0.007	0.007	0.006	0.002	0.002	0.001	0.002	0.002	0.004	0.006	0.004	0.005
Ni	0.007	0.007	0.008	0.000	0.000	0.000	0.000	0.000	0.000	0.000	0.000	0.000
Total	2.995	2.993	2.987	3.008	3.018	3.005	3.005	3.015	2.999	2.999	3.005	2.988

nd = not determined

Olivine analyses: "Water added" system

	PCW 25	PCW 26	PCW 26	PCW 26	PCW 28	PCW 28	PCW 31	PCW 31	PCW 31	PCW 31	PCW 31	PCW 31
kilobars	10	30	30	30	10	10	10	10	10	10	10	10
Celsius	1200	1150	1150	1150	1150	1150	1000	1000	1000	1000	1000	1000
minutes	90	270	270	270	270	270	60	60	60	60	60	60
SiO2	41.71	40.36	40.86	41.00	40.93	40.38	40.59	40.66	40.55	40.77	40.12	41.78
TiO2	0.06	0.05	0.10	0.07	0.07	0.04	0.03	0.02	0.06	0.04	0.02	0.03
Cr203	0.18	0.22	0.12	0.14	0.16	0.18	0.05	0.10	0.08	0.08	0.06	0.05
FeO	6.28	8.45	7.81	7.49	7.62	7 99	8.38	8.20	8.31	7.99	8.02	7.86
MnO	0.21	0.25	0.29	0.14	0.31	0.30	0.14	0.23	0.14	0.15	0.15	0.26
MgO	51.92	49.72	50.23	50.44	50.60	51.10	51.20	50.65	51.69	50.80	51.05	50.51
CaO	0.11	0.07	0.10	0.17	0.13	0.16	0.07	0.07	0.09	0.07	0.06	0.12
NiO	nd	nd	nd	nd	nd	nd	nd	nd	nd	nd	nd	nd
Total	100 47	99.12	99.51	99.45	99.82	100.15	100.46	99.93	100.92	99.90	99.48	100.61
Mg #	93.7	91.3	92.0	92.3	92.2	91.9	91.6	91.7	91.7	91.9	91.9	92.0
Structural formula calculations based on 4 oxygens												
Si	1.000	0.993	0.998	0.999	0.996	0.983	0.985	0.991	0.980	0.992	0.982	1.007
Ti	0.001	0.001	0.002	0.001	0.001	0.001	0.001	0.000	0.001	0.001	0.000	0.001
Cr	0.003	0.004	0.002	0.003	0.003	0.003	0.00	0.002	0.002	0.002	0.001	0.001
Mn	0.004	0.005	0.006	0.003	0.006	0.006	0.003	0.005	0.003	0.003	0.003	0.005
Fe	0.126	0.174	0.159	0.153	0.155	0.163	0.170	0.167	0.168	0.163	0.164	0.158
Mg	1.857	1.823	1.828	1.833	1.835	1.854	1.852	1.840	1.862	1.843	1.863	1.815
Ca	0.003	0.002	0.003	0.004	0.003	0.004	0.002	0.002	0.002	0.002	0.002	0.003
Ni	0.000	0.000	0.000	0.000	0.000	0.000	0.000	0.000	0.000	0.000	0.000	0.000
Total	2.994	3.002	2.998	2.996	2.999	3.014	3.014	3.007	3.018	3.006	3.015	2.99

nd = not determined

Olivine analyses: "Water added" system

	PCW 32	PCW 32	PCW 33	PCW 33	PCW 35	PCW 35	PCW 41	PCW 41	PCW 41	PCW 41
kilobars	20	20	20	20	30	30	30	30	30	30
Celsius	1020	1020	1130	1130	1050	1050	1200	1200	1200	1200
minutes	360	360	240	240	240	240	210	210	210	210
SiO2	41.27	41.05	41.77	41.31	40.38	40.25	41.03	41.68	41.38	41.46
TiO2	0.06	0.05	0.01	0.01	0.06	0.09	0.07	0.04	0.05	0.09
Cr203	0.00	0.00	0.00	0.09	0.00	0.00	0.15	0.13	0.11	0.07
FeO	7.23	6.94	6.58	5.64	7.49	7.31	5.04	4.97	6.09	6.16
MnO	0.13	0.20	0.25	0.20	0.17	0.24	0.16	0.20	0.17	0.16
MgO	50.75	50.59	51.15	51.83	51.96	52.16	52.53	53.08	52.38	52.16
CaO	0.06	0.13	0.14	0.15	0.05	0.09	0.13	0.08	0.09	0.10
NiO	nd	nd	nd	nd	nd	nd	0.41	0.40	0.30	0.34
Total	99.50	98.96	99.90	99.23	100.11	100.14	99.52	100.58	100.57	100.54
Mg #	92.6	92.9	93.3	94.3	92.5	92.7	94.9	95.0	93.9	93.8
Structural formula calculations based on 4 oxygens										
Si	1.003	1.002	1.008	1.000	0.980	0.977	0.992	0.996	0.993	0.995
Ti	0.001	0.001	0.000	0.000	0.001	0.002	0.001	0.001	0.001	0.002
Cr	0.000	0.000	0.000	0.002	0.000	0.000	0.003	0.002	0.002	0.001
Mn	0.003	0.004	0.005	0.004	0.003	0.005	0.003	0.004	0.003	0.003
Fe	0.147	0.142	0.133	0.114	0.152	0.148	0.102	0.099	0.122	0.124
Mg	1.839	1.842	1.840	1.871	1.880	1.887	1.893	1.890	1.874	1.867
Ca	0.002	0.003	0.004	0.004	0.001	0.002	0.003	0.002	0.002	0.003
Ni	0.000	0.000	0.000	0.000	0.000	0.000	0.008	0.008	0.006	0.007
Total	2.995	2.994	2.99	2.995	3.017	3.021	3.005	3.002	3.003	3.002

nd = not determined

Olivine analyses: "Fluorine added" system

	FPC 2	FPC 2	FPC 2	FPC 2	FPC 2	FPC 3	FPC 3	FPC 3	FPC 3	FPC 3	FPC 4	FPC 4
kilobars	20	20	20	20	20	20	20	20	20	20	20	20
Celsius	1300	1300	1300	1300	1300	1200	1200	1200	1200	1200	1100	1100
minutes	20	20	20	20	20	120	120	120	120	120	300	300
SiO2	41.07	40.54	40.09	40.29	40.06	40.00	40.89	40.42	40.85	40.38	40.78	39.74
TiO2	0.05	0.05	0.04	0.07	0.07	0.05	0.08	0.07	0.07	0.08	0.06	0.07
Cr2O3	0.17	0.15	0.22	0.20	0.12	0.25	0.16	0.21	0.15	0.20	0.20	0.07
FeO	4.34	4.33	4.29	4.18	4.22	5.08	5.28	5.26	5.10	5.95	6.46	6.61
MnO	0.06	0.09	0.09	0.09	0.10	0.10	0.15	0.12	0.10	0.12	0.11	0.17
MgO	54.83	53.74	54.51	54.27	54.65	54.25	53.93	54.06	54.10	53.24	52.72	53.06
CaO	0.11	0.10	0.10	0.11	0.10	0.11	0.15	0.12	0.11	0.13	0.11	0.11
NiO	0.22	0.23	0.24	0.21	0.26	0.26	0.28	0.27	0.29	0.29	0.31	0.23
Total	100.85	99.23	99.58	99.42	99.58	100.10	100.92	100.53	100.77	100.39	100.75	100.06
Mg #	95.8	95.7	95.8	95.9	95.9	95.0	94.8	94.8	95.0	94.1	93.6	93.5

Structural formula calculations based on 4 oxygens

Si	0.977	0.980	0.967	0.973	0.967	0.964	0.977	0.970	0.976	0.973	0.980	0.965
Ti	0.001	0.001	0.001	0.001	0.001	0.001	0.001	0.001	0.001	0.001	0.001	0.001
Cr	0.003	0.003	0.004	0.004	0.002	0.005	0.003	0.004	0.003	0.004	0.004	0.001
Mn	0.001	0.002	0.002	0.002	0.002	0.002	0.003	0.002	0.002	0.002	0.002	0.003
Fe	0.086	0.088	0.087	0.084	0.085	0.102	0.105	0.106	0.102	0.120	0.130	0.134
Mg	1.944	1.936	1.960	1.953	1.966	1.950	1.921	1.934	1.928	1.912	1.890	1.920
Ca	0.003	0.003	0.003	0.003	0.003	0.003	0.004	0.003	0.003	0.003	0.003	0.003
Ni	0.004	0.004	0.005	0.004	0.005	0.005	0.005	0.005	0.006	0.006	0.006	0.004
Total	3.019	3.017	3.029	3.024	3.031	3.032	3.019	3.025	3.021	3.021	3.016	3.031

nd = not determined

Olivine analyses: "Fluorine added" system

	FPC 4	FPC 4	FPC 4	FPC 4	FPC 4	FPC 6	FPC 6	FPC 6	FPC 7	FPC 7	FPC 7	FPC 7
kilobars	20	20	20	20	20	10	10	10	10	10	10	10
Celsius	1100	1100	1100	1100	1100	1000	1000	1000	1100	1100	1100	1100
minutes	300	300	300	300	300	360	360	360	300	300	300	300
SiO2	40.00	40.17	39.02	39.45	39.02	41.33	40.98	40.84	41.19	40.91	41.53	41.24
TiO2	0.07	0.06	0.04	0.10	0.11	0.06	0.03	0.04	0.02	0.08	0.01	0.12
Cr203	0.17	0.12	0.03	0.12	0.20	0.05	0.14	0.06	0.04	0.13	0.16	0.24
FeO	7.34	7.22	7.79	6.39	6.20	9.05	8.56	8.85	8.22	8.46	8.73	7.92
MnO	0.13	0.06	0.12	0.08	0.15	0.11	0.11	0.16	0.00	0.20	0.17	0.23
MgO	51.09	52.78	51.93	52.87	53.15	49.23	49.68	50.08	50.63	49.74	49.58	49.83
CaO	0.13	0.16	0.05	0.19	0.17	0.09	0.08	0.12	0.17	0.34	0.36	0.42
NiO	0.22	0.30	0.26	0.30	0.27	0.39	0.32	0.33	0.41	0.34	0.32	0.30
Total	99.15	100.87	99.24	99.50	99.27	100.31	99.90	100.48	100.68	100.20	100.86	100.30
Mg #	92.5	92.9	92.2	93.7	93.9	90.7	91.2	91.0	91.7	91.3	91.0	91.8
Structural formula calculations based on 4 oxygens												
Si	0.981	0.969	0.961	0.963	0.955	1.006	1.000	0.994	0.996	0.997	1.004	1.001
Ti	0.001	0.001	0.001	0.002	0.002	0.001	0.001	0.001	0.000	0.001	0.000	0.002
Cr	0.003	0.002	0.001	0.002	0.004	0.001	0.003	0.001	0.001	0.003	0.003	0.005
Mn	0.003	0.001	0.003	0.002	0.003	0.002	0.002	0.003	0.000	0.004	0.003	0.005
Fe	0.151	0.146	0.160	0.130	0.127	0.184	0.175	0.180	0.166	0.172	0.177	0.161
Mg	1.868	1.899	1.906	1.924	1.940	1.786	1.808	1.816	1.825	1.807	1.787	1.802
Ca	0.005	0.004	0.001	0.005	0.004	0.002	0.002	0.003	0.004	0.009	0.009	0.011
Ni	0.004	0.006	0.005	0.006	0.005	0.008	0.006	0.006	0.008	0.007	0.006	0.006
Total	3.014	3.028	3.038	3.034	3.040	2.990	2.997	3.004	3.000	3.000	2.989	2.993

nd = not determined

Olivine analyses: "Fluorine added" system

	FPC 7	FPC 7	FPC 7	FPC 8	FPC 8	FPC 8	FPC 8	FPC 9	FPC 9	FPC 9	FPC 9	FPC 10
kilobars	10	10	10	20	20	20	20	30	30	30	30	30
Celsius	1100	1100	1100	1000	1000	1000	1000	1200	1200	1200	1200	1100
minutes	300	300	300	300	300	300	300	180	180	180	180	180
SiO2	41.06	40.09	40.81	39.89	40.85	40.63	40.13	41.14	40.84	41.63	41.18	40.85
TiO2	0.10	0.10	0.09	0.06	0.05	0.02	0.06	0.08	0.11	0.05	0.04	0.08
Cr203	0.16	0.27	0.21	0.14	0.05	0.05	0.15	0.22	0.29	0.22	0.16	0.26
FeO	8.13	8.13	8.23	9.45	8.25	9.05	9.02	5.27	5.95	5.29	5.00	7.15
MnO	0.21	0.24	0.23	0.25	0.21	0.13	0.22	0.11	0.12	0.17	0.14	0.12
MgO	50.22	50.28	49.61	48.74	50.46	49.73	48.98	53.23	51.67	52.57	53.20	51.73
CaO	0.39	0.40	0.41	0.44	0.07	0.05	0.12	0.10	0.12	0.09	0.07	0.06
NiO	0.35	0.27	0.28	0.31	0.37	0.35	0.3[illegible]	nd	0.35	0.33	0.35	0.38
Total	100.62	99.78	99.87	99.28	100.31	100.01	99.01	100.15	99.45	100.35	100.14	100.63
Mg #	91.7	91.7	91.5	90.2	91.6	90.7	90.6	94.7	93.9	94.7	95.0	92.8
Structural formula calculations based on 4 oxygens												
Si	0.995	0.982	0.997	0.987	0.993	0.994	0.993	0.985	0.992	0.997	0.989	0.986
Ti	0.002	0.002	0.002	0.001	0.001	0.000	0.001	0.001	0.002	0.001	0.001	0.001
Cr	0.003	0.005	0.004	0.003	0.001	0.001	0.003	0.004	0.006	0.004	0.003	0.005
Mn	0.004	0.005	0.005	0.005	0.004	0.003	0.005	0.002	0.002	0.003	0.003	0.002
Fe	0.165	0.166	0.168	0.196	0.168	0.185	0.187	0.106	0.121	0.106	0.100	0.144
Mg	1.813	1.835	1.806	1.799	1.829	1.814	1.806	1.901	1.871	1.877	1.904	1.861
Ca	0.010	0.010	0.011	0.012	0.002	0.001	0.003	0.003	0.003	0.002	0.002	0.002
Ni	0.007	0.005	0.006	0.006	0.007	0.007	0.007	0.000	0.007	0.006	0.007	0.007
Total	2.999	3.010	2.999	3.009	3.005	3.005	3.005	3.002	3.004	2.996	3.009	3.008

nd = not determined

Olivine analyses: "Fluorine added" system

	FPC 10	FPC 10	FPC 10
kilobars	30	30	30
Celsius	1100	1100	1100
minutes	180	180	180
SIO2	40.94	40.60	40.76
TIO2	0.09	0.03	0.13
Cr203	0.15	0.09	0.21
FeO	6.49	7.77	6.93
MnO	0.15	0.08	0.19
MgO	50.99	50.53	51.83
CaO	0.07	0.06	0.11
NIO	0.31	0.37	0.32
Total	99.19	99.53	100.48
Mg #	93.3	92.1	93.0

Structural formula calculations based on 4 oxygens

SI	0.997	0.992	0.984
TI	0.002	0.001	0.002
Cr	0.003	0.002	0.004
Mn	0.003	0.002	0.004
Fe	0.132	0.159	0.140
Mg	1.852	1.841	1.865
Ca	0.002	0.002	0.003
NI	0.006	0.007	0.006
Total	2.997	3.006	3.008

nd = not determined

5.2 Clinopyroxene

Clinopyroxene analyses: Hypabyssal facies microphenocrysts (HYP)

	PC 30	PC 41	PC 30	PC 53	PC 53	PC 53	PC 53	PC 53	PC 53	PC 53	PC 36	PC 36
	core	core	core	core	core	core	core	core	core	core	core	core
SiO2	51.85	55.35	51.93	53.05	52.71	52.81	52.65	53.04	53.23	53.64	54.84	53.18
TiO2	1.03	0.09	2.59	1.57	1.84	1.79	1.71	1.38	1.46	1.05	1.18	2.15
Al203	0.08	0.00	1.20	0.16	0.23	0.35	0.25	0.22	0.23	0.08	0.18	0.38
Cr203	0.39	1.16	0.57	0.06	0.01	0.45	0.02	0.32	0.15	0.31	0.25	0.11
FeO	2.14	1.50	3.34	3.45	3.52	2.87	3.60	2.90	3.46	2.82	2.56	3.44
MnO	0.16	0.09	0.10	0.04	0.11	0.01	0.03	0.05	0.09	0.04	0.12	0.19
MgO	16.78	17.66	16.09	16.14	16.30	16.43	16.07	16.56	16.29	16.36	16.36	15.83
CaO	26.20	24.12	23.22	25.49	25.18	25.15	24.79	25.87	25.43	25.02	24.29	24.26
K2O	0.07	0.06	0.08	0.07	0.04	0.07	0.11	0.03	0.07	0.04	0.00	0.00
Na2O	0.25	0.57	0.62	0.47	0.40	0.45	0.59	0.30	0.48	0.42	0.41	0.44
Total	98.95	100.60	99.74	100.50	100.34	100.38	99.82	100.67	100.89	99.78	100.19	99.98
Mg #	93.3	95.5	89.6	89.3	89.2	91.1	88.8	91.1	89.4	91 2	91.9	89.1
Structural formula calculations based on 6 oxygens												
Si	1.930	1.997	1.912	1.946	1.936	1.936	1.944	1.939	1.944	1.970	1.993	1.952
Ti	0.029	0.002	0.072	0.043	0.051	0.049	0.047	0.038	0.040	0.029	0.032	0.059
IV Al	0.004	0.000	0.052	0.007	0.010	0.015	0.011	0.009	0.010	0.003	0.007	0.016
VI Al	0.000	0.000	0.000	0.000	0.000	0.000	0.000	0.000	0.000	0.000	0.001	0.000
Cr	0.011	0.033	0.017	0.002	0.000	0.013	0.001	0.009	0.004	0.009	0.007	0.003
Fe	0.067	0.045	0.103	0.106	0.108	0.088	0.111	0.089	0.106	0.087	0.078	0.106
Mn	0.005	0.003	0.003	0.001	0.003	0.000	0.001	0.002	0.003	0.001	0.004	0.006
Mg	0.931	0.950	0.883	0.882	0.893	0.896	0.884	0.903	0.887	0.896	0.886	0.866
Ca	1.045	0.932	0.916	1.002	0.991	0.986	0.980	1.013	0.995	0.984	0.946	0.954
K	0.003	0.003	0.004	0.003	0.002	0.003	0.005	0.001	0.003	0.002	0.000	0.000
Na	0.018	0.040	0.044	0.033	0.028	0.032	0.042	0.021	0.034	0.030	0.029	0.031
Total	4.043	4.005	4.006	4.025	4.022	4.018	4.026	4.024	4.026	4.011	3.983	3.993

Clinopyroxene analyses: Hypabyssal facies microphenocrysts (HYP)

	PC 36	PC 36	PC 36	PC 36	PC 23	PC 23	PC 29c	PC 29c	PC 29c	PC 29a	PC 29a	PC 20
	core	core	core	core	core	core	core	core	core	core	core	core
SiO2	53.54	53.85	54.38	53.67	52.08	54.39	54.22	53.39	53.05	52.71	52.33	53.88
TiO2	1.19	1.35	1.30	1.58	3.00	1.52	0.77	1.06	1.63	1.41	1.70	0.86
Al203	0.16	0.19	0.26	0.27	0.61	0.26	0.08	0.12	0.42	0.27	0.31	0.06
Cr203	0.24	0.12	0.08	0.16	0.31	0.19	0.28	0.20	0.62	0.32	0.25	0.27
FeO	3.13	2.80	3.19	2.96	4.10	3.49	2.21	2.90	2.99	3.27	3.53	2.18
MnO	0.16	0.11	0.13	0.14	0.13	0.17	0.11	0.16	0.00	0.13	0.08	0.00
MgO	16.30	16.61	16.45	16.01	15.25	15.90	17.05	16.77	16.89	16.17	16.74	17.15
CaO	24.54	24.36	24.37	24.57	23.28	23.01	25.72	25.97	25.08	25.26	25.05	25.69
K2O	0.00	0.00	0.00	0.00	0.00	0.00	0.00	0.00	0.00	0.00	0.00	0.04
Na2O	0.30	0.35	0.43	0.28	0.51	0.36	0.36	0.28	0.30	0.41	0.41	0.37
Total	99.56	99.74	100.59	99.64	99.27	99.29	100.80	100.85	100.98	99.95	100.40	100.50
Mg #	90.3	91.4	90.2	90.6	86.9	89.0	93.2	91.2	91.0	89.8	89.4	93.3
Structural formula calculations based on 6 oxygens												
Si	1.970	1.972	1.976	1.970	1.931	1.996	1.968	1.948	1.931	1.943	1.923	1.962
Ti	0.033	0.037	0.036	0.044	0.084	0.042	0.021	0.029	0.045	0.039	0.047	0.024
IV Al	0.007	0.008	0.011	0.012	0.027	0.004	0.003	0.005	0.018	0.012	0.013	0.003
VI Al	0.000	0.000	0.000	0.000	0.000	0.007	0.000	0.000	0.000	0.000	0.000	0.000
Cr	0.007	0.003	0.002	0.005	0.009	0.006	0.008	0.006	0.018	0.009	0.007	0.008
Fe	0.096	0.086	0.097	0.091	0.127	0.107	0.067	0.088	0.091	0.101	0.108	0.066
Mn	0.005	0.003	0.004	0.004	0.004	0.005	0.003	0.005	0.000	0.004	0.002	0.000
Mg	0.894	0.907	0.891	0.876	0.843	0.870	0.922	0.912	0.916	0.888	0.917	0.931
Ca	0.967	0.956	0.949	0.966	0.925	0.905	1.000	1.015	0.978	0.997	0.986	1.002
K	0.000	0.000	0.000	0.000	0.000	0.000	0.000	0.000	0.000	0.000	0.000	0.002
Na	0.021	0.025	0.030	0.020	0.037	0.026	0.025	0.020	0.021	0.029	0.029	0.026
Total	4.000	3.997	3.996	3.988	3.987	3.968	4.017	4.028	4.018	4.022	4.032	4.024

Clinopyroxene analyses: Hypabyssal facies microphenocrysts (HYP)

	PC 20	PC 29e	PC 30b	PC 30b	PC 53	PC 53	PC 53	PC 53	PC 30b	PC 30b	PC 20	PC 20
	core	core	core	edge	core	core	core	core	core	core	core	core
SiO2	52.80	53.96	53.27	54.24	52.38	52.96	52.71	52.11	52.72	53.49	53.25	54.24
TiO2	1.66	1.49	0.90	0.85	2.04	1.70	1.96	1.86	2.00	0.93	1.75	1.02
Al203	0.29	0.23	0.14	0.14	0.29	0.30	0.39	0.25	0.34	0.14	0.29	0.12
Cr203	0.27	0.22	0.38	0.32	0.17	0.26	0.18	0.14	0.16	0.45	0.22	0.39
FeO	3.10	2.80	2.37	2.23	3.54	3.11	3.66	3.10	3.26	2.23	3.60	2.44
MnO	0.00	0.06	0.13	0.09	0.04	0.07	0.08	0.05	0.11	0.09	0.14	0.19
MgO	16.40	16.64	17.04	17.15	15.94	16.21	16.14	16.31	16.67	17.56	16.44	16.87
CaO	25.45	24.97	26.06	25.55	25.19	25.40	25.32	24.71	24.92	25.50	24.77	25.20
K2O	0.07	0.00	0.03	0.06	0.10	0.12	0.14	0.12	0.12	0.05	0.00	0.00
Na2O	0.51	0.44	0.36	0.34	0.51	0.39	0.39	0.51	0.57	0.38	0.44	0.44
Total	100.55	100.81	100.68	100.97	100.20	100.52	100.97	99.16	100.87	100.82	100.90	100.91
Mg #	90.4	91.4	92.8	93.2	88.9	90.3	88.7	90.4	90.1	93.4	89.0	92.5
Structural formula calculations based on 6 oxygens												
Si	1.934	1.960	1.944	1.965	1.930	1.940	1.928	1.935	1.926	1.945	1.942	1.967
Ti	0.046	0.041	0.025	0.023	0.057	0.047	0.054	0.052	0.055	0.025	0.048	0.028
IV Al	0.013	0.010	0.006	0.006	0.013	0.013	0.017	0.011	0.015	0.006	0.012	0.005
VI Al	0.000	0.000	0.000	0.000	0.000	0.000	0.000	0.000	0.000	0.000	0.000	0.000
Cr	0.008	0.006	0.011	0.009	0.005	0.008	0.005	0.004	0.005	0.013	0.006	0.011
Fe	0.095	0.085	0.072	0.068	0.109	0.095	0.112	0.096	0.100	0.068	0.110	0.074
Mn	0.000	0.002	0.004	0.003	0.001	0.002	0.002	0.002	0.003	0.003	0.004	0.006
Mg	0.896	0.901	0.927	0.926	0.876	0.885	0.880	0.903	0.908	0.952	0.894	0.912
Ca	0.999	0.972	1.019	0.992	0.994	0.997	0.992	0.983	0.975	0.993	0.968	0.979
K	0.003	0.000	0.001	0.003	0.005	0.006	0.007	0.006	0.006	0.002	0.000	0.000
Na	0.036	0.031	0.025	0.024	0.036	0.028	0.028	0.037	0.040	0.027	0.031	0.031
Total	4.030	4.008	4.034	4.019	4.026	4.021	4.025	4.029	4.033	4.034	4.015	4.013

Clinopyroxene analyses: Hypabyssal facies microphenocrysts (HYP)

	PC 20	PC 20	PC 20	PC 20	PC 30	PC 30	PC 30	PC 30
	core	core	core	core	core	core	core	edge
SiO2	53.64	53.89	53.70	53.58	52.53	52.76	52.12	53.37
TiO2	1.34	0.84	1.29	0.87	1.61	1.60	1.63	0.91
Al203	0.16	0.08	0.14	0.09	1.38	0.87	0.38	0.33
Cr203	0.27	0.33	0.14	0.47	0.08	0.07	0.00	0.45
FeO	2.31	2.18	3.35	2.30	3.01	3.08	3.23	2.30
MnO	0.04	0.13	0.12	0.05	0.13	0.09	0.10	0.00
MgO	16.78	17.16	16.31	16.52	16.01	16.19	16.65	17.49
CaO	25.33	25.37	24.48	24.81	23.73	24.27	24.87	24.38
K2O	0.10	0.09	0.10	0.10	1.21	0.64	0.05	0.14
Na2O	0.82	0.41	0.51	0.55	0.52	0.51	0.48	0.44
Total	100.79	100.48	100.14	99.34	100.21	100.08	99.51	99.81
Mg #	92.8	93.4	89.7	92.8	90.5	90.4	90.2	93.1
Structural formula calculations based on 6 oxygens								
SI	1.952	1.963	1.968	1.973	1.931	1.939	1.929	1.954
TI	0.037	0.023	0.036	0.024	0.045	0.044	0.045	0.025
IV Al	0.007	0.003	0.006	0.004	0.060	0.038	0.017	0.014
VI Al	0.000	0.000	0.000	0.000	0.000	0.000	0.000	0.000
Cr	0.008	0.010	0.004	0.014	0.002	0.002	0.000	0.013
Fe	0.070	0.066	0.103	0.071	0.093	0.095	0.100	0.070
Mn	0.001	0.004	0.004	0.002	0.004	0.003	0.003	0.000
Mg	0.910	0.932	0.891	0.907	0.977	0.887	0.919	0.955
Ca	0.988	0.990	0.961	0.979	0.935	0.956	0.986	0.956
K	0.005	0.004	0.005	0.005	0.057	0.030	0.002	0.007
Na	0.058	0.029	0.036	0.039	0.037	0.036	0.034	0.031
Total	4.036	4.024	4.014	4.018	4.041	4.030	4.035	4.025

Clinopyroxene analyses: Diopside-richterite cognate xenoliths (DRX)

	PC 63	PC 63	PC 53	PC 53	PC 20	PC 20	PC 20	PC 20	PC 63	PC 54	PC 54	PC 40b
	core	core	core	core	core	core	core	core	core	core	core	core
SiO2	53.76	54.57	54.67	54.70	54.14	55.13	54.27	54.76	54.13	53.64	54.01	53.64
TiO2	0.56	0.59	0.43	0.41	0.31	0.33	0.29	0.51	0.63	1.23	1.14	1.07
Al203	0.01	0.06	0.04	0.04	0.02	0.04	0.06	0.04	0.09	0.13	0.09	0.31
Cr203	0.16	0.20	0.25	0.33	0.31	0.27	0.07	0.19	0.13	0.00	0.06	0.52
FeO	2.22	2.19	2.21	2.46	1.55	1.50	1.51	1.47	2.39	5.08	4.31	2.03
MnO	0.25	0.20	0.04	0.08	0.06	0.00	0.00	0.05	0.06	0.13	0.11	0.07
MgO	16.30	16.53	17.00	16.58	17.60	17.55	18.07	17.65	17.09	15.65	15.81	17.35
CaO	26.18	25.73	25.21	25.23	25.31	25.06	24.70	24.82	25.53	23.01	23.70	25.07
K2O	0.04	0.04	0.03	0.02	0.00	0.00	0.05	0.02	0.01	0.00	0.00	0.06
Na2O	0.42	0.47	0.41	0.44	0.30	0.34	0.27	0.41	0.48	1.70	1.17	0.38
Total	99.90	100.58	100.29	100.29	99.60	100.22	99.29	99.92	100.54	100.57	100.40	100.50
Mg #	92.9	93.1	93.2	92.3	95.3	95.4	95.5	95.5	92.7	84.6	86.7	93.8
Structural formula calculations based on 6 oxygens												
Si	1.974	1.984	1.988	1.992	1.979	1.996	1.984	1.989	1.97	1.97	1.979	1.951
Ti	0.015	0.016	0.012	0.011	0.009	0.009	0.008	0.014	0.017	0.034	0.031	0.029
IV Al	0.000	0.003	0.002	0.002	0.001	0.002	0.003	0.002	0.004	0.006	0.004	0.013
VI Al	0.000	0.000	0.000	0.000	0.000	0.000	0.000	0.000	0.000	0.000	0.000	0.000
Cr	0.005	0.006	0.007	0.009	0.009	0.008	0.002	0.005	0.004	0.000	0.002	0.015
Fe	0.068	0.067	0.067	0.075	0.047	0.045	0.046	0.045	0.073	0.156	0.132	0.062
Mn	0.008	0.006	0.001	0.002	0.002	0.000	0.000	0.002	0.002	0.004	0.003	0.002
Mg	0.892	0.896	0.922	0.900	0.959	0.947	0.985	0.956	0.927	0.857	0.864	0.941
Ca	1.030	1.002	0.982	0.984	0.991	0.972	0.967	0.966	0.995	0.906	0.930	0.977
K	0.002	0.002	0.001	0.001	0.000	0.000	0.002	0.001	0.000	0.000	0.000	0.003
Na	0.030	0.033	0.029	0.031	0.021	0.024	0.019	0.029	0.034	0.121	0.083	0.027
Total	4.024	4.015	4.011	4.007	4.018	4.003	4.016	4.009	4.026	4.054	4.028	4.020

Clinopyroxene analyses: Diopside-richterite cognate xenoliths (DRX)

	PC 54	PC 54	PC 29d	PC 53	PC 29c	PC 20	PC 63	PC 53	PC 53	PC 63	PC 54	PC 54
	core	core	core	core	core	core	core	edge	edge	edge	edge	edge
SiO2	53.77	53.51	53.33	54.59	54.18	54.36	54.03	53.99	54.23	53.40	53.43	53.36
TiO2	1.03	1.13	0.76	0.49	0.79	0.00	0.49	0.96	0.68	0.88	1.29	1.10
Al203	0.10	0.27	0.04	0.05	0.07	0.02	0.10	0.06	0.07	0.14	0.10	0.13
Cr203	0.01	0.00	0.00	0.19	0.22	4.69	0.07	0.21	0.20	0.04	0.01	0.00
FeO	4.31	4.43	2.15	2.39	2.08	0.81	2.49	2.54	2.40	2.41	5.09	4.47
MnO	0.11	0.10	0.01	0.04	0.00	0.00	0.04	0.02	0.06	0.00	0.12	0.11
MgO	15.72	15.73	16.29	16.96	17.29	15.05	17.31	16.89	16.75	16.70	15.66	15.67
CaO	24.08	23.57	25.87	25.41	25.89	22.19	25.36	25.18	25.14	25.17	22.79	23.15
K2O	0.00	0.00	0.01	0.03	0.00	0.05	0.00	0.02	0.01	0.00	0.00	0.00
Na2O	1.20	1.28	0.35	0.43	0.36	2.13	0.38	0.43	0.45	0.46	1.67	1.33
Total	100.33	100.02	98.81	100.58	100.88	99.30	100.27	100.30	99.99	99.20	100.16	99.32
Mg #	86.7	86.4	93.1	92.7	93.7	97.1	92.5	92.2	92.6	92.5	84.6	86.2
Structural formula calculations based on 6 oxygens												
Si	1.975	1.971	1.975	1.983	1.964	1.997	1.97	1.969	1.981	1.969	1.97	1.978
Ti	0.028	0.031	0.021	0.013	0.022	0.000	0.013	0.026	0.019	0.024	0.036	0.031
IV Al	0.004	0.012	0.002	0.002	0.003	0.001	0.004	0.003	0.003	0.006	0.004	0.006
VI Al	0.000	0.000	0.000	0.000	0.000	0.000	0.000	0.000	0.000	0.000	0.000	0.000
Cr	0.000	0.000	0.000	0.005	0.006	0.136	0.002	0.006	0.006	0.001	0.000	0.000
Fe	0.132	0.136	0.067	0.073	0.063	0.025	0.076	0.077	0.073	0.074	0.157	0.139
Mn	0.003	0.003	0.000	0.001	0.000	0.000	0.001	0.001	0.002	0.000	0.004	0.003
Mg	0.861	0.864	0.999	0.918	0.934	0.824	0.941	0.918	0.912	0.918	0.861	0.866
Ca	0.948	0.930	1.026	0.989	1.005	0.874	0.991	0.984	0.984	0.994	0.900	0.919
K	0.000	0.000	0.000	0.001	0.000	0.002	0.000	0.001	0.000	0.000	0.000	0.000
Na	0.085	0.091	0.025	0.030	0.025	0.152	0.027	0.030	0.032	0.033	0.119	0.096
Total	4.036	4.038	4.015	4.015	4.022	4.011	4.025	4.015	4.012	4.019	4.051	4.038

Clinopyroxene analyses: DRX

	PC 20	PC 63
	edge	edge
SiO2	54.94	53.95
TiO2	0.06	0.77
Al203	0.02	0.09
Cr203	2.25	0.00
FeO	1.18	2.58
MnO	0.00	0.00
MgO	16.63	17.07
CaO	23.93	25.06
K2O	0.06	0.01
Na2O	1.11	0.39
Total	100.18	99.92
Mg #	96.2	92.2
Structural formula calculations based on 6 oxygens		
Si	1.995	1.973
Ti	0.002	0.021
IV Al	0.001	0.004
VI Al	0.000	0.000
Cr	0.065	0.000
Fe	0.036	0.079
Mn	0.000	0.000
Mg	0.900	0.931
Ca	0.931	0.982
K	0.003	0.000
Na	0.078	0.028
Total	4.011	4.018

Clinopyroxene analyses: Corona rim 1 (CR1)

	PC 53	PC 22	PC 22	PC 22	PC 22	PC 22	PC 22
	core	core	core	core	core	core	core
SiO2	54.21	54.38	54.20	54.39	53.94	54.05	54.38
TiO2	0.61	0.47	0.86	0.70	1.09	0.88	0.87
Al203	0.05	0.06	0.05	0.05	0.06	0.08	0.11
Cr203	0.39	0.57	0.91	0.69	0.71	0.76	0.50
FeO	2.12	1.98	1.99	1.87	2.13	1.87	2.06
MnO	0.03	0.02	0.01	0.00	0.03	0.04	0.06
MgO	16.83	17.18	16.86	17.07	17.06	16.96	16.95
CaO	25.48	25.64	25.07	25.21	25.18	25.19	24.94
K2O	0.02	0.01	0.03	0.02	0.02	0.02	0.01
Na2O	0.52	0.44	0.56	0.52	0.57	0.59	0.54
Total	100.26	100.75	100.54	100.52	100.79	100.44	100.42
Mg #	93.4	93.9	93.8	94.2	93.5	94.2	93.6
Structural formula calculations based on 6 oxygens							
Si	1.976	1.972	1.970	1.974	1.958	1.966	1.976
Ti	0.017	0.013	0.024	0.019	0.030	0.024	0.024
IV Al	0.002	0.003	0.002	0.002	0.003	0.003	0.005
VI Al	0.000	0.000	0.000	0.000	0.000	0.000	0.000
Cr	0.011	0.016	0.026	0.020	0.020	0.022	0.014
Fe	0.065	0.060	0.060	0.057	0.065	0.057	0.063
Mn	0.001	0.001	0.000	0.000	0.001	0.001	0.002
Mg	0.915	0.929	0.913	0.924	0.923	0.920	0.918
Ca	0.995	0.996	0.976	0.981	0.980	0.982	0.971
K	0.001	0.000	0.001	0.001	0.001	0.001	0.000
Na	0.037	0.031	0.039	0.037	0.040	0.042	0.038
Total	4.020	4.021	4.011	4.015	4.021	4.018	4.011

Clinopyroxene analyses: Corona rim 1 (CR1)

	PC 29a core	PC 29a core	PC 20 core	PC 20 core	PC 20 core	PC 20 core	PC 63 core	PC 20 core	PC 20 core	PC 20 core	PC 20 core	PC 20 core
SiO2	54.07	53.24	54.81	51.16	54.43	53.76	53.26	54.74	55.17	54.89	53.50	55.13
TiO2	0.76	1.63	0.43	1.73	0.64	1.07	0.96	0.12	0.00	0.08	1.07	0.06
Al203	0.11	0.28	0.07	0.25	0.04	0.26	0.10	0.04	0.02	0.02	0.12	0.02
Cr203	0.68	0.32	0.60	0.16	0.37	0.54	0.58	2.56	3.45	3.34	0.64	2.17
FeO	1.95	2.78	2.16	3.07	2.16	2.50	2.29	1.11	0.94	1.00	1.97	1.32
MnO	0.08	0.11	0.14	0.19	0.12	0.00	0.02	0.06	0.00	0.00	0.00	0.00
MgO	17.29	16.47	17.08	16.18	17.43	17.02	16.65	16.21	15.66	15.76	16.87	16.43
CaO	25.01	25.25	25.05	26.02	25.36	25.14	24.91	24.46	23.56	23.31	24.94	24.61
K2O	0.00	0.07	0.00	0.00	0.00	0.00	0.02	0.00	0.04	0.02	0.02	0.03
Na2O	0.54	0.41	0.46	0.55	0.32	0.48	0.49	1.24	1.69	1.69	0.52	1.14
Total	100.49	100.56	100.80	99.31	100.87	100.77	99.28	100.54	100.53	100.11	99.65	100.91
Mg #	94.1	91.4	93.4	90.4	93.5	92.4	92.8	96.3	96.7	96.6	93.9	95.7
Structural formula calculations based on 6 oxygens												
Si	1.965	1.945	1.984	1.909	1.971	1.954	1.963	1.987	2.000	1.998	1.962	1.992
Ti	0.021	0.045	0.012	0.049	0.017	0.029	0.027	0.003	0.000	0.002	0.030	0.002
IV Al	0.005	0.012	0.003	0.011	0.002	0.011	0.004	0.002	0.000	0.001	0.005	0.001
VI Al	0.000	0.000	0.000	0.000	0.000	0.000	0.000	0.000	0.000	0.000	0.000	0.000
Cr	0.020	0.009	0.017	0.005	0.011	0.016	0.017	0.073	0.099	0.096	0.019	0.062
Fe	0.059	0.085	0.065	0.096	0.065	0.076	0.071	0.034	0.028	0.030	0.060	0.040
Mn	0.002	0.003	0.004	0.006	0.004	0.000	0.001	0.002	0.000	0.000	0.000	0.000
Mg	0.937	0.897	0.922	0.900	0.941	0.922	0.915	0.877	0.846	0.855	0.922	0.885
Ca	0.974	0.988	0.971	1.040	0.984	0.979	0.984	0.951	0.915	0.909	0.980	0.953
K	0.000	0.003	0.000	0.000	0.000	0.000	0.001	0.000	0.002	0.001	0.001	0.001
Na	0.038	0.029	0.032	0.040	0.022	0.034	0.035	0.087	0.119	0.119	0.037	0.080
Total	4.021	4.016	4.010	4.056	4.017	4.021	4.018	4.016	4.009	4.011	4.016	4.016

Clinopyroxene analyses: Corona rim 1 (CR1)

	PC 20 core	PC 20 core	PC 20 core	PC 63 core	PC 63 core	PC 63 core	PC 63 core	PC 63 core	PC 25 core	PC 20b core	PC 20b core	PC 20b core
SiO2	54.37	55.06	53.47	54.49	54.56	53.69	54.12	53.89	53.69	53.55	54.14	53.23
TiO2	0.03	0.72	0.66	1.20	0.77	1.12	1.09	0.92	1.46	1.08	0.41	0.85
Al203	0.02	0.07	0.19	0.10	0.08	0.21	0.11	0.08	0.23	0.19	0.15	0.23
Cr203	3.77	0.32	0.50	0.71	0.54	0.65	0.69	0.72	0.07	0.48	0.34	0.49
FeO	1.05	1.75	1.98	2.28	1.97	2.16	2.13	1.97	2.90	2.25	1.98	1.95
MnO	0.01	0.00	0.12	0.00	0.00	0.06	0.07	0.04	0.00	0.16	0.15	0.12
MgO	15.60	17.13	17.59	16.82	16.88	16.90	16.65	16.77	16.61	16.98	17.16	17.20
CaO	22.83	25.09	24.07	24.60	25.31	24.80	24.60	25.12	25.07	24.15	24.93	24.66
K2O	0.05	0.03	0.12	0.02	0.02	0.05	0.03	0.02	0.00	0.00	0.00	0.00
Na2O	1.71	0.37	0.47	0.57	0.47	0.59	0.59	0.54	0.43	0.66	0.53	0.53
Total	99.44	100.54	99.27	100.79	100.60	100.23	100.08	100.07	100.46	99.50	99.79	99.26
Mg #	96.4	94.6	94.1	92.9	93.9	93.3	93.3	93.8	91.1	93.1	93.9	94.0
Structural formula calculations based on 6 oxygens												
Si	1.994	1.991	1.965	1.973	1.979	1.959	1.974	1.968	1.958	1.965	1.979	1.959
Ti	0.001	0.020	0.018	0.033	0.021	0.031	0.030	0.025	0.040	0.030	0.011	0.024
IV Al	0.001	0.003	0.008	0.004	0.003	0.009	0.005	0.003	0.010	0.008	0.006	0.010
VI Al	0.000	0.000	0.000	0.000	0.000	0.000	0.000	0.000	0.000	0.000	0.000	0.000
Cr	0.109	0.009	0.017	0.020	0.015	0.019	0.020	0.021	0.002	0.014	0.010	0.014
Fe	0.032	0.053	0.061	0.069	0.060	0.066	0.065	0.060	0.088	0.069	0.061	0.060
Mn	0.000	0.000	0.004	0.000	0.000	0.002	0.002	0.001	0.000	0.005	0.005	0.004
Mg	0.853	0.923	0.964	0.908	0.913	0.919	0.905	0.913	0.903	0.929	0.935	0.944
Ca	0.897	0.972	0.948	0.954	0.983	0.970	0.961	0.983	0.980	0.950	0.976	0.972
K	0.002	0.001	0.006	0.001	0.001	0.002	0.001	0.001	0.000	0.000	0.000	0.000
Na	0.122	0.026	0.033	0.040	0.033	0.042	0.042	0.038	0.030	0.047	0.038	0.038
Total	4.011	3.988	4.024	4.002	4.008	4.019	4.005	4.013	4.011	4.017	4.017	4.021

Clinopyroxene analyses: Corona rim 2 (CR2)

	PC 53 core	PC 53 core	PC 22 core	PC 22 core	PC 22 core	PC 22 core	PC 22 core	PC 22 core	PC 22 core	PC 22 core	PC 29c core	PC 29a core
SiO2	54.31	54.38	53.94	54.10	53.92	53.87	54.29	52.89	53.07	54.17	54.14	54.59
TiO2	0.86	0.77	0.94	0.86	1.04	0.99	0.94	1.92	1.67	0.77	0.77	0.79
Al203	0.04	0.06	0.09	0.08	0.10	0.10	0.09	0.19	0.25	0.03	0.11	0.10
Cr203	0.56	0.44	0.58	0.47	0.57	0.48	0.44	0.22	0.04	0.38	0.54	0.61
FeO	2.02	2.28	1.99	2.16	2.23	2.01	2.21	3.11	3.38	2.29	2.00	1.91
MnO	0.10	0.01	0.04	0.02	0.04	0.01	0.01	0.06	0.10	0.08	0.00	0.07
MgO	16.79	16.63	17.03	17.03	17.03	17.03	16.97	16.54	16.32	17.01	17.07	16.81
CaO	25.36	25.74	25.19	25.40	24.97	25.62	25.47	25.37	25.30	25.74	25.26	25.22
K2O	0.03	0.05	0.03	0.02	0.03	0.04	0.03	0.02	0.03	0.04	0.00	0.00
Na2O	0.47	0.44	0.50	0.47	0.50	0.44	0.47	0.47	0.36	0.34	0.44	0.42
Total	100.54	100.80	100.33	100.61	100.43	100.59	100.92	100.79	100.57	100.85	100.33	100.52
Mg #	93.7	92.9	93.9	93.4	93.2	93.8	93.2	90.5	89.6	93.0	93.8	94.0
Structural formula calculations based on 6 oxygens												
Si	1.974	1.974	1.965	1.966	1.963	1.959	1.967	1.932	1.943	1.967	1.970	1.980
Ti	0.024	0.021	0.026	0.024	0.028	0.027	0.026	0.053	0.046	0.021	0.021	0.022
IV Al	0.002	0.003	0.004	0.003	0.004	0.004	0.004	0.008	0.011	0.001	0.005	0.004
VI Al	0.000	0.000	0.000	0.000	0.000	0.000	0.000	0.000	0.000	0.000	0.000	0.000
Cr	0.016	0.013	0.017	0.014	0.016	0.014	0.013	0.006	0.001	0.011	0.016	0.017
Fe	0.061	0.069	0.061	0.066	0.068	0.061	0.067	0.095	0.103	0.070	0.061	0.058
Mn	0.003	0.000	0.001	0.001	0.001	0.000	0.000	0.002	0.003	0.002	0.000	0.002
Mg	0.910	0.900	0.925	0.923	0.924	0.923	0.917	0.901	0.891	0.921	0.926	0.909
Ca	0.987	1.001	0.983	0.989	0.974	0.998	0.989	0.993	0.992	1.001	0.985	0.980
K	0.001	0.002	0.001	0.001	0.001	0.002	0.001	0.001	0.004	0.002	0.000	0.000
Na	0.033	0.031	0.035	0.033	0.035	0.031	0.033	0.033	0.026	0.024	0.031	0.030
Total	4.011	4.014	4.018	4.020	4.014	4.019	4.017	4.024	4.020	4.020	4.015	4.002

Clinopyroxene analyses: Corona rim 2 (CR2)

	PC 20 core	PC 20 core	PC 20 core	PC 20 core	PC 20 core	PC 20 core	PC 20 core	PC 20 core	PC 20 core	PC 20 core	PC 63 core	PC 63 core
SiO2	54.66	53.34	54.02	53.91	53.93	53.64	53.40	52.85	53.77	53.82	53.78	54.13
TiO2	0.70	0.90	1.07	0.87	1.49	0.81	0.87	1.29	0.91	1.06	1.00	0.83
Al2O3	0.08	0.12	0.12	0.10	0.12	0.08	0.07	0.20	0.10	0.11	0.12	0.07
Cr2O3	0.91	0.54	0.40	0.57	0.44	0.62	0.46	0.19	0.60	0.46	0.40	0.42
FeO	1.90	2.21	2.48	1.97	2.29	1.73	1.99	3.05	1.90	2.26	2.23	1.80
MnO	0.09	0.05	0.04	0.00	0.00	0.00	0.00	0.00	0.00	0.00	0.00	0.00
MgO	16.85	17.10	16.88	17.29	16.98	17.13	16.84	16.41	17.01	16.72	17.11	17.02
CaO	25.28	25.09	25.22	25.57	24.69	25.31	25.62	25.10	25.12	24.73	25.02	25.32
K2O	0.00	0.00	0.06	0.05	0.05	0.04	0.04	0.06	0.07	0.05	0.02	0.00
Na2O	0.49	0.50	0.43	0.45	0.75	0.52	0.46	0.42	0.50	0.44	0.45	0.36
Total	100.96	99.85	100.72	100.78	100.74	99.88	99.75	99.57	99.98	99.65	100.13	99.95
Mg #	94.1	93.2	92.4	94.0	93.0	94.6	93.8	90.6	94.1	93.0	93.2	94.4
Structural formula calculations based on 6 oxygens												
Si	1.976	1.956	1.963	1.957	1.958	1.962	1.960	1.951	1.965	1.972	1.963	1.975
Ti	0.019	0.025	0.029	0.024	0.041	0.022	0.024	0.036	0.025	0.029	0.027	0.023
IV Al	0.003	0.005	0.005	0.004	0.005	0.003	0.003	0.009	0.004	0.005	0.005	0.003
VI Al	0.000	0.000	0.000	0.000	0.000	0.000	0.000	0.000	0.000	0.000	0.000	0.000
Cr	0.026	0.016	0.011	0.016	0.013	0.018	0.013	0.006	0.017	0.013	0.012	0.012
Fe	0.057	0.068	0.075	0.060	0.070	0.053	0.061	0.094	0.058	0.069	0.068	0.055
Mn	0.003	0.002	0.001	0.000	0.000	0.000	0.000	0.000	0.000	0.000	0.000	0.000
Mg	0.908	0.935	0.915	0.936	0.919	0.934	0.921	0.903	0.927	0.913	0.931	0.926
Ca	0.979	0.986	0.982	0.995	0.960	0.992	1.008	0.993	0.984	0.971	0.978	0.990
K	0.000	0.000	0.003	0.002	0.002	0.002	0.002	0.003	0.003	0.002	0.001	0.000
Na	0.034	0.036	0.030	0.032	0.053	0.037	0.033	0.030	0.035	0.031	0.032	0.025
Total	4.005	4.029	4.014	4.026	4.021	4.023	4.025	4.025	4.018	4.005	4.017	4.009

Clinopyroxene analyses: Corona rim 2 (CR2)

	PC 63 core	PC 63 core	PC 63 core
SiO2	53.91	54.10	53.73
TiO2	0.95	0.91	1.02
Al203	0.11	0.08	0.11
Cr203	0.76	0.52	0.69
FeO	2.18	2.10	2.00
MnO	0.04	0.05	0.00
MgO	16.47	17.24	17.38
CaO	24.22	25.49	25.23
K2O	0.00	0.02	0.03
Na2O	0.56	0.39	0.53
Total	99.20	100.90	100.72
Mg #	93.1	93.6	93.9

Structural formula calculations based on 6 oxygens

SI	1.981	1.961	1.952
TI	0.026	0.025	0.028
IV Al	0.005	0.003	0.005
VI Al	0.000	0.000	0.000
Cr	0.022	0.015	0.020
Fe	0.067	0.064	0.061
Mn	0.001	0.002	0.000
Mg	0.902	0.932	0.941
Ca	0.954	0.990	0.982
K	0.000	0.001	0.001
Na	0.040	0.027	0.037
Total	3.998	4.020	4.027

Clinopyroxene analyses: Corona rim 3 (CR3)

	PC 29c core	PC 29a core	PC 20 core	PC 20 core	PC 20 core
SiO2	53.54	52.53	52.34	53.39	54.55
TiO2	1.52	1.76	2.08	0.76	0.74
Al203	0.43	0.42	0.43	0.06	0.07
Cr203	0.22	0.26	0.11	0.62	0.34
FeO	2.59	3.10	3.29	1.89	2.07
MnO	0.10	0.10	0.13	0.00	0.00
MgO	16.66	16.46	16.59	16.83	17.07
CaO	25.30	24.83	25.53	25.16	25.40
K2O	0.00	0 00	0.00	0.07	0.13
Na2O	0.39	0.49	0.45	0.45	0.46
Total	100.75	99.95	100.95	99.23	100.83
Mg #	92.0	90.4	90.0	94.1	93.6

Structural formula calculations based on 6 oxygens

SI	1.947	1.933	1.914	1.957	1.976
TI	0.042	0.049	0.057	0.021	0.020
IV Al	0.018	0.018	0.019	0.003	0.003
VI Al	0.000	0.000	0.000	0.000	0.000
Cr	0.006	0.008	0.003	0.018	0.010
Fe	0.079	0.095	0.101	0.058	0.063
Mn	0.003	0.003	0.004	0.000	0.000
Mg	0.903	0.903	0.904	0.924	0.922
Ca	0.986	0.979	1.000	0.993	0.986
K	0.000	0.000	0.000	0.003	0.006
Na	0.028	0.035	0.032	0.032	0.032
Total	4.012	4.023	4.034	4.019	4.018

Clinopyroxene analyses: Corona rim 3 (CR3)

	PC 20 core	PC 20 core	PC 20 core	PC 20 core	PC 20 core	PC 20 core	PC 20 core	PC 20 core	PC 20 core	PC 20 core	PC 20 core	PC 20 core
SiO2	54.53	52.31	54.08	53.70	52.95	52.71	52.14	53.22	51.90	53.53	53.15	53.89
TiO2	0.71	2.24	0.79	1.20	1.72	1.40	2.21	1.57	2.34	1.04	1.30	1.05
Al203	0.05	0.47	0.09	0.25	0.31	0.21	0.41	0.22	0.49	0.14	0.36	0.06
Cr203	0.41	0.22	0.41	0.46	0.19	0.17	0.21	0.05	0 17	0.22	0.28	0.47
FeO	2.03	3.60	2.00	2.51	2.97	3.58	2.76	3.50	3.70	2.87	2.97	2.49
MnO	0.01	0.00	0.01	0.09	0.04	0.00	0.02	0.08	0.12	0.08	0.02	0.00
MgO	17.23	16.24	16.93	16.78	16.89	16.20	16.22	16.28	15.85	16.99	16.60	17.03
CaO	25.43	25.32	25.64	25.01	25.15	24.33	24.52	25.16	24.46	25.02	24.37	25.32
K2O	0.06	0.07	0.10	0.07	0.10	0.10	0.23	0.13	0.13	0.10	0.12	0.10
Na2O	0.37	0.45	0.44	0.49	0.65	0.95	0.61	0.66	0.78	0.35	0.44	0.54
Total	100.83	100.92	100.49	100.56	100.97	99.65	99.33	100.87	99.94	100.34	99.61	100.95
Mg #	93.8	88.9	93.8	92.3	91.0	89.0	91.3	89.2	88.4	91.3	90.9	92.4
Structural formula calculations based on 6 oxygens												
Si	1.974	1.915	1.968	1.956	1.930	1.949	1.930	1.945	1.919	1.957	1.955	1.957
Ti	0.019	0.062	0.022	0.033	0.047	0.039	0.062	0.043	0.065	0.029	0.036	0.029
IV Al	0.002	0.020	0.004	0.011	0.013	0.009	0.018	0.009	0.021	0.006	0.016	0.003
VI Al	0.000	0.000	0.000	0.000	0.000	0.000	0.000	0.000	0.000	0.000	0.000	0.000
Cr	0.012	0.006	0.012	0.013	0.005	0.005	0.006	0.001	0.005	0.006	0.008	0.013
Fe	0.061	0.110	0.061	0.076	0.091	0.111	0.085	0.107	0.114	0.088	0.091	0.076
Mn	0.000	0.000	0.000	0.003	0.001	0.000	0.001	0.002	0.004	0.002	0.001	0.000
Mg	0.930	0.886	0.918	0.911	0.918	0.893	0.895	0.887	0.874	0.926	0.910	0.922
Ca	0.986	0.993	1.000	0.976	0.982	0.964	0.972	0.985	0.969	0.980	0.961	0.985
K	0.003	0.003	0.005	0.003	0.005	0.005	0.011	0.006	0.006	0.005	0.006	0.005
Na	0.026	0.032	0.031	0.035	0.046	0.068	0.044	0.047	0.056	0.025	0.031	0.038
Total	4.013	4.027	4.021	4.017	4.038	4.043	4.024	4.032	4.033	4.024	4.015	4.028

Clinopyroxene analyses: Corona rim 3 (CR3)

	PC 20 core	PC 20 core	PC 20 core	PC 20 core	PC 20 core	PC 20 core	PC 20 core	PC 63 core	PC 63 core	PC 63 core	PC 63 core	PC 63 core
SiO2	53.12	51.66	52.07	53.41	54.01	52.49	52.82	54.18	53.92	54.88	53.16	54.37
TiO2	1.66	2.65	2.32	1.30	0.71	1.87	1.63	0.97	1.19	0.91	1.47	0.80
Al203	0.29	0.35	0.43	0.15	0.17	0.29	0.35	0.10	0.14	0.09	0.27	0.09
Cr203	0.19	0.16	0.26	0.17	0.49	0.17	0.16	0.50	0.39	0.49	0.35	0.33
FeO	3.18	3.65	3.17	3.13	2.79	3.90	3.07	2.10	2.66	2.22	2.81	1.93
MnO	0.10	0.08	0.00	0.08	0.02	0.10	0.02	0.01	0.00	0.00	0.00	0.00
MgO	16.69	16.06	16.18	16.48	17.15	16.02	16.40	17.08	16.85	16.64	16.59	16.81
CaO	25.14	24.46	24.27	25.43	24.39	24.36	24.53	24.88	25.36	24.83	25.12	25.29
K2O	0.08	0.11	0.17	0.06	0.28	0.15	0.15	0.03	0.03	0.02	0.03	0.05
Na2O	0.40	0.92	0.56	0.57	0.90	0.77	0.53	0.48	0.39	0.40	0.39	0.33
Total	100.85	100.10	99.43	100.78	100.91	100.12	99.66	100.33	100.93	100.48	100.19	100.00
Mg #	90.3	88.7	90.1	90.4	91.6	88.0	90.5	93.6	91.9	93.0	91.3	94.0
Structural formula calculations based on 6 oxygens												
Si	1.938	1.909	1.927	1.950	1.963	1.936	1.946	1.971	1.958	1.989	1.947	1.982
Ti	0.046	0.074	0.065	0.036	0.019	0.052	0.045	0.027	0.032	0.025	0.040	0.022
IV Al	0.012	0.015	0.019	0.006	0.007	0.012	0.015	0.004	0.006	0.004	0.012	0.004
VI Al	0.000	0.000	0.000	0.000	0.000	0.000	0.000	0.000	0.000	0.000	0.000	0.000
Cr	0.005	0.005	0.008	0.005	0.014	0 005	0.005	0.014	0.011	0.014	0.010	0.010
Fe	0.097	0.113	0.098	0.096	0.085	0.120	0.095	0.064	0.081	0.067	0.086	0.059
Mn	0.003	0.003	0.000	0.002	0.001	0.003	0.001	0.000	0.000	0.000	0.000	0.000
Mg	0.908	0.885	0.893	0.897	0.929	0.881	0.901	0.926	0.912	0.899	0.906	0.913
Ca	0.983	0.969	0.962	0.995	0.950	0.963	0.968	0.970	0.987	0.964	0.986	0.988
K	0.004	0.005	0.008	0.003	0.013	0.007	0.007	0.001	0.001	0.001	0.001	0.002
Na	0.028	0.066	0.040	0.040	0.063	0.055	0.038	0.034	0.027	0.028	0.028	0.023
Total	4.024	4.044	4.020	4.030	4.044	4.034	4.021	4.011	4.015	3.991	4.016	4.003

Clinopyroxene analyses: Corona rim 3 (CR3)

	PC 63 core	PC 63 core	PC 63 core	PC 63 core	PC 63 core
SiO2	53.01	52.16	51.08	53.08	54.36
TiO2	1.15	2.11	2.76	1.83	0.96
Al203	0.18	0.39	0.41	0.37	0.14
Cr203	0.28	0.24	0.10	0.2[illegible]	0.37
FeO	2.80	3.50	4.35	3.25	2.49
MnO	0.03	0.08	0.05	0.05	0.04
MgO	16.72	16.03	15.59	16.40	17.11
CaO	25.28	25.06	24.56	24.68	24.71
K2O	0.05	0.05	0.11	0.09	0.05
Na2O	0.43	0.56	0.66	0.37	0.48
Total	99.93	100.18	99.67	100.38	100.71
Mg #	91.4	89.1	86.5	90.0	92.5

Structural formula calculations based on 6 oxygens

SI	1.949	1.923	1.902	1.943	1.971
TI	0.032	0.058	0.077	0.050	0.026
IV Al	0.008	0.017	0.018	0.016	0.006
VI Al	0.000	0.000	0.000	0.000	0.000
Cr	0.008	0.007	0.003	0.008	0.011
Fe	0.086	0.108	0.135	0.099	0.076
Mn	0.001	0.002	0.002	0.002	0.001
Mg	0.916	0.881	0.866	0.895	0.925
Ca	0.996	0.990	0.980	0.968	0.960
K	0.002	0.002	0.005	0.004	0.002
Na	0.031	0.040	0.048	0.026	0.034
Total	4.029	4.028	4.036	4.011	4.012

Clinopyroxene analyses: "No added volatile" system (LPD)

	EPC 25	EPC 25	EPC 25	EPC 25	EPC 43	EPC 43	EPC 43	EPC 43	EPC 50	EPC 50	EPC 50	EPC 50
kilobars	10	10	10	10	20	20	20	20	15	15	15	15
Celsius	1120	1120	1120	1120	1050	1050	1050	1050	1050	1050	1050	1050
minutes	240	240	240	240	240	240	240	240	360	360	360	360
SiO2	52.57	51.84	52.87	53.02	52.95	52.71	52.32	53.70	53.57	52.56	53.15	53.70
TiO2	1.15	1.51	0.77	0.88	1.92	1.59	1.16	0.60	0.87	1.47	1.50	0.93
Al203	0.15	0.44	0.08	0.13	0.35	0.37	0.30	0.39	0.11	0.23	0.25	0.13
Cr203	0.28	0.37	0.43	0.35	0.00	0.33	0.22	0.12	0.41	0.11	0.43	0.43
FeO	2.96	2.76	2.36	2.18	3.23	3.22	2.93	3.05	2.53	3.22	2.79	2.48
MnO	0.16	0.12	0.13	0.10	0.17	0.05	0.00	0.01	0.06	0.06	0.15	0.09
MgO	16.46	17.05	17.16	17.42	15.99	16.73	18.30	17.03	16.76	16.52	16.80	17.12
CaO	25.17	25.31	24.98	25.70	24.82	24.48	24.01	24.32	25.35	24.90	24.86	25.00
K2O	0.00	0.01	0.05	0.00	0.00	0.00	0.00	0.00	0.00	0.00	0.00	0.01
Na2O	0.39	0.41	0.54	0.34	0.47	0.47	0.18	0.22	0.33	0.39	0.37	0.32
Total	99.29	99.82	99.37	100.12	99.90	99.95	99.42	99.44	99.99	99.46	100.30	100.21
Mg #	90.8	91.7	92.8	93.4	89.8	90.3	91.8	90.9	92.2	90.1	91.5	92.5
Structural formula calculations based on 6 oxygens												
SI	1.948	1.914	1.952	1.943	1.947	1.938	1.928	1.972	1.963	1.943	1.944	1.961
IV Al	0.007	0.019	0.003	0.006	0.015	0.016	0.013	0.017	0.005	0.010	0.011	0.006
VI Al	0.000	0.000	0.000	0.000	0.000	0.000	0.000	0.000	0.000	0.000	0.000	0.000
TI	0.032	0.042	0.021	0.024	0.053	0.044	0.032	0.017	0.024	0.041	0.041	0.026
Cr	0.008	0.011	0.013	0.010	0.000	0.010	0.006	0.003	0.012	0.003	0.012	0.012
Fe	0.092	0.085	0.073	0.067	0.099	0.099	0.090	0.094	0.078	0.100	0.085	0.076
Mn	0.005	0.004	0.004	0.003	0.005	0.002	0.000	0.000	0.002	0.002	0.005	0.003
Mg	0.909	0.938	0.944	0.952	0.877	0.917	1.005	0.933	0.915	0.910	0.916	0.932
Ca	0.999	1.001	0.988	1.009	0.978	0.964	0.948	0.957	0.995	0.986	0.974	0.978
K	0.000	0.000	0.002	0.000	0.000	0.000	0.000	0.000	0.000	0.000	0.000	0.000
Na	0.028	0.029	0.039	0.024	0.034	0.033	0.013	0.016	0.023	0.028	0.026	0.023
Total	4.028	4.043	4.039	4.038	4.008	4.023	4.035	4.009	4.017	4.023	4.014	4.017

Clinopyroxene analyses: "Nc added volatile" system (LPD)

	EPC 50	EPC 51	EPC 51	EPC 51	EPC 51	EPC 51	EPC 52	EPC 52	EPC 59	EPC 59	EPC 59	EPC 59
kilobars	15	10	10	10	10	10	10	10	20	20	20	20
Celsius	1050	1000	1000	1000	1000	1000	1070	1070	1120	1120	1120	1120
minutes	360	420	420	420	420	420	360	360	180	180	180	180
SiO2	53.02	52.83	52.90	53.03	53.69	53.50	53.11	52.55	53.16	53.41	52.89	52.53
TiO2	1.17	1.49	1.45	1.93	1.58	1.22	1.36	1.35	0.88	0.80	1.11	1.48
Al203	0.24	0.26	0.15	0.31	0.20	0.19	0.29	0.33	0.13	0.13	0.13	0.33
Cr203	0.35	0.00	0.00	0.14	0.07	0.33	0.28	0.00	0.36	0.43	0.32	0.24
FeO	2.91	3.73	3.46	3.48	3.24	3.18	3.07	3.19	2.63	2.49	2.97	2.92
MnO	0.18	0.17	0.13	0.13	0.16	0.13	0.12	0.06	0.14	0.11	0.11	0.16
MgO	17.17	16.59	16.52	16.20	15.85	16.03	16.43	16.41	17.51	17.26	16.91	16.82
CaO	25.20	24.06	24.75	24.59	25.35	24.41	24.71	24.97	25.58	25.41	25.33	24.78
K2O	0.11	0.14	0.06	0.00	0.00	0.00	0.02	0.00	0.00	0.00	0.00	0.00
Na2O	0.34	0.53	0.42	0.48	0.41	0.41	0.39	0.32	0.35	0.36	0.40	0.46
Total	100.69	99.80	99.84	100.29	100.55	99.40	99.78	99.18	100.74	100.40	100.17	99.72
Mg #	91.3	88.8	89.5	89.3	89.7	90.0	90.5	90.2	92.2	92.5	91.0	91.1
Structural formula calculations based on 6 oxygens												
SI	1.937	1.948	1.949	1.944	1.962	1.972	1.953	1.947	1.939	1.951	1.942	1.936
IV Al	0.010	0.011	0.007	0.013	0.009	0.008	0.013	0.014	0.006	0.006	0.006	0.014
VI Al	0.000	0.000	0.000	0.000	0.000	0.000	0.000	0.000	0.000	0.000	0.000	0.000
TI	0.032	0.041	0.040	0.053	0.043	0.034	0.038	0.038	0.024	0.022	0.031	0.041
Cr	0.010	0.000	0.000	0.004	0.002	0.010	0.008	0.000	0.010	0.012	0.009	0.007
Fe	0.089	0.115	0.107	0.107	0.099	0.098	0.094	0.099	0.080	0.076	0.091	0.090
Mn	0.006	0.005	0.004	0.004	0.005	0.004	0.004	0.002	0.004	0.003	0.003	0.005
Mg	0.935	0.912	0.907	0.885	0.863	0.881	0.901	0.906	0.952	0.940	0.926	0.924
Ca	0.986	0.950	0.977	0.966	0.992	0.964	0.974	0.991	1.000	0.995	0.997	0.978
K	0.005	0.007	0.003	0.000	0.000	0.000	0.001	0.000	0.000	0.000	0.000	0.000
Na	0.024	0.038	0.030	0.034	0.029	0.029	0.028	0.023	0.025	0.025	0.028	0.033
Total	4.034	4.027	4.024	4.010	4.004	4.000	4.014	4.020	4.040	4.030	4.033	4.028

Clinopyroxene analyses: "Water added" system (LPD)

	PCW 31	PCW 31	PCW 31	PCW 31	PCW 31	PCW 32	PCW 32	PCW 32	PCW 32
kilobars	10	10	10	10	10	20	20	20	20
Celsius	1000	1000	1000	1000	1000	1020	1020	1020	1020
minutes	60	60	60	60	60	360	360	360	360
SiO2	53.36	53.14	54.31	52.93	51.48	53.43	52.74	53.39	52.77
TiO2	1.63	1.04	0.85	1.06	1.77	0.74	1.44	1.43	1.50
Al203	0.17	0.12	0.03	0.09	0.32	0.32	0.20	0.20	0.30
Cr203	0.24	0.27	0.29	0.15	0.32	0.00	0.29	0.19	0.40
FeO	3.13	3.15	2.82	3.03	3.18	2.89	2.91	2.85	3.06
MnO	0.01	0.08	0.05	0.18	0.14	0.14	0.14	0.13	0.02
MgO	16.00	16.60	16.56	17.04	16.27	18.36	16.57	16.39	16.29
CaO	24.48	25.57	25.43	25.39	25.13	24.53	25.33	25.33	25.02
K2O	0.07	0.12	0.08	0.08	0.02	0.06	0.02	0.03	0.04
Na2O	0.54	0.40	0.32	0.42	0.50	0.10	0.42	0.37	0.39
Total	99.63	100.49	100.74	100.37	99.13	100.57	100.06	100.31	99.79
Mg #	90.1	90.4	91.3	90.9	90.1	91.9	91.0	91.1	90.5
Structural formula calculations based on 6 oxygens									
SI	1.964	1.948	1.975	1.942	1.918	1.945	1.939	1.954	1.944
IV Al	0.007	0.005	0.001	0.004	0.014	0.014	0.009	0.009	0.013
VI Al	0.000	0.000	0.000	0.000	0.000	0.000	0.000	0.000	0.000
TI	0.045	0.029	0.023	0.029	0.050	0.020	0.040	0.039	0.042
Cr	0.007	0.008	0.008	0.004	0.009	0.000	0.008	0.005	0.012
Fe	0.096	0.097	0.086	0.093	0.099	0.088	0.089	0.087	0.094
Mn	0.000	0.002	0.002	0.006	0.004	0.004	0.004	0.004	0.001
Mg	0.878	0.907	0.898	0.932	0.904	0.996	0.908	0.894	0.895
Ca	0.965	1.004	0.991	0.998	1.003	0.957	0.998	0.993	0.988
K	0.003	0.006	0.004	0.004	0.001	0.003	0.001	0.001	0.002
Na	0.039	0.028	0.023	0.030	0.036	0.007	0.030	0.026	0.028
Total	4.004	4.034	4.011	4.042	4.038	4.034	4.026	4.012	4.019

Clinopyroxene analyses: "Fluorine added" system (LPD)

	FPC 6	FPC 6	FPC 6	FPC 6	FPC 6	FPC 8	FPC 8	FPC 8	FPC 8	FPC 8
kilobars	10	10	10	10	10	20	20	20	20	20
Celsius	1000	1000	1000	1000	1000	1000	1000	1000	1000	1000
minutes	360	360	360	360	360	300	300	300	300	300
SiO2	53.83	54.12	53.67	53.38	53.41	51.63	51.47	52.82	52.41	51.72
TiO2	0.80	0.77	1.21	0.78	0.95	1.73	1.87	0.91	1.61	2.04
Al203	0.07	0.04	0.18	0.05	0.14	0.27	0.43	0.10	0.22	0.30
Cr203	0.36	0.47	0.42	0.47	0.43	0.12	0.34	0.59	0.26	0.23
FeO	2.04	2.38	2.36	2.13	2.38	3.55	2.56	2.43	3.54	3.15
MnO	0.07	0.07	0.00	0.07	0.06	0.17	0.08	0.12	0.14	0.11
MgO	16.77	17.03	16.98	17.06	16.76	16.54	16.89	16.94	16.27	16.70
CaO	25.10	25.00	25.17	25.32	24.52	24.77	24.90	25.82	24.90	24.69
K2O	0.00	0.02	0.03	0.00	0.00	0.00	0.00	0.00	0.01	0.13
Na2O	0.00	0.49	0.47	0.44	0.42	0.44	0.47	0.52	0.59	0.60
Total	99.04	100.39	100.49	99.70	99.07	99.22	99.01	100.25	99.95	99.67
Mg #	93.6	92.7	92.8	93.5	92.6	89.3	92.2	92.6	89.1	90.4
Structural formula calculations based on 6 oxygens										
SI	1.981	1.971	1.955	1.960	1.970	1.922	1.913	1.939	1.935	1.915
IV Al	0.003	0.002	0.008	0.002	0.006	0.012	0.019	0.004	0.010	0.013
VI Al	0.000	0.000	0.000	0.000	0.000	0.000	0.000	0.000	0.000	0.000
TI	0.022	0.021	0.033	0.022	0.026	0.048	0.052	0.025	0.045	0.057
Cr	0.010	0.014	0.012	0.014	0.013	0.004	0.010	0.017	0.008	0.007
Fe	0.063	0.072	0.072	0.065	0.073	0.110	0.080	0.075	0.109	0.098
Mn	0.002	0.002	0.000	0.002	0.002	0.005	0.003	0.004	0.004	0.003
Mg	0.920	0.925	0.922	0.934	0.921	0.918	0.936	0.927	0.895	0.922
Ca	0.989	0.976	0.982	0.996	0.969	0.988	0.992	1.016	0.985	0.979
K	0.000	0.001	0.001	0.000	0.000	0.000	0.000	0.000	0.000	0.006
Na	0.000	0.035	0.033	0.031	0.030	0.032	0.034	0.037	0.042	0.043
Total	3.990	4.019	4.018	4.026	4.010	4.039	4.039	4.044	4.033	4.043

Clinopyroxene analyses: "No added volatile" system (HPA)

	EPC 7	EPC 7	EPC 7	EPC 7	EPC 45	EPC 45	EPC 45	EPC 60	EPC 60	EPC 60	EPC 60	EPC 60
kilobars	30	30	30	30	30	30	30	35	35	35	35	35
Celsius	1250	1250	1250	1250	1150	1150	1150	1200	1200	1200	1200	1200
minutes	30	30	30	30	180	180	180	180	180	180	180	180
SiO2	53.44	53.79	53.61	53.61	54.49	55.19	53.32	53.66	53.27	52.61	53.50	52.67
TiO2	0.36	0.37	0.36	0.33	0.34	0.34	0.20	0.29	0.36	0.30	0.33	0.38
Al203	1.50	1.43	1.14	1.07	0.74	0.88	1.00	1.04	1.32	1.18	1.05	1.51
Cr203	0.29	0.87	0.62	0.66	0.12	0.18	0.59	0.41	0.67	0.49	0.40	0.91
FeO	3.29	3.16	3.45	3.40	3.12	3.24	3.13	3.18	3.45	3.33	3.02	3.33
MnO	0.11	0.18	0.19	0.16	0.17	0.18	0.00	0.15	0.21	0.14	0.18	0.17
MgO	20.66	20.67	20.96	20.63	19.32	18.88	21.03	19.76	19.79	19.62	20.03	19.65
CaO	19.25	19.37	18.89	19.47	21.12	20.78	20.37	20.64	20.61	21.17	21.26	20.57
K2O	0.07	0.04	0.00	0.00	0.00	0.00	0.00	0.00	0.00	0.00	0.00	0.00
Na2O	0.14	0.33	0.30	0.34	0.26	0.25	0.29	0.27	0.34	0.30	0.28	0.34
Total	99.11	100.21	99.52	99.67	99.68	99.92	99.93	99.40	99.93	99.14	100.05	99.53
Mg #	91.8	92.1	91.6	91.5	91.7	91.2	92.3	91.7	91.1	91.3	92.2	91.3
Structural formula calculations based on 6 oxygens												
SI	1.945	1.939	1.946	1.946	1.977	1.993	1.933	1.955	1.936	1.931	1.941	1.924
IV Al	0.055	0.061	0.049	0.046	0.023	0.007	0.043	0.045	0.057	0.051	0.045	0.065
VI Al	0.009	0.000	0.000	0.000	0.009	0.030	0.000	0.000	0.000	0.000	0.000	0.000
Ti	0.010	0.010	0.010	0.009	0.009	0.009	0.005	0.008	0.010	0.008	0.009	0.010
Cr	0.008	0.025	0.018	0.019	0.003	0.005	0.017	0.012	0.019	0.014	0.011	0.026
Fe	0.100	0.095	0.105	0.103	0.095	0.098	0.095	0.097	0.105	0.102	0.092	0.102
Mn	0.003	0.005	0.006	0.005	0.005	0.006	0.000	0.005	0.006	0.004	0.006	0.005
Mg	1.121	1.111	1.134	1.116	1.045	1.016	1.137	1.073	1.068	1.074	1.083	1.070
Ca	0.751	0.748	0.734	0.757	0.821	0.804	0.791	0.806	0.803	0.833	0.826	0.805
K	0.003	0.002	0.000	0.000	0.000	0.000	0.000	0.000	0.000	0.000	0.000	0.000
Na	0.010	0.023	0.021	0.024	0.018	0.018	0.020	0.019	0.024	0.021	0.020	0.024
Total	4.015	4.019	4.023	4.025	4.005	3.986	4.041	4.020	4.028	4.038	4.033	4.031

Clinopyroxene analyses: HPA

	EPC 60	EPC 60
kilobars	35	35
Celsius	1200	1200
minutes	180	180
SiO2	53.10	53.20
TiO2	0.33	0.37
Al203	1.18	1.21
Cr203	0.44	0.49
FeO	3.25	3.18
MnO	0.14	0.16
MgO	19.44	19.30
CaO	21.24	21.83
K2O	0.01	0.00
Na2O	0.26	0.35
Total	99.39	100.09
Mg #	91.4	91.5
Structural formula calculations based on 6 oxygens		
SI	1.941	1.935
IV Al	0.051	0.052
VI Al	0.000	0.000
TI	0.009	0.010
Cr	0.013	0.014
Fe	0.099	0.097
Mn	0.004	0.005
Mg	1.059	1.046
Ca	0.832	0.851
K	0.000	0.000
Na	0.018	0.025
Total	4.026	4.035

Clinopyroxene analyses: "Water added" system (HPA)

	PCW 26	PCW 26	PCW 26	PCW 26	PCW 35
kilobars	30	30	30	30	30
Celsius	1150	1150	1150	1150	1050
minutes	270	270	270	270	240
SiO2	53.31	54.22	54.10	52.70	52.87
TiO2	0.43	0.48	0.41	0.42	1.86
Al203	1.00	0.97	0.83	0.88	0.40
Cr203	0.69	0.74	0.59	0.74	0.00
FeO	3.49	3.12	3.37	3.26	3.31
MnO	0.18	0.16	0.07	0.13	0.19
MgO	19.09	18.54	18.94	18.89	19.05
CaO	20.49	22.02	21.29	22.15	22.43
K2O	0.06	0.03	0.04	0.00	0.00
Na2O	0.46	0.37	0.41	0.33	0.46
Total	99.20	100.65	100.05	99.50	100.57
Mg #	90.7	91.4	90.9	91.2	91.1
SI	1.953	1.958	1.963	1.934	1.922
IV Al	0.043	0.041	0.036	0.038	0.017
VI Al	0.000	0.000	0.000	0.000	0.000
TI	0.012	0.013	0.011	0.012	0.051
Cr	0.020	0.021	0.017	0.021	0.000
Fe	0.107	0.094	0.102	0.100	0.101
Mn	0.006	0.005	0.002	0.004	0.006
Mg	1.042	0.998	1.025	1.033	1.032
Ca	0.804	0.852	0.828	0.871	0.874
K	0.003	0.001	0.002	0.000	0.000
Na	0.033	0.026	0.029	0.023	0.032
Total	4.023	4.009	4.015	4.036	4.035

Clinopyroxene analyses: "Fluorine added" system (HPA)

	FPC 10	FPC 10	FPC 10	FPC 10	FPC 10	FPC 10
kilobars	30	30	30	30	30	30
Celsius	1100	1100	1100	1100	1100	1100
minutes	180	180	180	180	180	180
SiO2	53.97	53.85	53.34	53.68	54.43	53.44
TiO2	0.43	0.33	0.37	0.32	0.37	0.39
Al203	0.80	0.68	0.82	0.75	0.86	0.77
Cr203	0.37	0.36	0.58	0.39	0.38	0.58
FeO	2.99	3.09	2.92	3.12	3.02	2.65
MnO	0.13	0.23	0.16	0.18	0.22	0.23
MgO	19.16	19.46	19.36	19.60	19.03	19.10
CaO	22.03	22.24	21.68	21.71	22.07	22.26
K2O	0.00	0.00	0.00	0.00	0.19	0.00
Na2O	0.25	0.25	0.24	0.25	0.26	0.25
Total	100.13	100.47	99.47	100.00	100.83	99.67
Mg #	92.0	91.8	92.2	91.8	91.8	92.8
Structural formula calculations based on 6 oxygens						
SI	1.957	1.950	1.948	1.951	1.962	1.949
IV Al	0.034	0.028	0.035	0.032	0.037	0.033
VI Al	0.000	0.000	0.000	0.000	0.000	0.000
TI	0.012	0.009	0.010	0.009	0.010	0.011
Cr	0.011	0.010	0.017	0.011	0.011	0.017
Fe	0.091	0.094	0.089	0.095	0.091	0.081
Mn	0.004	0.007	0.005	0.006	0.007	0.007
Mg	1.036	1.051	1.054	1.062	1.022	1.039
Ca	0.856	0.863	0.848	0.845	0.852	0.870
K	0.000	0.000	0.000	0.000	0.009	0.000
Na	0.018	0.018	0.017	0.018	0.018	0.018
Total	4.019	4.030	4.023	4.029	4.019	4.025

5.3 Phlogopite

Phlogopite analyses: Tuff facies phenocrystic phlogopite.

	PC 5	PC 5	PC 5	PC 5	PC 5	PC 5	PC 5	PC 5	PC 5	PC 5	PC 5
	c	e	e	c	c	ce	c	e	c	e	e
SiO2	40.37	41.07	41.00	41.82	40.17	42.72	40.73	41.05	40.22	40.77	41.49
TiO2	5.48	5.10	5.42	5.42	6.23	5.35	6.83	5.25	5.26	4.84	5.19
Al203	11.37	11.16	9.47	9.44	11.64	10.63	11.23	9.69	11.34	10.27	9.94
Cr203	0.56	0.41	0.16	0.23	0.00	0.24	0.43	0.15	0.42	0.11	0.19
FeO	4.35	4.54	5.42	5.51	4.59	4.25	3.99	5.71	4.92	5.45	5.28
MnO	0.02	0.00	0.05	0.02	0.00	0.04	0.00	0.04	0.06	0.05	0.03
MgO	22.30	22.53	21.90	22.42	21.95	23.92	21.15	22.17	22.20	22.18	22.19
CaO	0.01	0.04	0.02	0.00	0.00	0.00	0.00	0.02	0.00	0.01	0.07
BaO	0.21	0.19	0.20	0.19	0.35	0.21	0.15	0.18	0.19	0.11	0.12
K2O	10.01	9.72	9.78	10.16	10.33	10.46	10.11	9.97	10.47	10.06	10.30
Na2O	0.08	0.11	0.20	0.14	0.12	0.09	0.14	0.15	0.10	0.19	0.68
F	0.47	0.61	0.40	0.41	0.45	0.61	0.35	0.46	0.49	0.43	0.42
Total	95.23	95.48	94.02	95.76	95.83	98.52	95.11	94.84	95.67	94.47	95.90
O=F	0.20	0.26	0.17	0.17	0.19	0.26	0.15	0.19	0.21	0.18	0.18
Total	95.03	95.22	93.85	95.59	95.64	98.26	94.96	94.65	95.46	94.29	95.72
mg #	90.1	89.8	87.8	87.9	89.5	90.9	90.4	87.4	88.9	87.9	88.2
Structural formula calculations based on 22 oxygens.											
Si	5.769	5.837	5.955	5.969	5.724	5.888	5.813	5.922	5.754	5.897	5.923
Ti	0.589	0.545	0.592	0.582	0.668	0.555	0.733	0.570	0.566	0.526	0.557
Al	1.915	1.869	1.621	1.588	1.955	1.727	1.889	1.648	1.912	1.751	1.672
Cr	0.063	0.046	0.018	0.026	0.000	0.026	0.049	0.017	0.048	0.013	0.021
Mn	0.002	0.000	0.006	0.002	0.000	0.005	0.000	0.005	0.007	0.006	0.004
Fe	0.520	0.540	0.658	0.658	0.547	0.490	0.476	0.689	0.589	0.659	0.630
Mg	4.751	4.773	4.742	4.770	4.662	4.915	4.500	4.768	4.735	4.782	4.722
Ca	0.002	0.006	0.003	0.000	0.000	0.000	0.000	0.003	0.000	0.002	0.011
Ba	0.012	0.011	0.011	0.011	0.020	0.011	0.008	0.010	0.011	0.006	0.007
K	1.825	1.762	1.812	1.850	1.878	1.839	1.841	1.835	1.911	1.856	1.876
Na	0.022	0.030	0.056	0.039	0.033	0.024	0.039	0.042	0.028	0.053	0.188
F	0.212	0.274	0.184	0.185	0.203	0.266	0.158	0.210	0.222	0.197	0.190
Total	15.682	15.694	15.659	15.679	15.688	15.746	15.504	15.719	15.781	15.748	15.800

Phlogopite analyses: Hypabyssal facies poikilitic phlogopite (HYP).

	PC 29c	PC 29c	PC 30	PC 20b	PC 20b	PC 20b	PC 20b	PC 20b	PC 20b	PC 29b	PC 29a	PC 29a
	c	c	c	c	c	c	c	c	c	c	c	c
SiO2	42.80	43.03	43.49	42.80	43.37	42.46	42.33	44.19	43.26	43.00	42.62	43.19
TiO2	4.32	4.39	3.61	3.52	3.51	3.94	3.57	3.46	3.99	3.02	4.34	4.17
Al203	6.30	5.92	6.44	6.32	6.48	5.98	5.53	6.16	6.02	6.42	6.87	6.68
Cr203	0.13	0.12	0.10	0.04	0.10	0.00	0.00	0.00	0.00	0.00	0.05	0.00
FeO	7.50	8.29	7.60	8.03	7.06	7.83	7.62	7.25	7.67	7.00	8.05	7.25
MnO	0.03	0.06	0.00	0.00	0.00	0.00	0.00	0.00	0.00	0.00	0.03	0.00
MgO	22.60	22.22	23.22	22.87	23.18	23.19	22.95	23.33	23.30	24.29	22.66	22.42
CaO	0.05	0.05	0.06	0.07	0.04	0.06	0.08	0.05	0.04	0.04	0.10	0.02
BaO	0.73	0.85	0.53	0.66	0.74	0.93	0.94	0.72	1.02	0.52	0.96	0.54
K2O	10.71	10.76	10.32	10.04	10.16	9.95	10.16	10.02	9.75	10.29	9.86	10.28
Na2O	0.99	0.89	1.13	0.87	1.09	1.03	1.30	1.13	1.04	1.12	0.82	0.86
F	4.11	4.13	4.51	4.45	4.49	4.37	4.55	4.62	4.57	4.70	4.20	4.55
Total	100.27	100.71	101.01	99.67	100.22	99.74	99.03	100.93	100.66	100.40	100.56	99.96
O=F	1.73	1.74	1.90	1.87	1.89	1.84	1.92	1.95	1.92	1.98	1.77	1.92
Total	98.54	98.97	99.11	97.80	98.33	97.90	97.11	98.98	98.74	98.42	98.79	98.04
mg #	84.3	82.7	84.5	83.5	85.4	84.1	84.3	85.2	84.4	86.1	83.4	84.6
Structural formula calculations based on 22 oxygens.												
Si	5.959	5.991	5.981	5.977	6.000	5.941	5.978	6.059	5.978	5.939	5.908	5.985
Ti	0.452	0.460	0.373	0.370	0.365	0.415	0.379	0.357	0.415	0.314	0.452	0.435
Al	1.034	0.971	1.044	1.040	1.057	0.986	0.920	0.995	0.980	1.045	1.122	1.091
Cr	0.014	0.013	0.011	0.004	0.011	0.000	0.000	0.000	0.000	0.000	0.005	0.000
Mn	0.004	0.007	0.000	0.000	0.000	0.000	0.000	0.000	0.000	0.000	0.004	0.000
Fe	0.873	0.965	0.874	0.938	0.817	0.916	0.900	0.831	0.886	0.809	0.933	0.840
Mg	4.691	4.612	4.761	4.761	4.781	4.838	4.832	4.769	4.800	5.001	4.682	4.631
Ca	0.007	0.007	0.009	0.010	0.006	0.009	0.012	0.007	0.006	0.006	0.015	0.003
Ba	0.040	0.046	0.029	0.036	0.040	0.051	0.052	0.039	0.055	0.028	0.052	0.029
K	1.902	1.911	1.811	1.789	1.793	1.776	1.830	1.753	1.719	1.813	1.744	1.817
Na	0.267	0.240	0.301	0.236	0.292	0.279	0.356	0.300	0.279	0.300	0.220	0.231
F	1.810	1.818	1.962	1.965	1.964	1.934	2.032	2.003	1.997	2.053	1.841	1.994
Total	17.053	17.041	17.156	17.126	17.126	17.145	17.291	17.113	17.115	17.308	16.978	17.056

Phlogopite analyses: Hypabyssal facies poikilitic phlogopite (HYP).

	PC 29a	PC 29a	PC 20b	PC 20b	PC 20b	PC 20b	PC 20b	PC 20b	PC 20b	PC 20b	PC 20b	PC 20b
	c	c	ce	ce	ce	ce	ce	ce	ce	ce	ce	ce
SiO2	43.35	43.40	44.47	43.18	43.25	43.66	43.37	42.97	43.61	43.70	43.98	42.31
TiO2	4.30	4.54	3.35	2.98	3.13	3.22	3.52	4.09	3.76	3.59	3.54	4.36
Al203	6.24	6.24	6.31	6.39	6.29	6.59	5.96	5.88	6.16	6.28	6.44	6.57
Cr203	0.00	0.00	0.00	0.04	0.04	0.03	0.00	0.04	0.02	0.01	0.03	0.09
FeO	8.37	8.13	7.73	7.86	8.04	7.19	7.32	8.22	7.79	7.85	7.90	8.33
MnO	0.00	0.02	0.00	0.03	0.00	0.00	0.04	0.00	0.00	0.01	0.00	0.00
MgO	22.58	22.00	23.48	23.17	23.31	23.22	22.84	22.74	22.62	23.28	23.52	22.16
CaO	0.05	0.02	0.10	0.07	0.03	0.04	0.04	0.06	0.14	0.02	0.02	0.07
BaO	0.32	0.59	0.57	0.53	0.57	0.64	0.76	0.84	1.07	0.72	0.82	1.35
K2O	9.34	9.11	10.26	10.37	10.12	10.35	10.06	9.67	9.94	10.06	10.25	9.86
Na2O	0.73	0.69	0.91	1.00	1.03	1.00	1.18	1.02	1.17	0.95	0.99	0.90
F	4.55	4.48	4.43	4.41	4.68	4.61	4.66	4.21	4.37	4.40	4.55	4.19
Total	99.83	99.22	101.61	100.03	100.49	100.55	99.75	99.74	100.65	100.87	102.04	100.19
O=F	1.92	1.89	1.87	1.86	1.97	1.94	1.96	1.77	1.84	1.85	1.92	1.76
Total	97.91	97.33	99.74	98.17	98.52	98.61	97.79	97.97	98.81	99.02	100.12	98.43
mg #	82.8	82.8	84.4	84.0	83.8	85.2	84.8	83.1	83.8	84.1	84.2	82.6
Structural formula calculations based on 22 oxygens.												
Si	6.002	6.040	6.063	6.006	5.986	6.017	6.037	6.002	6.035	6.017	5.994	5.918
Ti	0.448	0.475	0.343	0.312	0.326	0.334	0.368	0.430	0.391	0.372	0.363	0.459
Al	1.018	1.023	1.014	1.046	1.026	1.070	0.978	0.968	1.005	1.019	1.035	1.083
Cr	0.000	0.000	0.000	0.004	0.004	0.003	0.000	0.004	0.002	0.001	0.003	0.010
Mn	0.000	0.002	0.000	0.004	0.000	0.000	0.005	0.000	0.000	0.001	0.000	0.000
Fe	0.969	0.946	0.881	0.914	0.931	0.829	0.852	0.960	0.902	0.904	0.900	0.974
Mg	4.661	4.564	4.772	4.804	4.809	4.771	4.740	4.735	4.666	4.778	4.779	4.621
Ca	0.007	0.003	0.015	0.010	0.004	0.006	0.006	0.009	0.021	0.003	0.003	0.010
Ba	0.017	0.032	0.030	0.029	0.031	0.035	0.041	0.046	0.058	0.039	0.044	0.074
K	1.650	1.617	1.785	1.840	1.787	1.820	1.786	1.723	1.755	1.767	1.782	1.759
Na	0.196	0.186	0.241	0.270	0.276	0.267	0.318	0.276	0.314	0.254	0.262	0.244
F	1.992	1.972	1.910	1.940	2.048	2.009	2.051	1.860	1.913	1.916	1.961	1.853
Total	16.960	16.860	17.054	17.181	17.228	17.161	17.182	17.013	17.062	17.071	17.126	17.005

Phlogopite analyses: Hypabyssal facies poikilitic phlogopite (HYP).

	PC 20b	PC 20b	PC 20b	PC 20b	PC 29b	PC 29b	PC 30	PC 20b	PC 20b	PC 20b	PC 20b	PC 20b
	ce	ce	ce	ce	•	•	•	•	•	•	•	•
SiO2	43.93	44.71	44.01	41.61	43.56	43.22	43.09	43.30	43.39	43.58	43.85	43.94
TiO2	3.79	3.45	3.78	3.44	3.73	3.68	3.80	3.51	1.92	2.81	2.06	3.04
Al203	5.84	6.36	5.87	6.56	7.35	6.43	6.45	6.29	6.96	6.85	5.50	6.56
Cr203	0.00	0.08	0.07	0.04	0.00	0.00	0.00	0.04	0.02	0.00	0.00	0.03
FeO	8.39	7.60	8.20	7.46	7.44	7.47	7.47	7.28	6.92	6.71	8.22	7.37
MnO	0.00	0.00	0.00	0.13	0.06	0.00	0.00	0.00	0.00	0.00	0.00	0.00
MgO	23.36	23.20	22.44	23.07	23.34	22.80	22.73	23.19	24.75	23.85	24.81	24.33
CaO	0.04	0.04	0.06	0.08	0.08	0.05	0.02	0.03	0.11	0.72	0.12	0.04
BaO	0.85	0.68	0.89	0.53	0.53	0.71	0.54	0.74	0.34	0.40	0.47	0.59
K2O	9.86	10.43	9.85	9.96	10.31	10.42	10.18	10.09	9.83	10.07	10.19	9.86
Na2O	1.04	1.08	1.08	1.03	0.73	0.99	0.99	1.04	0.62	0.92	1.04	0.92
F	4.26	4.55	4.59	4.96	3.89	4.51	4.60	4.37	4.49	4.19	4.64	4.16
Total	101.36	102.18	100.84	98.87	101.02	100.28	99.87	99.88	99.35	100.10	100.90	100.84
O=F	1.79	1.92	1.93	2.09	1.64	1.90	1.94	1.84	1.89	1.76	1.95	1.75
Total	99.57	100.26	98.91	96.78	99.38	98.38	97.93	98.04	97.46	98.34	98.95	99.09
mg #	83.2	84.5	83.0	84.7	84.8	84.5	84.4	85.0	86.4	86.4	84.3	85.5
Structural formula calculations based on 22 oxygens.												
Si	6.035	6.068	6.071	5.858	5.970	5.993	5.985	6.015	6.007	6.010	6.047	6.021
Ti	0.392	0.352	0.392	0.364	0.384	0.384	0.397	0.367	0.200	0.291	0.214	0.313
Al	0.946	1.017	0.954	1.088	1.187	1.051	1.056	1.030	1.136	1.113	0.894	1.059
Cr	0.000	0.009	0.008	0.004	0.000	0.000	0.000	0.004	0.002	0.000	0.000	0.003
Mn	0.000	0.000	0.000	0.016	0.007	0.000	0.000	0.000	0.000	0.000	0.000	0.000
Fe	0.964	0.863	0.946	0.878	0.853	0.866	0.868	0.846	0.801	0.774	0.948	0.845
Mg	4.784	4.694	4.615	4.842	4.769	4.713	4.707	4.802	5.108	4.903	5.100	4.970
Ca	0.006	0.006	0.009	0.012	0.012	0.007	0.003	0.004	0.016	0.106	0.018	0.006
Ba	0.046	0.036	0.048	0.029	0.028	0.039	0.029	0.040	0.018	0.022	0.025	0.032
K	1.728	1.806	1.733	1.789	1.803	1.843	1.804	1.788	1.736	1.772	1.793	1.724
Na	0.277	0.284	0.289	0.281	0.194	0.266	0.267	0.280	0.168	0.246	0.278	0.244
F	1.851	1.953	2.003	2.208	1.686	1.978	2.021	1.920	1.966	1.827	2.024	1.803
Total	17.029	17.088	17.068	17.369	16.893	17.140	17.137	17.096	17.156	17.064	17.341	17.020

Phlogopite analyses: Hypabyssal facies poikilitic phlogopite (HYP).

	PC 29b	PC 20b	PC 30b	PC 29a	PC 29a	PC 29b	PC 30	PC 30	PC 29b	PC 29b	PC 30	PC 30
	•	•	•	•	•	c	c	c	•	•	•	•
SiO2	43.53	44.04	42.49	43.78	42.30	41.56	44.01	43.17	42.85	43.09	42.41	43.41
TiO2	3.13	3.06	3.98	3.88	3.36	4.44	3.86	4.47	4.31	4.69	4.40	3.71
Al203	6.61	7.35	6.85	6.31	7.62	5.82	6.84	6.64	6.39	6.18	7.21	6.50
Cr203	0.01	0.06	0.13	0.00	0.00	0.00	0.00	0.07	0.00	0.03	0.00	0.05
FeO	7.31	6.58	8.04	7.68	7.31	8.10	7.42	7.35	7.60	7.57	7.73	7.57
MnO	0.01	0.16	0.07	0.00	0.04	0.12	0.00	0.00	0.00	0.05	0.00	0.00
MgO	24.29	23.45	24.02	22.89	23.04	22.61	23.57	23.04	22.35	22.39	22.80	22.95
CaO	0.10	0.02	0.03	0.01	0.07	0.08	0.10	0.08	0.06	0.01	0.05	0.06
BaO	0.50	0.40	0.60	0.27	0.34	1.07	0.62	0.84	1.03	1.08	1.16	0.62
K2O	10.09	10.43	10.11	10.16	9.28	9.87	9.94	9.33	10.06	8.79	9.78	9.88
Na2O	0.84	0.93	0.87	0.76	0.58	0.90	0.91	0.89	1.19	0.83	0.65	0.94
F	4.36	4.36	4.14	4.55	3.80	3.90	4.41	4.13	4.08	4.27	4.24	4.28
Total	100.78	101.51	101.33	100.29	97.74	98.47	101.68	100.01	99.94	99.38	100.43	99.97
O=F	1.84	2.12	1.74	1.92	1.60	1.64	1.86	1.74	1.72	1.80	1.79	1.80
Total	98.94	99.39	99.59	98.37	96.14	96.83	99.82	98.27	98.22	97.58	98.64	98.17
mg #	85.6	86.4	84.2	84.2	84.9	83.3	85.0	84.8	84.0	83.4	84.0	84.4
Structural formula calculations based on 22 oxygens.												
Si	5.976	5.980	5.845	6.034	5.953	5.918	5.984	5.968	5.979	6.005	5.878	6.015
Ti	0.323	0.312	0.412	0.402	0.356	0.475	0.395	0.465	0.452	0.491	0.459	0.387
Al	1.070	1.176	1.111	1.025	1.264	0.977	1.096	1.082	1.051	1.015	1.178	1.061
Cr	0.001	0.006	0.014	0.000	0.000	0.000	0.000	0.008	0.000	0.003	0.000	0.005
Mn	0.001	0.018	0.008	0.000	0.005	0.014	0.000	0.000	0.000	0.006	0.000	0.000
Fe	0.839	0.747	0.925	0.885	0.860	0.965	0.844	0.850	0.887	0.929	0.896	0.877
Mg	4.971	4.747	4.926	4.703	4.834	4.799	4.777	4.748	4.649	4.651	4.711	4.740
Ca	0.015	0.003	0.004	0.001	0.011	0.012	0.015	0.012	0.009	0.001	0.007	0.009
Ba	0.027	0.021	0.032	0.015	0.019	0.060	0.033	0.046	0.056	0.059	0.063	0.034
K	1.767	1.807	1.774	1.786	1.666	1.793	1.724	1.645	1.794	1.563	1.729	1.746
Na	0.224	0.245	0.232	0.203	0.158	0.248	0.240	0.239	0.322	0.224	0.175	0.253
F	1.893	2.160	1.801	1.983	1.691	1.756	1.896	1.806	1.801	1.882	1.859	1.875
Total	17.107	17.222	17.084	17.037	16.817	17.017	17.004	16.869	17.000	16.829	16.955	17.002

Phlogopite analyses: Hypabyssal facies poikilitic phlogopite (HYP).

	PC 29b	PC 29b	PC 30	PC 20b	PC 29a	PC 30
	e	e	e	ce	c	c
SiO2	42.74	43.74	42.58	43.96	43.70	44.10
TiO2	2.02	3.18	3.90	3.29	3.99	3.83
Al203	6.66	6.81	6.43	6.46	6.05	6.92
Cr203	0.05	0.05	0.00	0.01	0.12	0.02
FeO	7.96	7.10	7.99	6.94	7.80	6.72
MnO	0.00	0.00	0.09	0.00	0.13	0.00
MgO	24.47	24.04	23.52	22.93	22.07	22.45
CaO	0.04	0.08	0.02	0.04	0.01	0.06
BaO	0.49	0.60	0.48	0.60	0.69	0.67
K2O	10.13	9.92	10.48	10.16	10.24	10.11
Na2O	0.64	0.89	0.80	1.01	0.97	0.96
F	4.45	4.32	4.64	4.33	4.23	4.60
Total	99.65	100.73	100.93	99.73	100.00	100.44
O:F	1.87	1.82	1.95	1.82	1.78	1.94
Total	97.78	98.91	98.98	97.91	98.22	98.50
mg #	84.6	85.8	84.0	85.5	83.5	85.6
Structural formula calculations based on 22 oxygens.						
Si	5.957	5.996	5.883	6.087	6.077	6.053
Ti	0.212	0.328	0.405	0.343	0.417	0.395
Al	1.094	1.100	1.047	1.054	0.991	1.119
Cr	0.006	0.005	0.000	0.001	0.013	0.002
Mn	0.000	0.000	0.011	0.000	0.015	0.000
Fe	0.928	0.814	0.923	0.804	0.907	0.771
Mg	5.084	4.913	4.845	4.734	4.575	4.594
Ca	0.006	0.012	0.003	0.006	0.001	0.009
Ba	0.027	0.032	0.026	0.033	0.038	0.036
K	1.801	1.735	1.847	1.795	1.816	1.770
Na	0.173	0.237	0.214	0.271	0.262	0.255
F	1.962	1.873	2.028	1.896	1.860	1.997
Total	17.250	17.045	17.232	17.024	16.972	17.001

Phlogopite analyses: Hypabyssal facies tetraferriphlogopite phlogopite.

	PC 29c	PC 29c	PC 25	PC 25	PC 25	PC 53
	c	c	e	c	c	e
SiO2	45.45	45.60	44.27	48.43	45.00	44.80
TiO2	1.35	1.16	2.05	1.12	1.73	5.01
Al2O3	0.60	0.98	3.51	1.23	2.28	4.12
Cr2O3	0.14	0.07	0.00	0.00	0.09	0.00
FeO	15.15	15.00	11.20	9.11	11.60	10.48
MnO	0.27	0.24	0.00	0.00	0.02	0.05
MgO	19.10	19.37	22.76	22.56	22.96	21.05
CaO	0.02	0.01	0.09	0.04	0.10	0.01
BaO	0.00	0.00	0.66	0.10	0.72	0.53
K2O	10.34	9.81	9.91	10.20	9.79	9.64
Na2O	2.91	2.70	1.80	2.66	1.76	1.23
F	0.00	0.00	5.37	6.38	5.45	3.29
Total	95.33	94.94	101.62	101.83	101.50	100.21
O=F	0.00	0.00	2.26	2.69	2.29	1.39
Total	95.33	94.94	99.36	99.14	99.21	98.82
mg #	69.2	69.7	78.4	81.5	77.9	78.2
Structural formula calculations based on 22 oxygens.						
Si	6.897	6.906	6.163	6.609	6.280	6.263
Ti	0.154	0.132	0.215	0.115	0.182	0.527
Al	0.107	0.175	0.576	0.19[illegible]	0.375	0.679
Cr	0.017	0.008	0.000	0.000	0.010	0.000
Mn	0.035	0.031	0.000	0.000	0.002	0.006
Fe	1.923	1.900	1.304	1.040	1.354	1.225
Mg	4.321	4.373	4.723	4.589	4.777	4.387
Ca	0.003	0.002	0.013	0.006	0.015	0.001
Ba	0.000	0.000	0.036	0.005	0.039	0.029
K	2.002	1.895	1.760	1.776	1.743	1.719
Na	0.856	0.793	0.486	0.704	0.476	0.333
F	0.000	0.000	2.364	2.753	2.405	1.455
Total	16.315	16.214	17.640	17.794	17.658	16.624

Phlogopite analyses: Hypabyssal facies high-Ti phlogopite.

	PC 53	PC 53	PC 53	PC 53	PC 53	PC 53	PC 53	PC 53	PC 53	PC 53	PC 53	PC 53
	c	c	c	ce	ce	ce	ce	ce	ce	ce	ce	ce
SiO2	42.23	42.92	42.24	42.66	42.70	42.87	42.10	42.56	41.89	42.65	42.78	42.21
TiO2	5.68	5 77	5.59	5.78	5.85	5.78	5.63	5.84	5.38	5.66	5.41	5.22
Al203	7.48	7.62	7.79	6.37	6.95	7.44	7.54	6.65	7.52	7.55	7.55	7.15
Cr203	0.04	0.07	0.04	0.00	0.01	0.00	0.02	0.05	0.00	0.03	0.03	0.02
FeO	7.22	7.03	7.15	8.45	7.68	7.83	7.36	8.21	6.80	7.17	7.17	8.05
MnO	0.00	0.02	0.03	0.00	0.03	0.01	0.05	0.00	0.05	0.04	0.00	0.00
MgO	22.02	21.96	21.91	21.27	21.22	21.76	22.16	21.28	21.75	22.07	21.87	21.81
CaO	0.05	0.04	0.01	0.04	0.01	0.10	0.01	0.06	0.00	0.16	0.02	0.06
BaO	1.09	1.04	1.07	0.88	1.03	0.89	0.90	0.97	1.03	0.81	0.98	1.00
K2O	8.79	9.54	9.61	9.74	9.89	9.71	9.68	9.94	9.65	9.54	9.81	9.50
Na2O	0.54	0.60	0.63	0.93	0.85	0.66	0.66	0.81	0.66	0.67	0.71	0.69
F	2.80	2.86	3.19	2.87	3.26	3.15	3.11	2.99	3.17	3.06	3.29	3.31
Total	97.94	99.47	99.26	98.99	99.48	100.20	99.22	99.36	97.90	99.41	99.62	99.02
O=F	1.18	1.20	1.34	1.21	1.37	1.33	1.31	1.26	1.33	1.29	1.39	1.39
Total	96.76	98.27	97.92	97.78	98.11	98.87	97.91	98.10	96.57	98.12	98.23	97.63
mg #	84.5	84.8	84.5	81.8	83.1	83.2	84.3	82.2	85.1	84.6	84.5	82.9
Structural formula calculations based on 22 oxygens.												
Si	5.949	5.963	5.897	6.013	5.973	5.937	5.886	5.979	5.925	5.932	5.948	5.930
Ti	0.602	0.603	0.587	0.613	0.615	0.602	0.592	0.617	0.572	0.592	0.566	0.551
Al	1.242	1.248	1.282	1.058	1.146	1.214	1.242	1.101	1.254	1.238	1.237	1.184
Cr	0.004	0.008	0.004	0.000	0.001	0.000	0.002	0.006	0.000	0.003	0.003	0.002
Mn	0.000	0.002	0.004	0.000	0.004	0.001	0.006	0.000	0.006	0.005	0.000	0.000
Fe	0.851	0.817	0.835	0.996	0.898	0.907	0.861	0.965	0.804	0.834	0.834	0.946
Mg	4.624	4.548	4.560	4.469	4.425	4.493	4.619	4.456	4.586	4.576	4.533	4.568
Ca	0.008	0.006	0.001	0.006	0.001	0.015	0.001	0.009	0.000	0.024	0.003	0.009
Ba	0.060	0.057	0.059	0.049	0.056	0.048	0.049	0.053	0.057	0.044	0.053	0.055
K	1.580	1.691	1.712	1.751	1.765	1.716	1.727	1.781	1.741	1.693	1.740	1.703
Na	0.147	0.162	0.171	0.254	0.231	0.177	0.179	0.221	0.181	0.181	0.191	0.188
F	1.247	1.257	1.408	1.279	1.442	1.380	1.375	1.328	1.418	1.346	1.447	1.471
Total	16.314	16.361	16.518	16.488	16.557	16.490	16.540	16.516	16.546	16.466	16.555	16.606

Phlogopite analyses: Hypabyssal facies high-Ti phlogopite.

	PC 53	PC 53	PC 53
	ce	e	e
SiO2	43.13	43.24	42.78
TiO2	5.44	5.39	5.08
Al2O3	7.56	6.11	7.36
Cr2O3	0.04	0.07	0.05
FeO	7.38	8.38	7.82
MnO	0.00	0.03	0.02
MgO	21.65	21.56	22.60
CaO	0.04	0.04	0.05
BaO	1.02	0.67	0.87
K2O	9.54	10.04	9.58
Na2O	0.70	0.95	0.80
F	3.33	3.21	3.18
Total	99.83	99.69	100.19
O=F	1.40	1.35	1.34
Total	98.43	98.34	98.85
mg #	84.0	82.1	83.7
Structural formula calculations based on 22 oxygens.			
Si	5.976	6.046	5.926
Ti	0.567	0.567	0.529
Al	1.235	1.007	1.202
Cr	0.004	0.008	0.005
Mn	0.000	0.004	0.002
Fe	0.855	0.980	0.906
Mg	4.472	4.494	4.667
Ca	0.006	0.006	0.007
Ba	0.055	0.037	0.047
K	1.686	1.791	1.693
Na	0.188	0.258	0.215
F	1.459	1.419	1.393
Total	16.504	16.614	16.592

Phlogopite analyses: Phlogopite bearing cognate xenolith (DRX).

	PC 20b	PC 20b	PC 20b
	c	c	e
SiO2	42.14	45.74	43.67
TiO2	3.50	3.32	3.13
Al203	5.65	6.14	6.72
Cr203	0.00	0.07	0.00
FeO	7.42	7.01	6.90
MnO	0.00	0.11	0.00
MgO	21.98	22.87	23.41
CaO	0.00	0.00	0.00
BaO	0.95	0.48	0.54
K2O	10.44	10.25	10.48
Na2O	1.14	1.21	0.80
F	5.04	5.27	4.96
Total	98.26	102.47	100.61
O F	2.12	2.22	2.09
Total	96.14	100.25	98.52
mg #	84.1	85.3	85.8
Structural formula calculations based on 22 oxygens.			
Si	5.996	6.147	6.000
Ti	0.375	0.336	0.323
Al	0.948	0.973	1.088
Cr	0.000	0.007	0.000
Mn	0.000	0.013	0.000
Fe	0.883	0.788	0.793
Mg	4.662	4.582	4.795
Ca	0.000	0.000	0.000
Ba	0.053	0.025	0.029
K	1.895	1.757	1.837
Na	0.315	0.315	0.213
F	2.268	2.240	2.155
Total	17.394	17.183	17.235

Phlogopite analyses: Corona rim 2 phlogopite (CR2).

	PC 22	PC 22	PC 22	PC 22	PC 22	PC 22	PC 22
	c	c	ce	ce	ce	ce	ce
SiO2	43.09	42.92	42.91	43.63	43.09	41.73	42.76
TiO2	3.95	4.05	4.11	4.05	4.53	4.14	3.65
Al2O3	6.31	6.56	6.07	6.40	6.21	7.97	6.85
Cr2O3	0.00	0.00	0.00	0.00	0.00	0.02	0.00
FeO	7.21	7.16	7.60	7.26	7.27	7.03	7.27
MnO	0.00	0.00	0.01	0.00	0.02	0.03	0.00
MgO	22.09	22.97	22.91	22.58	22.08	23.69	23.43
CaO	0.02	0.05	0.01	0.03	0.06	0.07	0.03
BaO	0.65	0.42	0.66	0.45	0.62	0.78	0.25
K2O	10.05	10.09	9.88	9.77	9.64	9.19	10.15
Na2O	0.92	0.83	0.91	0.80	0.88	0.41	0.69
F	4.65	4.41	4.40	4.67	4.40	4.29	3.97
Total	98.94	99.46	99.47	99.64	98.80	99.35	99.05
O=F	1.96	1.86	1.85	1.97	1.85	1.81	1.67
Total	96.98	97.60	97.62	97.67	96.95	97.54	97.38
mg #	84.5	85.1	84.3	84.7	84.4	85.7	85.2
Structural formula calculations based on 22 oxygens.							
Si	6.032	5.969	5.988	6.037	6.028	5.794	5.966
Ti	0.416	0.424	0.431	0.421	0.477	0.432	0.383
Al	1.041	1.075	0.998	1.044	1.024	1.304	1.126
Cr	0.000	0.000	0.000	0.000	0.000	0.002	0.000
Mn	0.000	0.000	0.001	0.000	0.002	0.004	0.000
Fe	0.844	0.833	0.887	0.840	0.851	0.816	0.848
Mg	4.610	4.762	4.766	4.658	4.605	4.904	4.873
Ca	0.003	0.007	0.001	0.004	0.009	0.010	0.004
Ba	0.036	0.023	0.036	0.024	0.034	0.042	0.014
K	1.795	1.790	1.759	1.725	1.721	1.628	1.807
Na	0.250	0.224	0.246	0.215	0.239	0.110	0.187
F	2.059	1.940	1.942	2.044	1.947	1.884	1.752
Total	17.084	17.047	17.055	17.011	16.936	16.931	16.960

Phlogopite analyses: Corona rim 3 phlogopite (CR3).

	PC 53	PC 53	PC 22	PC 22	PC 22	PC 53	PC 22
	c	c	c	c	c	ce	e
SiO2	42.68	43.52	43.32	42.08	43.11	43.22	40.93
TiO2	5.62	5.58	4.19	4.53	4.16	5.76	3.51
Al2O3	7.15	7.11	5.96	6.11	6.49	7.60	6.87
Cr2O3	0.08	0.02	0.04	0.05	0.00	0.02	0.00
FeO	7.58	7.48	8.36	8.04	7.71	7.38	7.20
MnO	0.07	0.00	0.03	0.00	0.05	0.00	0.00
MgO	21.39	21.82	22.63	22.22	22.69	21.88	24.30
CaO	0.01	0.03	0.02	0.00	0.02	0.02	0.02
BaO	1.08	1.14	0.79	1.08	0.41	0.94	0.52
K2O	9.15	9.48	9.97	10.13	9.93	8.61	9.70
Na2O	0.68	0.69	1.05	0.82	0.78	0.50	0.90
F	3.16	3.37	3.78	4.34	4.57	2.86	4.67
Total	98.65	100.24	100.14	99.40	99.92	98.79	98.62
O:F	1.33	1.42	1.59	1.83	1.92	1.20	1.97
Total	97.32	98.82	98.55	97.57	98.00	97.59	96.65
mg #	83.4	83.9	82.8	83.1	84.0	84.1	85.8
Structural formula calculations based on 22 oxygens.							
Si	5.990	6.009	6.033	5.926	5.974	6.009	5.765
Ti	0.593	0.579	0.439	0.480	0.433	0.602	0.372
Al	1.183	1.157	0.978	1.014	1.060	1.245	1.140
Cr	0.009	0.002	0.004	0.006	0.000	0.002	0.000
Mn	0.008	0.000	0.004	0.000	0.006	0.000	0.000
Fe	0.890	0.864	0.974	0.947	0.893	0.858	0.848
Mg	4.475	4.491	4.698	4.665	4.687	4.535	5.102
Ca	0.002	0.004	0.003	0.000	0.003	0.003	0.003
Ba	0.059	0.062	0.043	0.060	0.022	0.051	0.029
K	1.638	1.670	1.771	1.820	1.755	1.527	1.743
Na	0.185	0.185	0.284	0.224	0.210	0.135	0.246
F	1.403	1.472	1.665	1.933	2.003	1.258	2.080
Total	16.434	16.495	16.896	17.073	17.047	16.225	17.328

Phlogopite analyses: Phlogopite-bearing cognate xenolith phlogopite (PBX).

	PC 40d	PC 40d	PC 40d	PC 40d	PC 40d	PC 40b	PC 40b	PC 40b	PC 40b	PC 40b	PC 40b	PC 40b
	c	c	c	c	c	c	c	c	c	c	c	c
SiO2	42.21	42.64	42.38	42.85	41.48	44.31	42.22	41.54	41.38	40.30	41.37	41.68
TiO2	4.34	4.57	4.51	4.59	4.91	3.89	4.52	4.69	4.60	4.57	4.65	4.98
Al203	7.57	7.53	7.58	7.43	8.14	7.42	8.16	7.65	7.86	8.18	7.83	8.05
Cr203	0.10	0.09	0.07	0.09	0.17	0.10	0.16	0.11	0.16	0.01	0.09	0.09
FeO	7.09	7.72	7.11	6.99	6.93	6.58	6.86	7.50	7.07	6.72	7.71	7.40
MnO	0.00	0.00	0.00	0.00	0.01	0.04	0.00	0.04	0.05	0.03	0.06	0.09
MgO	22.58	22.44	22.25	22.36	22.75	22.16	22.66	21.55	22.51	22.89	22.54	22.99
CaO	0.07	0.00	0.00	0.00	0.00	0.00	0.00	0.00	0.00	0.01	0.13	0.04
BaO	0.97	0.92	1.16	1.05	1.34	0.89	1.26	1.23	1.28	1.04	0.73	0.92
K2O	10.08	10.38	10.32	10.43	10.14	9.96	10.14	10.48	9.75	10.20	10.19	10.23
Na2O	0.61	0.67	0.71	0.73	0.39	0.46	0.50	0.61	0.45	0.46	0.51	0.44
F	0.00	0.00	0.00	0.00	0.00	0.00	0.00	0.00	0.00	3.46	4.11	3.81
Total	95.62	96.97	96.09	96.52	96.26	95.81	96.48	95.40	95.11	97.87	99.92	100.72
O=F	0.00	0.00	0.00	0.00	0.00	0.00	0.00	0.00	0.00	1.46	1.73	1.60
Total	95.62	96.97	96.09	96.52	96.26	95.81	96.48	95.40	95.11	96.41	98.19	99.12
mg #	85.0	83.8	84.8	85.1	85.4	85.7	85.5	83.7	85.0	85.9	83.9	84.7
Structural formula calculations based on 22 oxygens.												
Si	6.129	6.127	6.139	6.170	6.003	6.354	6.078	6.093	6.052	5.736	5.771	5.763
Ti	0.474	0.494	0.491	0.497	0.534	0.419	0.489	0.517	0.506	0.489	0.488	0.518
Al	1.295	1.275	1.294	1.261	1.388	1.254	1.385	1.323	1.355	1.372	1.287	1.312
Cr	0.011	0.010	0.008	0.010	0.019	0.011	0.018	0.013	0.019	0.001	0.010	0.010
Mn	0.000	0.000	0.000	0.000	0.001	0.005	0.000	0.005	0.006	0.004	0.007	0.011
Fe	0.861	0.928	0.861	0.842	0.839	0.789	0.826	0.920	0.865	0.800	0.899	0.856
Mg	4.888	4.806	4.805	4.799	4.908	4.737	4.863	4.712	4.908	4.857	4.688	4.739
Ca	0.011	0.009	0.000	0.000	0.000	0.000	0.000	0.000	0.000	0.002	0.019	0.006
Ba	0.055	0.052	0.066	0.059	0.076	0.050	0.071	0.071	0.073	0.058	0.040	0.050
K	1.867	1.904	1.907	1.916	1.872	1.822	1.862	1.961	1.819	1.852	1.814	1.805
Na	0.172	0.187	0.199	0.204	0.109	0.127	0.140	0.173	0.128	0.127	0.138	0.118
F	0.000	0.000	0.000	0.000	0.000	0.000	0.000	0.000	0.000	1.558	1.813	1.666
Total	15.763	15.783	15.772	15.758	15.750	15.568	15.732	15.789	15.729	16.856	16.975	16.852

Phlogopite analyses: Phlogopite-bearing cognate xenolith phlogopite (PBX).

	PC 40b	PC 40b	PC 40b	PC 40b	PC 40d	PC 40b	PC 40b	PC 40b	PC 20b
	c	c	c	c	e	e	e	e	e
SiO2	39.81	40.57	40.51	42.31	40.25	40.18	37.68	39.60	40.76
TiO2	4.62	5.50	4.99	4.78	4.22	4.88	4.66	4.91	4.26
Al203	8.37	8.94	8.38	7.79	7.64	8.32	7.38	8.75	9.50
Cr203	0.03	0.10	0.07	0.05	0.10	0.13	0.00	0.17	0.08
FeO	6.71	7.38	6.83	7.03	7.20	7.51	7.69	6.97	6.38
MnO	0.00	0.00	0.04	0.03	0.00	0.00	0.00	0.00	0.17
MgO	23.18	22.53	22.76	22.45	22.55	22.98	22.81	22.86	23.17
CaO	0.00	0.07	0.04	0.02	0.32	0.03	0.00	0.00	0.00
BaO	0.96	1.45	1.12	1.00	1.23	1.01	0.84	1.49	1.98
K2O	10.31	9.30	10.12	9.58	9.92	9.82	9.91	10.09	9.42
Na2O	0.46	0.25	0.71	0.56	0.46	0.30	0.42	0.32	0.45
F	3.30	3.57	2.83	3.05	0.00	3.22	3.26	3.20	4.50
Total	97.75	99.66	98.40	98.65	93.89	98.38	94.65	98.36	100.67
O=F	1.39	1.50	1.19	1.28	0.00	1.36	1.37	1.35	1.89
Total	96.36	98.16	97.21	97.37	93.89	97.02	93.28	97.01	98.78
mg #	86.0	84.5	85.6	85.1	84.8	84.5	84.1	85.4	86.6
Structural formula calculations based on 22 oxygens.									
Si	5.680	5.665	5.742	5.932	5.995	5.697	5.599	5.637	5.634
Ti	0.496	0.578	0.532	0.504	0.473	0.520	0.521	0.526	0.443
Al	1.408	1.471	1.400	1.287	1.341	1.390	1.292	1.468	1.547
Cr	0.003	0.011	0.008	0.006	0.012	0.015	0.000	0.019	0.009
Mn	0.000	0.000	0.005	0.004	0.000	0.000	0.000	0.000	0.020
Fe	0.801	0.862	0.810	0.824	0.897	0.890	0.956	0.830	0.737
Mg	4.931	4.690	4.810	4.693	5.007	4.857	5.053	4.851	4.774
Ca	0.000	0.010	0.006	0.003	0.051	0.005	0.000	0.000	0.000
Ba	0.054	0.079	0.062	0.055	0.072	0.056	0.049	0.083	0.107
K	1.877	1.657	1.830	1.714	1.885	1.776	1.878	1.832	1.661
Na	0.127	0.068	0.195	0.152	0.133	0.082	0.121	0.088	0.121
F	1.489	1.577	1.269	1.353	0.000	1.444	1.532	1.441	1.967
Total	16.865	16.667	16.669	16.526	15.865	16.732	17.000	16.775	17.020

Phlogopite analyses: "No added volatile" system (HPP)

	EPC 7	EPC 7	EPC 7	EPC 7	EPC 7	EPC 43	EPC 43	EPC 43	EPC 43	EPC 43	EPC 43	EPC 43
kilobars	30	30	30	30	30	20	20	20	20	20	20	20
Celsius	1250	1250	1250	1250	1250	1050	1050	1050	1050	1050	1050	1050
minutes	30	30	30	30	30	240	240	240	240	240	240	240
SiO2	40.53	42.20	41.66	40.64	41.87	40.60	40.96	40.18	40.75	40.91	42.08	39.70
TiO2	2.13	2.16	2.25	2.30	1.97	1.99	2.15	1.99	1.91	1.87	2.07	1.98
Al2O3	12.40	10.94	12.14	11.78	12.42	11.57	11.02	11.67	12.04	12.11	12.33	11.77
Cr2O3	1.61	1.02	0.49	0.28	0.93	0.18	0.14	0.10	0.12	0.33	0.18	0.19
FeO	4.50	5.30	4.59	4.88	4.79	5.12	5.74	5.66	5.46	5.23	5.73	5.32
MnO	0.00	0.03	0.00	0.05	0.07	0.13	0.07	0.12	0.00	0.00	0.00	0.00
MgO	22.68	23.05	22.82	22.34	23.72	23.33	23.25	22.85	22.80	23.17	23.21	22.86
CaO	0.12	0.09	0.08	0.25	0.12	0.09	0.07	0.04	0.01	0.01	0.03	0.04
K2O	10.03	10.52	11.10	10.64	10.08	9.57	8.64	9.88	8.57	10.31	9.26	9.89
Na2O	0.00	0.05	0.00	0.00	0.08	0.06	0.00	0.07	0.05	0.08	0.04	0.13
BaO	0.47	0.52	0.00	0.00	0.39	0.00	0.00	0.00	0.46	0.53	0.56	0.60
F	0.00	0.00	0.36	0.31	0.40	0.00	0.00	0.00	0.22	0.29	0.29	0.32
Total	94.47	95.88	95.49	93.47	96.84	92.64	92.04	92.56	92.39	94.84	95.78	92.80
O=F	0.00	0.00	0.15	0.13	0.17	0.00	0.00	0.00	0.09	0.12	0.12	0.13
Total	94.47	95.88	95.34	93.34	96.67	92.64	92.04	92.56	92.30	94.72	95.66	92.67
mg #	89.98	88.57	89.86	89.08	89.82	89.04	87.84	87.80	88.16	88.76	87.84	88.45
Structural formula calculations based on 22 oxygens												
Si	5.852	6.026	5.938	5.926	5.882	5.943	6.011	5.916	5.960	5.895	5.960	5.856
Ti	0.231	0.232	0.241	0.252	0.208	0.219	0.237	0.220	0.210	0.203	0.220	0.220
Al	2.110	1.841	2.039	2.025	2.056	1.996	1.906	2.025	2.076	2.057	2.058	2.046
Cr	0.184	0.115	0.055	0.032	0.103	0.021	0.016	0.012	0.014	0.038	0.020	0.022
Mn	0.000	0.004	0.000	0.006	0.008	0.016	0.009	0.015	0.000	0.000	0.000	0.000
Fe	0.543	0.633	0.547	0.595	0.563	0.627	0.704	0.697	0.668	0.630	0.679	0.656
Mg	4.881	4.906	4.849	4.856	4.967	5.091	5.087	5.016	4.972	4.977	4.901	5.026
Ca	0.019	0.014	0.012	0.039	0.018	0.014	0.011	0.006	0.002	0.002	0.005	0.006
Ba	0.027	0.029	0.000	0.000	0.021	0.000	0.000	0.000	0.026	0.030	0.031	0.035
K	1.847	1.916	2.018	1.979	1.806	1.787	1.618	1.856	1.599	1.895	1.673	1.861
Na	0.000	0.014	0.000	0.000	0.022	0.017	0.000	0.020	0.014	0.022	0.011	0.037
F	0.000	0.000	0.162	0.143	0.178	0.000	0.000	0.000	0.102	0.132	0.130	0.149
Total	15.694	15.730	15.864	15.854	15.833	15.731	15.599	15.783	15.642	15.880	15.688	15.914

Phlogopite analyses: "No added volatile" system (HPP)

	EPC 45	EPC 45	EPC 45	EPC 45	EPC 45	EPC 45	EPC 45	EPC 45	EPC 45	EPC 45	EPC 45	EPC 60
kilobars	30	30	30	30	30	30	30	30	30	30	30	35
Celsius	1150	1150	1150	1150	1150	1150	1150	1150	1150	1150	1150	1200
minutes	180	180	180	180	180	180	180	180	180	180	180	180
SiO2	40.34	39.86	40.98	41.28	40.24	40.92	41.22	40.63	41.97	40.56	40.18	39.83
TiO2	1.76	1.65	1.65	1.73	1.36	1.36	1.42	1.38	1.42	1.39	1.40	1.18
Al2O3	11.74	11.70	11.56	11.71	11.88	11.99	11.84	12.05	11.71	11.76	12.05	11.44
Cr2O3	0.27	0.43	0.62	0.25	0.84	0.47	0.65	0.70	0.15	0.26	0.58	0.39
FeO	5.63	5.22	5.53	5.33	5.17	4.84	5.12	4.66	5.66	4.21	5.25	5.42
MnO	0.08	0.11	0.08	0.09	0.00	0.00	0.00	0.00	0.00	0.00	0.00	0.06
MgO	22.62	24.22	22.80	23.49	24.04	24.03	23.30	23.83	23.98	24.14	23.78	24.83
CaO	0.04	0.10	0.04	0.04	0.01	0.05	0.02	0.00	0.03	0.06	0.03	0.01
K2O	9.49	9.04	9.70	9.89	10.50	10.39	9.76	10.41	9.10	10.32	10.53	10.80
Na2O	0.04	0.04	0.04	0.01	0.10	0.11	0.08	0.09	0.04	0.06	0.06	0.03
BaO	0.00	0.00	0.00	0.00	0.29	0.35	0.33	0.36	0.34	0.37	0.41	0.26
F	0.00	0.00	0.00	0.00	0.14	0.12	0.13	0.11	0.11	0.19	0.00	0.29
Total	92.01	92.37	93.00	93.82	94.57	94.63	93.87	94.23	94.51	93.32	94.27	94.54
O:F	0.00	0.00	0.00	0.00	0.06	0.05	0.05	0.05	0.05	0.08	0.00	0.12
Total	92.01	92.37	93.00	93.82	94.51	94.58	93.82	94.18	94.46	93.24	94.27	94.42
mg #	87.75	89.21	88.02	88.71	89.23	89.85	89.03	90.11	88.31	91.09	88.98	89.09
Structural formula calculations based on 22 oxygens												
Si	5.955	5.851	5.988	5.972	5.831	5.898	5.968	5.883	6.011	5.911	5.844	5.795
Ti	0.195	0.182	0.181	0.188	0.148	0.147	0.155	0.150	0.153	0.152	0.153	0.129
Al	2.042	2.024	1.991	1.997	2.029	2.037	2.020	2.058	1.976	2.020	2.066	1.962
Cr	0.032	0.050	0.072	0.029	0.096	0.054	0.074	0.080	0.017	0.030	0.067	0.045
Mn	0.010	0.014	0.010	0.011	0.000	0.000	0.000	0.000	0.000	0.000	0.000	0.007
Fe	0.695	0.641	0.676	0.645	0.627	0.583	0.620	0.564	0.678	0.513	0.639	0.659
Mg	4.978	5.300	4.966	5.066	5.193	5.164	5.029	5.143	5.120	5.244	5.156	5.386
Ca	0.006	0.016	0.006	0.006	0.002	0.008	0.003	0.000	0.005	0.009	0.005	0.002
Ba	0.000	0.000	0.000	0.000	0.016	0.020	0.019	0.020	0.019	0.021	0.023	0.015
K	1.787	1.693	1.808	1.825	1.941	1.911	1.803	1.923	1.663	1.919	1.954	2.005
Na	0.011	0.011	0.011	0.003	0.028	0.031	0.022	0.025	0.011	0.017	0.017	0.008
F	0.000	0.000	0.000	0.000	0.064	0.055	0.060	0.050	0.050	0.088	0.000	0.133
Total	15.712	15.782	15.709	15.741	15.975	15.907	15.773	15.897	15.702	15.924	15.922	16.146

Phlogopite analyses: "No added volatile" system (HPP)

	EPC 60	EPC 60	EPC 60	EPC 60
kilobars	35	35	35	35
Celsius	1200	1200	1200	1200
minutes	180	180	180	180
SiO2	39.05	38.90	39.54	39.87
TiO2	1.26	1.25	1.33	1.23
Al203	11.30	12.18	12.11	11.91
Cr203	0.36	0.80	0.39	0 48
FeO	5.08	4.83	4.86	4.86
MnO	0.10	0.11	0.05	0.06
MgO	24.68	24.53	25.08	24.62
CaO	0.00	0.02	0.02	0.01
K2O	10.15	10.32	10.38	10.46
Na2O	0.04	0.06	0.07	0.04
BaO	0.29	0.33	0.33	0.31
F	0.21	0.31	0.29	0.27
Total	92.52	93.64	94.45	94.12
O:F	0.09	0.13	0.12	0.11
Total	92.43	93.51	94.33	94.01
mg #	89.65	90.05	90.20	90.03
Structural formula calculations based on 22 oxygens				
Si	5.786	5.700	5.733	5.797
Ti	0.140	0.138	0.145	0.134
Al	1.973	2.103	2.069	2.041
Cr	0.042	0.093	0.045	0.055
Mn	0.013	0.014	0.006	0.007
Fe	0.629	0.592	0.589	0.591
Mg	5.451	5.358	5.421	5.337
Ca	0.000	0.003	0.003	0.002
Ba	0.017	0.019	0.019	0.018
K	1.919	1.929	1.920	1.940
Na	0.011	0.017	0.020	0.011
F	0.098	0.144	0.133	0.124
Total	16.060	16.109	16.102	16.058

Phlogopite analyses: "Water added" system (HPP)

	PCW 26	PCW 26	PCW 26	PCW 26	PCW 26
kilobars	30	30	30	30	30
Celsius	1150	1150	1150	1150	1150
minutes	270	270	270	270	270
SiO2	41.33	40.47	40.95	42.31	42.36
TiO2	1.98	1.63	1.62	1.69	1.66
Al203	12.78	12.56	12.10	12.39	12.49
Cr203	1.15	1.34	0.96	1.26	1.09
FeO	5.20	4.73	4.77	4.91	4.68
MnO	0.05	0.06	0.09	0.06	0.00
MgO	23.66	23.08	22.82	22.86	22.98
CaO	0.14	0.06	0.03	1.00	0.04
K2O	11.27	11.71	9.75	10.32	9.55
Na2O	0.16	0.17	0.05	0.09	0.05
BaO	0.49	0.58	0.48	0.57	0.59
F	0.00	0.00	0.00	0.16	0.10
Total	98.21	96.39	93.62	97.62	95.59
O F	0.00	0.00	0.00	0.07	0.04
Total	98.21	96.39	93.62	97.55	95.55
mg #	89.02	89.69	89.50	89.25	89.75
Structural formula calculations based on 22 oxygens					
Si	5.794	5.799	5.949	5.928	5.999
Ti	0.209	0.176	0.177	0.178	0.177
Al	2.111	2.121	2.072	2.046	2.085
Cr	0.127	0.152	0.110	0.140	0.122
Mn	0.006	0.007	0.011	0.007	0.000
Fe	0.610	0.567	0.580	0.575	0.554
Mg	4.944	4.930	4.942	4.775	4.852
Ca	0.021	0.009	0.005	0.150	0.006
Ba	0.027	0.033	0.027	0.031	0.033
K	2.015	2.141	1.807	1.845	1.726
Na	0.043	0.047	0.014	0.024	0.014
F	0.000	0.000	0.000	0.071	0.045
Total	15.908	15.982	15.694	15.771	15.612

Phlogopite analyses: "Water added" system (HPP)

	PCW 26	PCW 26	PCW 32	PCW 32	PCW 32	PCW 32	PCW 32	PCW 32	PCW 32	PCW 32	PCW 32	PCW 32
kilobars	30	30	20	20	20	20	20	20	20	20	20	20
Celsius	1150	1150	1020	1020	1020	1020	1020	1020	1020	1020	1020	1020
minutes	270	270	360	360	360	360	360	360	360	360	360	360
SiO2	39.57	40.18	39.69	39.81	41.31	39.17	39.96	39.66	40.71	40.71	40.25	39.35
TiO2	1.44	1.58	1.75	1.66	1.75	1.76	1.77	1.81	1.56	1.69	1.65	1.71
Al2O3	12.32	12.46	11.61	11.69	10.97	11.04	11.14	11.26	12.08	12.30	12.23	11.56
Cr2O3	0.87	1.03	0.33	0.30	0.16	0.32	0.10	0.29	0.00	0.08	0.13	0.00
FeO	4.67	4.39	5.24	5.23	5.60	5.30	5.57	5.52	5.12	5.57	5.41	5.23
MnO	0.00	0.00	0.06	0.02	0.08	0.11	0.06	0.00	0.00	0.00	0.00	0.00
MgO	23.07	23.26	23.66	23.77	23.45	23.97	23.93	24.14	24.48	23.76	23.61	23.28
CaO	0.00	0.02	0.01	0.02	0.01	0.02	0.06	0.01	0.14	0.05	0.10	0.10
K2O	10.52	10.55	9.57	9.70	9.73	9.75	9.58	9.71	10.08	9.32	10.13	10.01
Na2O	0.06	0.08	0.04	0.05	0.06	0.09	0.07	0.04	0.16	0.11	0.16	0.16
BaO	0.35	0.45	0.68	0.74	0.74	0.67	0.59	0.65	0.60	0.67	0.68	0.65
F	0.13	0.13	0.00	0.00	0.00	0.00	0.00	0.00	0.27	0.25	0.30	0.31
Total	93.00	94.13	92.64	92.99	93.81	92.20	92.83	93.09	95.20	94.51	94.65	92.36
O:F	0.05	0.05	0.00	0.00	0.00	0.00	0.00	0.00	0.11	0.11	0.13	0.13
Total	92.95	94.08	92.64	92.99	93.81	92.20	92.83	93.09	95.09	94.40	94.52	92.23
mg #	89.80	90.43	88.95	89.01	88.19	88.96	88.45	88.63	89.50	88.38	88.61	88.81
Structural formula calculations based on 22 oxygens												
Si	5.822	5.833	5.858	5.858	6.015	5.833	5.890	5.840	5.842	5.867	5.828	5.842
Ti	0.159	0.172	0.194	0.184	0.192	0.197	0.196	0.200	0.168	0.183	0.180	0.191
Al	2.136	2.132	2.020	2.027	1.883	1.938	1.935	1.954	2.043	2.089	2.087	2.023
Cr	0.101	0.118	0.039	0.035	0.018	0.038	0.012	0.034	0.000	0.009	0.015	0.000
Mn	0.000	0.000	0.008	0.002	0.010	0.014	0.007	0.000	0.000	0.000	0.000	0.000
Fe	0.575	0.533	0.647	0.644	0.682	0.660	0.687	0.680	0.615	0.671	0.655	0.649
Mg	5.060	5.034	5.206	5.214	5.090	5.321	5.258	5.300	5.237	5.105	5.096	5.153
Ca	0.000	0.003	0.002	0.003	0.002	0.003	0.009	0.002	0.022	0.008	0.016	0.016
Ba	0.020	0.026	0.039	0.043	0.039	0.039	0.034	0.038	0.034	0.038	0.039	0.038
K	1.975	1.954	1.802	1.821	1.807	1.852	1.801	1.824	1.846	1.714	1.871	1.896
Na	0.017	0.023	0.011	0.014	0.017	0.026	0.020	0.011	0.045	0.031	0.045	0.046
F	0.060	0.060	0.000	0.000	0.000	0.000	0.000	0.000	0.123	0.114	0.137	0.146
Total	15.926	15.887	15.825	15.845	15.755	15.921	15.851	15.883	15.974	15.829	15.968	15.999

Phlogopite analyses: "Water added" system (HPP)

	PCW 33	PCW 33	PCW 33	PCW 33	PCW 33	PCW 35	PCW 35	PCW 35	PCW 35	PCW 35	PCW 35
kilobars	20	20	20	20	20	30	30	30	30	30	30
Celsius	1130	1130	1130	1130	1130	1050	1050	1050	1050	1050	1050
minutes	240	240	240	240	240	240	240	240	240	240	240
SiO2	41.40	40.76	39.34	40.22	38.93	41.33	41.10	41.52	40.16	40.44	40.34
TiO2	2.12	2.00	1.75	1.68	1.86	1.37	1.47	1.47	1.86	1.64	1.63
Al203	13.15	13.26	12.17	12.08	12.23	12.05	12.42	11.19	12.30	12.32	11.89
Cr203	1.10	1.21	1.32	1.21	1.32	0.20	0.25	0.19	0.30	0.28	0.18
FeO	4.61	4.88	4.75	4.59	4.62	5.05	5.12	4.74	4.93	5.00	5.20
MnO	0.03	0.00	0.07	0.11	0.01	0.05	0.00	0.00	0.00	0.00	0.00
MgO	23.93	23.40	24.20	23.83	23.55	24.12	23.72	23.27	23.32	23.45	24.01
CaO	0.04	0.09	0.01	0.00	0.01	0.02	0.02	0.13	0.00	0.01	0.04
K2O	10.15	9.97	9.49	10.06	10.20	9.88	10.27	10.23	10.41	10.36	10.09
Na2O	0.12	0.24	0.03	0.06	0.11	0.09	0.09	0.10	0.16	0.09	0.17
BaO	0.42	0.36	0.34	0.46	0.39	0.69	0.63	0.60	0.70	0.61	0.68
F	0.00	0.00	0.15	0.22	0.18	0.27	0.34	0.29	0.22	0.21	0.19
Total	97.07	96.17	93.62	94.52	93.41	95.12	95.43	93.73	94.36	94.41	94.42
O=F	0.00	0.00	0.06	0.09	0.08	0.11	0.14	0.12	0.09	0.09	0.08
Total	97.07	96.17	93.56	94.43	93.33	95.01	95.29	93.61	94.27	94.32	94.34
mg #	90.25	89.53	90.08	90.25	90.09	89.49	89.20	89.74	89.40	89.32	89.17
Structural formula calculations based on 22 oxygens											
Si	5.805	5.778	5.733	5.813	5.714	5.920	5.881	6.035	5.831	5.858	5.850
Ti	0.224	0.213	0.192	0.183	0.205	0.148	0.158	0.161	0.203	0.179	.178
Al	2.173	2.215	2.090	2.058	2.116	2.034	2.095	1.917	2.105	2.103	2.032
Cr	0.122	0.136	0.152	0.138	0.153	0.023	0.028	0.022	0.034	0.032	0.021
Mn	0.004	0.000	0.009	0.013	0.001	0.006	0.000	0.000	0.000	0.000	0.000
Fe	0.541	0.579	0.579	0.555	0.567	0.605	0.613	0.576	0.599	0.606	0.631
Mg	5.002	4.945	5.257	5.134	5.153	5.150	5.060	5.042	5.048	5.064	5.190
Ca	0.006	0.014	0.002	0.000	0.002	0.003	0.003	0.020	0.000	0.002	0.006
Ba	0.023	0.020	0.019	0.026	0.022	0.039	0.035	0.034	0.040	0.035	0.039
K	1.816	1.803	1.764	1.855	1.910	1.805	1.875	1.897	1.928	1.914	1.867
Na	0.033	0.066	0.008	0.017	0.031	0.025	0.025	0.028	0.045	0.025	0.048
F	0.000	0.000	0.069	0.101	0.084	0.122	0.154	0.133	0.101	0.096	0.087
Total	15.748	15.768	15.875	15.893	15.959	15.880	15.926	15.865	15.934	15.914	15.947

Phlogopite analyses: "Fluorine added" system (HPP)

	FPC 4	FPC 4	FPC 4	FPC 4	FPC 4	FPC 4	FPC 8	FPC 8	FPC 8	FPC 8	FPC 8	FPC 8
kilobars	20	20	20	20	20	20	20	20	20	20	20	20
Celsius	1100	1100	1100	1100	1100	1100	1000	1000	1000	1000	1000	1000
minutes	300	300	300	300	300	300	300	300	300	300	300	300
SiO2	40.16	41.13	41.29	41.42	41.83	41.46	40.82	40.83	40.40	40.77	40.62	40.02
TiO2	1.45	1.39	1.48	1.43	1.49	1.41	1.75	1.68	1.78	1.79	1.72	1.80
Al2O3	12.13	12.60	12.23	10.94	11.65	11.58	11.88	11.88	11.36	12.03	12.01	11.92
Cr2O3	0.62	0.97	0.65	0.47	0.92	0.91	0.14	0.16	0.19	0.18	0.14	0.15
FeO	5.26	5.35	5.43	5.71	5.33	5.39	4.90	4.63	4.60	4.78	4.48	4.82
MnO	0.03	0.04	0.00	0.00	0.09	0.06	0.08	0.07	0.07	0.09	0.14	0.09
MgO	24.47	24.19	25.05	24.12	24.53	25.15	25.04	24.69	24.37	24.73	24.43	24.70
CaO	0.00	0.00	0.00	0.03	0.02	0.14	0.07	0.04	0.04	0.05	0.08	0.04
K2O	10.22	9.66	10.44	9.91	9.99	9.59	9.77	8.89	8.96	8.92	8.88	9.41
Na2O	0.00	0.00	0.00	0.02	0.03	0.07	0.19	0.20	0.15	0.16	0.18	0.18
BaO	0.55	0.53	0.46	0.49	0.34	0.42	1.01	0.94	1.00	0.92	1.02	1.02
F	0.83	0.85	0.75	0.58	0.93	0.91	1.57	1.55	1.43	1.54	1.45	1.43
Total	95.72	96.71	97.78	95.12	97.15	97.09	97.22	95.56	94.35	95.98	95.15	95.58
O=F	0.35	0.36	0.32	0.24	0.39	0.38	0.66	0.65	0.60	0.65	0.61	0.60
Total	95.37	96.35	97.46	94.88	96.76	96.71	96.56	94.91	93.75	95.33	94.54	94.98
mg #	89.24	88.96	89.16	88.28	89.14	89.27	90.11	90.48	90.43	90.22	90.67	90.13
Structural formula calculations based on 22 oxygens												
Si	5.751	5.798	5.782	5.952	5.872	5.825	5.745	5.801	5.825	5.773	5.798	5.724
Ti	0.156	0.147	0.156	0.155	0.157	0.149	0.185	0.179	0.193	0.191	0.185	0.194
Al	2.047	2.093	2.018	1.853	1.927	1.918	1.971	1.989	1.930	2.008	2.020	2.009
Cr	0.070	0.108	0.072	0.053	0.102	0.101	0.016	0.018	0.022	0.020	0.016	0.017
Mn	0.004	0.005	0.000	0.000	0.011	0.007	0.010	0.008	0.009	0.011	0.017	0.011
Fe	0.630	0.631	0.636	0.686	0.626	0.633	0.577	0.550	0.555	0.566	0.535	0.577
Mg	5.224	5.084	5.229	5.167	5.134	5.268	5.254	5.229	5.238	5.220	5.198	5.267
Ca	0.000	0.000	0.000	0.005	0.003	0.021	0.011	0.006	0.006	0.008	0.012	0.006
Ba	0.031	0.029	0.025	0.028	0.019	0.023	0.056	0.052	0.057	0.051	0.057	0.057
K	1.867	1.737	1.865	1.817	1.789	1.719	1.754	1.611	1.648	1.611	1.617	1.717
Na	0.000	0.000	0.000	0.006	0.008	0.019	0.052	0.055	0.042	0.049	0.050	0.050
F	0.376	0.379	0.332	0.264	0.413	0.404	0.699	0.696	0.652	0.690	0.655	0.647
Total	16.156	16.012	16.116	15.983	16.061	16.088	16.329	16.197	16.177	16.198	16.160	16.276

Phlogopite analyses: "Fluorine added" system (HPP)

	FPC 8	FPC 9	FPC 9	FPC 9	FPC 10	FPC 10	FPC 10	FPC 10	FPC 10
kilobars	20	30	30	30	30	30	30	30	30
Celsius	1000	1200	1200	1200	1100	1100	1100	1100	1100
minutes	300	180	180	180	180	180	180	180	180
SiO2	40.59	38.99	38.68	40.18	40.34	39.33	40.45	40.01	39.25
TiO2	1.65	1.36	1.34	1.33	1.28	1.27	1.20	1.22	1.31
Al203	11.46	12.44	12.24	11.96	11.37	11.34	11.11	11.20	11.54
Cr203	0.08	1.32	1.37	1.38	0.23	0.44	0.29	0.45	0.49
FeO	5.03	4.46	4.31	4.56	4.62	4.87	4.85	4.85	4.59
MnO	0.05	0.07	0.11	0.09	0.05	0.11	0.07	0.02	0.10
MgO	24.33	23.56	23.90	23.86	25.30	25.33	24.83	24.54	24.73
CaO	0.02	0.02	0.03	0.00	0.03	0.02	0.03	0.02	0.04
K2O	8.91	10.25	10.36	8.42	10.65	10.38	10.32	10.25	10.23
Na2O	0.20	0.06	0.07	0.03	0.08	0.04	0.07	0.07	0.08
BaO	0.95	0.31	0.46	0.30	0.41	0.37	0.39	0.36	0.38
F	1.61	0.98	0.97	0.70	1.08	0.88	1.08	0.93	1.00
Total	94.88	93.82	93.84	92.81	95.44	94.38	94.69	93.92	93.74
O=F	0.68	0.41	0.41	0.29	0.45	0.37	0.45	0.39	0.42
Total	94.20	93.41	93.43	92.52	94.99	94.01	94.24	93.53	93.32
mg #	89.61	90.40	90.81	90.32	90.71	90.26	90.12	90.02	90.57
Structural formula calculations based on 22 oxygens									
Si	5.823	5.689	5.658	5.845	5.786	5.719	5.841	5.826	5.733
Ti	0.178	0.149	0.147	0.146	0.138	0.139	0.130	0.134	0.144
Al	1.938	2.139	2.110	2.051	1.922	1.944	1.891	1.922	1.987
Cr	0.009	0.152	0.158	0.159	0.026	0.051	0.033	0.052	0.057
Mn	0.006	0.009	0.014	0.011	0.006	0.014	0.009	0.002	0.012
Fe	0.603	0.544	0.527	0.555	0.554	0.592	0.586	0.591	0.561
Mg	5.203	5.125	5.212	5.175	5.410	5.491	5.345	5.327	5.385
Ca	0.003	0.003	0.005	0.000	0.005	0.003	0.005	0.003	0.006
Ba	0.053	0.018	0.026	0.017	0.023	0.021	0.022	0.021	0.022
K	1.631	1.908	1.933	1.563	1.949	1.926	1.901	1.904	1.906
Na	0.056	0.017	0.020	0.008	0.022	0.011	0.020	0.020	0.023
F	0.730	0.452	0.449	0.322	0.490	0.405	0.493	0.428	0.462
Total	16.234	16.205	16.261	15.851	16.332	16.315	16.274	16.229	16.297

Phlogopite analyses: "Water added" system (LPP)

	PCW 31	PCW 31	PCW 31	PCW 31	PCW 31	PCW 31	PCW 31
kilobars	10	10	10	10	10	10	10
Celsius	1000	1000	1000	1000	1000	1000	1000
minutes	60	60	60	60	60	60	60
SiO2	41.57	42.94	42.34	43.86	42.29	44.11	40.86
TiO2	4.58	4.60	4.55	4.15	3.99	4.08	4.01
Al203	7.29	6.18	6.32	6.32	5.84	6.15	6.62
Cr203	0.09	0.06	0.13	0.07	0.02	0.13	0.09
FeO	7.99	7.77	7.69	7.73	7.98	7.31	7.60
MnO	0.00	0.05	0.01	0.02	0.05	0.00	0.07
MgO	22.39	21.89	22.41	22.41	22.77	22.51	21.68
CaO	0.06	0.08	0.11	0.07	0.06	0.05	0.07
K2O	11.41	11.56	11.86	10.14	9.49	9.90	9.67
Na2O	0.04	0.02	0.00	0.01	0.05	0.02	0.23
BaO	1.13	0.68	0.75	1.06	1.34	1.04	0.61
F	0.00	0.00	0.00	3.08	3.42	3.85	3.16
Total	96.55	95.83	96.17	98.92	97.30	99.15	94.67
O=F	0.00	0.00	0.00	1.30	1.44	1.62	1.33
Total	96.55	95.83	96.17	97.62	95.86	97.53	93.34
mg #	83.3	83.4	83.9	83.8	83.6	84.6	83.6
Structural formula calculations based on 22 oxygens							
Si	6.060	6.268	6.182	6.148	6.054	6.144	5.993
Ti	0.502	0.505	0.500	0.437	0.430	0.427	0.442
Al	1.253	1.063	1.088	1.044	0.985	1.010	1.144
Cr	0.010	0.007	0.015	0.008	0.002	0.014	0.010
Mn	0.000	0.006	0.001	0.002	0.006	0.000	0.009
Fe	0.974	0.949	0.939	0.906	0.955	0.852	0.932
Mg	4.866	4.763	4.878	4.683	4.859	4.674	4.740
Ca	0.009	0.013	0.017	0.011	0.009	0.007	0.011
Ba	0.065	0.039	0.043	0.058	0.075	0.057	0.035
K	2.122	2.153	2.209	1.813	1.733	1.759	1.809
Na	0.011	0.006	0.000	0.003	0.014	0.005	0.065
F	0.000	0.000	0.000	1.365	1.548	1.696	1.466
Total	15.873	15.771	15.872	16.479	16.671	16.647	16.658

Phlogopite analyses: "Fluorine added" (LPP)

	FPC 6	FPC 6	FPC 6	FPC 6
kilobars	10	10	10	10
Celsius	1000	1000	1000	1000
minutes	360	360	360	360
SiO2	43.69	43.11	41.16	42.78
TiO2	4.63	4.20	4.91	4.41
Al2O3	6.09	6.94	7.69	6.36
Cr2O3	0.12	0.12	0.09	0.14
FeO	7.52	7.58	7.75	7.88
MnO	0.12	0.07	0.06	0.14
MgO	22.66	24.08	22.16	22.00
CaO	0.12	0.22	0.09	0.08
K2O	9.27	8.68	9.89	10.35
Na2O	0.11	0.23	0.17	0.17
BaO	0.95	0.69	1.48	0.72
F	4.29	4.17	4.63	5.10
Total	99.57	100.09	100.08	100.13
O=F	1.81	1.76	1.95	2.15
Total	97.76	98.33	98.13	97.98
mg #	84.3	85.0	83.6	83.3
Structural formula calculations based on 22 oxygens				
Si	6.056	5.924	5.751	5.945
Ti	0.483	0.434	0.516	0.461
Al	0.995	1.124	1.266	1.042
Cr	0.013	0.013	0.010	0.015
Mn	0.014	0.008	0.007	0.016
Fe	0.872	0.871	0.906	0.916
Mg	4.682	4.933	4.616	4.558
Ca	0.018	0.032	0.013	0.012
Ba	0.052	0.037	0.081	0.039
K	1.639	1.522	1.763	1.835
Na	0.030	0.061	0.046	0.046
F	1.880	1.812	2.046	2.241
Total	16.732	16.771	17.022	17.127

5.4 Spinel

Spinel analyses: Hypabyssal facies (HYP)

	PC 29	PC 29	PC 29	PC 29	PC 29	PC 29	PC 29	PC 29	PC 29	PC 29	PC 29	PC 29
	101c	102c	103c	103c	103c	103ce	104c	104c	104ce	104ce	104c	105c
Al2O3	0.00	0.00	0.01	0.04	1.15	0.12	0.17	0.23	0.30	0.09	0.09	0.10
Cr2O3	17.67	16.82	12.21	21.74	46.55	26.24	32.72	33.24	32.49	30.14	29.16	30.55
FeO	62.70	63.57	67.58	58.71	40.66	56.46	50.84	49.78	50.32	54.26	54.11	52.39
MgO	3.85	3.23	2.39	3.71	5.15	4.01	4.70	4.72	4.55	4.35	4.35	4.27
TiO2	9.40	9.49	9.96	8.82	3.50	7.92	7.12	6.96	7.22	6.67	6.98	6.81
MnO	1.13	1.31	1.32	1.36	0.86	1.26	0.80	1.03	1.04	1.16	1.07	1.27
Total	94.75	94.42	93.47	94.38	97.87	96.01	96.35	95.96	95.92	96.67	95.76	95.39
Based on stoichiometry												
FeO	32.40	33.12	34.56	31.68	26.22	31.04	29.74	29.24	29.67	29.67	29.74	29.39
Fe2O3	33.70	33.85	36.73	30.02	15.97	28.27	23.47	22.84	23.00	27.31	27.15	25.55
Total	98.15	97.83	97.18	97.38	99.40	98.85	98.73	98.26	98.27	99.39	98.54	97.94
Structural formula calculations based on 4 oxygens												
Ti	0.265	0.269	0.287	0.250	0.095	0.220	0.197	0.193	0.201	0.184	0.194	0.191
Al	0.000	0.000	0.000	0.002	0.049	0.005	0.007	0.010	0.013	0.004	0.004	0.004
Cr	0.523	0.502	0.370	0.647	1.327	0.767	0.951	0.969	0.949	0.874	0.853	0.899
Fe3+	0.948	0.960	1.056	0.851	0.434	0.787	0.648	0.634	0.637	0.754	0.754	0.716
Fe2+	1.014	1.046	1.108	0.998	0.792	0.960	0.914	0.901	0.917	0.910	0.921	0.914
Mn	0.036	0.042	0.043	0.043	0.026	0.039	0.025	0.032	0.033	0.036	0.034	0.040
Mg	0.215	0.182	0.136	0.208	0.277	0.221	0.258	0.260	0.251	0.238	0.240	0.237
Total	3.000	3.000	3.000	3.000	3.000	3.000	3.000	3.000	3.000	3.000	3.000	3.000
Molecular proportions												
MgAl2O4	0.00	0.00	0.01	0.06	1.60	0.17	0.24	0.32	0.42	0.13	0.13	0.14
Mg2TiO4	7.67	6.43	4.75	7.36	7.03	7.89	9.22	9.22	8.82	8.59	8.59	8.42
Mn2TiO4	1.77	2.05	2.06	2.13		1.97	1.25	1.61	1.63	1.81	1.67	1.99
Fe2TiO4	13.85	15.53	19.17	12.29		9.19	5.81	5.01	6.27	4.87	5.88	5.32
MnCr2O4					2.70							
MgCr2O4					5.56							
FeCr2O4	26.02	24.77	17.98	32.02	59.37	38.64	48.19	48.95	47.85	44.39	42.94	44.99
Fe3O4	48.85	49.09	53.25	43.53	23.21	40.98	34.04	33.11	33.34	39.59	39.36	37.05

Spinel analyses: Hypabyssal facies (HYP)

	PC 29	PC 29	PC 29	PC 29	PC 29	PC 29	PC 29	PC 29	PC 29	PC 29	PC 29
	106ce	106c	106c	106c	107ce	107ce	105c	105c	105c	105ce	106ce
Al2O3	3.79	3.37	2.62	2.49	2.22	0.35	0.94	0.96	0.73	1.02	0.36
Cr2O3	44.93	45.23	44.83	45.45	44.60	44.22	50.94	49.98	48.94	50.76	37.16
FeO	37.92	39.46	39.19	40.37	39.67	42.44	37.05	37.44	38.89	37.11	47.11
MgO	5.62	5.47	5.20	5.39	5.17	4.82	5.04	5.02	4.95	5.09	4.95
TiO2	2.97	3.21	3.46	3.36	3.44	4.22	2.69	2.80	3.27	2.67	5.89
MnO	0.83	0.84	0.88	0.80	0.90	1.00	0.92	0.91	1.04	0.96	0.92
Total	96.06	97.58	96.18	97.86	96.00	97.05	97.58	97.11	97.82	97.61	96.39
FeO	24.93	25.79	25.79	26.01	25.72	26.87	25.43	25.43	26.08	25.36	28.16
Fe2O3	14.53	15.17	14.85	15.97	15.49	17.25	12.94	13.25	14.21	13.09	21.08
Total	97.60	99.08	97.63	99.47	97.54	98.73	98.90	98.36	99.22	98.96	98.52
Structural formula calculations based on 4 oxygens											
Ti	0.081	0.086	0.095	0.090	0.095	0.116	0.073	0.077	0.089	0.073	0.162
Al	0.161	0.142	0.112	0.105	0.096	0.015	0.040	0.041	0.031	0.044	0.016
Cr	1.284	1.277	1.290	1.285	1.288	1.278	1.461	1.440	1.402	1.454	1.078
Fe3+	0.393	0.409	0.408	0.429	0.427	0.475	0.352	0.365	0.389	0.356	0.582
Fe2+	0.753	0.770	0.785	0.779	0.785	0.822	0.773	0.776	0.790	0.768	0.863
Mn	0.025	0.025	0.027	0.024	0.028	0.031	0.028	0.028	0.032	0.029	0.029
Mg	0.303	0.291	0.282	0.287	0.282	0.263	0.273	0.273	0.267	0.275	0.271
Total	3.000	3.000	3.000	3.000	3.000	3.000	3.000	3.000	3.000	3.000	3.000
Molecular proportions											
MgAl2O4	5.29	4.70	3.66	3.47	3.10	0.49	1.31	1.34	1.02	1.42	0.50
Mg2TiO4	5.97	6.45	6.95	6.75	6.91	8.48	5.40	5.62	6.57	5.36	9.57
Mn2TiO4											1.44
Fe2TiO4											1.70
MnCr2O4	2.61	2.64	2.77	2.51	2.83	3.14	2.89	2.86	3.27	3.02	
MgCr2O4	5.37	4.29	3.21	4.85	3.92	2.02	9.33	8.66	6.50	9.51	
FeCr2O4	57.30	58.97	59.50	58.77	58.28	59.61	61.26	60.65	61.23	60.66	54.73
Fe3O4	20.98	22.06	21.58	23.10	22.52	25.04	18.68	19.31	20.67	18.95	30.56

Spinel analyses: Hypabyssal facies (HYP)

	PC 29 106c	PC 29 106c	PC 29 106c	PC 29 106ce	PC 29 107c	PC 29 107c	PC 30 108c	PC 30 c	PC 29 e	PC 29 e	PC 29 e	PC 29 ce
Al2O3	0.29	0.30	0.19	0.22	0.04	0.48	18.64	0.22	0.06	0.01	0.12	0.02
Cr2O3	38.55	37.07	36.11	37.72	21.45	14.21	45.80	15.02	18.72	13.74	21.74	16.25
FeO	46.05	46.62	48.01	45.74	60.24	64.35	19.00	66.00	61.91	66.73	60.60	63.99
MgO	4.97	4.88	4.98	4.87	4.17	4.82	12.72	4.55	4.76	3.68	3.80	3.85
TiO2	5.89	5.95	6.40	5.90	8.65	10.26	0.34	9.22	10.32	9.50	8.21	8.83
MnO	1.06	1.00	0.93	0.94	1.13	1.01	0.39	0.72	0.93	1.18	0.99	1.16
Total	96.81	95.82	96.62	95.39	95.68	95.13	96.89	95.73	96.70	94.84	95.46	94.10
FeO	28.09	28.02	28.59	27.88	31.54	32.04	14.58	31.97	32.62	32.83	31.76	31.68
Fe2O3	19.96	20.60	21.56	19.80	31.94	35.93	4.95	37.85	32.58	37.69	32.10	35.93
Total	98.81	97.82	98.76	97.33	98.92	98.75	97.43	99.55	99.99	98.63	98.71	97.73
Structural formula calculations based on 4 oxygens												
Ti	0.162	0.165	0.176	0.165	0.241	0.284	0.008	0.255	0.283	0.267	0.230	0.230
Al	0.012	0.013	0.008	0.010	0.002	0.021	0.704	0.010	0.003	0.000	0.005	0.001
Cr	1.114	1.082	1.045	1.107	0.628	0.414	1.160	0.436	0.540	0.406	0.639	0.483
Fe3+	0.550	0.574	0.594	0.554	0.889	0.996	0.119	1.045	0.892	1.060	0.897	1.016
Fe2+	0.858	0.865	0.876	0.866	0.975	0.988	0.390	0.983	0.996	1.025	0.988	0.997
Mn	0.033	0.031	0.029	0.030	0.035	0.032	0.011	0.022	0.029	0.037	0.031	0.037
Mg	0.271	0.269	0.272	0.269	0.230	0.265	0.608	0.249	0.259	0.205	0.211	0.216
Total	3.000	3.000	3.000	3.000	3.000	3.000	3.000	3.000	3.000	3.000	3.000	3.000
Molecular proportions												
MgAl2O4	0.40	0.42	0.27	0.31	0.06	0.67	26.01	0.31	0.08	0.01	0.17	0.03
Mg2TiO4	9.67	9.48	9.77	9.52	8.27	9.22	0.68	8.89	9.43	7.32	7.47	7.65
Mn2TiO4	1.66	1.56	1.45	1.47	1.77	1.58		1.13	1.45	1.84	1.55	1.81
Fe2TiO4	1.34	1.87	2.84	1.76	10.90	14.28		12.29	14.28	14.53	11.01	12.22
MnCr2O4							1.23					
MgCr2O4							23.90					
FeCr2O4	56.77	54.59	53.18	55.55	31.59	20.93	38.40	22.12	27.57	20.23	32.02	23.93
Fe3O4	28.94	29.87	31.26	28.71	46.31	52.10	7.17	54.87	47.23	54.64	46.54	52.10

Spinel analyses: Hypabyssal facies (HYP)

	PC 29	PC 29	PC 29	PC 29	PC 29	PC 29	PC 29	PC 29	PC 29	PC 29	PC 29	PC 29
	•	ce	ce	•	ce	ce	ce	•	•	ce	•	ce
Al2O3	0.04	0.00	0.07	0.12	0.07	0.06	0.02	0.02	0.16	0.03	0.00	0.04
Cr2O3	10.21	12.47	24.40	10.69	11.10	24.12	18.31	18.55	9.99	23.68	12.45	24.38
FeO	70.41	67.25	56.82	70.28	70.08	57.80	62.03	62.94	70.32	59.15	66.27	58.98
MgO	3.58	3.81	4.16	3.76	3.90	4.11	3.91	3.99	3.58	3.95	3.36	3.93
TiO2	9.40	9.59	7.84	9.36	9.32	8.16	8.85	8.71	8.17	7.71	10.35	8.21
MnO	1.08	1.14	1.27	1.09	1.23	1.18	1.24	1.16	1.26	1.37	0.98	1.11
Total	94.72	94.26	94.56	95.30	95.70	95.43	94.36	95.37	93.48	95.89	93.41	96.65
FeO	32.98	32.55	30.25	32.91	32.62	30.97	31.61	31.76	31.33	30.82	33.77	31.76
Fe2O3	41.52	38.65	29.54	41.52	41.68	29.86	33.85	34.65	43.28	31.46	36.09	30.18
Total	98.81	98.20	97.53	99.45	99.92	98.46	97.80	98.84	97.76	99.02	97.00	99.61
Structural formula calculations based on 4 oxygens												
Ti	0.264	0.271	0.221	0.261	0.259	0.228	0.250	0.243	0.232	0.215	0.296	0.227
Al	0.002	0.000	0.003	0.005	0.003	0.003	0.001	0.001	0.007	0.001	0.000	0.002
Cr	0.302	0.370	0.723	0.313	0.324	0.709	0.543	0.545	0.298	0.693	0.374	0.708
Fe3+	1.169	1.089	0.832	1.160	1.156	0.833	0.956	0.968	1.231	0.877	1.034	0.836
Fe2+	1.031	1.021	0.948	1.019	1.006	0.963	0.992	0.986	0.990	0.954	1.074	0.977
Mn	0.034	0.036	0.040	0.034	0.038	0.037	0.039	0.036	0.040	0.043	0.032	0.035
Mg	0.199	0.213	0.232	0.208	0.214	0.228	0.219	0.221	0.202	0.218	0.190	0.215
Total	3.000	3.000	3.000	3.000	3.000	3.000	3.000	3.000	3.000	3.000	3.000	3.000
Molecular proportions												
MgAl2O4	0.06	0.00	0.10	7	0.10	0.08	0.03	0.03	0.22	0.04	0.00	0.06
Mg2TiO4	7.10	7.59	8.23	7.39	7.71	8.14	7.77	7.93	7.00	7.84	6.69	7.79
Mn2TiO4	1.69	1.78	1.99	1.70	1.92	1.84	1.94	1.81	1.97	2.14	1.53	1.74
Fe2TiO4	14.72	14.47	8.48	14.18	13.40	9.64	11.99	11.50	11.12	8.49	18.10	10.37
MnCr2O4												
MgCr2O4												
FeCr2O4	15.04	18.36	35.93	15.74	16.35	35.52	26.97	27.32	14.71	34.87	18.34	35.90
Fe3O4	60.20	56.03	42.83	60.20	60.43	43.30	49.09	50.24	62.75	45.61	52.33	43.76

Spinel analyses: Hypabyssal facies (HYP)

	PC 29	PC 29	PC 29	PC 29	PC 29
	ce	e	e	e	ce
Al2O3	0.06	0.00	0.03	0.03	0.75
Cr2O3	15.92	9.65	15.85	12.12	48.16
FeO	64.24	70.37	63.98	67.74	39.75
MgO	3.99	3.23	3.95	3.71	4.90
TiO2	10.22	10.61	9.49	10.12	3.37
MnO	1.25	1.31	1.19	1.15	0.95
Total	95.68	95.17	94.49	94.87	97.88
FeO	33.12	34.49	32.19	33.34	26.37
Fe2O3	34.65	39.92	35.29	38.17	14.85
Total	99.21	99.21	97.99	98.63	99.35
Structural formula calculations based on 4 oxygens					
Ti	0.284	0.298	0.267	0.284	0.092
Al	0.003	0.000	0.001	0.001	0.032
Cr	0.466	0.285	0.469	0.358	1.379
Fe3+	0.963	1.120	0.995	1.073	0.406
Fe2+	1.025	1.077	1.009	1.041	0.798
Mn	0.039	0.041	0.038	0.036	0.029
Mg	0.220	0.180	0.221	0.206	0.265
Total	3.000	3.000	3.000	3.000	3.000
Molecular proportions					
MgAl2O4	0.08	0.00	0.04	0.04	1.05
Mg2TiO4	7.90	6.43	7.84	7.36	6.77
Mn2TiO4	1.95	2.05	1.86	1.80	
Fe2TiO4	15.63	18.67	13.76	16.25	
MnCr2O4					2.99
MgCr2O4					5.74
FeCr2O4	23.45	14.21	23.34	17.85	61.24
Fe3O4	50.24	57.88	51.17	55.34	21.58

Spinel analyses: Chromite Series

	EPC 10	EPC 10	EPC 10	EPC 10	PCW 25	PCW 25	PCW 25
kilobars	20	20	20	20	10	10	10
Celsius	1200	1200	1200	1200	1200	1200	1200
minutes	45	45	45	45	90	90	90
Al2O3	4.71	7.02	7.91	6.75	4.83	4.81	4.42
Cr2O3	55.70	48.51	42.41	41.87	57.98	57.82	54.16
FeO	20.25	22.35	25.64	28.99	17.02	16.70	21.75
MgO	13.59	13.62	15.35	14.32	12.68	14.29	11.99
TiO2	2.60	2.79	4.24	4.35	2.56	2.83	2.66
MnO	0.32	0.40	0.36	0.37	0.21	0.24	0.31
Total	97.17	94.69	95.91	96.65	95.28	96.69	95.29
Based on stoichiometry							
FeO	13.27	12.93	12.23	13.97	14.07	12.30	15.12
Fe2O3	7.76	10.48	14.92	16.69	3.27	4.90	7.36
Total	97.95	95.74	97.41	98.32	95.61	97.19	96.03
Structural formula calculations based on 4 oxygens							
Ti	0.066	0.071	0.106	0.109	0.067	0.072	0.069
Al	0.187	0.282	0.308	0.264	0.197	0.191	0.181
Cr	1.484	1.307	1.109	1.101	1.585	1.541	1.488
Fe3+	0.197	0.269	0.371	0.417	0.085	0.124	0.192
Fe2+	0.374	0.368	0.338	0.389	0.407	0.347	0.439
Mn	0.009	0.012	0.010	0.010	0.006	0.007	0.009
Mg	0.683	0.692	0.757	0.710	0.654	0.718	0.621
Total	3.000	3.000	3.000	3.000	3.000	3.000	3.000
Molecular proportions							
MgAl2O4	6.57	9.79	11.04	9.42	6.74	6.71	6.17
Mg2TiO4	5.22	5.60	8.52	8.74	5.14	5.69	5.34
Mn2TiO4							
Fe2TiO4							
MnCr2O4	1.01	1.26	1.13	1.16	0.66	0.75	0.97
MgCr2O4	43.44	38.31	37.91	34.65	39.07	45.48	36.07
FeCr2O4	30.45	25.58	17.19	20.16	39.25	31.45	36.80
MgFe2O4							
Fe3O4	11.25	15.19	21.61	24.19	4.75	7.10	10.67

Spinel analyses: Magnetite Series

	EPC 50	EPC 50	EPC 50	EPC 50	EPC 50	EPC 50	EPC 50	EPC 51	EPC 51	PCW 31	PCW 31	PCW 31
kilobars	15	15	15	15	15	15	15	10	10	10	10	10
Celsius	1050	1050	1050	1050	1050	1050	1050	1000	1000	1000	1000	1000
minutes	360	360	360	360	360	360	360	420	420	60	60	60
Al2O3	3.39	3.30	3.36	4.09	4.09	3.11	3.74	3.60	2.55	0.62	1.20	1.35
Cr2O3	16.97	17.41	15.36	13.45	13.93	19.22	13.06	14.81	18.21	24.48	20.66	8.48
FeO	59.71	61.34	60.47	63.11	63.46	62.09	64.55	59.94	65.94	56.44	64.43	73.29
MgO	9.91	10.19	9.65	10.62	10.57	10.08	10.26	8.40	6.67	9.37	9.74	8.39
TiO2	4.95	4.59	8.30	5.59	5.58	3.62	4.70	9.15	3.69	4.33	2.15	4.53
MnO	0.47	0.32	0.28	0.35	0.26	0.29	0.26	0.27	0.31	1.13	0.52	0.65
Total	95.40	97.15	97.42	97.21	97.89	98.41	96.57	96.17	97.37	96.37	98.70	96.69
Based on stoichiometry												
FeO	20.68	20.66	24.87	21.04	21.42	20.38	20.66	27.14	25.20	20.11	19.20	22.76
Fe2O3	43.37	45.21	39.57	46.76	46.73	46.36	48.79	36.44	45.27	40.37	50.27	56.16
Total	99.75	101.68	101.39	101.90	102.57	103.06	101.46	99.82	101.91	100.41	103.75	102.32
Structural formula calculations based on 4 oxygens												
Ti	0.129	0.118	0.214	0.142	0.141	0.092	0.121	0.241	0.097	0.114	0.055	0.119
Al	0.139	0.133	0.136	0.163	0.162	0.124	0.151	0.149	0.105	0.026	0.048	0.055
Cr	0.467	0.470	0.416	0.360	0.371	0.513	0.353	0.410	0.505	0.679	0.556	0.234
Fe3+	1.135	1.162	1.020	1.192	1.184	1.179	1.255	0.960	1.195	1.066	1.286	1.473
Fe2+	0.602	0.590	0.713	0.596	0.603	0.578	0.590	0.795	0.739	0.590	0.546	0.664
Mn	0.014	0.009	0.008	0.010	0.007	0.008	0.008	0.008	0.009	0.034	0.015	0.019
Mg	0.514	0.519	0.493	0.536	0.531	0.508	0.523	0.438	0.349	0.490	0.494	0.436
Total	3.000	3.000	3.000	3.000	3.000	3.000	3.000	3.000	3.000	3.000	3.000	3.000
Molecular proportions												
MgAl2O4	4.73	4.60	4.69	5.71	5.71	4.34	5.22	5.02	3.56	0.87	1.67	1.88
Mg2TiO4	9.94	9.22	16.67	11.23	11.21	7.27	9.44	13.89	7.41	8.70	4.32	9.10
Mn2TiO4								0.42				
Fe2TiO4								5.83				
MnCr2O4	1.48	1.01	0.88	1.10	0.82	0.91	0.82		0.97	3.55	1.63	2.04
MgCr2O4	17.06	20.30	-0.25	16.05	15.86	23.53	15.82		9.25	22.69	24.73	8.97
FeCr2O4	3.65	1.00	22.03	0.02	1.24			21.81	15.07	6.07		
MgFe2O4						1.32	3.59	52.84			9.49	6.98
Fe3O4	62.88	65.55	57.36	67.79	67.74	65.68	66.57	99.81	65.64	58.54	61.88	73.34

Spinel analyses: Magnetite Series

	PCW 35	PCW 35	PCW 35	PCW 35	PCW 35	FPC 4	FPC 4	FPC 4	FPC 4	FPC 4	FPC 4	FPC 4
kilobars	30	30	30	30	30	20	20	20	20	20	20	20
Celsius	1050	1050	1050	1050	1050	1100	1100	1100	1100	1100	1100	1100
minutes	240	240	240	240	240	300	300	300	300	300	300	300
Al2O3	3.74	3.89	2.93	3.91	3.57	3.00	2.81	2.59	2.64	2.83	2.80	2.63
Cr2O3	24.54	21.07	23.76	24.47	23.30	26.26	25.33	22.18	26.12	21.68	22.43	21.85
FeO	52.73	56.29	53.84	53.43	53.80	50.13	53.18	56.54	52.16	55.08	56.17	56.56
MgO	13.29	13.22	13.40	13.34	12.87	12.07	11.79	11.58	11.80	11.56	11.80	11.59
TiO2	3.17	3.75	4.05	3.20	3.33	3.84	3.87	4.43	3.62	4.44	4.32	4.26
MnO	0.24	0.23	0.25	0.23	0.29	0.43	0.08	0.17	0.00	0.15	0.15	0.17
Total	97.71	98.45	98.23	98.58	97.16	95.73	97.06	97.49	96.34	95.74	97.67	97.06
Based on stoichiometry												
FeO	14.92	15.86	15.58	15.19	15.45	16.37	17.60	18.49	17.18	18.00	18.16	18.19
Fe2O3	42.03	44.94	42.53	42.51	42.62	37.53	39.54	42.29	38.89	41.20	42.24	42.64
Total	101.93	102.96	102.49	102.85	101.44	99.49	101.02	101.72	100.24	99.87	101.90	101.33
Structural formula calculations based on 4 oxygens												
Ti	0.079	0.093	0.101	0.079	0.084	0.099	0.099	0.113	0.093	0.115	0.110	0.109
Al	0.146	0.151	0.114	0.152	0.141	0.121	0.112	0.103	0.106	0.115	0.111	0.105
Cr	0.645	0.549	0.623	0.637	0.617	0.712	0.680	0.594	0.706	0.589	0.598	0.587
Fe3+	1.051	1.114	1.061	1.053	1.074	0.969	1.010	1.077	1.001	1.066	1.072	1.090
Fe2+	0.414	0.437	0.432	0.418	0.433	0.469	0.500	0.523	0.491	0.518	0.512	0.517
Mn	0.007	0.006	0.007	0.006	0.008	0.012	0.002	0.005	0.000	0.004	0.004	0.005
Mg	0.658	0.649	0.662	0.655	0.643	0.617	0.597	0.584	0.602	0.593	0.593	0.587
Total	3.000	3.000	3.000	3.000	3.000	3.000	3.000	3.0[illegible]	3.000	3.000	3.000	3.000
Molecular proportions												
MgAl2O4	5.22	5.43	4.09	5.46	4.98	4.19	3.92	3.61	3.68	3.95	3.91	3.67
Mg2TiO4	6.37	7.53	8.14	6.43	6.69	7.71	7.77	8.90	7.27	8.92	8.68	8.56
Mn2TiO4												
Fe2TiO4												
MnCr2O4	0.75	0.72	0.79	0.72	0.91	1.35	0.25	0.53	0.00	0.47	0.47	0.53
MgCr2O4	30.40	26.03	29.38	30.34	28.69	32.06	31.83	27.60	33.05	27.02	27.97	27.18
FeCr2O4												
MgFe2O4	11.13	12.12	9.91	10.96	10.35	1.44	0.51	1.50	0.88	1.48	2.34	2.75
Fe3O4	48.06	51.11	50.19	48.94	49.81	52.74	56.73	59.58	55.35	58.03	58.53	58.63

Spinel analyses: Magnetite Series

	FPC 4	FPC 4	FPC 9	FPC 9	FPC 9
kilobars	20	20	30	30	30
Celsius	1100	1100	1200	1200	1200
minutes	300	300	180	180	180
Al2O3	2.72	2.83	1.59	5.02	4.94
Cr2O3	25.49	26.86	30.15	30.53	29.50
FeO	53.33	52.46	42.38	45.42	44.96
MgO	11.68	12.06	11.42	13.99	13.80
TiO2	3.90	3.43	9.83	2.62	2.73
MnO	0.07	0.15	0.14	0.20	0.24
Total	97.19	97.79	95.51	97.78	96.17
Based on stoichiometry					
FeO	17.83	16.96	22.50	13.50	13.31
Fe2O3	39.44	39.46	22.10	35.47	35.16
Total	101.14	101.75	97.73	101.33	99.69
Structural formula calculations based on 4 oxygens					
Ti	0.100	0.087	0.259	0.065	0.069
Al	0.109	0.112	0.066	0.195	0.195
Cr	0.684	0.715	0.835	0.795	0.781
Fe3+	1.008	0.999	0.582	0.880	0.886
Fe2+	0.506	0.477	0.659	0.372	0.373
Mn	0.002	0.004	0.004	0.006	0.007
Mg	0.591	0.605	0.596	0.687	0.689
Total	3.000	3.000	3.000	3.000	3.000
Molecular proportions					
MgAl2O4	3.80	3.95	2.22	7.00	6.89
Mg2TiO4	7.83	6.89	19.75	5.26	5.48
Mn2TiO4					
Fe2TiO4					
MnCr2O4	0.22	0.47	0.44	0.63	0.75
MgCr2O4	31.82	33.58	4.17	38.08	36.67
FeCr2O4	0.27		39.11		
MgFe2O4		2.20		6.85	6.98
Fe3O4	57.19	54.66	32.04	43.51	42.91

Spinel analyses: Transitional Series

	EPC 25	EPC 25	EPC 25	EPC 25	EPC 25	EPC 52	EPC 52	EPC 52	EPC 52	EPC 52	EPC 59
kilobars	10	10	10	10	10	10	10	10	10	10	20
Celsius	1120	1120	1120	1120	1120	1070	1070	1070	1070	1070	1120
minutes	240	240	240	240	240	360	360	360	360	360	180
Al2O3	5.97	5.15	4.28	7.09	6.07	8.12	5.02	8.94	5.37	6.33	2.28
Cr2O3	19.06	24.84	22.94	22.47	16.30	24.54	25.37	26.36	20.84	21.31	23.19
FeO	44.52	42.53	48.02	38.24	48.82	39.69	41.36	34.38	42.67	45.01	52.23
MgO	12.61	11.58	11.71	15.65	13.44	13.32	12.61	14.82	12.73	12.79	9.21
TiO2	11.96	9.55	10.10	13.00	12.41	11.90	13.43	11.48	16.40	14.07	8.77
MnO	0.35	0.37	0.26	0.26	0.34	0.34	0.39	0.29	0.40	0.32	0.24
Total	94.47	94.02	97.31	96.71	97.38	97.91	98.18	96.27	98.41	99.83	95.92
Based on stoichiometry											
FeO	22.78	21.84	23.28	19.97	22.92	22.99	25.00	19.90	27.59	26.15	25.22
Fe2O3	24.11	23.00	27.47	20.28	28.74	18.52	18.20	16.13	16.77	20.92	30.02
Total	96.84	96.33	100.04	98.72	100.22	99.74	100.03	97.92	100.10	101.89	98.93
Structural formula calculations based on 4 oxygens											
Ti	0.309	0.250	0.257	0.321	0.309	0.294	0.337	0.284	0.410	0.346	0.232
Al	0.241	0.212	0.171	0.274	0.237	0.315	0.198	0.347	0.211	0.244	0.095
Cr	0.517	0.685	0.614	0.583	0.427	0.638	0.670	0.686	0.548	0.550	0.645
Fe3+	0.624	0.603	0.701	0.501	0.717	0.459	0.457	0.398	0.420	0.515	0.796
Fe2+	0.653	0.638	0.659	0.548	0.636	0.632	0.698	0.549	0.768	0.714	0.742
Mn	0.010	0.011	0.007	0.007	0.010	0.009	0.011	0.008	0.011	0.009	0.007
Mg	0.645	0.602	0.591	0.766	0.664	0.653	0.628	0.728	0.632	0.623	0.483
Total	3.000	3.000	3.000	3.000	3.000	3.000	3.000	3.000	3.000	3.000	3.000
Molecular proportions											
MgAl2O4	8.33	7.19	5.97	9.89	8.47	11.33	7.00	12.47	7.49	8.83	3.18
Mg2TiO4	20.41	19.00	19.95	25.58	21.98	20.13	21.16	22.47	21.12	20.48	16.54
Mn2TiO4	0.55	0.58	0.41	0.41	0.53	0.53	0.61	0.45	0.63	0.50	0.38
Fe2TiO4	4.49	-0.33	0.07	0.33	3.57	4.72	7.50	0.36	15.84	10.33	1.12
MnCr2O4											
MgCr2O4											
FeCr2O4	28.07	36.58	33.78	33.09	24.01	36.14	37.36	38.82	30.69	31.38	34.15
MgFe2O4											
Fe3O4	34.96	33.34	39.82	29.41	41.68	26.86	26.40	23.39	24.31	30.33	43.53

Spinel analyses: Transitional Series

	EPC 59	EPC 59	EPC 59	PCW 6	PCW 6	PCW 6	PCW 6	PCW 6	PCW 28	PCW 28	PCW 28
kilobars	20	20	20	10	10	10	10	10	10	10	10
Celsius	1120	1120	1120	1100	1100	1100	1100	1100	1150	1150	1150
minutes	180	180	180	360	360	360	360	360	270	270	270
Al2O3	3.76	4.00	2.52	7.18	4.24	6.83	4.99	6.49	11.51	10.09	10.87
Cr2O3	22.40	17.24	22.69	23.47	31.51	28.72	34.28	23.51	36.99	32.07	31.59
FeO	54.80	52.58	49.61	29.88	31.82	31.44	32.40	37.49	17.48	19.53	20.44
MgO	11.78	12.33	10.04	13.53	12.30	13.46	12.00	13.92	19.29	20.09	17.12
TiO2	3.80	9.60	8.04	14.26	13.08	13.42	10.72	16.11	12.42	16.41	13.83
MnO	0.28	0.33	0.26	0.28	0.37	0.32	0.42	0.31	0.39	0.41	0.30
Total	96.82	96.08	93.16	88.60	93.32	94.19	94.81	97.83	98.08	98.60	94.15
Based on stoichiometry											
FeO	17.46	21.48	22.42	21.55	23.35	22.63	22. .	25.51	14.58	16.88	17.89
Fe2O3	41.52	34.49	30.18	9.26	9.42	9.74	11.34	13.25	3.19	2.87	2.87
Total	101.00	99.48	96.15	89.54	94.27	95.12	96.02	99.10	98.38	98.83	94.47
Structural formula calculations based on 4 oxygens											
Ti	0.097	0.246	0.217	0.387	0.347	0.346	0.280	0.401	0.292	0.385	0.343
Al	0.150	0.160	0.107	0.305	0.176	0.276	0.204	0.253	0.425	0.371	0.422
Cr	0.599	0.464	0.644	0.670	0.879	0.779	0.941	0.615	0.915	0.791	0.823
Fe3+	1.057	0.885	0.816	0.251	0.250	0.253	0.295	0.331	0.076	0.069	0.070
Fe2+	0.494	0.611	0.672	0.651	0.689	0.649	0.646	0.706	0.382	0.440	0.493
Mn	0.008	0.010	0.008	0.009	0.011	0.009	0.012	0.009	0.010	0.011	0.008
Mg	0.594	0.625	0.537	0.728	0.647	0.688	0.621	0.686	0.900	0.934	0.841
Total	3.000	3.000	3.000	3.000	3.000	3.000	3.000	3.000	3.000	3.000	3.000
Molecular proportions											
MgAl2O4	5.25	5.58	3.52	10.02	5.92	9.53	6.96	9.06	16.06	14.08	15.17
Mg2TiO4	7.63	19.29	16.15	21.29	21.15	21.43	19.97	22.61	24.95	32.06	25.53
Mn2TiO4				0.44	0.58	0.50	0.66	0.48		0.64	0.47
Fe2TiO4				9.81	6.55	7.20	1.52	13.10		0.61	2.66
MnCr2O4	0.88	1.04	0.82						1.23		
MgCr2O4	27.58	5.07	4.45						10.54		
FeCr2O4		18.44	27.42	34.56	46.40	42.30	50.48	34.62	40.97	47.23	46.52
MgFe2O4	3.37										
Fe3O4	56.27	50.12	43.84	13.43	13.66	14.12	16.44	19.22	4.65	4.17	4.17

Spinel analyses: Transitional Series

	PCW 28	PCW 28	PCW 28	PCW 28	FPC 6	FPC 6	FPC 6	FPC 6	FPC 6	FPC 6	FPC 7
kilobars	10	10	10	10	10	10	10	10	10	10	10
Celsius	1150	1150	1150	1150	1000	1000	1000	1000	1000	1000	1100
minutes	270	270	270	270	360	360	360	360	360	360	300
Al2O3	6.07	8.83	6.92	8.35	3.69	2.93	3.51	3.45	1.40	2.87	4.22
Cr2O3	39.71	36.53	38.46	29.87	17.55	23.01	22.53	25.03	34.69	20.67	28.48
FeO	20.98	20.75	22.51	20.83	48.69	51.86	50.31	47.87	42.52	58.82	41.39
MgO	14.95	15.64	16.05	19.24	10.15	9.79	10.05	10.22	10.68	8.05	12.45
TiO2	12.55	13.15	12.13	17.50	13.52	10.45	11.40	10.22	8.63	6.90	9.88
MnO	0.30	0.27	0.21	0.37	0.47	0.00	0.20	0.17	0.22	0.28	0.38
Total	94.56	95.17	96.28	96.16	94.07	98.04	98.00	96.96	98.14	97.59	96.80
Based on stoichiometry											
FeO	19.47	19.54	18.18	18.18	27.30	26.80	27.09	25.43	23.28	26.01	21.55
Fe2O3	1.76	1.28	4.79	3.03	23.79	27.79	25.71	24.91	21.40	36.57	22.04
Total	94.81	95.24	96.74	96.54	96.48	100.77	100.49	99.44	100.30	101.35	99.00
Structural formula calculations based on 4 oxygens											
Ti	0.321	0.329	0.302	0.424	0.360	0.270	0.293	0.265	0.223	0.180	0.252
Al	0.244	0.347	0.270	0.317	0.154	0.118	0.141	0.140	0.057	0.118	0.169
Cr	1.069	0.962	1.007	0.762	0.492	0.624	0.609	0.683	0.943	0.568	0.764
Fe3+	0.044	0.033	0.119	0.072	0.633	0.719	0.663	0.647	0.554	0.954	0.563
Fe2+	0.554	0.545	0.504	0.489	0.810	0.769	0.775	0.735	0.669	0.755	0.611
Mn	0.009	0.008	0.006	0.010	0.014	0.000	0.006	0.005	0.006	0.008	0.011
Mg	0.759	0.777	0.792	0.925	0.536	0.501	0.512	0.526	0.548	0.417	0.630
Total	3.000	3.000	3.000	3.000	3.000	3.000	3.000	3.000	3.000	3.000	3.000
Molecular proportions											
MgAl2O4	8.47	12.32	9.66	11.65	5.15	4.09	4.90	4.81	1.95	4.00	5.89
Mg2TiO4	24.99	24.19	24.37	31.74	17.31	17.19	17.25	17.63	17.34	13.86	19.85
Mn2TiO4	0.47	0.42		0.58	0.73	0.00	0.31	0.27			
Fe2TiO4	-0.17	2.67		4.18	12.99	5.30	7.56	3.77			
MnCr2O4			0.66						0.69	0.88	1.19
MgCr2O4			5.14						6.77	-0.22	3.88
FeCr2O4	58.48	53.80	50.00	43.99	25.85	33.89	33.18	36.86	42.51	29.81	36.22
MgFe2O4											
Fe3O4	2.55	1.85	6.94	4.40	34.50	40.29	37.28	36.12	31.02	52.91	31.97

Spinel analyses: Transitional Series

	FPC 7	FPC 7	FPC 7	FPC 7	FPC 7	FPC 7	FPC 7	FPC 7
kilobars	10	10	10	10	10	10	10	10
Celsius	1100	1100	1100	1100	1100	1100	1100	1100
minutes	300	300	300	300	300	300	300	300
Al2O3	5.38	4.33	7.38	5.89	6.89	5.87	5.79	4.16
Cr2O3	24.83	26.76	26.93	26.33	23.15	25.29	24.73	26.39
FeO	42.60	44.57	39.49	42.67	42.09	43.67	43.43	45.63
MgO	12.79	13.00	14.75	13.99	14.43	13.64	13.36	12.44
TiO2	11.85	9.99	10.36	10.75	12.16	11.19	10.83	9.53
MnO	0.24	0.00	0.00	0.11	0.07	0.16	0.14	0.17
Total	97.69	98.65	98.91	99.74	98.79	99.82	98.28	98.32
Based on stoichiometry								
FeO	23.42	21.84	20.05	21.48	21.91	22.42	21.98	21.98
Fe2O3	21.40	25.23	21.72	23.47	22.36	23.63	23.79	26.19
Total	99.91	101.15	101.18	102.03	100.97	102.20	100.63	100.86
Structural formula calculations based on 4 oxygens								
Ti	0.298	0.249	0.252	0.262	0.297	0.273	0.269	0.239
Al	0.212	0.169	0.281	0.225	0.264	0.225	0.225	0.164
Cr	0.656	0.702	0.688	0.675	0.595	0.650	0.645	0.697
Fe3+	0.537	0.630	0.527	0.575	0.547	0.579	0.592	0.660
Fe2+	0.654	0.606	0.541	0.583	0.596	0.608	0.607	0.615
Mn	0.007	0.000	0.000	0.003	0.002	0.004	0.004	0.005
Mg	0.637	0.643	0.711	0.677	699	0.661	0.657	0.620
Total	3.000	3.000	3.000	3.000	3.000	3.000	3.000	3.000
Molecular proportions								
MgAl2O4	7.51	6.04	10.30	8.22	9.61	8.19	8.08	5.80
Mg2TiO4	21.23	20.07	20.81	21.60	23.31	22.48	21.76	19.14
Mn2TiO4	0.38				0.11			
Fe2TiO4	3.2				1.45			
MnCr2O4		0.00	0.00	0.35		0.50	0.44	0.53
MgCr2O4		5.77	6.59	3.89		0.14	0.69	5.63
FeCr2O4	36.57	32.69	31.99	33.90	34.09	36.57	35.17	31.77
MgFe2O4								
Fe3O4	31.03	36.61	31.39	34.15	32.42	34.30	34.53	38.06

Spinel analyses: Ulvospinel-magnetite Series

	EPC 43	EPC 43	EPC 43	EPC 43	EPC 43	EPC 43	EPC 45	EPC 45	EPC 45	EPC 45	EPC 45
kilobars	20	20	20	20	20	20	30	30	30	30	30
Celsius	1050	1050	1050	1050	1050	1050	1150	1150	1150	1150	1150
minutes	240	240	240	240	240	240	180	180	180	180	180
Al2O3	0.70	0.55	0.58	0.51	0.48	0.49	1.30	1.18	0.54	0.63	0.56
Cr2O3	0.85	1.73	5.75	2.06	1.44	2.36	11.10	8.76	5.92	10.70	9.96
FeO	60.63	58.65	56.21	60.50	56.40	57.15	56.81	56.79	57.98	57.10	56.88
MgO	6.70	6.80	6.82	6.57	6.61	6.77	6.05	6.20	6.35	5.88	5.49
TiO2	30.26	30.19	28.27	29.34	29.05	29.79	21.43	22.28	27.98	24.05	22.72
MnO	0.14	0.12	0.14	0.07	0.17	0.11	0.06	0.10	0.13	0.00	0.07
Total	99.28	98.04	97.77	99.05	94.15	96.67	96.75	95.31	98.90	98.36	95.68
Based on stoichiometry											
FeO	49.00	48.35	46.48	48.35	46.34	47.63	41.53	41.53	47.35	44.54	43.04
Fe2O3	12.94	11.34	10.70	13.41	11.18	10.54	16.93	16.93	11.82	13.89	15.33
Total	100.58	99.08	98.74	100.32	95.27	97.69	98.39	96.97	100.08	99.70	97.17
Structural formula calculations based on 4 oxygens											
Ti	0.803	0.811	0.761	0.781	0.812	0.811	0.582	0.614	0.748	0.647	0.629
Al	0.029	0.023	0.024	0.021	0.021	0.021	0.055	0.051	0.023	0.027	0.024
Cr	0.024	0.049	0.163	0.058	0.042	0.068	0.317	0.254	0.166	0.303	0.290
Fe3+	0.342	0.306	0.290	0.359	0.313	0.289	0.463	0.468	0.316	0.376	0.427
Fe2+	1.446	1.445	1.393	1.432	1.440	1.443	1.255	1.272	1.407	1.334	1.326
Mn	0.004	0.004	0.004	0.002	0.005	0.003	0.002	0.003	0.004	0.000	0.002
Mg	0.352	0.362	0.364	0.347	0.366	0.366	0.326	0.339	0.336	0.314	0.302
Total	3.000	3.000	3.000	3.000	3.000	3.000	3.000	3.000	3.000	3.000	3.000
Molecular proportions											
MgAl2O4	0.98	0.77	0.81	0.71	0.67	0.68	1.81	1.65	0.75	0.88	0.78
Mg2TiO4	12.79	13.11	13.12	12.68	12.78	13.09	11.02	11.42	12.22	11.21	10.49
Mn2TiO4	0.22	0.19	0.22	0.11	0.27	0.17	0.09	0.16	0.20	0.00	0.11
Fe2TiO4	66.64	66.04	60.61	64.33	63.22	64.95	44.52	46.29	61.07	51.68	48.86
MnCr2O4											
MgCr2O4											
FeCr2O4	1.25	2.55	8.47	3.03	2.12	3.48	16.35	12.90	8.72	15.76	14.67
MgFe2O4											
Fe3O4	18.75	16.44	15.51	19.45	16.21	15.28	24.54	24.54	17.13	20.14	22.23

Spinel analyses: Ulvospinel-magnetite Series

	EPC 45	EPC 60	EPC 60	EPC 60	PCW 32	PCW 32	PCW 32	PCW 32	PCW 32	PCW 32	PCW 32
kilobars	30	35	35	35	20	20	20	20	20	20	20
Celsius	1150	1200	1200	1200	1020	1020	1020	1020	1020	1020	1020
minutes	180	180	180	180	360	360	360	360	360	360	360
Al2O3	0.54	1.59	1.20	1.56	0.63	0.65	0.66	0.65	0.65	0.56	0.68
Cr2O3	5.98	16.16	15.23	12.07	3.76	4.05	3.47	5.37	6.77	0.89	6.37
FeO	56.80	55.73	59.37	58.43	58.48	57.97	58.93	58.87	56.45	58.84	57.56
MgO	6.37	5.27	4.70	5.80	6.42	6.58	6.62	6.39	6.37	6.38	6.36
TiO2	27.54	17.09	16.06	19.35	24.96	25.02	25.08	24.38	24.40	27.41	25.04
MnO	0.09	0.13	0.05	0.05	0.24	0.25	0.32	0.16	0.30	0.31	0.08
Total	97.32	95.97	96.61	97.26	94.49	94.52	95.08	95.82	94.94	94.39	96.09
Based on stoichiometry											
FeO	46.48	38.58	38.80	40.31	43.11	42.89	43.04	43.18	42.75	45.26	43.90
Fe2O3	11.50	19.16	22.84	20.12	17.09	16.77	17.73	17.41	15.17	15.17	15.17
Total	98.50	97.98	98.87	99.26	96.20	96.21	96.91	97.54	96.41	95.98	97.60
Structural formula calculations based on 4 oxygens											
Ti	0.747	0.470	0.441	0.523	0.694	0.694	0.692	0.669	0.676	0.764	0.686
Al	0.023	0.069	0.052	0.066	0.027	0.028	0.029	0.028	0.028	0.024	0.029
Cr	0.171	0.467	0.439	0.343	0.110	0.118	0.101	0.155	0.197	0.026	0.183
Fe3+	0.312	0.525	0.628	0.545	0.475	0.465	0.488	0.480	0.423	0.422	0.415
Fe2+	1.402	1.179	1.183	1.211	1.333	1.325	1.320	1.316	1.317	1.402	1.338
Mn	0.003	0.004	0.002	0.002	0.008	0.008	0.010	0.005	0.009	0.010	0.002
Mg	0.343	0.287	0.256	0.311	0.354	0.362	0.362	0.348	0.350	0.352	0.345
Total	3.000	3.000	3.000	3.000	3.000	3.000	3.000	3.000	3.000	3.000	3.000
Molecular proportions											
MgAl2O4	0.75	2.22	1.67	2.18	0.88	0.91	0.92	0.91	0.91	0.78	0.95
Mg2TiO4	12.26	9.24	8.41	10.32	12.29	12.59	12.66	12.21	12.17	12.26	12.13
Mn2TiO4	0.14	0.20	0.08	0.08	0.38	0.39	0.50	0.25	0.47	0.48	0.13
Fe2TiO4	59.85	34.75	33.14	39.69	52.35	52.08	52.04	50.96	50.85	59.13	53.05
MnCr2O4											
MgCr2O4											
FeCr2O4	8.81	23.80	22.43	17.78	5.54	5.96	5.11	7.91	9.97	1.31	9.38
MgFe2O4											
Fe3O4	16.67	27.78	33.11	29.17	24.77	24.31	25.70	25.24	22.00	22.00	22.00

Spinel analyses: Ulvospinel-magnetite Series

	PCW 32	PCW 32	FPC 8	FPC 8	FPC 8	FPC 8	FPC 8	FPC 8	FPC 8	FPC 8	FPC 8
kilobars	20	20	20	20	20	20	20	20	20	20	20
Celsius	1020	1020	1000	1000	1000	1000	1000	1000	1000	1000	1000
minutes	360	360	300	300	300	300	300	300	300	300	300
Al2O3	0.56	0.56	0.51	0.54	0.53	0.53	0.53	0.49	0.51	0.64	0.66
Cr2O3	2.45	0.71	0.95	7.72	2.96	7.97	8.22	5.55	1.93	8.33	6.56
FeO	59.44	61.19	53.59	53.65	55.50	53.73	54.96	54.41	54.49	57.62	54.53
MgO	5.99	6.13	6.57	6.03	6.51	5.99	6.15	6.40	6.82	5.42	6.25
TiO2	26.44	27.89	34.48	29.37	33.72	29.54	29.37	30.56	33.86	26.93	30.66
MnO	0.15	0.04	0.39	0.00	0.01	0.17	0.06	0.13	0.19	0.17	0.16
Total	95.03	96.52	96.49	97.31	99.23	97.93	99.29	97.54	97.80	99.11	98.82
Based on stoichiometry											
FeO	45.34	46.99	51.66	48.64	52.38	48.86	49.00	49.07	51.37	47.85	49.79
Fe2O3	15.65	15.81	2.08	5.59	3.51	5.43	6.55	5.91	3.51	10.86	5.27
Total	96.57	98.13	96.63	97.89	99.62	98.49	99.88	98.11	98.19	100.20	99.35
Structural formula calculations based on 4 oxygens											
Ti	0.734	0.762	0.946	0.801	0.901	0.802	0.785	0.830	0.915	0.723	0.823
Al	0.024	0.024	0.022	0.023	0.022	0.023	0.022	0.021	0.022	0.027	0.028
Cr	0.072	0.020	0.027	0.221	0.083	0.227	0.231	0.158	0.055	0.235	0.185
Fe3+	0.436	0.431	0.059	0.153	0.093	0.147	0.176	0.161	0.094	0.291	0.142
Fe2+	1.400	1.429	1.577	1.475	1.556	1.474	1.457	1.481	1.544	1.430	1.485
Mn	0.005	0.001	0.012	0.000	0.000	0.005	0.002	0.004	0.006	0.005	0.005
Mg	0.330	0.332	0.357	0.326	0.345	0.322	0.326	0.344	0.365	0.289	0.332
Total	3.000	3.000	3.000	3.000	3.000	3.000	3.000	3.000	3.000	3.000	3.000
Molecular proportions											
MgAl2O4	0.78	0.78	0.71	0.75	0.74	0.74	0.74	0.68	0.71	0.89	0.92
Mg2TiO4	11.49	11.77	12.68	11.58	12.55	11.51	11.83	12.36	13.18	10.29	11.93
Mn2TiO4	0.23	0.06	0.61	0.00	0.02	0.27	0.09	0.20	0.30	0.27	0.25
Fe2TiO4	57.75	61.60	78.21	66.06	76.87	66.36	65.62	68.10	76.10	60.76	68.94
MnCr2O4											
MgCr2O4											
FeCr2O4	3.61	1.05	1.40	11.37	4.36	11.74	12.11	8.17	2.84	12.27	9.66
MgFe2O4											
Fe3O4	22.69	22.92	3.01	8.10	5.09	7.87	9.49	8.57	5.09	15.74	7.64

Spinel analyses: Ulvospinel-magnetite Series

	FPC 8	FPC 10	FPC 10	FPC 10	FPC 10	FPC 10	FPC 10	FPC 10
kilobars	20	30	30	30	30	30	30	30
Celsius	1000	1100	1100	1100	1100	1100	1100	1100
minutes	300	180	180	180	180	180	180	180
Al2O3	0.50	0.85	0.76	0.79	0.91	0.81	0.85	0.83
Cr2O3	2.69	7.21	3.30	5.76	9.41	6.98	10.34	6.04
FeO	54.76	59.81	62.30	60.63	57.99	60.10	58.15	59.41
MgO	6.57	6.04	6.22	6.10	5.65	6.13	5.73	6.10
TiO2	33.54	23.30	25.74	24.21	22.31	24.27	22.08	24.15
MnO	0.16	0.09	0.06	0.10	0.05	0.08	0.09	0.05
Total	98.22	97.30	98.38	97.59	96.32	98.37	97.24	96.58
Based on stoichiometry								
FeO	51.66	43.32	45.62	44.11	42.75	44.40	42.68	43.75
Fe2O3	3.51	18.36	18.52	18.36	16.93	17.41	17.25	17.41
Total	98.63	99.18	100.23	99.44	98.01	100.08	99.01	98.33
Structural formula calculations based on 4 oxygens								
Ti	0.904	0.631	0.689	0.654	0.612	0.650	0.600	0.659
Al	0.021	0.036	0.032	0.033	0.039	0.034	0.036	0.035
Cr	0.076	0.205	0.093	0.163	0.271	0.197	0.295	0.173
Fe3+	0.094	0.497	0.497	0.496	0.466	0.469	0.469	0.474
Fe2+	1.548	1.304	1.357	1.324	1.303	1.322	1.289	1.327
Mn	0.005	0.003	0.002	0.003	0.002	0.002	0.003	0.002
Mg	0.351	0.324	0.330	0.326	0.307	0.328	0.309	0.330
Total	3.000	3.000	3.000	3.000	3.000	3.000	3.000	3.000
Molecular proportions								
MgAl2O4	0.70	1.19	1.06	1.10	1.27	1.13	1.19	1.16
Mg2TiO4	12.69	11.36	11.79	11.52	10.53	11.57	10.74	11.49
Mn2TiO4	0.25	0.14	0.09	0.16	0.08	0.13	0.14	0.08
Fe2TiO4	75.93	49.24	55.52	51.54	47.68	51.68	46.69	51.49
MnCr2O4								
MgCr2O4								
FeCr2O4	3.96	10.62	4.86	8.48	13.86	10.28	15.23	8.90
MgFe2O4								
Fe3O4	5.09	26.63	26.86	26.63	24.54	25.24	25.01	25.24

5.5 Titan potassic richterite

Titan potassic richterite analyses: amphibole from the hypabyssal facies (HYP).

	PC 29d	PC 29c	PC 63	PC 29c	PC 22	PC 63	PC 22	PC 25	PC 63	PC 63	PC 30
	c	c	c	c	•	c	c	c	c	c	c
SiO2	50.23	55.44	53.49	55.44	54.01	52.74	54.11	55.97	52.74	53.51	54.16
TiO2	4.97	3.64	4.07	3.64	2.42	4.24	2.87	1.96	4.24	4.30	3.32
Al2O3	0.48	0.58	0.44	0.58	0.54	0.80	0.41	0.69	0.80	0.78	0.46
Cr2O3	0.00	0.30	0.00	0.30	0.04	0.00	0.00	0.03	0.00	0.00	0.00
MnO	0.00	0.09	0.21	0.09	0.09	0.12	0.00	0.00	0.12	0.11	0.07
FeO	4.94	4.30	3.65	4.30	3.04	3.55	2.68	2.83	3.55	3.65	3.46
MgO	23.89	20.87	20.19	20.87	21.21	20.49	20.80	23.33	20.49	20.38	21.43
CaO	4.25	6.11	6.07	6.11	6.17	5.99	5.69	6.66	5.99	6.17	6.00
K2O	3.95	4.87	5.18	4.87	4.97	5.02	4.74	5.09	5.02	5.02	4.99
Na2O	3.20	4.55	4.80	4.55	3.93	3.96	3.75	3.86	3.96	3.64	4.34
BaO	0.00	0.00	0.00	0.00	0.00	0.00	0.00	0.00	0.00	0.00	0.00
F	0.00	2.66	0.00	2.66	3.05	0.00	3.05	3.32	0.00	0.00	2.97
Total	95.91	103.41	98.10	103.41	99.47	96.91	98.10	103.74	96.91	97.56	101.20
O:F	0.00	1.12	0.00	1.12	1.28	0.00	1.28	1.40	0.00	0.00	1.25
Total	95.91	102.29	98.10	102.29	98.19	96.91	96.82	102.34	96.91	97.56	99.95
Mg#	89.6	89.6	90.8	89.6	92.6	91.1	93.3	93.6	91.1	90.9	91.7
Structural formula calculations based on 23 oxygens											
Si	7.280	7.466	7.610	7.466	7.514	7.565	7.584	7.456	7.565	7.610	7.435
Ti	0.542	0.369	0.435	0.369	0.253	0.457	0.303	0.196	0.457	0.460	0.343
Al	0.082	0.092	0.074	0.092	0.089	0.135	0.068	0.108	0.135	0.131	0.074
Cr	0.000	0.032	0.000	0.032	0.004	0.000	0.000	0.003	0.000	0.000	0.000
Mn	0.000	0.010	0.025	0.010	0.011	0.015	0.000	0.000	0.015	0.013	0.008
Fe	0.599	0.484	0.434	0.484	0.354	0.426	0.314	0.315	0.426	0.434	0.397
Mg	5.161	4.190	4.282	4.190	4.399	4.381	4.346	4.633	4.381	4.321	4.386
Ca	0.660	0.882	0.925	0.882	0.920	0.921	0.855	0.951	0.921	0.940	0.882
Ba	0.000	0.000	0.000	0.000	0.000	0.000	0.000	0.000	0.000	0.000	0.000
K	0.730	0.837	0.940	0.837	0.882	0.919	0.848	0.865	0.919	0.911	0.874
Na	0.899	1.188	1.324	1.188	1.060	1.101	1 019	0.997	1.101	1.004	1.155
F	0.000	1.133	0.000	1.133	1.342	0.000	1.352	1.399	0.000	0.000	1.289
Total	15.953	16.682	16.050	16.682	16.828	15.920	16.688	16.923	15.920	15.822	16.844

Titan potassic richterite analyses: amphibole from the hypabyssal facies (HYP).

	PC 30	PC 30	PC 29a	PC 22	PC 22	PC 25	PC 25	PC 30	PC 29b	PC 29b	PC 29c	PC 22
	c	c	c	c	c	c	c	e	c	c	c	c
SiO2	53.55	53.06	51.91	55.15	54.11	55.32	55.97	53.32	54.15	54.15	53.73	56.02
TiO2	2.78	3.89	4.23	2.32	2.87	2.45	1.96	3.88	1.60	1.60	3.75	1.45
Al2O3	0.81	0.60	0.36	0.41	0.41	0.68	0.69	0.49	0.51	0.51	0.33	0.44
Cr2O3	0.00	0.00	0.00	0.00	0.00	0.00	0.03	0.00	0.19	0.19	0.00	0.00
MnO	0.09	0.05	0.04	0.11	0.00	0.07	0.00	0.08	0.00	0.00	0.08	0.11
FeO	3.42	3.54	3.86	3.15	2.68	2.93	2.83	3.92	2.24	2.24	4.02	2.57
MgO	21.80	21.13	21.21	22.10	20.80	22.28	23.33	21.60	22.03	22.03	21.08	22.53
CaO	5.63	5.67	5.31	6.47	5.69	6.52	6.66	5.72	6.32	6.32	5.45	6.41
K2O	5.18	5.09	5.06	5.08	4.74	5.04	5.09	5.12	4.69	4.69	5.30	5.04
Na2O	4.15	4.24	4.25	3.82	3.75	3.77	3.86	4.37	3.98	3.98	4.69	3.86
BaO	0.00	0.00	0.00	0.00	0.00	0.00	0.00	0.00	0.00	0.00	0.00	0.00
F	2.70	2.92	2.55	2.99	3.05	3.17	3.32	2.95	2.75	2.75	2.40	2.91
Total	100.11	100.19	98.78	101.60	98.10	102.23	103.74	101.45	98.46	98.46	100.83	101.34
O=F	1.14	1.23	1.07	1.26	1.28	1.33	1.40	1.24	1.16	1.16	1.01	1.23
Total	98.97	98.96	97.71	100.34	96.82	100.90	102.34	100.21	97.30	97.30	99.82	100.11
Mg#	91.9	91 4	90.7	92.6	93.3	93.1	93.6	90.8	94.6	94.6	90.3	94.0
Structural formula calculations based on 23 oxygens												
Si	7.430	7.370	7.335	7.515	7.584	7.479	7.456	7.335	7.570	7.570	7.440	7.613
Ti	0.290	0.406	0.449	0.238	0.303	0.249	0.196	0.401	0.168	0.168	0.390	0.148
Al	0.132	0.098	0.060	0.066	0.068	0.108	0.108	0.079	0.084	0.084	0.054	0.070
Cr	0.000	0.000	0.000	0.000	0.000	0.000	0.003	0.000	0.021	0.021	0.000	0.000
Mn	0.011	0.006	0.005	0.013	0.000	0.008	0.000	0.009	0.000	0.000	0.009	0.013
Fe	0.397	0.411	0.456	0.359	0.314	0.331	0.315	0.451	0.262	0.262	0.466	0.292
Mg	4.509	4.375	4.468	4.489	4.346	4.491	4.633	4.430	4.591	4.591	4.351	4.564
Ca	0.837	0.844	0.804	0.945	0.855	0.944	0.951	0.843	0.947	0.947	0.809	0.933
Ba	0.000	0.000	0.000	0.000	0.000	0.000	0.000	0.000	0.000	0.000	0.000	0.000
K	0.917	0.902	0.912	0.883	0.848	0.869	0.865	0.899	0.836	0.836	0.936	0.874
Na	1.116	1.142	1.164	1.009	1.019	0.988	0.997	1.166	1.079	1.079	1.259	1.017
F	1.185	1.283	1.140	1.289	1.352	1.355	1.399	1.284	1.216	1.216	1.051	1.251
Total	16.823	16.838	16.793	16.805	16.688	16.824	16.923	16.897	16.775	16.775	16.766	16.775

Titan potassic richterite analyses: amphibole from the hypabyssal facies (HYP).

	PC 29c	PC 20b	PC 30b	PC 30b
	c	c	c	e
SiO2	54.34	54.18	54.18	54.20
TiO2	3.49	2.62	2.89	2.83
Al203	0.57	0.77	0.72	0.65
Cr203	0.03	0.03	0.06	0.05
MnO	0.09	0.19	0.07	0.12
FeO	4.03	3.04	3.01	3.08
MgO	20.40	21.09	21.96	21.97
CaO	5.95	6.39	6.52	6.43
K2O	5.17	4.90	5.04	4.93
Na2O	4.26	4.20	4.33	4.28
BaO	0.00	0.00	0.00	0.00
F	2.48	3.14	3.01	3.05
Total	100.81	100.55	101.79	101.59
O=F	1.04	1.32	1.27	1.28
Total	99.77	99.23	100.52	100.31
Mg#	90.0	92.5	92.9	92.7
Structural formula calculations based on 23 oxygens				
Si	7.504	7.469	7.395	7.407
Ti	0.362	0.272	0.297	0.291
Al	0.093	0.125	0.116	0.105
Cr	0.003	0.003	0.006	0.005
Mn	0.011	0.022	0.008	0.014
Fe	0.465	0.350	0.344	0.352
Mg	4.200	4.334	4.468	4.476
Ca	0.880	0.944	0.953	0.941
Ba	0.000	0.000	0.000	0.000
K	0.911	0.862	0.878	0.860
Na	1.141	1.123	1.146	1.134
F	1.083	1.369	1.299	1.318
Total	16.653	16.872	16.909	16.903

Titan potassic richterite analyses: amphibole from the round diopside-richterite xenoliths (RD-DRX).

	PC 53	PC 53	PC 22	PC 63	PC 22	PC 29c	PC 29a	PC 22a	PC 22	PC 22	PC 22	PC 29c
	c	c	c	c	c	c	c	c	c	c	c	c
SiO2	53.99	52.68	54.42	52.52	53.82	52.82	51.75	53.33	53.37	53.67	53.24	50.56
TiO2	4.98	6.13	3.79	5.12	3.76	4.94	5.85	3.33	3.23	3.54	3.52	5.85
Al2O3	0.14	0.39	0.44	0.33	0.41	0.40	0.49	1.40	0.66	0.91	0.66	0.20
Cr2O3	0.00	0.00	0.00	0.06	0.00	0.08	0.00	0.00	0.00	0.00	0.00	0.00
MnO	0.05	0.06	0.04	0.03	0.07	0.06	0.17	0.09	0.00	0.00	0.07	0.15
FeO	7.58	4.95	3.34	5.54	3.40	3.81	4.22	3.37	3.53	3.84	3.34	11.44
MgO	17.12	19.61	21.12	19.15	20.85	19.94	20.34	21.32	21.15	20.46	21.35	16.21
CaO	3.45	5.13	5.81	4.46	5.49	5.12	5.59	5.12	6.19	5.72	6.04	2.43
K2O	5.06	5.23	5.05	5.19	5.20	5.21	5.22	5.05	5.02	4.45	4.98	5.05
Na2O	6.10	4.63	4.40	5.17	4.31	4.76	4.47	4.40	4.11	3.19	3.96	6.27
BaO	0.15	0.20	0.22	0.22	0.00	0.23	0.16	0.00	0.00	0.00	0.00	0.20
F	1.55	1.52	1.91	2.24	3.09	2.37	2.33	3.11	2.94	2.95	2.68	2.35
Total	100.17	100.53	100.54	100.03	100.40	99.74	100.59	100.52	100.20	98.73	99.84	100.71
O=F	0.65	0.64	0.80	0.94	1.30	1.00	0.98	1.31	1.24	1.24	1.13	0.99
Total	99.52	99.89	99.74	99.09	99.10	98.74	99.61	99.21	98.96	97.49	98.71	99.72
Mg#	80.1	87.6	91.9	86.0	91.6	90.3	89.6	91.9	91.4	90.5	91.9	71.6
Structural formula calculations based on 23 oxygens												
Si	7.620	7.366	7.520	7.396	7.445	7.403	7.233	7.358	7.407	7.494	7.406	7.276
Ti	0.529	0.645	0.394	0.542	0.391	0.521	0.615	0.345	0.337	0.372	0.368	0.633
Al	0.023	0.064	0.072	0.055	0.067	0.066	0.081	0.228	0.108	0.150	0.108	0.034
Cr	0.000	0.000	0.000	0.007	0.000	0.009	0.000	0.000	0.000	0.000	0.000	0.000
Mn	0.006	0.007	0.005	0.004	0.008	0.007	0.020	0.011	0.000	0.000	0.008	0.018
Fe	0.895	0.579	0.386	0.652	0.393	0.447	0.493	0.389	0.410	0.448	0.389	1.377
Mg	3.602	4.088	4.351	4.020	4.300	4.166	4.238	4.385	4.376	4.259	4.427	3.477
Ca	0.522	0.769	0.860	0.673	0.814	0.769	0.837	0.757	0.920	0.856	0.900	0.375
Ba	0.008	0.011	0.012	0.012	0.000	0.013	0.009	0.000	0.000	0.000	0.000	0.011
K	0.911	0.933	0.890	0.932	0.918	0.932	0.931	0.889	0.889	0.793	0.884	0.927
Na	1.669	1.255	1.179	1.412	1.156	1.294	1.211	1.177	1.106	0.864	1.068	1.749
F	0.692	0.672	0.835	0.998	1.352	1.051	1.030	1.357	1.291	1.303	1.179	1.070
Total	16.476	16.388	16.502	16.702	16.843	16.676	16.698	16.894	16.844	16.539	16.737	16.947

Titan potassic richterite analyses: amphibole from the round diopside-richterite xenolith, (RD-DRX).

	PC 29c	PC 29c	PC 22	PC 29c	PC 29c	PC 22a	PC 22	PC 63	PC 29c	PC 29c	PC 22	PC 22
	c	c	c	c	c	c	e	e	e	e	e	e
SiO2	51.52	52.35	54.71	50.42	50.80	52.40	53.68	53.60	52.42	52.16	53.09	52.85
TiO2	5.60	5.30	3.05	7.16	6.65	3.40	4.15	4.36	5.22	5.83	3.62	3.18
Al2O3	0.25	0.24	0.07	0.32	0.27	1.04	0.70	0.41	0.49	0.50	0.78	0.63
Cr2O3	0.00	0.00	0.23	0.00	0.04	0.00	0.00	0.00	0.00	0.01	0.00	0.00
MnO	0.15	0.18	0.13	0.06	0.10	0.12	0.09	0.00	0.00	0.14	0.07	0.05
FeO	6.48	5.90	4.42	5.19	7.05	3.41	5.15	4.18	5.11	4.52	3.65	3.09
MgO	18.81	19.43	20.37	19.56	18.64	21.47	21.12	19.43	20.37	19.77	21.11	20.89
CaO	4.25	4.58	4.31	4.56	3.58	6.19	4.64	5.24	4.87	5.02	6.00	6.15
K2O	5.14	5.26	5.12	5.16	5.15	5.03	4.66	5.26	5.12	5.18	5.02	4.98
Na2O	5.28	4.85	5.13	4.98	5.50	4.00	4.49	4.65	4.82	4.81	3.94	4.15
BaO	0.22	0.27	0.00	0.32	0.33	0.00	0.19	0.15	0.27	0.25	0.00	0.00
F	2.51	2.46	3.43	1.93	2.13	2.93	1.76	2.39	2.27	2.48	2.76	2.93
Total	100.21	100.82	100.97	99.66	100.24	99.99	100.63	99.67	100.96	100.67	100.04	98.90
O=F	1.06	1.04	1.44	0.81	0.90	1.23	0.74	1.01	0.96	1.04	1.16	1.23
Total	99.15	99.78	99.53	98.85	99.34	98.76	99.89	98.66	100.00	99.63	98.88	97.67
Mg#	83.8	85.4	89.1	87.0	82.5	91.8	88.0	89.2	87.7	88.6	91.2	92.3
Structural formula calculations based on 23 oxygens												
Si	7.292	7.337	7.541	7.163	7.219	7.301	7.444	7.505	7.305	7.283	7.383	7.422
Ti	0.596	0.559	0.316	0.765	0.711	0.356	0.433	0.459	0.547	0.612	0.379	0.336
Al	0.042	0.040	0.011	0.054	0.045	0.171	0.114	0.068	0.080	0.082	0.128	0.104
Cr	0.000	0.000	0.025	0.000	0.004	0.000	0.000	0.000	0.000	0.001	0.000	0.000
Mn	0.018	0.021	0.015	0.007	0.012	0.014	0.011	0.000	0.000	0.017	0.008	0.006
Fe	0.767	0.692	0.510	0.617	0.838	0.397	0.597	0.489	0.596	0.528	0.424	0.363
Mg	3.969	4.060	4.186	4.142	3.949	4.460	4.366	4.056	4.232	4.115	4.376	4.373
Ca	0.645	0.688	0.637	0.694	0.545	0.924	0.689	0.786	0.727	0.751	0.894	0.925
Ba	0.012	0.015	0.000	0.018	0.018	0.000	0.010	0.008	0.015	0.014	0.000	0.000
K	0.928	0.940	0.900	0.935	0.934	0.894	0.824	0.940	0.910	0.923	0.891	0.892
Na	1.449	1.318	1.371	1.372	1.515	1.081	1.207	1.262	1.302	1.302	1.062	1.130
F	1.124	1.090	1.495	0.867	0.957	1.291	0.772	1.058	1.000	1.095	1.214	1.301
Total	16.841	16.759	17.008	16.633	16.748	16.890	16.468	16.632	16.714	16.723	16.758	16.852

Ti-K richterite analyses: RD-DRX

	PC 22
	e
SiO2	53.07
TiO2	3.34
Al203	0.57
Cr203	0.00
MnO	0.07
FeO	3.36
MgO	21.48
CaO	6.00
K2O	4.99
Na2O	4.04
BaO	0.00
F	2.80
Total	99.72
O=F	1.18
Total	98.54
Mg#	91.9
Structural formula calculations based on 23 oxygens	
Si	7.397
Ti	0.350
Al	0.094
Cr	0.000
Mn	0.008
Fe	0.392
Mg	4.463
Ca	0.896
Ba	0.000
K	0.887
Na	1.092
F	1.234
Total	16.813

Ti-K richterite analyses: amphibole from the angular DRX (ANG-DRX).

	PC 20	PC 20	PC 20	PC 20	PC 22	PC 34	PC 20	PC 20b
	c	c	c	c	c	ce	c	c
SiO2	57.41	55.53	57.35	56.72	55.30	57.35	56.41	54.06
TiO2	0.38	0.45	0.50	0.42	2.08	0.49	0.31	2.41
Al203	0.13	0.15	0.17	0.16	0.09	0.14	0.04	0.80
Cr203	0.95	0.31	1.05	0.07	0.18	0.01	0.16	0.00
MnO	0.07	0.02	0.06	0.00	0.05	0.00	0.04	0.00
FeO	1.07	1.50	1.38	0.91	3.92	2.06	0.98	2.94
MgO	22.09	22.60	21.77	22.71	20.60	22.58	22.51	21.00
CaO	5.93	6.61	6.19	6.92	4.97	6.76	6.76	6.94
K2O	5.39	5.07	5.11	5.42	5.20	5.00	5.27	4.92
Na2O	4.37	4.07	4.46	3.88	4.86	4.05	4.08	3.84
BaO	0.08	0.10	0.06	0.00	0.00	0.01	0.04	0.00
F	3.02	3.00	2.89	3.36	3.26	2.43	3.24	3.24
Total	100.89	99.41	100.99	100.57	100.51	100.88	99.84	99.73
O=F	1.27	1.26	1.22	1.41	1.37	1.02	1.36	1.19
Total	99.62	98.15	99.77	99.16	99.14	99.86	98.48	98.54
Mg#	97.4	96.4	96.6	97.8	90.4	95.1	97.6	92.7
Si	7.792	7.676	7.784	7.719	7.633	7.792	7.739	7.505
Ti	0.039	0.047	0.051	0.043	0.216	0.050	0.032	0.252
Al	0.021	0.024	0.027	0.026	0.015	0.022	0.006	0.131
Cr	0.102	0.034	0.113	0.008	0.020	0.001	0.017	0.000
Mn	0.008	0.002	0.007	0.000	0.006	0.000	0.005	0.000
Fe	0.121	0.173	0.157	0.104	0.452	0.234	0.112	0.341
Mg	4.469	4.657	4.405	4.608	4.239	4.573	4.604	4.346
Ca	0.862	0.979	0.900	1.009	0.735	0.984	0.994	1.032
Ba	0.004	0.005	0.003	0.000	0.000	0.001	0.002	0.000
K	0.933	0.894	0.885	0.941	0.916	0.867	0.922	0.871
Na	1.150	1.091	1.174	1.024	1.301	1.067	1.085	1.034
F	1.296	1.312	1.[illegible]	1.446	1.423	1.044	1.406	1.238
Total	16.798	16.896	16.[illegible]	16.927	16.954	16.635	16.924	16.750

Ti-K richterite analyses: amphibole from the angular DRX (ANG-DRX).

	PC 34	PC 20
	•	•
SiO2	57.71	56.08
TiO2	1.02	0.32
Al203	0.11	0.11
Cr203	0.00	0.40
MnO	0.01	0.00
FeO	3.03	1.70
MgO	21.27	22.10
CaO	6.17	6.55
K2O	4.96	5.05
Na2O	4.13	4.34
BaO	0.05	0.04
F	2.48	2.93
Total	100.94	99.62
O:F	1.04	1.23
Total	99.90	98.39
Mg#	92.6	95.9
Structural formula calculations based on 23 oxygens		
Si	7.849	7.734
Ti	0.104	0.033
Al	0.018	0.018
Cr	0.000	0.044
Mn	0.001	0.000
Fe	0.345	0.196
Mg	4.312	4.544
Ca	0.899	0.968
Ba	0.003	0.002
K	0.851	0.888
Na	1.089	1.160
F	1.067	1.278
Total	16.546	16.065

REFERENCES

Allsopp, H. L., Bristow, J. W., Skinner, E. M. W., Scott-Smith, B. H., and Danchin, R. V. 1985. Rb-Sr geochronology of some Miocene West Australian lamproites. Transactions of the Geological Society of South Africa, **88**: 341-345.

Anderson, O. L. 1979. The role of fracture dynamics in kimberlite pipe formation. *In* Kimberlites, Diatremes and Diamonds: Their Geology, Petrology, and Geochemistry. *Edited by* F. R. Boyd, and M. O. A. Meyer. Proceeding of the Second International Kimberlite Conference, American Geophysical Union, Washington, D.C., **1**:344-353.

Aoki, K., and Kanisawa, S. 1979. Fluorine contents of some hydrous minerals derived from upper mantle and lower crust. Lithos, **12**: 167-171.

Arculus, R. J., and Delano, J. W. 1987. Oxidation state of the upper mantle: present conditions, evolution, and controls. *In* Mantle Xenoliths. *Edited by* P. H. Nixon, 589-599,.J. Wiley & Sons, London.

Arima, M., and Edgar, A. D. 1983. A high pressure experimental study on a magnesian-rich leucite-lamproite from the West Kimberley area, Australia: petrogenetic implications. Contributions to Mineralogy and Petrology, **84**: 228-234.

Arima, M., and Edgar, A. D. 1983a. High pressure experimental studies on a Katungite and their bearing on the genesis of some potassium-rich magmas of the West Branch of the African Rift. Journal of Petrology **24**: 160-187.

Arima, M., and Edgar, A. D. 1981. Substitution mechanisms and solubility of titanium in phlogopites from rocks of probable mantle origin. Contributions to Mineralogy and Petrology, **77**: 140-152.

Arima, M., and Edgar, A. D. 1980. Stability of wadeite ($Zr_2K_4Si_6O_{18}$) under upper mantle conditions: Petrological implications. Contributions to Mineralogy and Petrology, **72**: 191-195.

Artyushkov, E. V., and Sobolev, S. V. 1984. Physics of the kimberlite magmatism. *In* Kimberlites and related rocks,*Edited by* J. Kornprobst. Proceedings of the Third International Kimberlite Conference, Elsevier, Amsterdam, **1**: 309-322.

Atkinson, W. J. 1989. Diamond exploration philosophy, practice and promises: a review. *In* Kimberlite and related rocks: Their composition, occurrence, origin and emplacement. Proceedings of the 4th International Kimberlite Conference, Perth 1986. Geological Society of America Special Publication Number 14, **1**: 1075-1107.

Atkinson, W. J., Hughes, F. E., and Smith, C. B. 1984. A review of the kimberlitic rocks of Western Australia. *In* Kimberlites and related rocks, *Edited by* J. Komprobst. Proceedings of the Third International Kimberlite Conference, Elsevier, Amsterdam, **1**: 195-225.

Bachinski, S. W., and Simpson, E. L. 1984. Ti-phlogopites of the Shaw's Cove minette: a comparison with micas of other lamprophyres, potassic rocks, kimberlites, and mantle xenoliths. American Mineralogist, **69**: 41-56.

Bailey, D. K. 1987. Mantle metasomatism - perspective and prospect. *In* Alkaline Igneous Rocks. *Edited by* J. G. Fitton and B. G. J. Upton, Geological Society Special Publication Number **30**: 1-13.

Bailey, D. K. 1985. Fluids, melts, flowage and styles of eruption in alkaline ultramafic magmatism. Transactions of the Geological Society of South Africa, **88**: 449-457.

Bailey, D. K. 1984. Kimberlite: "The mantle sample" formed by ultrametasomatism. *In* Kimberlites and related rocks, *Edited by* J. Komprobst. Proceedings of the Third International Kimberlite Conference, Elsevier, Amsterdam, **1**: 323-333.

Bailey, D. K. 1982, Mantle metasomatism - continuing chemical change within the Earth. Nature, **296**: 525-530.

Bailey, D. K. 1980. Volatile flux, geotherms and the generation of the kimberlite - carbonatite - alkaline magma spectrum. Mineralogical Magazine, **43**: 695-699.

Barton, M. 1979. A comparative study of some minerals occurring in the potassium-rich alkaline rocks of the Leucite Hills, Wyoming, the Vico Volcano, Western Italy, and the Toro-Ankole Region, Uganda. Neues Jahrbuch fur Geologie und Palaontologie Abhandlungen, **137**: 113-134.

Barton, M., and Hamilton, D. L. 1978. Water-saturated melting relations to 5 kilobars of three Leucite Hills lavas. Contributions to Mineralogy and Petrology, **66**: 41-49.

Barton, M., and Hamilton, D. L. 1979. The melting relationships of a madupite from the Leucite Hills, Wyoming, to 30 kilobars. Contributions to Mineralogy and Petrology, **69**: 133-142.

Barton, M., and van Bergen, M. J. 1981. Green clinopyroxenes and associated phases in a potassium-rich lava from Leucite Hills, Wyoming. Contributions to Mineralogy and Petrology, **77**: 101-114.

Bergman, S. C. 1987. Lamproites and other potassium-rich igneous rocks: A review of their occurrence, mineralogy and geochemistry. *In* Alkaline Igneous Rocks. *Edited by* J. G. Fitton and B. G. J. Upton. Geological Society Special Publication Number **30**: 103-190.

Bolivar, S. L., and Brookins, D. G. 1979. Geophysical and Rb-Sr study of Prairie Creek, Arkansas, Kimberlites. *In* Kimberlites, Diatremes and Diamonds: Their Geology, Petrology, and Geochemistry. *Edited by* F. R. Boyd, and M. O. A. Meyer. Proceeding of the Second International Kimberlite Conference, American Geophysical Union, Washington, D.C., **1**:289-299.

Bolivar, S. L., Brookins, D. G., Lewis, R. D., and Meyer, H. O. A. 1976. Geophysical studies of the Prairie Creek kimberlite, Murfreesboro, Arkansas. EOS Transactions, **57**: 761.

Boyd, F. R., and Finnerty, A. A. 1980. Conditions of origin of natural diamonds of peridotite affinity. Journal of Geophysical Research, **85**: 6911-6918.

Boyd, F. R., and Nixon, 1978. Ultramafic nodules from the Premier kimberlite pipe, South Africa. Geochimica Cosmochimica Acta, **42**: 1367-1382.

Boyd, F. R., and Nixon, 1975. Origins of the ultramafic nodules from some kimberlites of northern Lesotho and the Monastery Mine, South Africa, Physics and Chemistry of the Earth, **9**: 431-434.

Boyd, F. R., and England, J. L. 1963. Effect of pressures on the melting of diopside, $CaMgSi_2O_6$, and albite, $NaAlSi_3O_8$, in the range up to 50 kilobars. Journal of Geophysical Research. **68**: 311-323.

Boyd, F. R., and England, J. L. 1960. Apparatus for phase equilibrium measurements at pressures up to 50 kilobars and temperatures to 1750°C. Journal of Geophysical Research, **65**: 741-748.

Branner, J. C., and Brackett, R. N. 1890. The peridotite of Pike County, Arkansas. American Journal of Science, 3rd Series, **38**: 50-59.

Brey, G. 1976. CO_2 solubility and solubility mechanisms in silicate melts at high pressures. Contributions to Mineralogy and Petrology, **57**: 215-221.

Brey, G., and Green, D. H. 1977. Systematic study of liquidus phase relations in olivine melilite + H_2O + CO_2 at high pressures and petrogenesis of an olivine melilite magma. Contributions to Mineralogy and Petrology **61**: 141-162.

Brey, G., and Green, D. H. 1975. The role of CO_2 in the genesis of olivine melilite, Contributions to Mineralogy and Petrology, **49**: 93-103.

Cameron, M., and Papike, J. J. 1981. Structural and chemical variations in pyroxenes. American Mineralogist, **66**:1-50.

Cameron, M., and Papike, J. J. 1980. Crystal chemistry of silicate pyroxenes. *In* Reviews in Mineralogy. *Edited by* Prewitt, C. T., Mineralogical Society of America, **7**: 5-92.

Carmichael, I. S. E. 1967. The mineralogy and petrology of the volcanic rocks from the Leucite Hills, Wyoming. Contributions to Mineralogy and Petrology, **19**: 97-124.

Carmichael, I. S. E. 1967a. The iron-titanium oxides of sialic volcanic rocks and their associated ferromagnesian silicates. Contributions to Mineralogy and Petrology, **14**: 36-64.

Carmichael, I. S. E. 1967b. Iron-titanium oxides and oxygen fugacities in volcanic rocks. Journal of Geophysical Research, **72**: 4665-4687.

Clement, C. R., Skinner, E. M. W., and Scott-Smith, B. H. 1984. Kimberlite redefined. Journal of Geology, **92**: 223-228.

Clement, C. R., Skinner, E. M. W., and Scott, B. H. 1977. Kimberlite redefined. Second International Kimberlite Conference, Santa Fe, New Mexico. Extended Abstracts.

Colby, J. W. 1971. Majic IV, a computer program for quantitative electron microprobe analysis. Bell Telephone Laboratories, Allentown, Pennsylvania.

Coopersmith, H. G., and Mitchell, R. H. 1989. Geology and exploration of the Rose lamproite, south-east Kansas, U.S.A. *In* Kimberlite and related rocks: Their composition, occurrence, origin and emplacement. Proceedings of the 4th International Kimberlite Conference, Perth 1986. Geological Society of America Special Publication Number 14, **1**: 1179-1191.

Cullers, R. L., Ramakrisnnan, S., Berendsen, P., and Griffin, T. 1985. Geochemistry and petrogenesis of lamproites, Late Cretaceous Age, Woodsen County, Kansas, United States of America. Geochimica Cosmochimica Acta, **49**: 1383-1402.

Cundari, A., and Ferguson, A. K. 1982. Significance of the pyroxene chemistry from leucite-bearing and related assemblages. Tschermaks Mineralogische und Petrographische Mitteilungen, **30**: 189-204.

Cundari, A., and Salviulo, G. 1989. Ti solubility in diopsidic pyroxene from a suite of New South Wales Leucitites (Australia), Lithos, **22**: 191-198.

Dawson, J. B. 1989. Geographic and time distribution of kimberlites and lamproites: relationships to tectonic processes. *In* Kimberlite and related rocks: Their composition, occurrence, origin and emplacement. Proceedings of the 4th International Kimberlite Conference, Perth 1986. Geological Society of America Special Publication Number 14, 1: 323-342.

Dawson, J. B. 1987a. The kimberlite clan: relationship with olivine and leucite lamproites, and inferences for upper-mantle metasomatism. *In* Alkaline Igneous Rocks. *Edited by* J. G. Fitton and B. G. J. Upton, Geological Society Special Publication Number 30: 95-101.

Dawson, J. B. 1987b Metasomatized harzburgites in kimberlite and alkaline magmas: Enriched restites and "Flushed" lherzolite. *In* Mantle Metasomatism. *Edited by* M. A. Menzies and C. J. Hawkesworth, p125-144, Academic Press, London

Dawson, J. B. 1987c. The MARID suite of xenoliths in kimberlite: relationship to veined and metasomatized peridotite xenoliths. *In* Mantle Xenoliths. *Edited by* P. H. Nixon, p465-473,.J. Wiley & Sons, London.

Dawson, J. B. 1967. A review of the geology of kimberlite, *In* Ultramafic and Related Rocks, *Edited by* P. J. Wyllie, 241-278 John Wiley and Sons Limited, New York.

Dawson, J. B., and Smith, J. V. 1977. The MARID (mica-amphibole-rutile-ilmenite-diopside) suites of xenoliths in kimberlite, Geochimica Cosmochimica Acta, 41: 309-323.

Dal Negro, A., Carbonin, S., Molin, G, M., Cundari, A., and Piccirillo, E. M. 1982. Intracrystalline cation distribution in natural clinopyroxenes of tholeiitic transitional, and alkaline basaltic rocks. *In* Advances in physical geochemistry. *Edited by* S. K. Saxena, Springer-Verlag, New York, 2: 117-150.

Dal Negro, A., Carbonin, S., Salviulo, G., Piccirillo, E. M., and Cundari, A. 1985. Crystal chemistry and site configuration of the clinopyroxene from leucite-bearing rocks and related genetic significance: the Sabatini Lavas, Roman Region, Italy. Journal of Petrology, 26: 1027-1040.

Dingwell, D. B. 1989. Effect of fluorine on the viscosity of diopside liquid. American Mineralogist, 74: 333-338.

Donaldson, C. H. 1976. An experimental investigation of olivine morphology. Contributions to Mineralogy and Petrology, 57: 187-213.

Dubeau, M. L., and Edgar, A. D. 1985. Priderite stability in the system $K_2MgTi_7O_{16}$ - $BaMgTi_7O_{16}$. Mineralogical Magazine, 49: 603-606.

Droop, G. T. R. 1987. A general equation for estimating Fe3+ concentrations in ferromagnesian silicates and oxides from microprobe analyses, using stoichiometric criteria. Mineralogical Magazine, **51**: 431-435.

Downes, H. 1989. Magma mixing in undersaturated alkaline volcanics, Central, Massif Central, France. Mineralogical Magazine, **53**: 43-53.

Edgar, A. D. 1989. Barium- and strontium-enriched apatites in lamproites from West Kimberley, Western Australia. American Mineralogist, **74**: 889-895.

Edgar, A. D. 1987. The genesis of alkaline magmas with emphasis on their source regions: inferences from experimental studies.*In* Alkaline Igneous Rocks. *Edited by* J. G. Fitton and B. G. J. Upton, Geological Society Special Publication Number **30**: 29-52.

Edgar, A. D. 1983. Relationship of ultrapotassic magmatism in the western U.S.A. to the Yellowstone plume. Neues Jahrbuch fur Mineralogie Abhandlungen, **147**: 35-46.

Edgar, A. D., and Arima, M. 1985. Fluorine and chlorine contents of phlogopites crystallized from ultrapotassic rock compositions in high pressure experiments: implication for halogen reservoirs in source regions. American Mineralogist, **70**: 529-536.

Edgar, A. D., and Arima, M. 1983. Conditions of phlogopite crystallization in ultrapotassic rocks. Mineralogical Magazine, **47**: 11-19.

Edgar, A. D., and Arima, M. 1981. Geochemistry of three potassium-rich ultrabasic lavas from the west branch of the African Rift: inferences on their genesis. Neues Jahrbuch fur Mineralogie Abhandlungen, **12**: 539-552.

Edgar, A. D., Green, D. H., and Hibberson, W. O. 1976. Experimental petrology of a highly potassic magma. Journal of Petrology, **17**: 339-356.

Edgar, A. D., Arima, M., Baldwin, D. K., bell, D. R., Shee, S. R., Michael, E., Skinner, W., and Walker, E. C. 1989. High-pressure-high-temperature melting experiments on a SiO_2-poor aphanitic kimberlite from the Wesselton mine, Kimberley, South Africa. The American Mineralogist, **72**: 524-533.

Edgar, A. D., Condliffe, E., Barnett, R. L., and Shirran, R. J. 1980. An experimental study of an olivine Ugandite magma and mechanisms for the formation of its K-enriched derivatives. Journal of Petrology, **21**,:475-497.

Eggler, D. H. 1983. Upper mantle oxidation state: evidence from Ol - Opx - ilmenite assemblages. Geophysical Research Letters, **10**: 365-368.

Eggler, D. H., and Wendlandt, R. F. 1979. Experimental studies on the relationship between kimberlite magmas and partial melting of peridotite. *In* Kimberlites, Diatremes and Diamonds: Their Geology, Petrology, and Geochemistry. *Edited by* F. R. Boyd, and M. O. A. Meyer. Proceeding of the Second International Kimberlite Conference, American Geophysical Union, Washington, D.C., 1:330-338.

Ellis, D. J., and Green, D. H. 1979. An experimental study of the effect of Ca upon garnet-clinopyroxene Fe-Mg exchange equilibria, Contributions to Mineralogy and Petrology, **71**: 13-22.

Ellis, D. J. and Wyllie, P. J. 1979. a model of phase relations in the system MgO-SiO_2-H_2O-CO_2 and prediction of the compositions of liquids coexisting with forsterite and enstatite. *In* Kimberlites, Diatremes and Diamonds: Their Geology, Petrology, and Geochemistry. *Edited by* F. R. Boyd, and M. O. A. Meyer. Proceeding of the Second International Kimberlite Conference, American Geophysical Union, Washington, D.C., 1: 313-318.

Es'Kova, E. M., and Kazakova, M. E. 1954. Shcherbakovite - a new mineral. Doklady Akad. Nauk. S.S.S.R., **99**: 837-841 (in Russian). Translated in 1955, American Mineralogist, **40**: 788.

Esperanca, S., and Holloway, J. R. 1987. On the origin of some mica lamprophyres: experimental evidence from a mafic minette. Contributions to Mineralogy and Petrology. **95**: 207-216.

Farmer, G. L., and Boettcher, A. L. 1981. Petrologic and crystal chemical significance of some deep-seated phlogopites. American Mineralogist, **66**: 1154-1163.

Finger, L. W. 1972. The uncertainty of the calculated ferric iron content of a microprobe analysis. Carnegie Institute of Washington, Yearbook, **71**: 600-603.

Finger, L. W., and Ohashi, Y. 1976. The thermal expansion of diopside to 800°C and refinement of the crystal structure at 700°C. American Mineralogist, **61**: 303-310.

Flowers, M. F. J. 1971. Evidence for the role of phlogopite in the genesis of alkali basalts. Contributions to Mineralogy and Petrology, **32**: 126-137.

Foley, S. F. 1990. Experimental constraints on phlogopite chemistry in lamproites: 2. Effect of pressure-temperature variations. European Journal of Mineralogy, **2**: 327-341.

Foley, S. F. 1989. The genesis of lamproitic magmas in a reduced fluorine-rich mantle. *In* Kimberlite and related rocks: Their composition, occurrence, origin and emplacement. Proceedings of the 4th International Kimberlite Conference, Perth 1986. Geological Society of America Special Publication Number 14, **1**: 616-631.

Foley, S. F. 1989a. Experimental constraints on phlogopite chemistry in lamproites: 1. The effect of water activity and oxygen fugacity. European Journal of Mineralogy, **1**: 417-426.

Foley, S. F. 1985. The oxidation state of lamproitic magmas. Tschermaks Mineralogische und Petrographische Mitteilungen, **34**: 217-238.

Foley, S. F., Taylor, W. R., and Green, D. H. 1986a. The effect of fluorine on phase relationships in the system $KAlSiO_4$-Mg_2SiO_4-SiO_2 at 28 kilobars and the solution mechanism of fluorine in silicate melts. Contributions to Mineralogy and Petrology, **93**: 46-55.

Foley, S. F., Taylor, W. R., and Green, D. H. 1986b. The role of fluorine and oxygen fugacity in the genesis of the ultrapotassic rocks. Contribution to Mineralogy and Petrology, **94**: 183-192.

Foley, S. F., Venturelli, G., Green, D. H., and Toscani, L. 1987. The ultrapotassic rocks: Characteristics, classification, and constraints for petrogenetic models. Earth-Science Reviews, **24**: 81-134.

Ford, C. E. 1978. Platinum-iron alloy sample containers for melting experiments on iron-bearing rocks, minerals and related systems. Mineralogical Magazine, **42**: 271-275.

Forbes, W. C., and Flower, M. F. J. 1974. Phase relations of titan-phlogopite, $K_2Mg_4TiAl_2Si_6O_{20}(OH)_4$: A refractory phase in the upper mantle? Earth and Planetary Science Letters, **22**: 60-66.

Friedemann, F. 1981. Mechanism of the water and carbon dioxide solubility in oxides and silicates and the role of O^-. Contributions to Mineralogy and Petrology, **76**: 474-482.

Friel, J. J., Harker, R. I., and Ulmar, G. C. 1977. Armalcolite stability as a function of pressure and oxygen fugacity. Geochimica Cosmochimica Acta, **41**: 403-410.

Fudali, R. F. 1963. Experimental studies bearing on the origin of pseudoleucite and associated problems of alkalic rock systems. Geological Society of America, Bulletin, **74**: 1101-1126.

Giardini, A. A., and Melton, C. E. 1975. The nature of cloud-like inclusions in two Arkansas diamonds. American Mineralogist, **60**: 931-933.

Gilbert, M. C., Helz, R. T., Popp, R. K., and Spear, F. s. 1982. Experimental studies of amphibole stability. *In* Amphiboles: Petrology and experimental phase relations. *Edited by* D. R. Veblen, and P. H. Ribbe. Reviews in Mineralogy, Mineralogical Society of America, **9B**: 229-354.

Gogineni,S. V. C., Melton, E., and Giardini, A. A. 1978. Some petrological aspects of the Prairie Creek diamond-bearing kimberlite diatreme, Arkansas. Contributions to Mineralogy and Petrology, **66**: 251-261.

Green, D. H., Falloon, T. J., and Taylor, W. R. 1987. Mantle - derived magmas - roles of variable source peridotite and variable C- H - O fluid compositions. *In* Magmatic Processes : physico-chemical principles. *Edited by* B. O. Mysen, Geochemical Society Special Publication **1**: 139-154.

Grove, T. L. 1981. Use of FePt alloys to eliminate the iron loss problem in 1 atmosphere gas mixing experiments: Theoretical and practical considerations. **78**: 298-304.

Guo, J., and Green, T. H. 1990. Experimental study of barium partitioning between phlogopite and silicate liquid at upper-mantle pressure and temperature. Lithos, **24**: 83-95.

Gupta, A. K. 1972. The system forsterite-diopside-akermanite-leucite and its significance in the origin of potassium-rich mafic and ultramafic volcanic rocks. The American Mineralogist, **57**: 1242-1259.

Gupta, A. K., and Green, D. H. 1988. The liquidus surface of the system forsterite-kalsilite-quartz at 28 kilobars under dry conditions, in the presence of H_2O and of CO_2. Mineralogy and Petrology, **39**: 163-174.

Gupta, A. K., and Yagi, K. 1979. Experimental study on two picrites with reference to the genesis of kimberlite. *In* Kimberlites, Diatremes and Diamonds: Their Geology, Petrology, and Geochemistry. *Edited by* F. R. Boyd, and M. O. A. Meyer. Proceeding of the Second International Kimberlite Conference, American Geophysical Union, Washington, D.C., **1**:339-343.

Gupta, A. K., Onuma, K., Yagi, K., and Lidiak, E. G. 1973. Effect of silica concentration on the diopsidic pyroxenes in the system diopside-$CaTiAl_2O_6$-SiO_2. Contributions to Mineralogy and Petrology, **41**: 333-344.

Hall, A. E., and Smith, C. B. 1985. Lamproite diamonds - are they different. *In* Kimberlite occurrence and origin: A basis for conceptual models in exploration, *Edited by* Glover, J. E., and Harris, P. G., Geological Society of Australia, 167-211.

Hawkesworth, C. J., Fraser, K. S., and Rodgers, N. W. 1985. Kimberlites and lamproites: Extreme products of mantle enrichment processes. Transactions of the Geological Society of South Africa, **88**: 439-447.

Jaques, A. L., and Foley, S. F. 1985. The origin of Al-rich spinel inclusions in leucite from the leucite lamproites of Western Australia. American Mineralogist, **70**: 1143-1150.

Jaques, A. L., O'Neill, H. St. C., Smith, C. B., Moon, J., and Chappell, B. W. 1990. Diamondiferous peridotite xenoliths from the Argyle (AK1) lamproite pipe, Western Australia. Contributions to Mineralogy and Petrology, **104**: 255-276.

Jaques, A. L., Sun, S.-S., and Chappell, B. W. 1989a. Geochemistry of the Argyle (AK1) lamproite pipe, Western Australia. *In* Kimberlite and related rocks: Their composition, occurrence, origin and emplacement. Proceedings of the 4th International Kimberlite Conference, Perth 1986. Geological Society of America Special Publication Number 14, 1:170-188.

Jaques, A. L., Haggerty, S. E., Lucas, H., and Boxer, G. L. 1989b. Mineralogy and Petrology of the Argyle (AK1) lamproite pipe, Western Australia. *In* Kimberlite and related rocks: Their composition, occurrence, origin and emplacement. Proceedings of the 4th International Kimberlite Conference, Perth 1986. Geological Society of America Special Publication Number 14, 1:153-169.

Jaques, A. L., Lewis, J. D., and Smith, C. B. 1986. The kimberlites and lamproites of Western Australia. Geological Survey of Western Australia Bulletin, **132**: 268p.

Jaques, A. L., Ferguson, J., and Smith, C. B. 1985. Kimberlites in Australia. *In* Kimberlite occurrence and origin: A basis for conceptual models in exploration, *Edited by* Glover, J. E., and Harris, P. G., Geological Society of Australia, 227-274.

Jaques, A. L., Lewis, J. D., Smith, C. B., Gregory, G. P., Ferguson, J., Chappell, B. W., and McCulloch, M. T. 1984a. The diamond-bearing ultrapotassic (lamproitic) rocks of the West Kimberley Region, Western Australia. *In* Kimberlites and related rocks, *Edited by* J. Kornprobst. Proceedings of the Third International Kimberlite Conference, Elsevier, Amsterdam, **1**: 225-254.

Jaques, A. L, Creaser, R. A., Ferguson J., and Smith, C. B. 1984b. A review of the alkaline rocks of Australia. Transactions of the Geological Society of South Africa, **288**: 311-334.

Johannes, W., and Bode, B. 1978. Loss of iron to the Pt-container in melting experiments with basalts and a method to reduce it. Contributions to Mineralogy and Petrology, **67**: 221-225.

Johannes, W., Bell, P. M., Mao, H. K., Boettcher, A. L., Chipman, D. W., Hays, J. F., Newton, R. C., and Seifert, F. 1971. An interlaboratory comparison of piston-cylinder calibration using the albite breakdown reaction. Contributions to Mineralogy and Petrology, **32**: 24-38.

Kadik, A. A., and Lukanin, O. A. 1985a. Paths of mantle outgassing during melting: the role of partial melting of upper mantle rocks in the evolution of fluid composition and redox regime. International Geological Review, **27**: 563-572.

Kadik, A. A., and Lukanin, O. A. 1985b. Paths for mantle outgasing during melting: changes in fluid composition and conditions in basaltic magmas during migration to the surface. International Geological Review, **27**: 573-586.

Kennedy, C. S., and Kennedy, G. C. 1976. The equilibrium boundary between graphite and diamond. Journal of Geophysical Research **81**: 2467-2470.

Kuroda, Y., Suzuoki, T., Matsuo, S., and Aoki, K. 1975. D/H ratios of the coexisting phlogopite and richterite from mica nodules and a peridotite in South African kimberlites. Contributions to Mineralogy and Petrology, **52**: 315-318.

Kushiro, I., Syono, Y., and Akimoto, S. 1967. Stability of phlogopite at high pressures and possible presence of phlogopite in the Earth's upper mantle. Earth and Planetary Science Letters, **3**: 197-203.

Kushiro, I. 1960. Si-Al relation in clinopyroxenes from igneous rocks. American Journal of Science, **258**: 548-554.

LeBas, M. J. 1962. The role of aluminum in igneous clinopyroxenes with relation to heir parentage. American Journal of Science, **260**: 267-288.

Lewis, R. D., and Bolivar, S. L. 1976. Mineralogy of the diamond bearing "Kimberlite", Murfreesboro, Arkansas. EOS Transactions of the American Geophysical Union, **57**: 761.

Lewis, R. D., Meyer, H. O. A., Bolivar, S. L., and Brookins, D. G. 1976. Mineralogy of the diamond-bearing "kimberlite", Murfreesboro, Arkansas. Eos, Transaction of the American Geophysical Union, **57**: 761.

Lindsley, D. H., and Dixon, S. S. 1976. Coexisting diopside and enstatite at 20 kilobars and 900-1200°C. American Journal of Science, **276**: 1285-1301.

Lloyd, F. E. 1987a. Characterization of mantle metasomatic fluids in spinel lherzolites and alkali clinopyroxenites from the West Eifel and South West Uganda. *In* Mantle Metasomatism. *Edited by* M. A. Menzies and C. J. Hawkesworth, p91-123, Academic Press, London.

Lloyd, F. E. 1987b Regional K-metasomatism in the mantle beneath the west branch of the East African Rift: alkali clinopyroxenite xenoliths in highly potassic magmas. *In* Mantle Xenoliths. *Edited by* P. H. Nixon, 641-659,.J. Wiley & Sons, London.

Lloyd, F. E. 1985. Experimental melting and crystallization of glassy olivine melilitites. Contributions to Mineralogy and Petrology **90**: 236-243.

Luth, R. W. 1989. Natural versus experimental control of oxidation state: Effects on the composition and speciation of C-O-H fluids. American Mineralogist, **74**: 50-57.

Luth, W. C. 1967. Studies in the system $KAlSiO_4$-Mg_2SiO_4-SiO_2-H_2O: I, Inferred phase relations and petrologic applications. Journal of Petrology, **8**: 372-416.

MacGregor, I. D. 1974. The system MgO-Al_2O_3-SiO_2: solubility of Al_2O_3 in enstatite for spinel and garnet peridotite compositions. American Mineralogist, **59**: 110-119.

Mansker, W. L., Ewing, R. C., and Keil, K. 1979. Barian-titanian biotites in nephelinites from Oahu, Hawaii. American Mineralogist, **64**: 156-159.

Mattioli, G. S., and Wood, B. J. 1986. Upper mantle oxygen fugacity recorded by spinel lherzolites. Nature, **322**: 626-628.

McCauley, J. W., Newnham, R. E., and Gibbs, G. V. 1973. Crystal structure analysis of synthetic fluorophlogopite. American Mineralogist, **58**: 249-254.

Mengel, K., and Green, D. H. 1989. Stability of amphibole and phlogopite in metasomatized peridotite under water-saturated and water-undersaturated conditions. *In* Kimberlite and related rocks: Their composition, occurrence, origin and emplacement. Proceedings of the 4th International Kimberlite Conference, Perth 1986. Geological Society of America Special Publication Number 14, **1**: 571-581.

Merrill, R. B., and Wyllie, P. J. 1973. Absorption of iron by platinum capsules in high pressure rock melting experiments. American Mineralogist, **58**: 16-20.

Meyer, H. O. A. 1985. Genesis of diamond: a mantle saga. American Mineralogist, **70**: 344-355.

Miser, H. D., and Ross, C. S. 1923. Diamond-bearing peridotite in Pike County, Arkansas. Contributions to Economic Geology, United States Geological Society Bulletin, **735**: 279-322.

Miser, H. D. 1912. New areas of diamond-bearing peridotite in Arkansas. United States Geological Survey Bulletin, **540**: 534-546.

Mitchell, R. H. 1989. Aspects of the petrology of kimberlites and lamproites: some definitions and distinctions. *In* Kimberlite and related rocks: Their composition, occurrence, origin and emplacement. Proceedings of the 4th International Kimberlite Conference, Perth 1986. Geological Society of America Special Publication Number 14, **1**: 7-45.

Mitchell, R. H. 1985. A review of the mineralogy of lamproites. Transactions of the Geological Society of South Africa, **88**: 411-437.

Mitchell, R. H. 1981. Titaniferous phlogopites from the leucite lamproites of the West Kimberley area, Western Australia. Contributions to Mineralogy and Petrology, **76**: 342-251.

Mitchell, R. H. 1975. Theoretical aspects of gaseous and isotopic equilibria in the system C-H-O-S with application to kimberlite. Physical Chemistry of the Earth, **9**: 903-915.

Mitchell, R. H. 1986. Kimberlites: Mineralogy, Geochemistry and Petrology. Plenum Publishing Corporation, New York, 442pp

Mitchell, R. H., and Bergman, S. C. 1991. Petrology of Lamproites.Plenum Publishing Corporation, New York, 441pp.

Mitchell, R. H., and Meyer, H. O. A. 1989. Mineralogy of micaceous kimberlites from the new Elands and Star Mines, Orange Free State, South Africa *In* Kimberlite and related rocks: Their composition, occurrence, origin and emplacement. Proceedings of the 4th International Kimberlite Conference, Perth 1986. Geological Society of America Special Publication Number 14, **1**: 83-96.

Mitchell, R. H., and Lewis, R. D. 1983. Priderite-bearing xenoliths from the Prairie Creek Mica Peridotite, Arkansas. Canadian Mineralogist, **21**: 59-64.

Mitchell, R. H., Platt, R. G., and Downey, M., 1987. Petrology of lamproites from Smoky Butte, Montana. Journal of Petrology, **28**: 645-677.

Modreski, P. J., and Boettcher, A. L. 1972. The stability of phlogopite + enstatite at high pressures: A model for micas in the interior of the earth. American Journal of Science, **272**: 852-869.

Modreski, P. J., and Boettcher, A. L. 1973. Phase relationships of phlogopite in the system K_2O-MgO-CaO-Al_2O_3-SiO_2-H_2O to 35 kilobars: A better model for micas in the interior of the earth. American Journal of Science, **273**: 385-414.

Morimoto, N., and others 1988. Nomenclature of pyroxenes. Mineralogy and Petrology, **39**: 55-76.

Montana, A., and Brearley, M. 1989. An appraisal of the stability of phlogopite in the crust and in the mantle. American Mineralogist, **74**: 1-4.

McCulloch, M, T., Jaques, A. L., Nelson, D. R., and Lewis, J. D. 1983. Nd and Sr isotopes in kimberlites and lamproites from Western Australia: an enriched mantle origin. Nature, **302**: 400-403.

Mysen, B. O., Virgo, D., Harrison, W. J., and Scarfe, C. M. 1980. Solubility mechanisms of H_2O in silicate melts at high pressures and temperatures: a Raman Spectroscopic study. American Mineralogist **65**: 900-914.

Nelson, D. R. 1989. Isotopic characteristics and petrogenesis of the lamproites and kimberlites of central-west Greenland. Lithos, **22**: 265-274.

Nicholls, I. A., and Whitford, D. J 1983. Potassium-rich volcanic rocks of the Muriah complex Java, Indonesia: Products of multiple magma sources? Journal of Volcanology and Geothermal Research, **18**: 337-359.

Nicolas, A. 1986. A melt extraction model based on structural studies in mantle peridotites. Journal of Petrology, **27**: 999-1022.

Nixon, P. H., Boyd, F. R., and Lee, D. C. 1987. Western Australian xenoliths form kimberlites and lamproites. *In* Mantle Xenoliths. *Edited by* P. H. Nixon, p281-256,.J. Wiley & Sons, London.

Nixon, P. H., Thirlwall, M. F., Buckley, F., and Davies, C. J. 1984. Spanish and Western Australian lamproites: Aspects of whole rock geochemistry. *In* Kimberlites and related rocks, *Edited by* J. Kornprobst. Proceedings of the Third International Kimberlite Conference, Elsevier, Amsterdam, **1**: 285-296.

Norrish, K., 1951. Priderite, a new mineral from the leucite lamproites of the West Kimberley area, Western Australia. Mineralogical Magazine, **29**: 496-501.

Olafsson, M., and Eggler, D. H. 1983. Phase relations of amphibole, amphibole - carbonate, and phlogopite - carbonate peridotite: petrologic constraints on the asthenosphere. Earth and Planetary Science Letters, **64**: 305-315.

O'Neill, H. C., and Wall, V. J. 1987. The olivine - orthopyroxene - spinel oxygen geobarometer, the oxygen fugacity of the Earth's upper mantle. Journal of Petrology, **28**: 1169-1191.

Papike, J. J., and White, C. 1979. Pyroxenes from planetary basalts: characterization of "other" than quadrilateral components. Geophysical Research Letters, **6**: 913-916.

Pidgeon, R. T., Smith, C. B. and Fanning, C. M. 1989. Kimberlite and lamproite emplacement ages in Western Australia. *In* Kimberlite and related rocks: Their composition, occurrence, origin and emplacement. Proceedings of the 4th International Kimberlite Conference, Perth 1986. Geological Society of America Special Publication Number 14, **1**: 369-381.

Prider, R. T. 1982. A glassy lamproite from the West Kimberley area, Western Australia. Mineralogical Magazine, **45**: 279-282.

Prider, R. T. 1960. The leucite lamproites of the Fitzroy Basin, Western Australia. Geological Society of Australia, **6**: 67-118.

Prider, R. T., 1939. Some minerals from the Leucite-rich rocks of the West Kimberley area, Western Australia. The Mineralogical Magazine, **25**: 373-387.

Purdue, A. H. 1908. A new discovery of peridotite in Arkansas. Economic Geology, **3**: 525-528.

Richardson, S. W., Bell, P. M., and Gilbert, M. C. 1968. Kyanite-sillimanite equilibrium between 700oC and 1500°C. American Journal of Science, **266**: 513-541.

Robert, J. -L. 1976. Titanium solubility in synthetic phlogopite solid solutions. Chemical Geology, **17**: 213-227.

Robinson, P. 1980. the composition space of Terrestrial pyroxenes - internal and external limits. *In* Reviews in Mineralogy. *Edited by* Prewitt, C. T., Mineralogical Society of America, **7**: 419-494.

Rock, N. M. S. 1989. Kimberlites as varieties of lamprophyres: implications for geological mapping, petrological research and mineral exploration. *In* Kimberlite and related rocks: Their composition, occurrence, origin and emplacement. Proceedings of the 4th International Kimberlite Conference, Perth 1986. Geological Society of America Special Publication Number 14, **1**: 46-59.

Rock, N. M. S. 1986. The nature and origin of ultramafic lamprophyres: alnoites and allied rocks. Journal of Petrology, **27**: 155-196.

Rock, N. M. S. 1977. the nature and origin of lamprophyres: some definitions, distinctions and derivations. Earth Science Reviews, **13**: 123-169.

Ryabchikov, I. D., Schreyer, W., and Abraham, K. 1982. Compositions of aqueous fluids in equilibrium with pyroxenes and olivines at mantle pressures and temperatures. Contributions to Mineralogy and Petrology, **79**: 80-84.

Schneider, P. F. 1908. A unique collection of peridotite. Science new series, **28**: 92-93.

Scott-Smith, B. H., and Skinner, E. M. W. 1984a. A new look at Prairie Creek, Arkansas. *In* Kimberlites and related rocks,*Edited by* J. Kornprobst, : Proceedings of the Third International Kimberlite Conference, American Geophysical Union, Washington, D.C., **1**: 255-284.

Scott-Smith, B. H., and Skinner, E. M. W. 1984b. Diamondiferous Lamproites. Journal of Geology, **92**: 433-438.

Scott-Smith, B. H., and Skinner, E. M. W. 1984c. Kimberlite and American Mines, near Prairie Creek, Arkansas. Ann. Sci. Univ. Clermont-Ferrand. II, **74**: 27-36.

Scott-Smith, B. H., Skinner, E. M. W., and Loney, P. E. 1989. The Kapamba lamproites of the Luangwa valley, Eastern Zambia. *In* Kimberlite and related rocks: Their composition, occurrence, origin and emplacement. Proceedings of the 4th International Kimberlite Conference, Perth 1936. Geological Society of America Special Publication Number 14, **1**: 189-205.

Scott, D. R., and Stevenson, D. J. 1989. A self-consistent model of melting, magma migration and buoyancy-driven circulation beneath mid-ocean ridges. Journal of Geophysical Research, **94**: 2973-2988.

Sekine, T., and Wyllie, P. J. 1982. Phase relationships in the system $KAlSiO_4$ - Mg_2SiO_4 - SiO_2 - H_2O as a model for hybridization between hydrous siliceous melts and peridotite. Contributions to Mineralogy and Petrology, **79**: 368-374.

Sheraton, J. W., and Cundari, A. 1980. Leucitites from Gaussberg, Antarctica. Contributions to Mineralogy and Petrology, **71**: 417-427.

Skinner, E. M. W., Smith, C. B., Bristow, J. W., Scott-Smith, B. H., and Dawson, J. B. 1984. Proterozoic kimberlites and lamproites and a preliminary age for the Argyle lamproite pipe, Western Australia. Transactions of the Geological Society of South Africa, **88**: 335-340.

Smith, B. H. 1979. Petrogenesis of kimberlites and associated potassic lamprophyres form central west Greenland. *In* Kimberlites, Diatremes and Diamonds: Their Geology, Petrology, and Geochemistry. *Edited by* F. R. Boyd, and M. O. A. Meyer. Proceeding of the Second International Kimberlite Conference, American Geophysical Union, Washington, D.C., **1**: 190-205.

Smith, C. B., and Lorenz, V. 1989. Volcanology of the Ellendale lamproite pipes, Western Australia. *In* Kimberlite and related rocks: Their composition, occurrence, origin and emplacement. Proceedings of the 4th International Kimberlite Conference, Perth 1986. Geological Society of America Special Publication Number 14, **1**: 505-519.

Smith, J. V., Delaney, J. S., Hervig, R. L., and Dawson, J. B. 1981. Storage of F and Cl in the upper mantle: geochemical implications. Lithos, **14**: 133-147.

Sobolev, A. V., Sobolev, N. V., Smith, C. B., and Dubessy, J. 1989. Fluid and melt compositions in lamproites and kimberlites based on the study of inclusions in olivine. *In* Kimberlite and related rocks: Their composition, occurrence, origin and emplacement. Proceedings of the 4th International Kimberlite Conference, Perth 1986. Geological Society of America Special Publication Number 14, **1**: 220-240.

Spence, D. A., and Turcotte, D. L. 1990. Buoyancy-driven magma fracture: A mechanism for ascent through the lithosphere and the emplacement of diamonds. Journal of Geophysical Research, **95**: 5133-5139.

Spence, D. A., and Turcotte, D. L. 1985. Magma-driven propagation of cracks. Journal of Geophysical Research, **90**: 575-580.

Spence, D. A., Sharp, P. W., and Turcotte, D. L. 1987. Buoyancy-driven crack propagation: A mechanism for magma migration. Journal of Fluid Mechanics, **174**: 135-153.

Spera, F. J. 1987. Dynamics of translithosphereic migration of metasomatic fluid, and alkaline magma. *In* Mantle Metasomatism. *Edited by* M. A. Menzies and C. J. Hawkesworth, p1-20, Academic Press, London.

Stanin, F. T., and Taylor, L. A. 1980. Armalcolite: An oxygen fugacity indicator. Proceeds Lunar and Planetary Science Conference, **11**: 117-124.

Steele, K. F., and Wagner, G. H. 1979. Relationship of the Murfreesboro kimberlite and other igneous rocks of Arkansas, U.S.A. *In* Kimberlites, Diatremes and Diamonds: Their Geology, Petrology, and Geochemistry. *Edited by* F. R. Boyd, and M. O. A. Meyer. Proceeding of the Second International Kimberlite Conference, American Geophysical Union, Washington, D.C., 1:393-399.

Stern, C. R., and Wyllie, P. J. 1975. Effect of iron absorption by noble-metal capsules on phase boundaries in rock - melting experiments at 30 kilobars. American Mineralogist, **60**: 681-689.

Stevens, R. E. 1944. Composition of some chromites of the Western Hemisphere. American Mineralogist, **29**: 1-34.

Stopler, E., Walker, D., Bradford, H., Hager, H., and Hays, J. F. 1981. Melt segregation form partially molten source regions: The importance of melt density and source region size. Journal of Geophysical Research, **87**: 6261-6271.

Taylor, W. R., and Green, D. H. 1989. The role of reduced C-O-H fluids in mantle partial melting. *In* Kimberlite and related rocks: Their composition, occurrence, origin and emplacement. Proceedings of the 4th International Kimberlite Conference, Perth 1986. Geological Society of America Special Publication Number 14, **1**: 592-602.

Taylor, W. R., and Green, D. H. 1987. The petrogenetic role of methane: Effect on liquidus phase relations and the solubility mechanism of reduced C - H volatiles. *In* Magmatic Processes : physico-chemical principles. *Edited by* B. O. Mysen, Geochemical Society Special Publication **1**: 121-137.

Thompson, R. N. 1977. Primary basalts and magma genesis III: Albian Hills, Roman comagmatic province, Central Italy. Contributions to Mineralogy and Petrology, **60**: 91-108.

Thy, P. 1982. Richterite-arfvedsonite-riebeckite-actinolite assemblage from MARID dykes associated with ultrapotassic magmatic activity in central west Greenland. Terra Cognita, **2**: 247-249.

Thy, P., Stecher, O., and Korstgard, J. A. 1987. Mineral chemistry and crystallization sequences in kimberlite and lamproite dykes from the Sisimuit area, central west Greenland. Lithos, **20**: 391-417.

Tronnes, R. G., Edgar, A. D., and Arima, M. 1985. A high pressure-high temperature study of TiO_2 solubility in Mg-rich phlogopite: implications to phlogopite chemistry. Geochimica Cosmochimica Acta **49**:2323-2329.

Turcotte, D. L. 1987. Physics of magma segregation processes. *In* Magmatic Processes : physico-chemical principles. *Edited by* B. O. Mysen, Geochemical Society Special Publication **1**: 69-74.

Turcotte, D. L. 1981. Some thermal problems associated with magma migration. Journal of Volcanology and Geothermal Research, **10**: 267-278.

Ulmer, P. 1989. The dependence of the Fe2+-Mg cation-partitioning between olivine and basaltic liquid on pressure, temperature, and composition. An experimental study to 30 kilobars. Contributions to Mineralogy and Petrology, **101**: 261-273.

Ulmer, G. C., Grandstaff, D. E., Weiss, D., Moats, M. A., Buntin, T. J., Gold, D. P., Hatton, C. J., Kadik, A., Koseluk, R. A., and Rosenhauer, M. 1987. The mantle redox state; An unfinished story? Geological Society of America, Special Paper **215**: 5-23.

Velde, D. 1975. Armalcolite-Ti-phlogopite-diopside-analcite-bearing lamproites from Smoky Butt, Garfield County, Montana. The American Mineralogist, **60**: 566-573.

Velde, D., 1979. Trioctahedral micas in Melilite-bearing eruptive rocks. Carnegie Institute of Washington, Yearbook, **78**: 468-475.

Venturelli, G., Mariani, E. S., Foley, S. F., Capedri, S., and Crawford, A. J. 1988. Petrogenesis and conditions of crystallization of Spanish lamproitic rocks. Canadian Mineralogist, **26**: 67-79.

Verhoogen, J. 1962. Distribution of titanium between silicates and oxides in igneous rocks. American Journal of Science, **260**: 211-220.

Wade, A., and Prider, R. T. 1939. The leucite-bearing rocks of the West Kimberley area, Western Australia. Quarterly J ·rnal of the Geological Society of London, **96**: 39-98.

Wagner, C., and Velde, D. 1986. The mineralogy of K-richterite-bearing lamproites. American Mineralogist, **71**: 17-37.

Waldman, M. A., McCandless, T. E., and Dummett, H. T. 1987. Geology and petrography of the Twin Knobs #1 lamproite, Pike County, Arkansas. Geological Society of America Special Paper, **215**: 205-216.

Wallace, M. E., and Green, D. H. 1988. An experimental determination of primary carbonatite magma composition. Nature, **335**: 343-347.

Waters, F. G. 1987. A suggested origin of MARID xenoliths in kimberlites by high pressure crystallization of an ultrapotassic rock such as lamproite. Contributions to Mineralogy and Petrology, **95**: 523-533.

Wendlandt, R. F. 1985. An experimental and theoretical analysis of partial melting in the system $KAlSiO_4$-CaO-MgO-SiO_2-CO_2 and applications to the genesis of potassic magmas, carbonatites and kimberlites. *In* Kimberlites and related rocks,*Edited by* J. Kornprobst, : Proceedings of the Third International Kimberlite Conference, American Geophysical Union, Washington, D.C , **1**: 359-369.

Wendlandt, R. F., and Eggler, D. H. 1980a. The origins of potassic magmas: 1. Melting relations in the systems $KAlSiO_4$- Mg_2SiO_4-SiO_2 and $KAlSiO_4$-MgO-SiO_2-CO_2 to 30 kilobars. American Journal of Science, **280**: 385-420.

Wendlandt, R. F., and Eggler, D. H. 1980b. The origins of potassic magmas:2. Stability of phlogopite in natural spinel lherzolite and in the system $KAlSiO_4$-MgO-SiO_2-H_2O-CO_2 at high pressures and high temperatures. American Journal of Science, **280**: 421-458.

Wendlandt, R. F., and Eggler, D. H. 1980c. Stability of sanidine + forsterite and its bearing on the genesis of potassic magmas and the distribution of potassium in the upper mantle. Earth and Planetary Science Letters, **51**: 215-220.

Whitehead, J. A. 1986. Buoyancy - driven instabilities of low-viscosity zones as models of magma-rich zones. Journal of Geophysical Research, **91**: 9303-9314.

Wones, D. R., and Gilbert, M. C. 1982. Amphiboles: Petrology and experimental phase relations. *In* Amphiboles: Petrology and experimental phase relations. *Edited by* D. R. Veblen, and P. H. Ribbe. Reviews in Mineralogy, Mineralogical Society of America, **9B**: 355-385.

Wyllie, P. J., and Sekine, T. 1982. The formation of mantle phlogopite in subduction zone hybridization. Contributions to Mineralogy and Petrology, **79**: 375-380.

Wyllie, P. J. 1979a. Kimberlite magmas from the system peridotite - CO_2 - H_2O. *In* Kimberlites, Diatremes and Diamonds: Their Geology, Petrology, and Geochemistry. *Edited by* F. R. Boyd, and M. O. A. Meyer. Proceeding of the Second International Kimberlite Conference, American Geophysical Union, Washington, D.C., 1:319-329.

Wyllie, P. J. 1979. Magmas and volatile components. American Mineralogist, **64**: 469-500.

Wyllie, P. J., and Huang, W.-L. 1976. Carbonation and melting reactions in the system CaO - MgO - SiO_2 - CO_2 at mantle pressures with geophysical and petrological applications. Contributions to Mineralogy and Petrology, **54**: 79-107.

Yoder, H. S., Jr. 1986. Potassium-rich rocks: Phase analysis and heteromorphic relations. Journal of Petrology, **27**: 1215-1228.

Yoder, H. S., Jr., and Kushiro, I., 1969. Melting of a hydrous phase: Phlogopite. American Journal of Science, **26**: 558-582.